

Liquid Phase Pyrolysis

Dipl.-Ing. Dr. techn.
Nikolaus Schwaiger
Graz, June 2016

► www.icvt.tugraz.at



Eidesstattliche Erklärung

Ich erkläre an Eides statt, dass ich die vorliegende Arbeit selbstständig verfasst, andere als die angegebenen Quellen/Hilfsmittel nicht benutzt, und die den benutzten Quellen wörtlich und inhaltlich entnommene Stellen als solche kenntlich gemacht habe.

Graz, am
(Dipl.-Ing. Dr. techn. Nikolaus Schwaiger)

Statutory Declaration

I declare that I have authored this thesis independently, that I have not used other than the declared sources / resources, and that I have explicitly marked all material which has been quoted either literally or by content from the used sources.

Graz, am
(Dipl.-Ing. Dr. techn. Nikolaus Schwaiger)

Acknowledgement

This page is dedicated to those friends and supporters which made this Thesis possible

My supervisors

Matthäus Siebenhofer

Edgar Ahn

Peter Pucher

Verena Witek

My PhD colleagues

Roland Feiner

Hannes Pucher

Jürgen Ritzberger

My master students

Thomas Glatz

Angela Pieber

Lisa Steiner

Michael Derntl

Joachim Drack

Michael Schadler

Andrea Rollett

Klara Treusch

Thomas Pichler

Roland Wilhelm

Anna Magdalena Mauerhofer

Manuel Tandl

Klaus Schlackl

Roland Nagl

My BDI and CEET colleagues

Hertha Luttenberger

Peter Letonya

Sarah Kunis

Tanja Weiß

Bettina Koch

Jutta Freismuth

Kerstin Zahel

Susanne Neuhold

Lisa Ellmaier

My parents

Bruno

Ingrid

My beloved wife Anna with our unborn child

Abstract

This habilitation thesis describes introductorily three methods for the production of substitute fuels from lignocellulose. These three methods are indirect liquefaction of biomass, direct liquefaction of biomass and lignocellulose pulping followed by processing of the products to fuels. These three strategies are different approaches to obtaining fuels from lignocellulose. The spectrum of fuels discussed, ranges from low-molecular-weight compounds from synthesis gas such as methanol to oxygen-rich multicomponent mixtures which arise from the hydrodeoxygenation of pyrolysis oil.

The main focus of this work is based on liquid phase pyrolysis of lignocellulose and subsequent side product upgrading to liquid fuels. Emphasis is set on process analysis to describe the reaction mechanisms of pyrolytic degradation of lignocellulose. Consequently the next step has been upscaling of the liquid phase pyrolysis process to pilot scale. Moreover it is shown how to synthesize a Diesel fuel with 28% of biogenic carbon. Additionally a liquefaction route for the pyrolysis by-product biochar is presented. This mechanism is based on a hydrogen donor system, which consists of tetralin and naphthalene. A dehydration pathway for liquid phase pyrolysis oil, followed by continuous hydrodeoxygenation is presented too. Finally an overall estimation of fuel production from lignocellulose via liquid phase pyrolysis and side product upgrading has been elucidated.

Kurzfassung

Diese Habilitationsschrift zeigt einleitend drei Strategien um aus Lignozellulose Treibstoffe zu gewinnen. Diese drei Methoden sind die Indirekte Biomasseverflüssigung, die Direkte Biomasseverflüssigung und Aufschlussverfahren für Lignozellulose und Verwertung der gewonnenen Komponenten zu Treibstoffen. Das aufgezeigte Spektrum der Kraftstoffe aus diesen Biomasseverflüssigungsstrategien reicht von niedermolekularen Verbindungen wie Methanol aus Synthesegas bis zu sauerstoffreichen Vielstoffgemischen die bei der Hydrodeoxygenierung von Pyrolyseöl entstehen.

Der Hauptteil der Arbeit beschäftigt sich mit der Flüssigphasenpyrolyse von Lignozellulose und der Aufarbeitung der Produkte der Flüssigphasenpyrolyse zu Treibstoffen. Dabei werden im Detail die Mechanismen der pyrolytischen Zersetzung von Lignozellulose beschrieben. Dann wird das Upscaling der Flüssigphasenpyrolyse in den Pilotmassstab gezeigt. Es wird dargestellt wie man aus Flüssigphasenpyrolyseöl Dieseltreibstoff mit einem biogenen Kohlenstoffanteil von 28% gewinnt. Ebenso wird eine Methode dargestellt biogene Kohle zu verflüssigen. Dies wird durch den Wasserstoffdonor Tetralin ermöglicht. Um einen Kreisprozess zu generieren, wird auch die Rehydrierung von Naphthalin in Tetralin demonstriert. Darüber hinaus wird entwässertes und unbehandeltes Pyrolyseöl in einem kontinuierlichen Hydrierverfahren zu Kohlenwasserstoffen umgesetzt. Abschließend wird eine erste Abschätzung der Gesamteffizienz der Umwandlung von Lignozellulose in Treibstoffe durch Flüssigphasenpyrolyse und nachgeschaltete Upgradingschritte durchgeführt.

Chapter 1

Introduction

1 Introduction

This habilitation thesis shows the academic outcomes of the biomass liquefaction projects done by me and my colleagues at the Institute of Chemical Engineering and Environmental Technology at Graz University of Technology and at BDI-Bioenergy International AG starting in 2008 until spring 2016.

I started my work on biomass liquefaction with my master thesis which was finished in November 2008. Until summer 2011 I did my PhD thesis on optimization of liquid phase pyrolysis. Since autumn 2011 until spring 2016 I worked as Post-Doc on the upgrading of liquid phase pyrolysis sideproducts to fuels.

All the work I did was based on research projects, funded by the Austrian science funding agency, (österreichische Forschungsförderungsgesellschaft; FFG). My project partners were the companies BDI-BioEnergy International AG, OMV AG, AVL List GmbH, Vienna University of Technology and the “Comet Zentrum” Flippr GmbH, which is also funded by Sappi, Mondi and the Heinzl Group.

The names of the projects, I participated, are listed in chronological order, with a short comment on results and outcomes according to this habilitation thesis:

| | |
|-----------|---|
| 2008-2010 | FFG project Lab4BtL; Fundamentals and basics of liquid phase pyrolysis were investigated; invention of the bioCRACK process |
| 2010-2014 | FFG project bioCRACK; Results of the Project Lab4BtL were upscaled to pilot plant scale. The pilot plant was integrated in the OMV refinery at Schwechat, Austria |
| 2012-2014 | FFG project bioBOOST; Liquid and solid side products of the bioCRACK process were upgraded to substitute Diesel fuels |
| 2014-2017 | FFG project OxyGen 2; Basic engineering, ecological and economical design of several biomass conversion processes was performed |
| 2014-2015 | FFG project bioCRACK Scale-up; A continuous hydrodeoxygenation lab-scale plug flow reactor for liquid phase pyrolysis oil was set in operation |
| 2015-2016 | Comet project Flippr, working title “Hydrogen Shuttle”; a process simulation for lignin liquefaction. |
| 2016-2018 | FFG project bioBOOST ⁺ ; goal: long term operations of a continuous hydrodeoxygenation lab-scale plug flow reactor for liquid phase pyrolysis oil |

This thesis is divided in 14 chapters. The first and the last one are an introduction and a summary of my work. Chapter 2 is based on a study of fundamentals of biomass conversion technologies for the OxyGen 2 project. Chapters 3 to 13 are peer reviewed papers in various scientific journals. Chapter 2 and a part of chapter 13 were translated with the support of Ben Hemmens.

Chapter 2

Biomass liquefaction

2 Biomass liquefaction

Independent of the threatening scenario of global warming [1], the decline in availability of the fossil resources oil, coal and gas [2] is an inevitable fact. The irreplaceable loss of carbon-based organic substances due to combustion for heating and transport [3] means that barriers to extraction of fossil raw materials are growing steadily higher. High risks have been accepted to access deposits, as the Deepwater Horizon disaster illustrates, but also increasing amounts of environmental damage are being accepted [4].

As an alternative to these phenomena this work describes processes for making substitute fuels from renewable energy sources.

The following criteria are defined as conditions that these substitute fuels must fulfil:

1. The fuels must originate in a renewable source
2. Competition of resources with production of food is not acceptable.

By defining the categories 1 and 2 it is important to restrict the scope of this work to so-called 'second generation biofuels'. These fuels have in common that they are designed by making use of whole plant material. This does not mean that the whole plant is converted to fuel. Wheat is a good example; it would be possible to use the wheat grain in the food industry and the rest of the plant (straw) for making fuel.

Having thus defined the criteria for manufacturing this type of fuel, it is the next step to turn to the processes involved in converting lignocellulose to substitute fuel. To begin with, biomass properties are explained in more detail, with spruce wood as an example.

2.1 Lignocellulose in Spruce Wood

Lignocellulose is a highly complex composite material. In this Chapter, using spruce wood as an example, it is mandatory to describe the structure of lignocellulose, beginning with its elemental composition, then consider its molecular constituents and finally look at its macrostructure.

2.1.1 Elemental Composition

As a first approximation it is possible to say that wood is effectively a combination of carbon, oxygen and hydrogen. Even the nitrogen content is so small as to be negligible, at less than 1% (Table 1).

Table 1: Elemental composition of spruce wood without inorganic components:

| C | H | N | O |
|----|---|----|----|
| % | % | % | % |
| 50 | 6 | <1 | 43 |

In addition, the ash content of spruce wood is small, less than 1%. The main inorganic components of spruce wood are shown in Table 2.

Table 2: Main constituents of the ash of spruce wood [5]

| Element | Mass |
|---------|------|
| | mg/g |
| Ca | 0.27 |
| K | 0.33 |
| Na | 0.01 |
| S | 0.08 |

From the elemental composition it is shown that wood does not have a high energy density. The main aspect that limits its potential as an energy store is the high oxygen content.

Table 3: Calorific values of diesel and wood

| Material | Lower Calorific value kJ/kg |
|-------------|--------------------------------|
| Spruce wood | 19123 |
| Diesel | 43113 |

Even if wood is dried at 105°C for 24h, so that the water which is not chemically fixed is removed, the calorific value is still less than half that of diesel fuel, as shown in Table 3. To express the composition of spruce wood as an empirical formula, this would be approximately $\text{CH}_{1.54}\text{O}_{0.65}$.

2.1.2 Molecular Composition

The empirical formula calculated in chapter 2.1.1 reflects a considerable variety of functional groups, which is also apparent in the infrared spectrum (Figure 1).

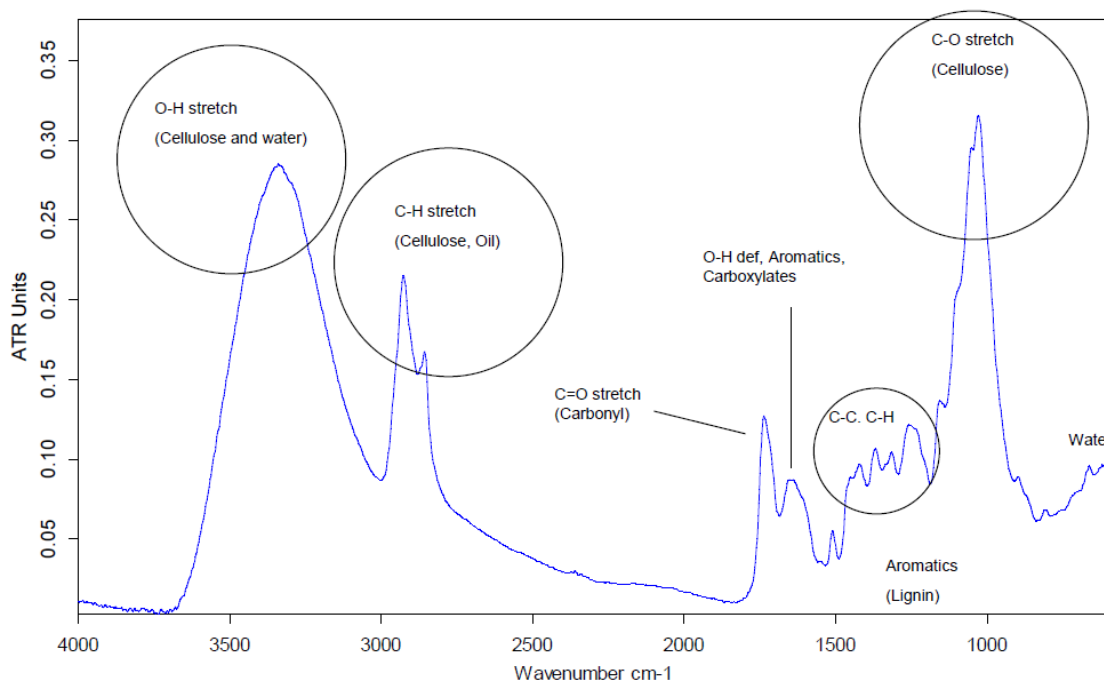


Figure 1: ATR-IR spectrum of spruce wood [5]

Figure 1 shows an ATR-IR spectrum of spruce wood, in which the most important functional groups are visible. The only exception are the aromatic groups, which are difficult to detect in infra-red spectra, because they interact with infra-red radiation very weakly and their absorption of these frequencies is minimal. The functional groups shown in Figure 1 are listed in Table 4 along with their respective mean bond enthalpies.

Table 4: Types of bonds found in ATR-IR of spruce wood [6]

| Bond type | | Mean bond energy kJ/mol |
|---------------------------|-----|----------------------------|
| Hydrogen-oxygen bond | O–H | 463 |
| Carbon-hydrogen bond | C–H | 412 |
| Carbon-oxygen double bond | C=O | 743 |
| Carbon–carbon bond | C–C | 348 |
| Carbon-oxygen single bond | C–O | 360 |
| Aromatic C–C bond | C≈C | 838 |

Like all forms of lignocellulose, spruce wood consists mainly of three categories of polymer: these are cellulose, hemicellulose and lignin.

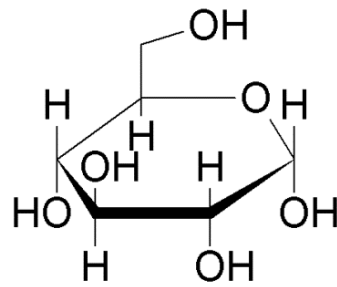
Table 5: Categorization of molecular components in spruce wood [7]

| Name | Extractives | Lignin | Cellulose | Glucomannan | Glucuronoxylan | Other polysaccharides |
|---------------|-------------|--------|-----------|-------------|----------------|-----------------------|
| | % | % | % | % | % | % |
| Norway Spruce | 1.7 | 27.4 | 41.7 | 16.3 | 8.6 | 3.4 |

Table 5 shows the main molecular components in spruce wood. Glucomannan and glucuronoxylan are subtypes of hemicellulose. Extractives are low-molecular weight component, which can be extracted in organic solvents. For example, 2.2% of spruce wood is soluble in acetone. These compounds can then be further classified as soluble or insoluble in ethyl ether and petroleum ether. The soluble compounds include free fatty acids, longer-chain alcohols, terpenes, waxes, resins and many other molecules [7].

2.1.2.1 Cellulose

Figure 2 shows β -D-glucopyranose, the (only) monomer of cellulose. In cellulose, β -D-glucopyranose is polymerized via a 1- \rightarrow 4 glycosidic linkage [8].

Figure 2: β -D-Glucopyranose

The linkage of the first carbon atom to the fourth carbon atom means that the molecule has a reducing end on one side and a non-reducing end on the other side.

non-reducing end

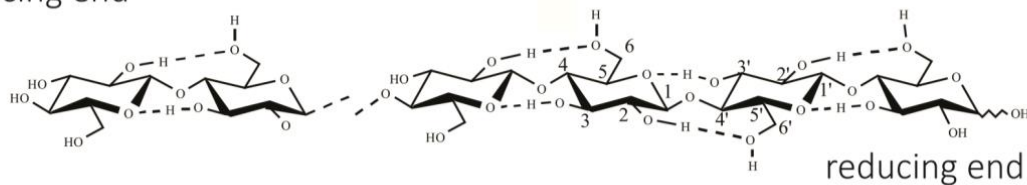


Figure 3: Cellulose polymer [9]

Figure 3 shows two details of the polymer. Firstly, it shows the non-reducing and the reducing ends. In addition, the figure shows two intramolecular hydrogen bonds. One is between the hydroxyl group of the C₆ and the C₂ carbon; the other is from the C₃ hydroxyl to the oxygen atom of the acetal group.

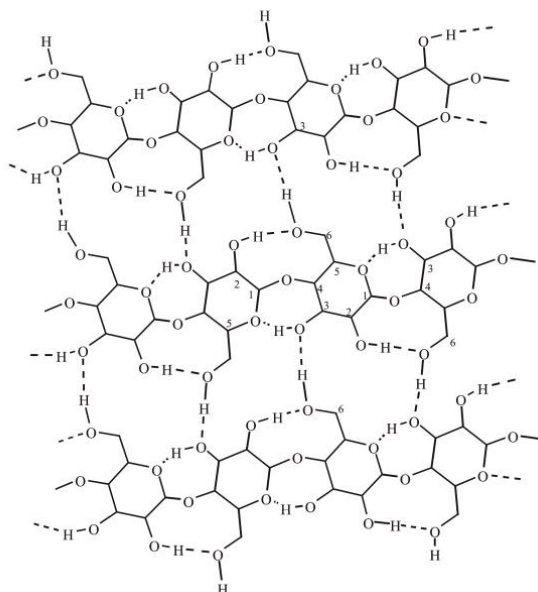


Figure 4: Intermolecular hydrogen bonds in cellulose [10]

Figure 4 shows the crosslinking between cellulose molecules by hydrogen bonds between the hydroxyl groups on the C₆ and C₃ carbons.



Figure 5: Three-dimensional representation of two glucose dimers linked by hydrogen bonds [11]

The three additional bonds, which are shown in a close-up view in Figure 5, give cellulose its characteristic properties, such as its insolubility in water or the relatively slow degradation by microorganisms compared to other carbohydrates. These bonds assemble the individual cellulose polymer molecules into cellulose sheets. The cellulose sheets turn into aggregates to form fibrils held together by Van-der-Waal forces and hydrophobic interactions. Finally, the fibrils combine to form cellulose fibres [12].

2.1.2.2 Hemicellulose

The term hemicellulose is an umbrella term for a diverse category of carbohydrate-based polymers isolated from plants. The prefix hemi- (Greek: half) is rather misleading because neither in the molecular sense nor in terms of their properties as macromolecules is it accurate to describe hemicelluloses as ‘half-’ celluloses.

At the molecular level, hemicellulose differs from cellulose in two important respects:

- The building blocks of hemicellulose are not only glucose and carbohydrates.
- Hemicellulose is not a straight-chain polymer.

Additionally, the composition of hemicelluloses present in plants materials differs quite strongly between different taxonomic groups. In this chapter, the chemical structure of hemicellulose based on the hemicelluloses of spruce wood, glucuronoxylan and glucomannan is described.

Glucuronoxylan

Glucuronoxylan, as its name suggests, is composed of the components xylose and glucuronic acid. Side-chains may be formed by glucuronic acid or methyl groups. Spruce wood contains a special type of glucuronoxylan, called arabinoglucuronoxylan, whose structure is shown schematically in Figure 6. The mean molecular mass of arabinoglucuronoxylan in spruce wood is approximately 19200 g/mol [13].

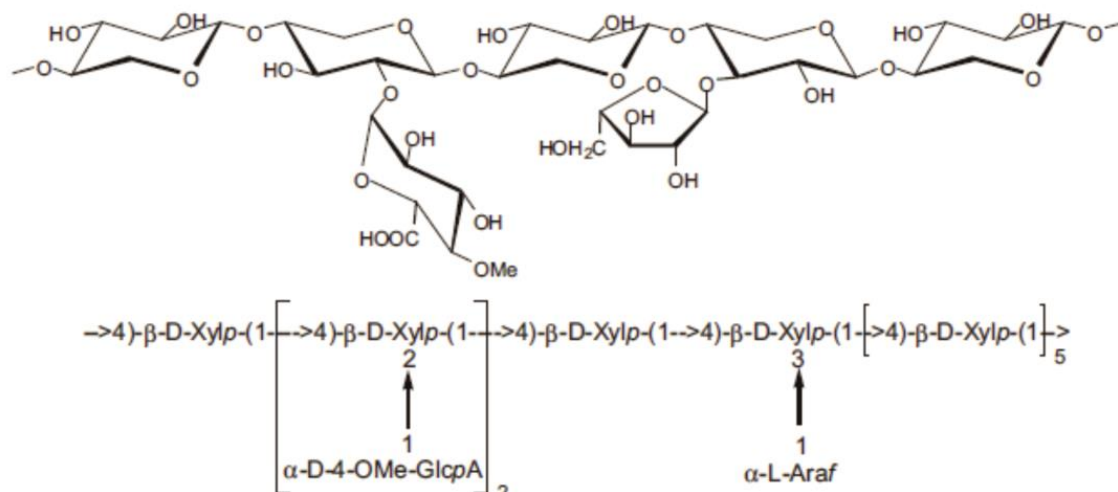


Figure 6: Representative detail of an arabino-4-O-methylglucuronoxylan chain [13]

Glucomannan

As with glucuronoxylan, spruce also contains a special subtype of glucomannan, called galactoglucomannan, shown schematically in Figure 7. Its mean molecular mass is 20200 g/mol. It is composed mainly of glucose and mannose. The side chains are acetate groups connected via ester linkages and galactose connected via an acetal [13].

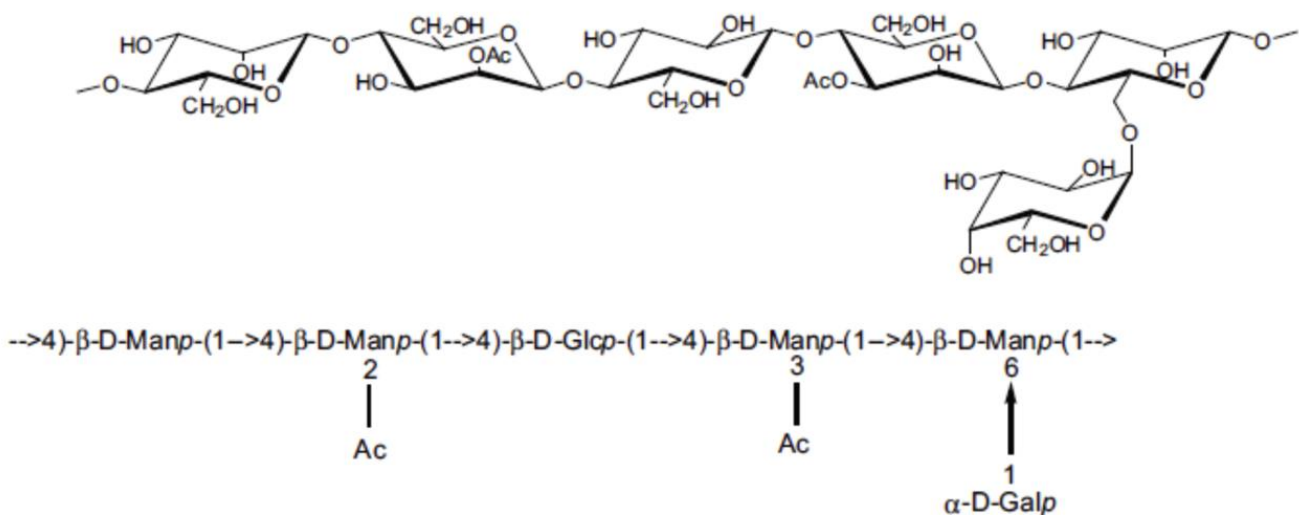


Figure 7: Detail of galactoglucomannan [13]

2.1.2.3 Lignin

'Lignin' is derived from the Latin word *lignum*, for wood. This term is no less misleading than 'hemicellulose'. In reality, the lignin content of wood ranges from minimum values of about 20% in hard woods to maximum values of around 33% in soft woods [14]. Lignin differs from cellulose and hemicellulose in that its three basic building blocks are coumaryl alcohol, coniferyl alcohol and sinapyl alcohol.

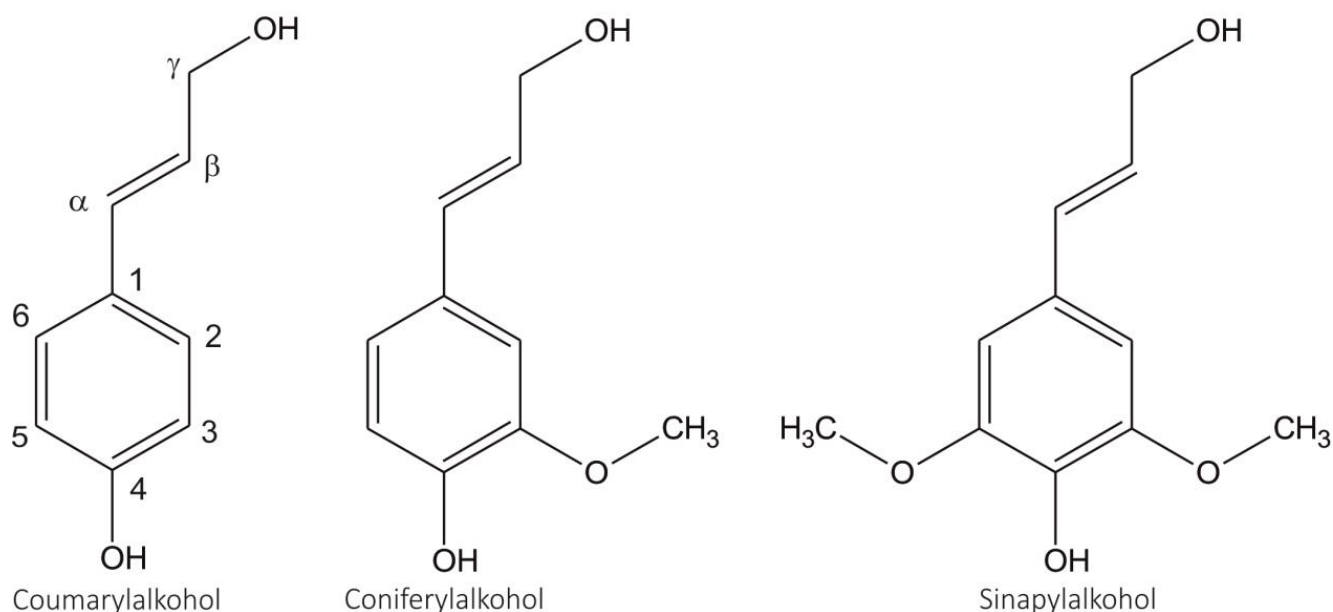


Figure 8: Monomers of lignin with numbering/naming of their carbon centres

As shown in Figure 8, these three monomers are very similar in structure. They are based on 4-[(*E*)-3-hydroxyprop-1-enyl]-phenol, with extra methoxy groups in position 3 in coniferyl alcohol and in positions 3 and 5 in sinapyl alcohol. The centres in lignin are numbered as shown in Figure 8 [15].

Table 6: Relative amounts of the monomer residues coumaryl alcohol, coniferyl alcohol and sinapyl alcohol in different categories of plants: hard and softwood and annual plants [10]

| Plant type | Coumaryl alcohol | Coniferyl alcohol | Sinapyl alcohol |
|------------|------------------|-------------------|-------------------------|
| Softwood | <5 | >95 | Not detectable / traces |
| Hardwood | 0–8 | 25–50 | 46–75 |
| Annuals | 5–33 | 33–80 | 20–54 |

Table 6 shows the relative abundance of the monomer types in lignin from different categories of wood. It is possible to see that lignin from soft wood such as spruce has a simpler chemical composition than the lignin from hard wood or annual plants. The formation of lignin from the monomers mostly proceeds via dehydrogenation of the phenol hydroxyl group [15]. This leads to formation of phenoxy radicals and thus to polymerisation.

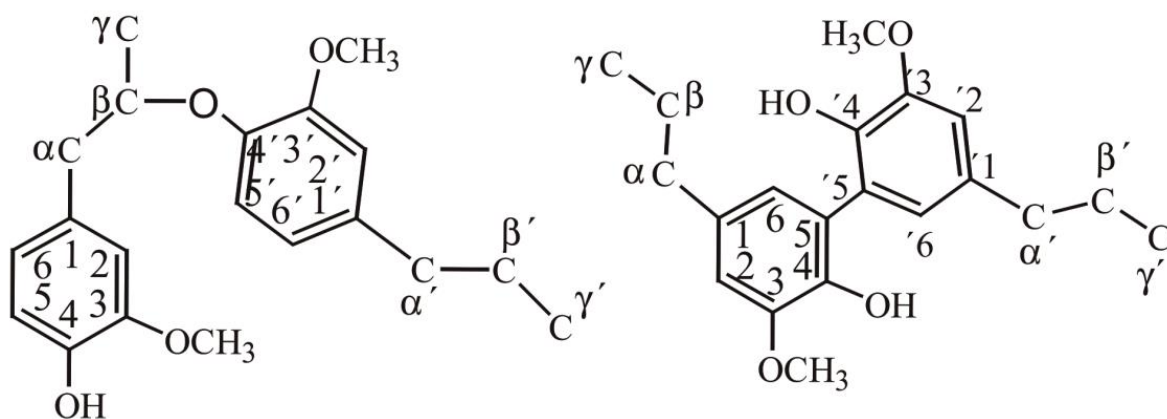
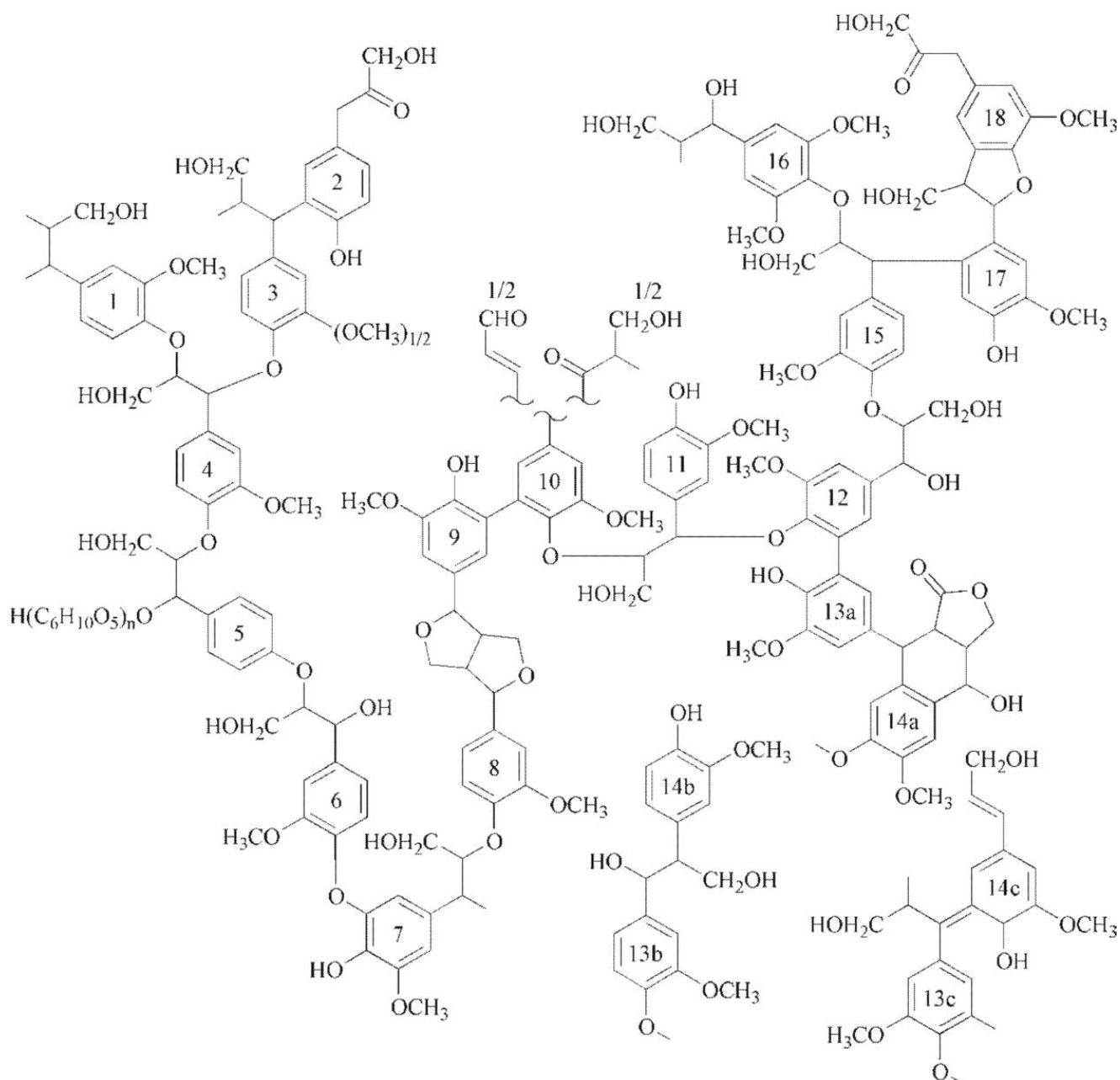
Figure 9: β -o-4 und 5-5' bonds in lignin [10]

Figure 10: Structure of lignin according to Freudenberg

Figure 10 shows a model of lignin structure and possible bonds, whereas Figure 9 shows two representative linkages between the phenylpropanoid units in lignin. The β -O-4 linkage between the β -carbon of the propane side chain and the hydroxyl of the phenol is one of the common types of linkage in lignin, accounting for 35 to 60 % of the linkages in lignin of soft wood [10]. In addition, lignin also contains some carbon-carbon bonds, including the 5-5' bond between the position 5 carbons of two phenyl rings (Figure 9).

Because of the multiple different kind of linkage and the additional crosslinking of lignin with polymeric carbohydrates, it is not really possible to give a definitive description of lignin as a whole molecule. Every wood pulping process damages the lignin framework in one way or another. Acidic processes such as the magnefite process [16] or other bisulphite processes [17], yield lignin in the form of liginosulphonate with mean molecular weights from 4600 to 398000 g/mol and a degree of polymerisation of 1.3 to 3.5 [18]. An acidic organosolv process yields molecular weights of more than 4600 g/mol [19]. In order to describe lignin better in its natural state, it is necessary to rely on hypothetical models of its structure.

2.1.3 Macroscopic Structure of Wood

The three polymers described above – lignin, hemicellulose and cellulose – are combined with each other and interact with each other to form the macroscopic structure of wood.

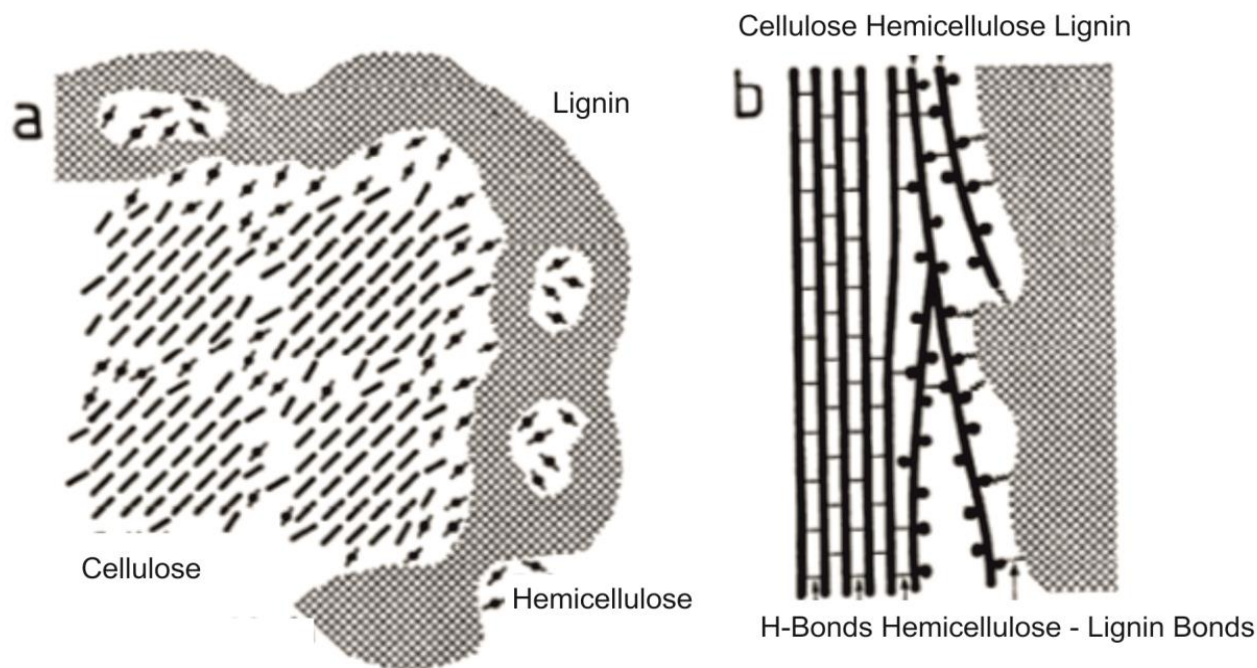


Figure 11: Model of the internal structure of a wood cell wall a) transverse section, b) longitudinal section [7]

The interaction between the components is difficult to detect at the molecular level and has the overall title of 'lignin-carbohydrate complex' (LCC). Some clues about the structure of LCC have been obtained from studying the fragments that remain in softwood cellulose produced

by the kraft process. It was found that 92% of the lignin fragments are bound to xylan and glucomannan. Only 8% are bound to cellulose [20]. This allows to create a schematic structural model of the polymers.

Figure 11 shows the schematic arrangement of wood in a wood cell. It shows how the hemicellulose connects the lignin with the cellulose. Figure 12 shows the formation of the different layers in the wood cell.

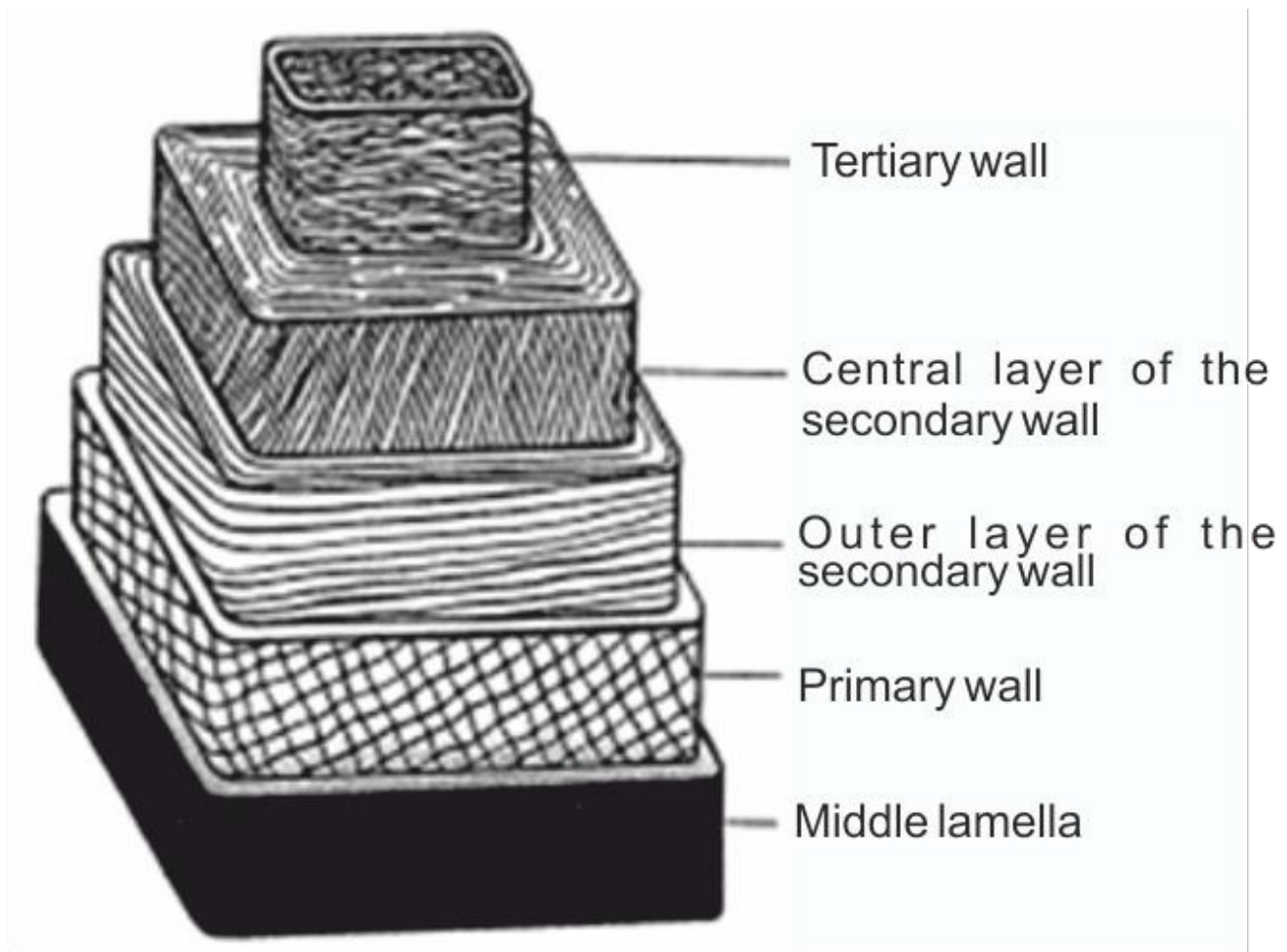


Figure 12: Cell-wall layers of a conifer tracheid [21]

Middle lamella: This layer consists of pectin and carbohydrate-free lignin. The middle lamella must be broken up in the maceration process. Along with the insolubility of cellulose in water, this is certainly one of the most difficult steps in the liquefaction of cellulosic biomass.

Primary wall: 10% of this layer consists of cellulose fibres; the rest is made up of lignin, pectin and hemicellulose. The lignin content can be 70%.

Secondary wall: This layer is mostly composed of cellulose microfibrils [21].

Figure 13 shows the distribution of lignin in a wood cell. This agrees with the structures shown in Figure 11 and Figure 12.

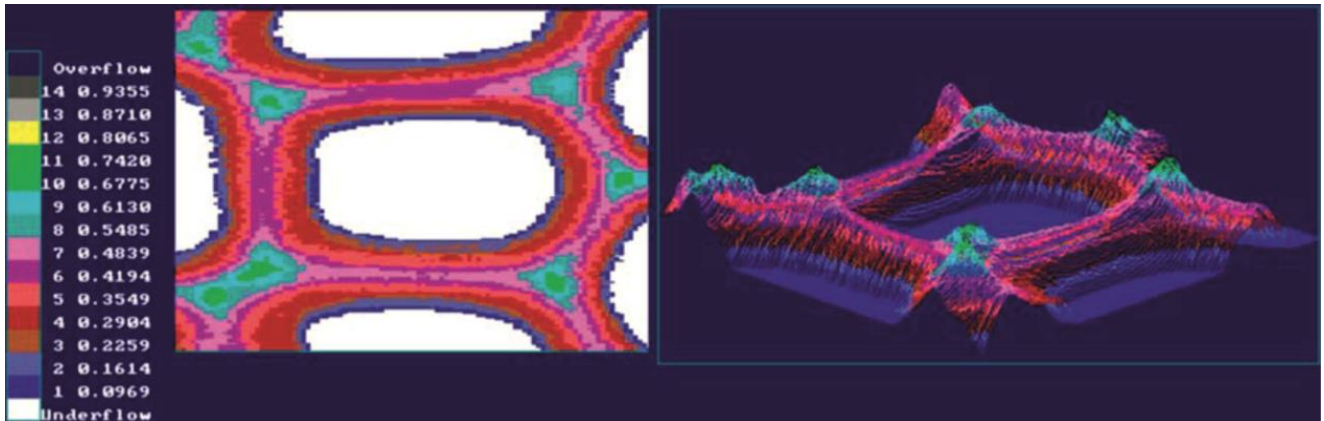


Figure 13: Image of wood cell (spruce) made by UV microspectrophotometry at 280 nm [14]

This basic introduction into lignocellulosic biomass and the nature of constituents of lignocellulosic biomass has to be linked with technologies for hydrocarbon formation, the topic of this habilitation thesis

2.2 Substitute Fuels from Lignocellulose

There are different process options for synthesizing substitute fuels from biomass. In this chapter 3 individual process strategies are picked out in detail.

2.2.1 Indirect liquefaction of Biomass to Fuels

The indirect liquefaction of biomass is a multi-step process as shown schematically in Figure 14. By neglecting the harvesting and transport of the biomass raw material, four main process steps are identified.

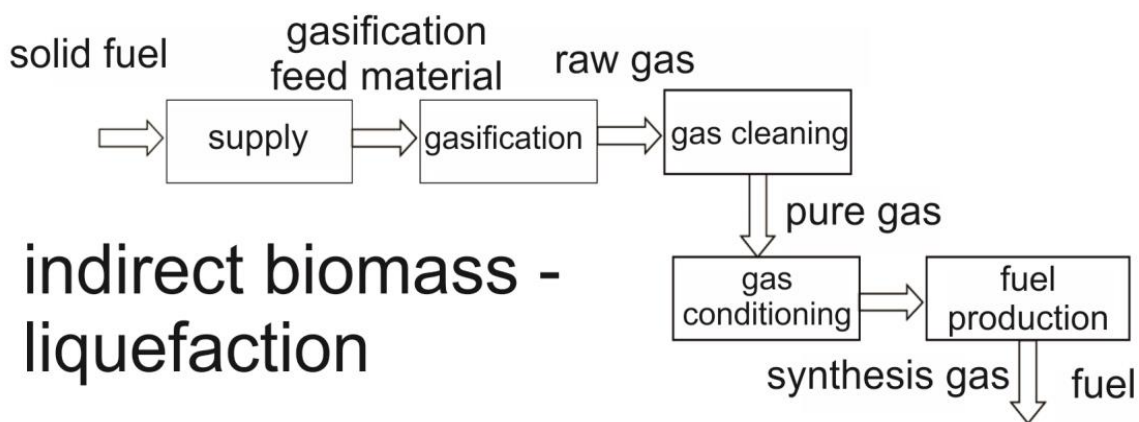


Figure 14: Scheme for indirect liquefaction of biomass [22, 23]

These are the gasification of the biomass, gas purification, gas conditioning and the final step of fuel production. These four steps and the many alternative methods for realizing them will be discussed in detail in the following sections.

2.2.1.1 Gasification of Biomass

There are several variables that influence biomass gasification; the most important are the reactor and the energy input, the gasification medium, and the reaction parameters temperature and pressure. These factors are discussed in this section.

The gasification temperatures reported in the literature covers a wide range, from 740 to 1400°C [24]. Most gasification reactors are operated at atmospheric pressure. However there are examples of reactors that run at 50 mbar [25]. There are also reports of experiments on biogenic hydrogen production in which the entire reaction system (biomass feed, gasification reactor and particle separator) is pressurized [26]. It is also possible to blow only a partial flow (oxygen as gasification medium) under pressure into the gasifier [27]. The gas quality is defined in terms of the energy content per volume. This can be between 1 and 20 MJ/m³ [28].

The basic reactions in gasification of biomass are very similar to those involved in gasification of coal.

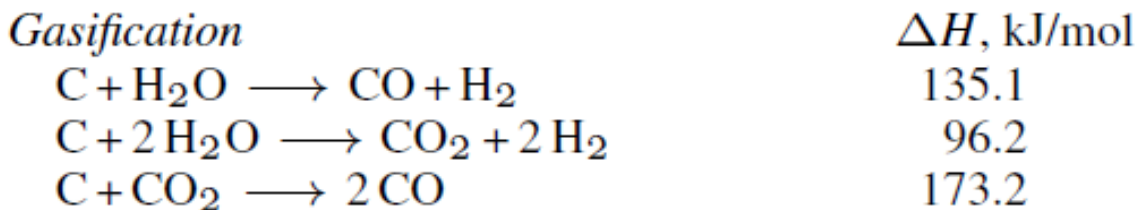


Figure 15: Reactions in gasification of carbon, oxygen and hydrogen [29]

Figure 15 shows the basic reactions involved in the gasification of carbon. These reactions are all endothermic. In addition, depending on the gasification medium, combustion reactions can occur within the gasification process, which are shown in Figure 16.

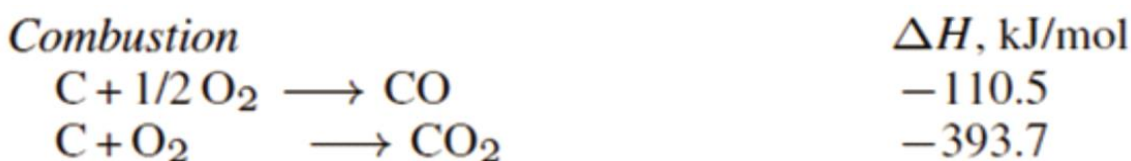


Figure 16: Combustion reactions in biomass gasification [29]

This leads to the next aspect of gasification, the choice of the gasification medium. The choice of gasification medium also determines the mode of energy input into the gasifier.

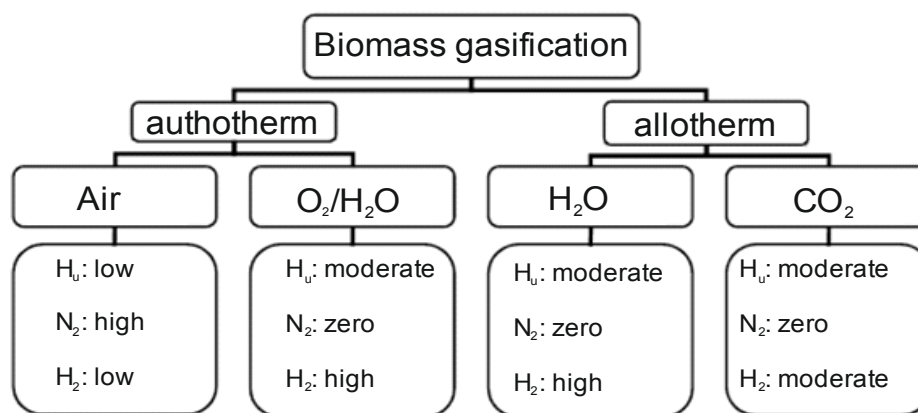


Figure 17: Operational modes of biomass gasification [30]

As shown in Figure 17, the gasifier can be operated 'autothermally' or 'allothermally'; this defines how the endothermic gasification is driven. Autothermal operation means that part of the biomass is burnt so that the energy of combustion can be used for the gasification of the remainder. As can be seen in Figure 17, the reaction mode has a major effect on the composition of the resulting gas. In particular, autothermal operation generates CO_2 , which has to be washed out of the gas with considerable effort; on the other hand, if the energy for gasification is not obtained from the biomass, it must be supplied from another source, again with considerable effort.

The choice between autothermal and allothermal energy supply leads to the next choice in the design of the gasification process, the design of the reactor. As analysed by Hofbauer [30], reactors for biomass gasification can be classified into three types: packed bed, fluidized bed

and entrained flow. A variety of designs exist for each type; here it will suffice to show representative basic forms. Figure 18 shows a counter current packed-bed gasifier. A highly innovative application of this type of gasifier is to combine it with a Stirling engine [31]. This configuration can achieve electrical efficiencies of up to 17.5% [30].

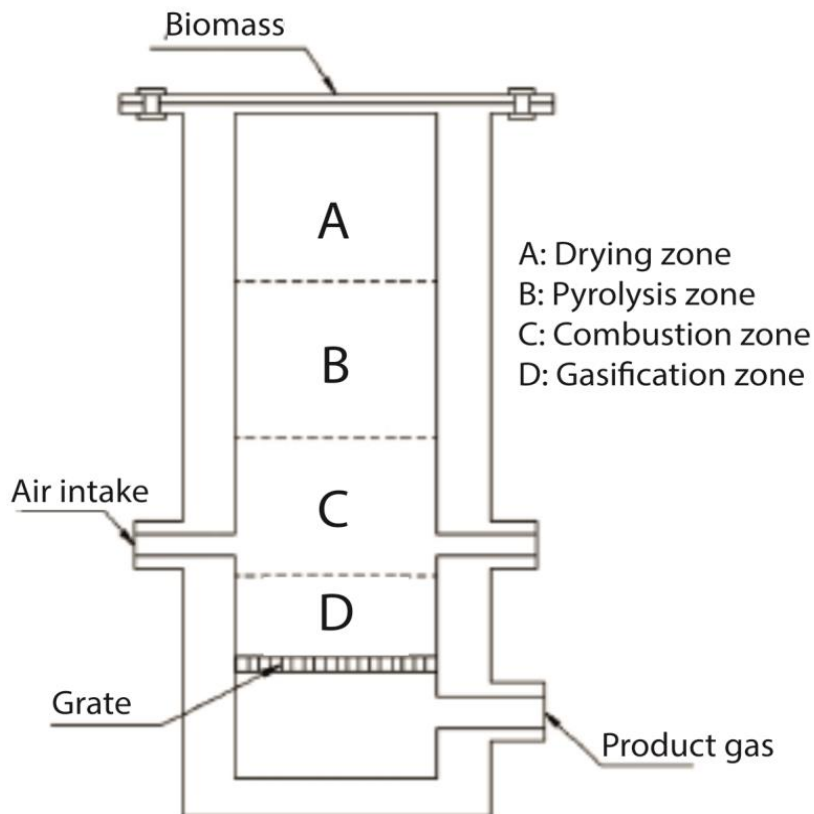


Figure 18: Autothermal counterflow packed-bed gasifier [31]

The reactor is divided into four reaction zones. From the top to the bottom, biomass is fed in, then dried, pyrolyzed, partially combusted and finally gasified.

The next reactor type is the fluidized-bed gasifier. Fluidized-bed reactors are designed in different types and can be divided into several subtypes, for example stationary, circulating and twin-bed reactors. In the stationary fluidized-bed reactor, the sand used as the heat carrier remains in the reactor. In a circulating fluidized-bed reactor, the heat carrier is transported out of the reactor and is usually separated from the product gas in a cyclonic separator. Figure 19 shows a twin-bed fluidized-bed system [34]. In this form, biomass is gasified in a stationary fluidized bed. Subsequently, the heat carrier and the char formed in the gasification step are transferred into a circulating fluidized bed and burned. This step supplies energy for the gasification process while at the same time cleaning the ash and char out of the stationary fluidized-bed material. Separating the gasification from the combustion makes the gas production much simpler, because the gas is not contaminated with CO_2 . Currently, numerous research groups are working actively on the gasification of biomass in fluidized beds [35–39].

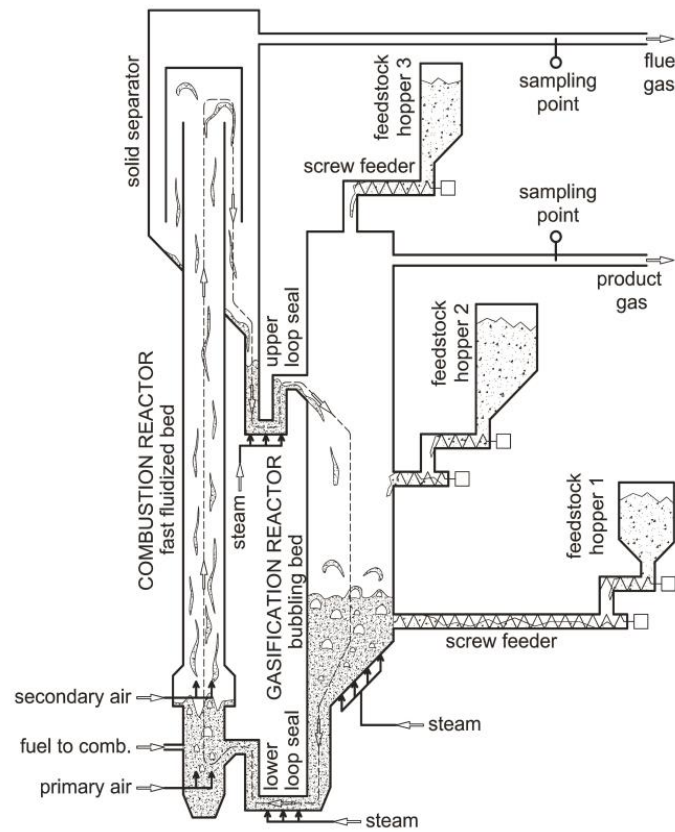


Figure 19: Twin circulating fluidized bed [34]

The third reactor technology described in the literature is the entrained-flow gasifier. The leading example of this reactor type is perhaps the bioliq process of the Karlsruhe Institute of Technology [38]. In this reactor type, the biomass and the gasification medium are blown into the reactor in the same gas stream, as shown in Figure 20.

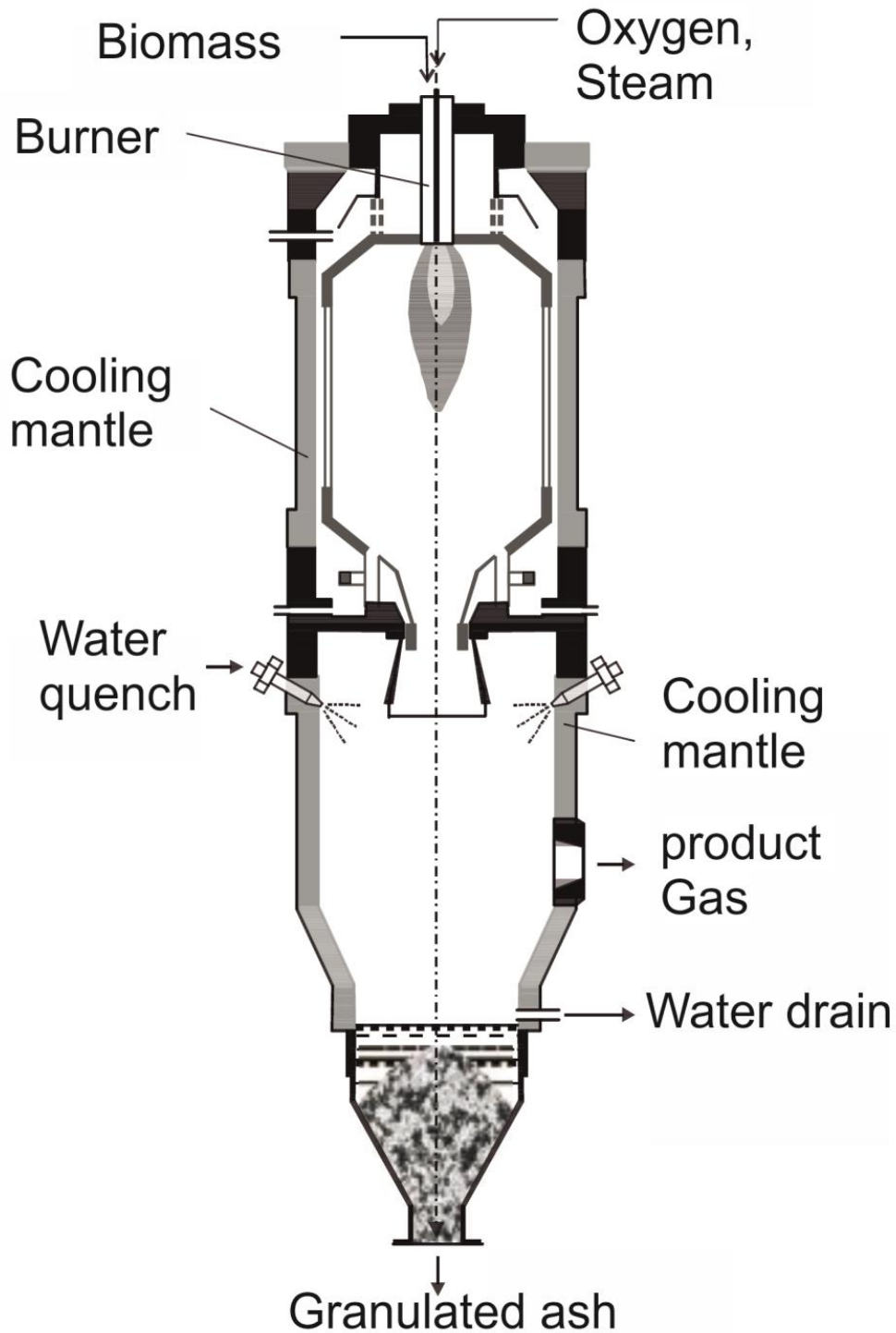


Figure 20: Entrained-flow gasifier [38]

In the bioliq process, the input material injected into the reactor is not raw biomass but pyrolysis oil. This has the advantage that a conversion of the biomass to a more energy-dense form already takes place upstream of the gasification unit [41]. Currently, entrained-flow gasification is the subject of intensive research [27, 42, 43].

2.2.1.2 Gas Cleaning and Gas Conditioning

The gasification of biomass is followed by cleaning and conditioning of the raw gas. These are essential steps en route to biofuel. In this section there is a brief review of the purity shown, which depends on the subsequent use of the gas, and the technical solutions for achieving the required purity.

Table 7: Composition of Eucalyptus ash [44]

| Substance | Mass fraction % |
|--------------------------------|--------------------|
| SiO ₂ | 2.82 |
| CaO | 59.47 |
| Al ₂ O ₃ | 0.27 |
| Fe ₂ O ₃ | 0.94 |
| Na ₂ O | 3.4 |
| K ₂ O | 10.67 |
| MgO | 5.79 |
| P ₂ O ₅ | 3.53 |
| CO ₂ | 5.64 |
| Rest | 7.47 |

There are three components of the gasified biomass that can cause problems with the subsequent utilization of the gases. These are the inorganic components, which can include salts, oxides, acids and bases. The composition of the ash of gasification residues depends on the type of biomass. For example, annual plants have an exoskeleton made of silicates, which means that they have a much higher silicate content than perennial plants. The dry mass of Eucalyptus has an ash content of 0.95% [44]. The substances of the ash are listed in Table 7. For comparison, the main components of gasification residues of olive mill waste are shown in Table 8. This shows clearly how widely the composition of inorganic components can vary. In the publication series 'Nachwachsende Rohstoffe', Volume 29 [43] is stated "problems rarely arise because a dust separator is a standard part of the plant".

Tars are formed in every pyrolysis process, regardless of whether the goal is gasification, liquefaction or coking. They may originate from different components of the biomass: for example, they can be formed by recombination of pyrolysis fragments [44], or they may represent fragments of lignin or carbohydrates that did not remain in the gasifier long enough to be completely decomposed into the target substances CO and H₂.

Table 8: Ash content of gasification residues of olive mill waste [45]

| Substance | Mass fraction % |
|--------------------------------|--------------------|
| CaO | 11.15 |
| MgO | 7.90 |
| Fe ₂ O ₃ | 9.115 |
| Al ₂ O ₃ | 13.61 |
| SiO ₂ | 53.93 |
| K ₂ O | 0.48 |
| Na ₂ O | 3.49 |

In practice, inorganic dust and char particles do not pose any serious problems for the workup of raw gas to synthesis gas; removing the tar fraction takes much more effort.

A detailed account of tar formation in biomass gasification is given by Font Palma [46]. The reactor design has a large influence on the tar content of the synthesis gas. The tar content is particularly high in a contraflow gasifier (10–150 g/m³) and lowest in the twin-bed fluidized-bed reactor (0.5–2 g/m³) [28].

Table 9: Maximum tar levels in the synthesis gas depending on the application [47]

| Tar content in synthesis gas depending on gasifier type | 0.1 to 100 g/Nm ³ |
|---|------------------------------|
| Maximum tar content, depending on the application | |
| Gas-fired combustion engine | <100 mg/m ³ |
| Gas turbine | <50 mg/m ³ |
| Molten carbonate fuel cell (MCFC) | <2000 ppmv |
| Polymer electrolyte fuel cell (PEMFC) | <100 ppmv |
| Fischer-Tropsch synthesis (F-T) | <1 ppmv |

Table 9 shows the range of average values for tar contamination from the literature compared to the maximum tolerable tar levels for different applications of the synthesis gas. It is clear that significant effort is needed to reduce the tar content to the required levels. Table 10 shows the tar separation levels achieved with different cleaning technologies. Simple separators can remove more than 99% of the dust particles from the gas, but much more effort is needed to reduce the tar contamination to levels compatible with using the gas to synthesise fuels. So-called ‘hot gas’ tar removal technologies use catalysts to decompose the tar, similar to crackers or reformers used in the petrochemical industry. These units use iron- and nickel-based catalysts at high temperatures (600–900°C) [48].

Table 10: Separation of particulates and tar by different cleaning technologies [49]

| | Particle separation % | Tar removal % |
|-----------------------------------|--------------------------|---------------------|
| Sand bed filter | 70–99 | 50–97 |
| Washing towers | 60–98 | 10–25 |
| Venturi washer | | 50–90 |
| Wet electrostatic precipitator | >99 | 0–60 |
| Fabric filter | 70–95 | 0–50 |
| Rotary separator | 85–90 | 30–70 |
| Granular bed adsorption | | 50 |

One example of these processes are silicon carbide filters doped with magnesium, calcium or cerium. In tests with naphthalene these filters achieved removal nearly levels of 100% [50].

In contrary to the removal of solid and liquid contaminants, the removal of gaseous contaminants is a much more difficult step in the synthesis gas production. The sensitivity of the catalysts to poisoning by several contaminants necessitates strenuous efforts to clean the synthesis gas. For example, methanol synthesis with nickel catalysts requires the sulphur content of the gas to be reduced to less than 0.1 ppmv [51]. For Fischer-Tropsch synthesis of alkanes, the gas has to be cleaned even more stringently and must contain less than 10 ppb of sulphur and less than 20 ppb of nitrogen (as NH_3 und HCN) [52].

Table 11: Absorption-based gas cleaning [53]

| Solvent for the absorption | Type | Applicable for | | | | Process name |
|---------------------------------------|----------|----------------|----------------------|--------------|--------|-----------------|
| | | CO_2 | H_2S | COS | Thiols | |
| Monoethanolamine | Chemical | yes | yes | no | no | MEA |
| Diethanolamine | Chemical | yes | yes | no | no | DEA |
| Potassium carbonate | Chemical | yes | yes | yes | yes | Benfield |
| Methanol | Physical | yes | yes | yes | yes | Rectisol |
| N-methylpyrrolidone | Physical | yes | yes | yes | yes | Purisol |
| Polyethylene glycol dimethyl ether | Physical | yes | yes | yes | yes | Selexol |

In contrary to the removal of solid and liquid contaminants, the removal of gaseous contaminants is a much more difficult step in the synthesis gas production. The sensitivity of the catalysts to poisoning by several contaminants necessitates strenuous efforts to clean the synthesis gas. For example, methanol synthesis with nickel catalysts requires the sulphur content of the gas to be reduced to less than 0.1 ppmv [51]. For Fischer-Tropsch synthesis of alkanes, the gas has to be cleaned even more stringently and must contain less than 10 ppb of sulphur and less than 20 ppb of nitrogen (as NH_3 und HCN) [52].

Table 11 shows a list of gas-cleaning processes and their brand names. The best known of these is certainly the Rectisol process. This process was developed by the companies Linde and Lurgi. Figure 21 shows a diagram of the process. It shows clearly how small the actual absorber unit is, relative to the laborious and complex regeneration of the cleaning agent.

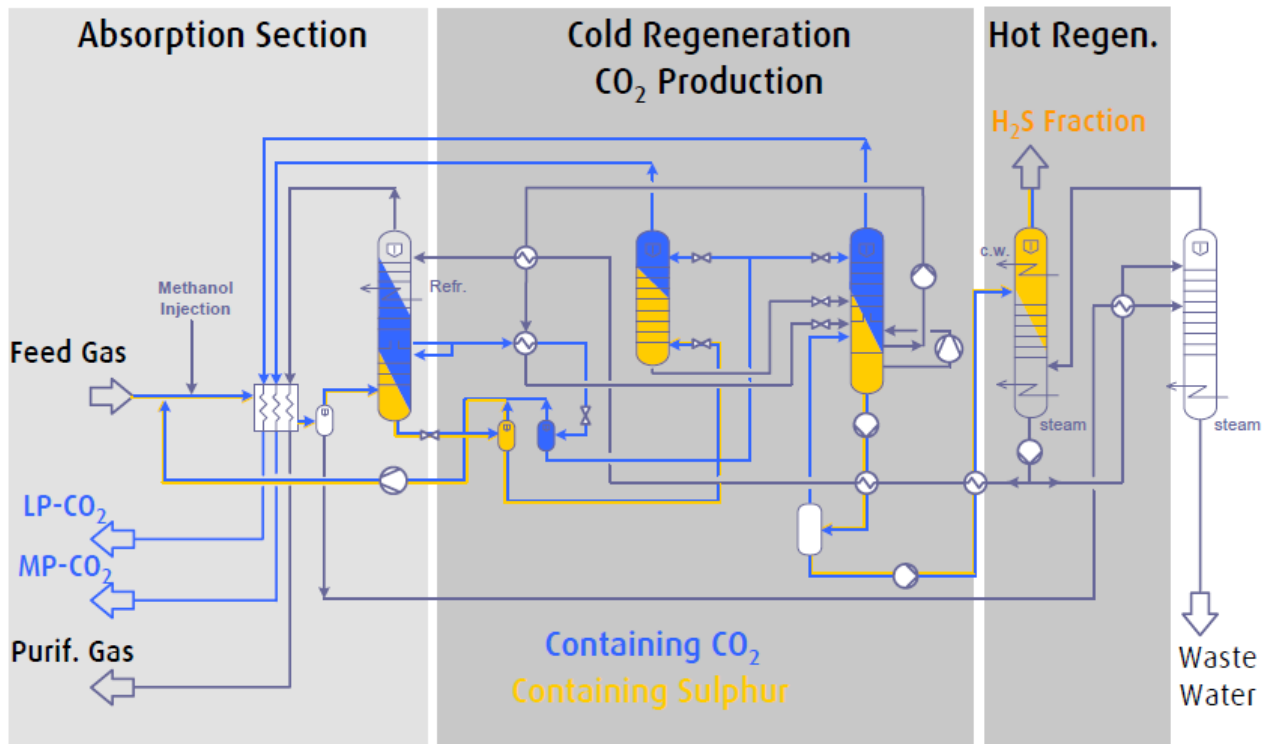


Figure 21: Simplified diagram of the Rectisol process [54]

However, the complexity of the plant is not the greatest obstacle to cleaning of synthesis gas. What makes the process difficult in economic terms is most of all the process temperature. Figure 22 shows the process concept for an Aspen simulation of a single-stage Rectisol cleaning plant. Notable are the temperatures of the material streams MEOH1, at -50°C , and RAWGAS at -20.59°C [55].

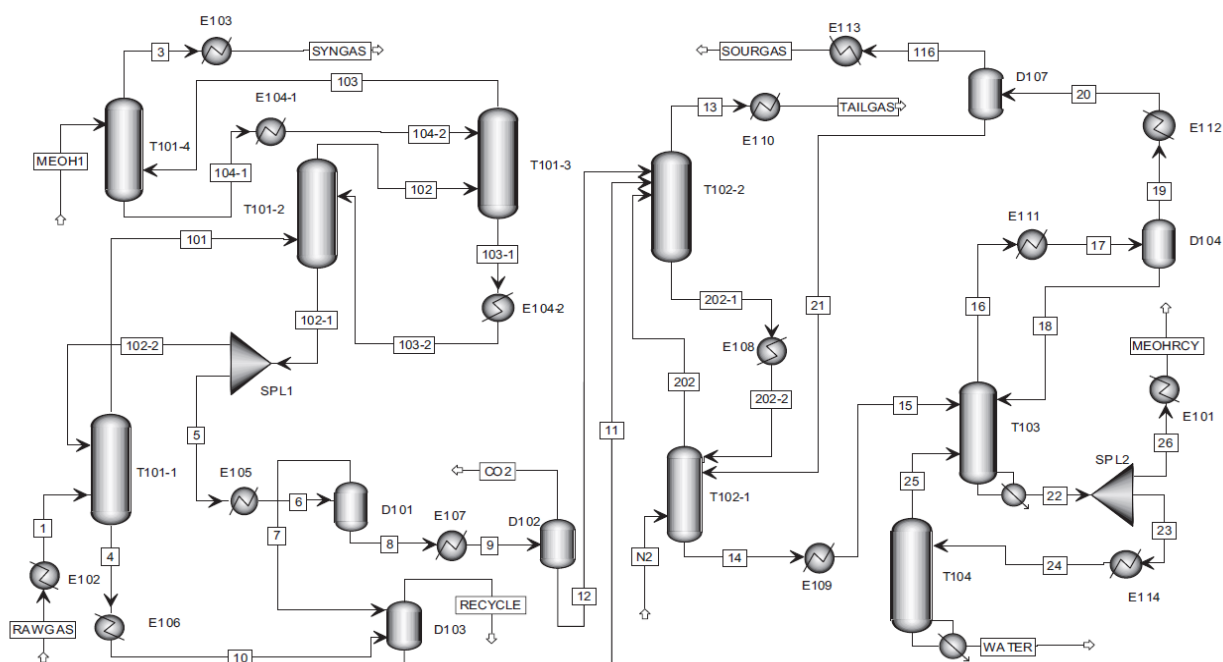


Figure 22: Flow diagram of the Aspen simulation of a single-stage Rectisol gas-washing plant [55]

This means that the synthesis gas has to be cooled from the gasification temperature, somewhere between 700°C und 1400°C, to a temperature as low as -20°C. Additional to gas cleaning, the synthesis gas has to be adjusted to the ideal ratio of its components for a methanol or Fischer-Tropsch synthesis. This is done by means of a water-gas shift reaction [56], for which a further reactor is needed. For methanol synthesis, the ratio of H₂ to CO has to be about 2 with little excess. For Fischer-Tropsch synthesis the H₂ to CO ration needs to be approximately 2.15 if cobalt catalysts are being used, or a little less if iron catalysts are being used, because the iron catalysts also catalyse the water-gas shift reaction [51].

Fuel Production from Synthesis Gas

Figure 23 shows the two platforms of synthesis gas and methanol that form the basis of a chemical industry based on synthesis gas. In this study, the Fischer-Tropsch synthesis is discussed only briefly. The main focus of interest is on methanol and the compounds that can be derived from it.

Fischer-Tropsch synthesis

Since the original synthesis of methane and its homologues by Hans Fischer and Franz Tropsch was published in the 1920s, using iron oxide and cobalt oxide mixtures at 270°C [57], many variants of the Fischer-Tropsch synthesis process have been developed. In the literature, these processes are mainly divided into high-temperature (HTFT=300–350°C) and low-temperature (LTFT=200–240°C) processes [37]. The most commonly used catalysts are iron, nickel, cobalt and ruthenium. Ruthenium has the disadvantage of its high price, while nickel has the disadvantage of forming too much methane [58].

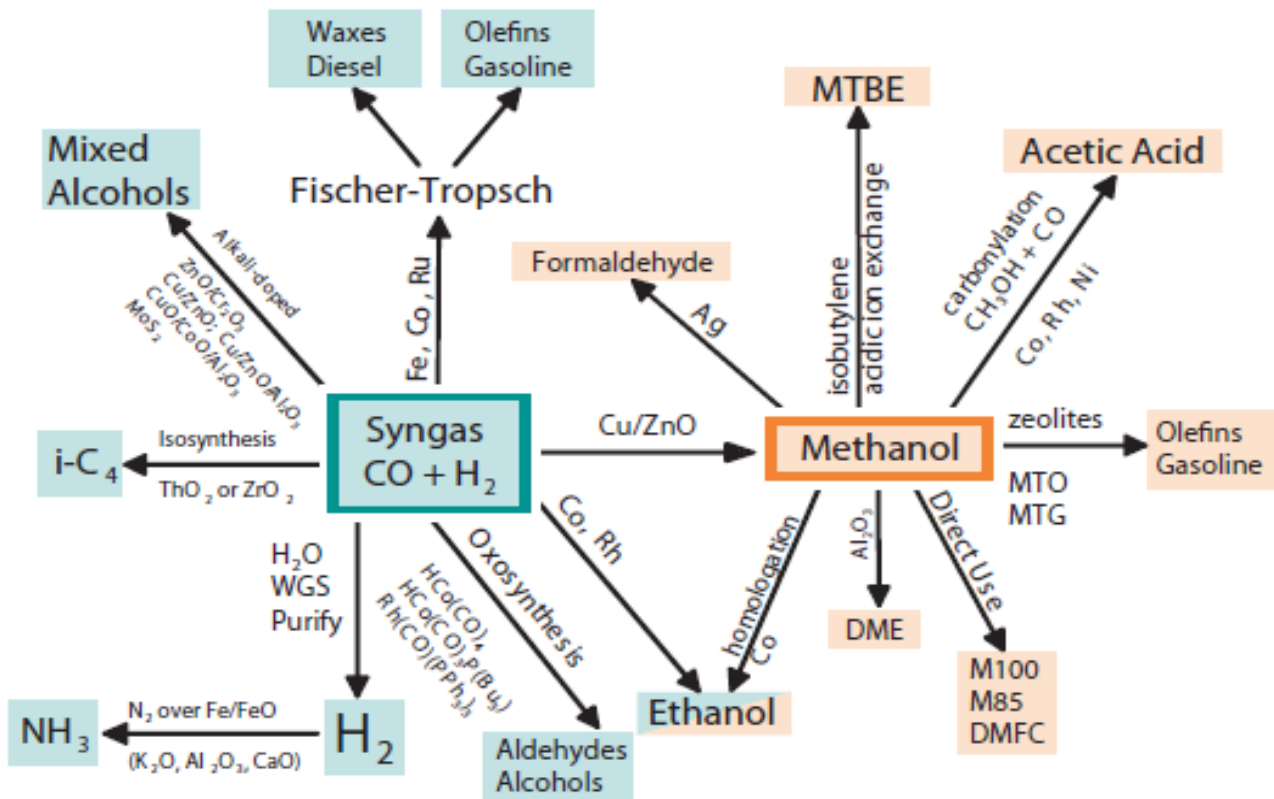


Figure 23: Fuel production from synthesis gas [51]

One of the most important factors in the Fischer-Tropsch synthesis is the so-called chain growth probability α , which should be as close as possible to 1 in order to minimize the amount of methane produced [52].

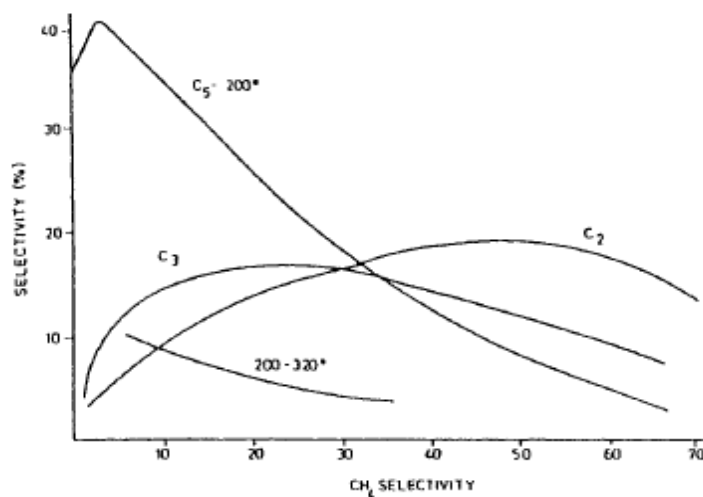


Figure 24: Relationships between formation of methane and other hydrocarbons (by carbon number) in a HT Fischer-Tropsch synthesis process. [58]

Figure 24 and Figure 25 show the product distributions for HT and LT Fischer-Tropsch syntheses. The X axis of both graphs immediately shows the drawback of both synthesis variants. In the HT Fischer-Tropsch synthesis, the high temperature causes formation of a

large amount of methane; it then has to be separated from the other products and recycled. In contrast, while the LT Fischer-Tropsch synthesis produces smaller amounts of short-chain products, it favours formation of longer chains to the extent that the boiling-point ranges of the product mixtures can reach temperatures as high as 500°C.

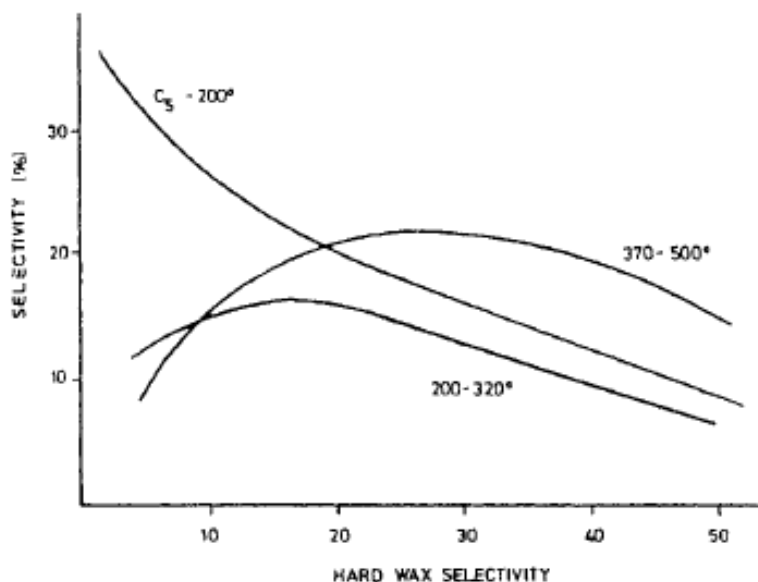


Figure 25: Relationships between the formation of hard waxes (i.e. compounds with boiling points higher than 500°C) and other hydrocarbons (by carbon number) in a LT Fischer-Tropsch synthesis. [58]

It is clear that such products cannot be used directly in diesel engines. Also, the product still needs to be worked up with considerable effort in a refinery [53]. Figure 26 shows a diagram of the HT Fischer-Tropsch synthesis plant of the company Sasol in South Africa. This flow diagram indicates that the plant is fed with coal, but it is also reported that natural gas is supplied to the site [59]. In reality it is not very accurate to call this plant a Fischer-Tropsch plant, because this step is only a small part of the total process at the site. The facility is more likely a whole refinery.

The effort invested in production of Fischer-Tropsch fuels results in fuels of the highest quality. Before the final distillation, they have to be isomerized [60] – to improve the knock resistance of gasoline, among other reasons.

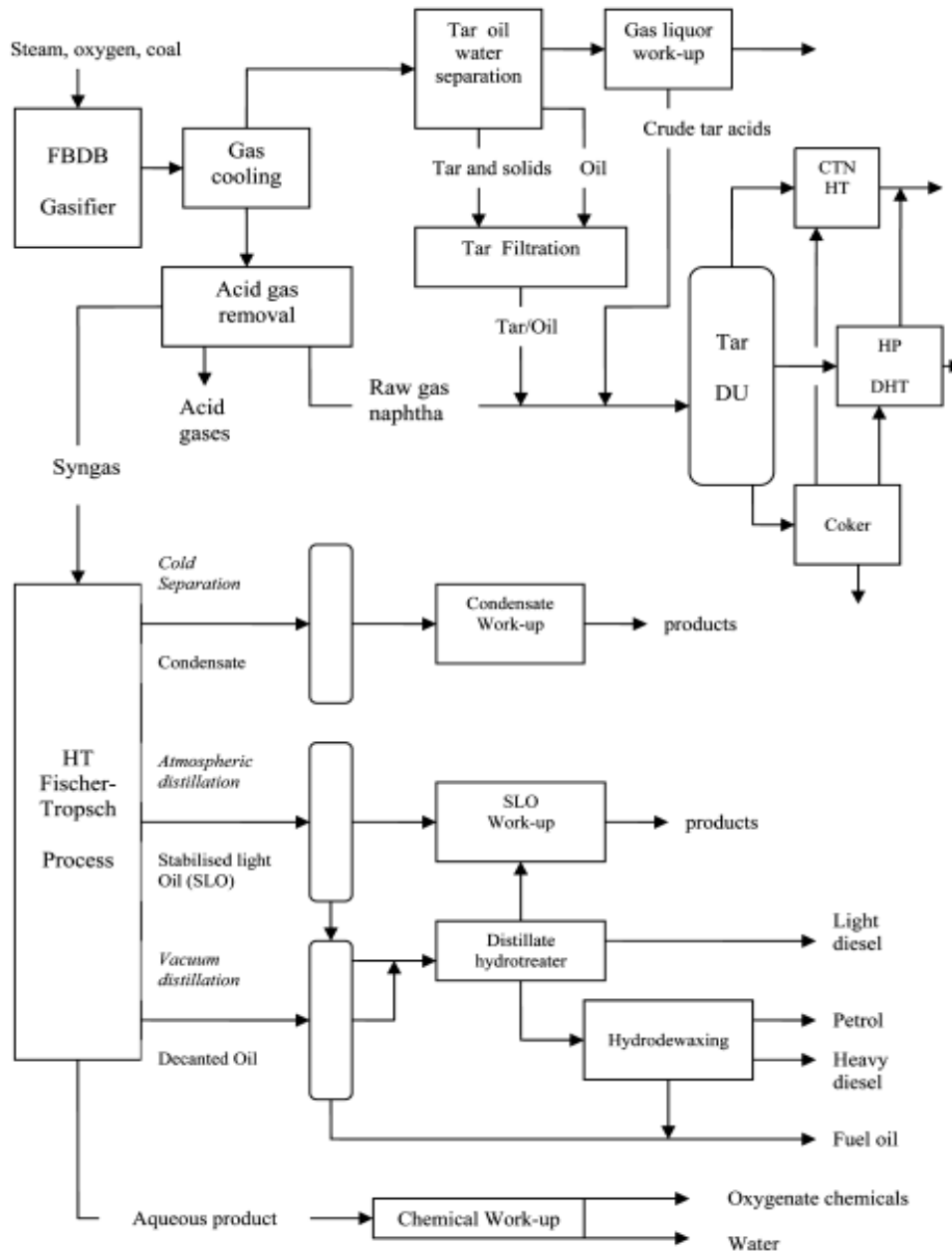
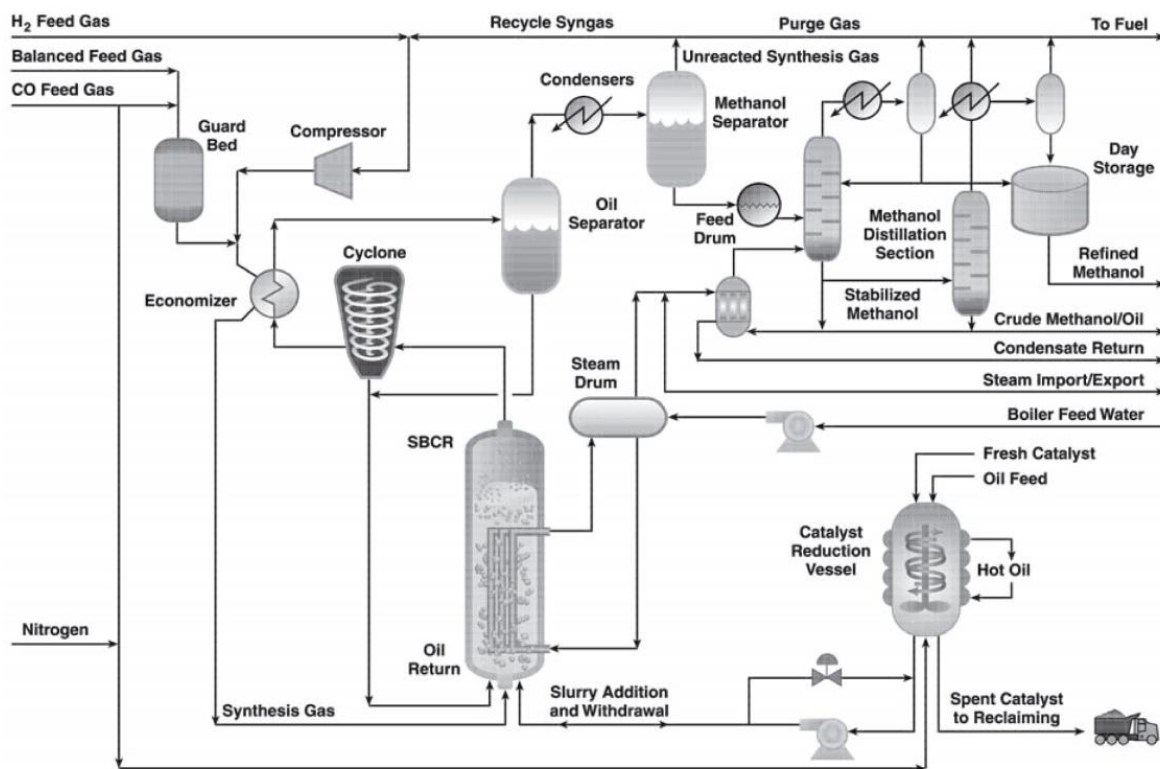


Figure 26: Coal-based HT Fischer-Tropsch synthesis plant, with a so-called ‘fixed bed d bottom’ gasifier, separate Fischer-Tropsch synthesis and tar refinery (Sasol Synfuels Refine 2004, Secunda, South Africa). CTN: coal tar naphtha; DHT: distillate hydrotreater, HP: hi pressure, HT: Hydrotreater [61]

Methanol synthesis

The complicated and expensive workup of the products of Fischer-Tropsch synthesis is one the many disadvantages of this technology. As Figure 23 shows, a very good alternative exists in the form of methanol as a platform chemical. Methanol production from synthesis gas is an extensively researched technology. The first commercial methanol synthesis was developed in 1923 by BASF; it used Zn-Cr₂O₃ catalysts at 240–300 bar and 350–400°C [64]. In the 1960s, low-temperature methanol synthesis was developed in the USA by ICI [65]. This process used co-precipitated Cu/Zn catalysts and was operated at 250°C and 50–100 bar [66]. Nowadays methanol synthesis is mostly done in slurry reactors; there are several examples of th

technology in operation including reactors developed by Lurgi and also ICI [67]. One technology that has been described very positively in the literature is the test plant of Air Products Liquid Phase Conversion Company, which uses the LPMEOH process. This process operates at only 50 bar and 200°C [68].



LPMEOH™ Demonstration Unit Process Flow Diagram

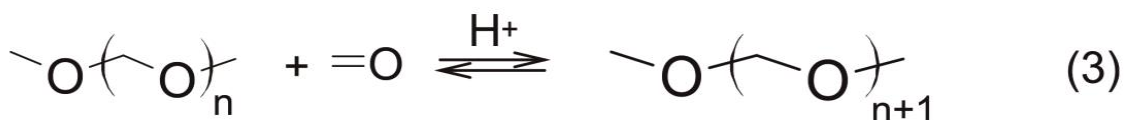
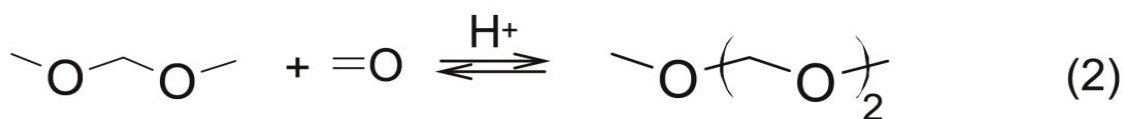
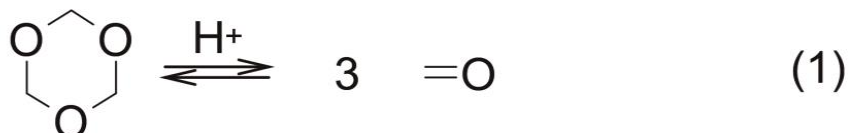
Figure 27: Process diagram of the LPMEOH plant of Air Products Liquid Phase Conversion Company [68]

Figure 27 shows a process diagram of the LPMEOH plant [69]. It can be seen that the workup of the methanol still takes a considerable effort, but is not nearly as elaborate as the refining of Fischer-Tropsch fuels. Most importantly, it only requires thermal separation steps; it is not necessary to use hydrocrackers.

In subsequent process steps, the methanol can be converted, for example, to dimethyl ether. It has the advantage of a much higher energy density than methanol; the disadvantage of dimethyl ether is its boiling point of -24.8°C [70]. It can be produced directly or indirectly. The question is only whether to first synthesize methanol from synthesis gas and then dehydrate it over an acidic catalyst, or if the process should be done as a unit operation with mixed catalysts [71]. At present, research is being done on catalyst modifications to improve stability and selectivity [72].

Production of poly(oxymethylene) dimethyl ether

The disadvantages of methanol as a fuel are its low energy content, its low boiling point, its high solubility in water and its high toxicity [73]. Conversion to poly(oxymethylene) dimethyl ethers (POMDME [74]) with two to five repeating units achieves the following improvements: better autoignition, unlimited miscibility with diesel, good compatibility with materials and avoidance of the toxicity problem.[75]. However, the synthetic route to these products is both complex and costly. First, the methanol must be converted to formaldehyde.



Formula 1: Reaction scheme of POMDME synthesis [76]

This is done at 680–720°C over a silver catalyst [77]. Then, part of the formaldehyde must be reacted with methanol in an acidic medium to yield methylal, the acetal of formaldehyde [8]. Alternatively, methylal can also be made directly from methanol [78]. As well as methylal, trioxane is needed as an additional reagent for the further synthesis; it is also synthesized from formaldehyde [77].

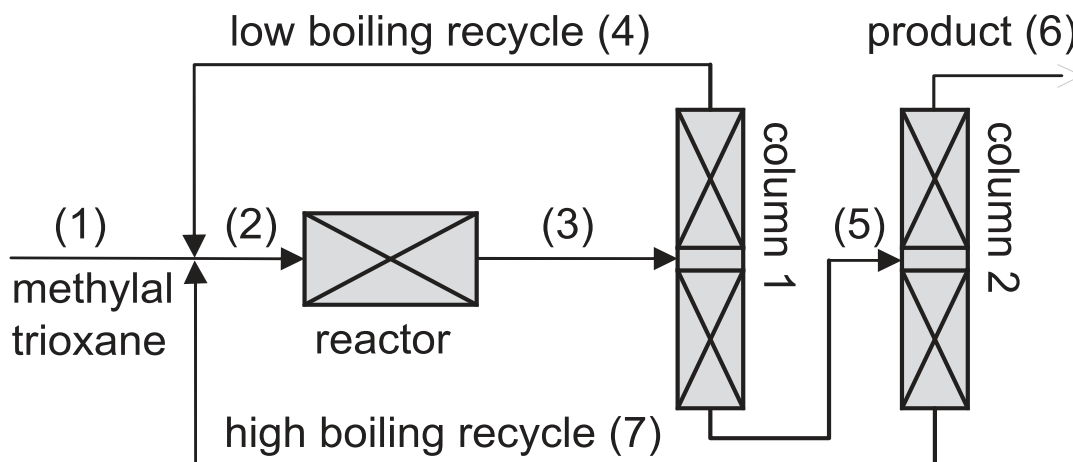


Figure 28: Block flow diagram of POMDME production [79]

Formula 1 shows the synthesis of POMDME from trioxane and methylal according to Burger [76]. First the trioxane is cleaved and then the fuel is synthesized with a variable chain length. To obtain at a suitable distribution of melting and boiling points for use as a diesel substitute

fuel, a mixture of POMDMEs with three and four repeating units is desirable. The block flow diagram of the production process with the recycling loops is shown in Figure 28. It can be seen that the process has a high level of complexity, like the Fischer-Tropsch fuels [80, 81]. However, the advantage is that no high-pressure and high-temperature processes are needed. As an alternative to this type of process, it is also possible to synthesize POMDMEs using polyvinylpyrrolidone-stabilized hetero-polyacids [82].

2.2.1.3 Conclusions on indirect liquefaction of Biomass to Fuels

In Chapter 2.2.1 it was shown how intensively lignocellulose must be processed to obtain fuels of high quality. However, it was also possible to see, that it is imperative to keep the effort and complexity of processing as low as possible. This can be done if methanol is chosen as a fuel or if it is used as a platform chemical for making other fuels such as DME or POMDMEs.

2.2.2 Direct Liquefaction of Biomass

Direct liquefaction of biomass is a synonyme for the thermochemical conversion of lignocellulose with the goal to obtain a majority of products, which are liquid at room temperature.

2.2.2.1 Pyrolysis

For the search term 'pyrolysis', Google finds about 15800000 (fifteen million, eight hundred thousand) results in 0.17s [83]. The meanings of this umbrella term are correspondingly complex. *"The term pyrolysis, is used for the thermal decomposition of organic waste materials under exclusion of air"* [84]. This description is true except for the restriction to waste materials, because reusable materials can also be pyrolyzed.

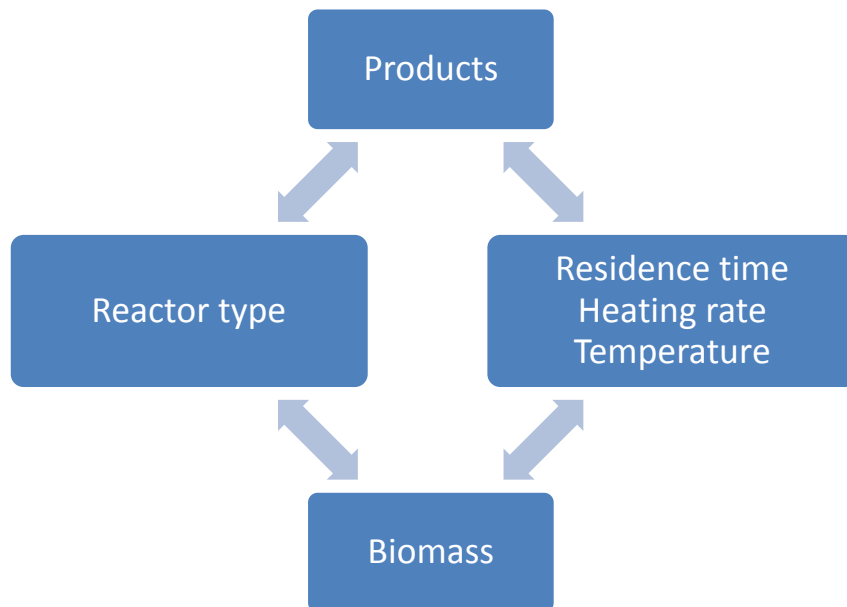


Figure 29: Interactions of the main variables controlling pyrolysis

Pyrolysis processes are subject to many different variables. By neglecting the factor heat transfer, Figure 29 describes the four most fundamental variables. To simplify the scope of this review, it is necessary to confine the discussion to pyrolysis methods that have direct liquefaction as their goal; hydrothermal carbonisation is not discussed[84]. [5]

2.2.2.2 Reactor Types

The type of reactor used for pyrolysis has a central effect on the type of products obtained. Various reactor types are shown in Figure 30. Ablative reactors have the advantage that they do not need a carrier gas, but they are difficult to heat without large losses. Stationary and recirculating fluidized-bed reactors can be operated at very high temperatures and can therefore achieve high liquefaction yields [85]. The disadvantage of these reactors is however that the biomass particles are physically broken up in the fluidized bed and very fine ash and char particles are then carried out in the stream of liquid products [86]. In the pyrolysis process, the char and ash particles promote molecular cracking and thus increase the amount of water of reaction formed. In addition, the process requires exact technical control in operation, especially in terms of the particle sizes: fluidized-bed reactors require feed particles of no more than 2 mm, whereas recirculating fluidized-bed reactors can accept particles of up to 6 mm [87]. Reactors operated under vacuum have the advantage that they extract gases rapidly and thus keep the residence times in the high-temperature zones short. However, continuous operation under vacuum is difficult.

A twin-screw reactor is in use at the Karlsruhe Institute of Technology [43]. This reactor cannot be directly compared to the others. It is certainly a pyrolysis reactor, but in this case the pyrolysis oil and the solid residue are worked into a slurry. The concept is that this slurry, which can be pumped and transported, should be produced by many of these reactors deployed decentrally at the sources of the biomass. The slurry should then be transported to a central synthesis-gas and Fischer Tropsch plant to be processed to waxes in a Fischer Tropsch process. Subsequently these could be converted into fuels [43]. [5]

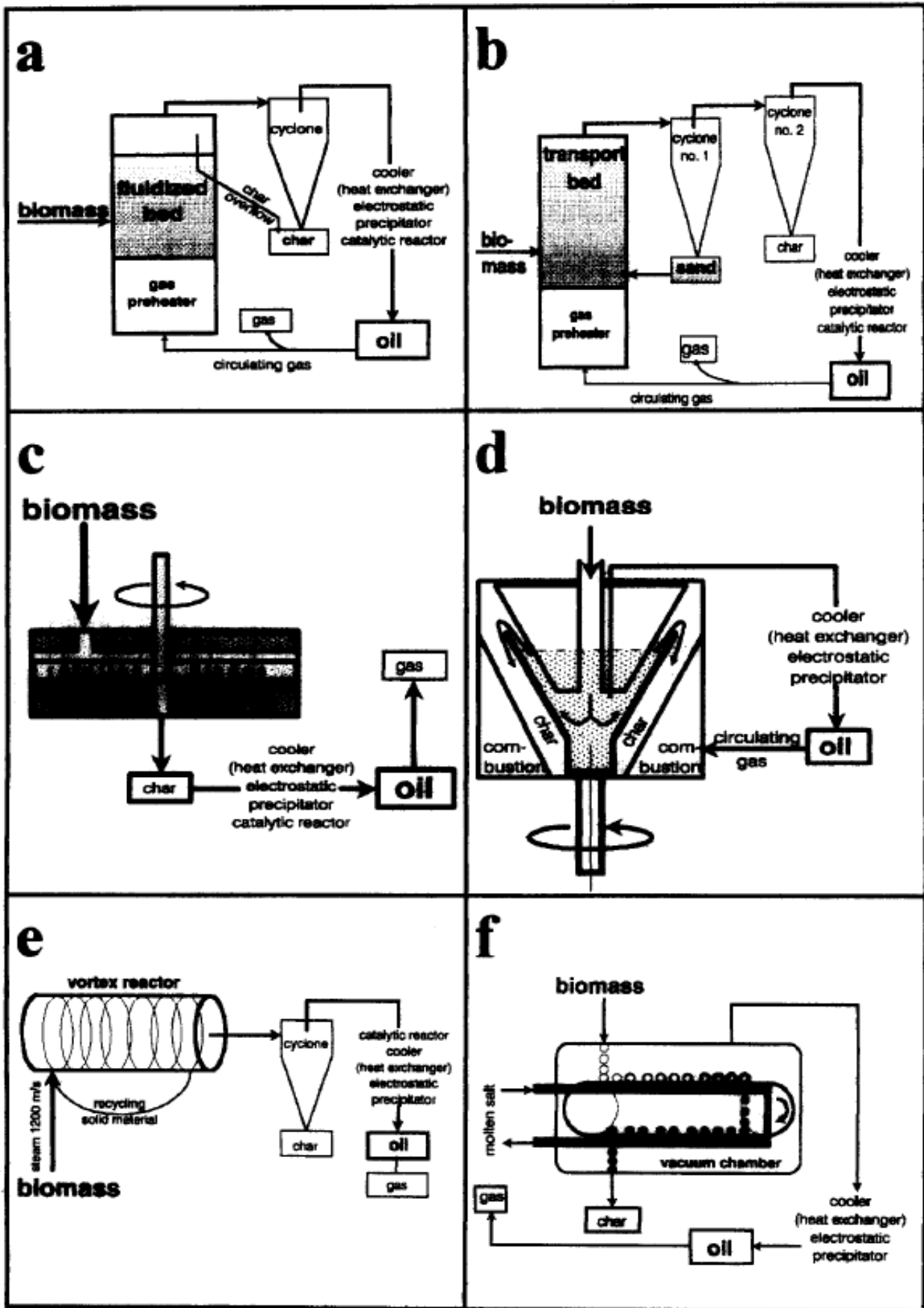


Figure 30: Reactors for flash pyrolysis of biomass: a) stationary fluidized-bed reactor, b) recirculating fluidized-bed reactor, c, d, e) ablative reactors, f) reactor under vacuum [88]

2.2.2.3 Temperature Range, Residence Time and Heating Rate

The variables temperature range, residence time and heating rate are as essential for characterizing pyrolysis processes as the reactor geometry.

Table 12: Pyrolysis processes and their variable parameters according to Huber [89]

| Pyrolysis process | Residence time | Temperature [°C] | Heating rate | Major products |
|----------------------------|-------------------|------------------|--------------|-------------------------|
| Conventional carbonisation | Hours to days | 300–500 | Very slow | Biochar |
| Pressurized carbonisation | 15 min to 2 hours | 450 | Intermediate | Biochar |
| Conventional pyrolysis | Hours | 400–600 | Slow | Biochar, liquids, gases |
| Conventional pyrolysis | 5–30 min | 700–900 | Intermediate | Biochar, gases |
| Flash pyrolysis | 0.1–2 s | 400–650 | High | Liquids |
| Flash pyrolysis | <1 s | 650–900 | High | Liquids, gases |
| Flash pyrolysis | <1 s | 1000–3000 | Very high | Gases |
| Vacuum pyrolysis | 2–30 s | 350–450 | Intermediate | Liquids |
| Pressurized hydrolysis | <10 s | >500 | High | Liquids |

Table 12 offers an overview of the temperature ranges that are used in pyrolysis processes. It is essential to draw particular attention to the temperature range between 400 and 500°C. This is the range with the highest potential for liquefaction, with residence times of less than 1 s and high heating rates [85]. Figure 31 shows this graphically.

Pyrolysis begins with the decomposition of the individual components. The decomposition of hemicellulose (xylan) begins at about 240°C [90]. Below this temperature, at atmospheric pressure without reaction mediators or solubilizers, hardly any liquefaction reactions can take place. At temperatures below 350°C, char with high oxygen content is the main product. The working range of gasification technology begins from 550°C upwards. This topic will be examined in more detail in Section 2.2.1.1 Gasification of Biomass.

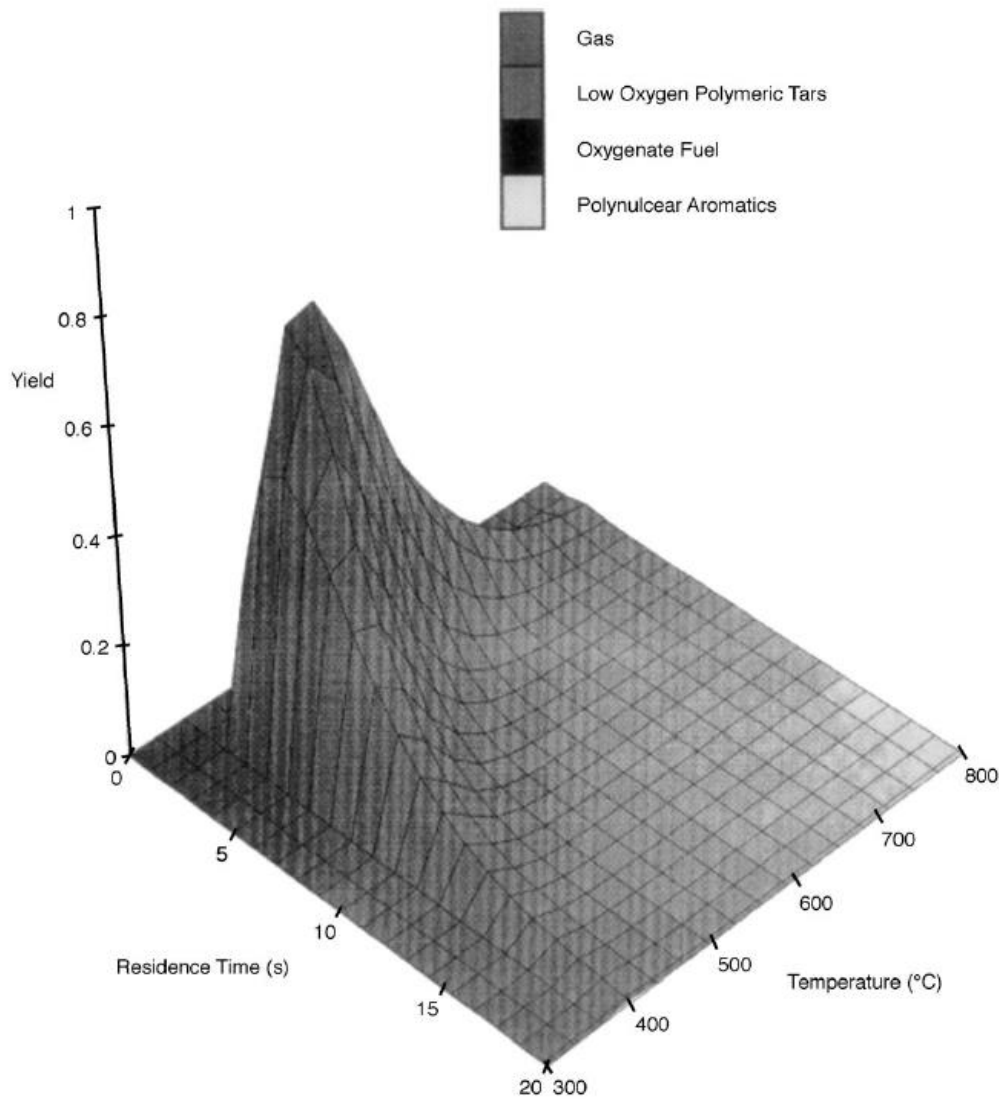


Figure 31: Yield of liquid products in flash pyrolysis according to Bridgwater [85]

This short residence time is necessary for two reasons. Firstly, longer residence times lead to decomposition of products that are liquid at room temperature, to gaseous products and water [91]. Secondly, after the “initial step of depolymerisation and fragmentation of the biomass” into smaller molecular units, a process of “recondensation, recyclization and repolymerization” [92] occurs, if the fragments formed initially are exposed to high temperatures for too long. [5]

2.2.2.4 Products

The products of pyrolysis can be classified into three groups according to their physical characteristics. These are: gases that are non-condensable at room temperature; pyrolysis oil; and biochar. In this section pyrolysis products are identified under these headings.

Gases that are non-condensable at room temperature

The formation of gases during biomass pyrolysis depends on the factors shown in Figure 29. It is stated, that the transition between pyrolysis for liquefaction and gasification is a continuous one. Figure 32 shows the temperature dependence of the relative yields of gas and char.

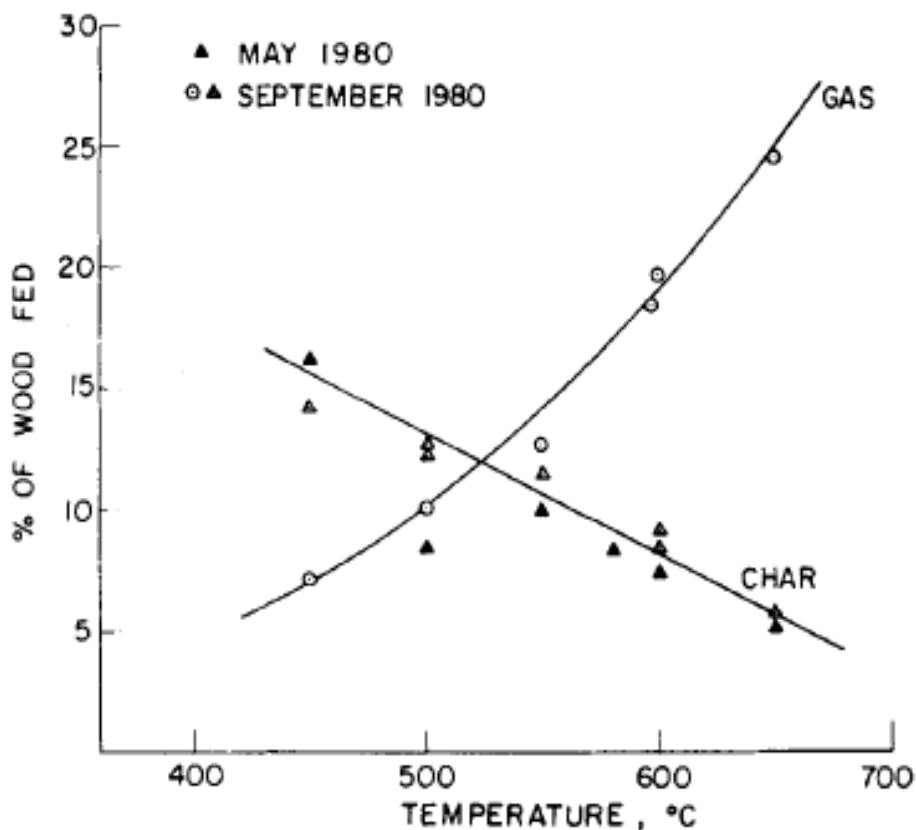


Figure 32: Temperature dependence of formation of gas and biochar [93]

The temperature dependence of gas yield differs strongly between pyrolysis process types. Bridgwater found elevated formation of gas only from 500°C upwards, and not in the range 400–500°C [85]. As well as the amount of gas formed, the composition of the gas changes, as Figure 33 shows — depending primarily on the temperature and less on the type of biomass. The Boudouard equilibrium has a stronger effect on the main components of the gas, carbon monoxide and carbon dioxide, than the biomass used as feedstock. The number of gaseous components is not very high, because lignocellulose consists mainly of carbon, hydrogen and oxygen and these elements are the origin of the gases formed. If biomass rich in nitrogen or sulphur is used, the range of gases formed can change considerably.

In fluidized-bed reactors, the molecular composition of the gases is also altered by the additional carrier gas. In this type of process, the carrier gas, usually nitrogen, has to be separated from the products gases. This step is difficult and costly to realise in industrial-scale plants.

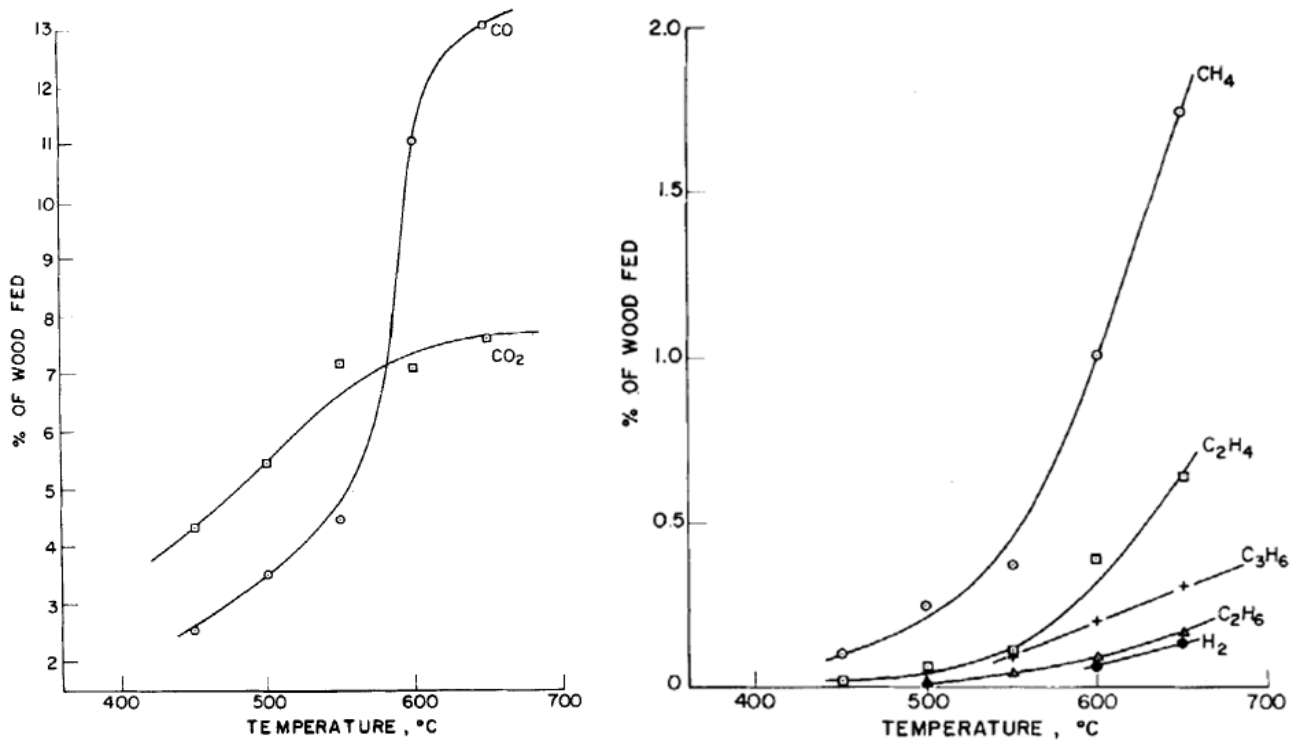


Figure 33: Temperature dependence of formation of different gas components [93]

Biochar

In the context of pyrolysis for production of liquid fuels, biochar (carbonized biogenic material resulting from any kind of pyrolysis process) is an undesired side product, because it reduces the yield of liquids. The direct inverse relationship between char and gas formation is shown in Figure 32. The fact that biochar is – depending on the pyrolysis temperature – an energy-rich material low in sulphur and nitrogen has attracted the attention of many pyrolysis researchers. Biochar has a similar calorific value to brown coal [94], but with the advantage of a relatively low ash content. Slow pyrolysis processes are designed to maximize the biochar yield, which (e.g. using algal biomass) can be in the range 37 to 63% [95]. This contrasts with the Hamburg fluidized-bed process, in which char usually accounts for less than 10% of the total product yield, because this process is optimized for liquefaction. This biochar yield is quite typical of fast or flash pyrolysis in terms of reactor type and operating temperature.

One possible application of biochar, apart from using it as a fuel, is as a means of carbon sequestration. In this case biochar is ploughed into soil in order to reduce the level of CO₂ in the atmosphere [96] and to improve the soil quality, especially the water retention and formation of organic material [97]. [5]

Pyrolysis oil

Pyrolysis oil or 'biocrude' is currently the most important product of the various biomass liquefaction routes. The components of this oil mixture represent the complete spectrum of

organic chemicals of the elements carbon, hydrogen and oxygen, except for peroxides, which are too unstable because of the low dissociation energy of the oxygen-oxygen bond. The subfractions of pyrolysis oil can be categorized in many different ways. Fundamentally, the composition of pyrolysis oil depends on the production process variant and the parameters shown in Figure 29. It is a dark to black, more or less viscous liquid with an odour of 'campfire'. The simplest characterization is in terms of the elements oxygen, nitrogen, carbon and hydrogen.

Table 13: Elemental composition of pyrolysis oil

| Element | Czernik [98] [w%] | Gerdes [99] [w%] | Garcia [100] [w%] |
|---------|-------------------|------------------|-------------------|
| C | 54–58 | 36.62 | 39.7 |
| H | 5.5–7.0 | 8.54 | 6.5 |
| N | 0–0.2 | <0.27 | 0.1 |
| O | 35–40 | 54.57 | 53.6 |

Table 13 shows the elemental compositions of pyrolysis oil from various raw materials and pyrolysis processes.

Table 14: Physical and chemical properties of pyrolysis oil

| Parameter | Unit | Czernik [98] | Bayerbach [101] | Meier [88] |
|-----------------|----------------------|--------------|-----------------|------------|
| Water content | [w%] | 15–30 | 26.4 | 20 |
| pH | | 2.5 | 2.4 | 2.5 |
| Density | [g/cm ³] | 1.2 | — | 1.2 |
| Calorific value | [MJ/kg] | 16–19 | — | 20 |

Table 14 shows how much the amount of water in pyrolysis oil can vary. Even if the raw material is absolutely dry biomass, a significant amount of water is produced, depending mainly on the temperature and residence time. As described in Section 2.2.2.3, additional water of reaction can be formed in secondary reactions. The only parameter that is similar in all biocrudes is the pH value: all biocrudes have a low pH of around 2.5. This is due to the high concentration of acetic acid, which is formed from the carbohydrates of the lignocellulose or

by cleavage of esters. At high yields of liquids, with the correspondingly low water content, the oils have a calorific value approaching that of absolutely dry wood.

A further important characteristic of the liquid products besides their elemental composition and chemical properties is their molecular composition. An important though undesirable molecule is water. An impression of the diversity of molecular compositions of biocrudes can be obtained from Figure 36 and Figure 37. With standard GC-MS methods, more than 250 compounds can be detected. Pyrograms of cellulose and lignin from beech wood reveal that the molecular composition varies quite strongly depending on the source of the biomass. However, GC-MS only gives a partial picture of the molecular composition of the pyrolysis oil. Important components are dimers, trimers and oligomers which are decomposition products of the individual biopolymers [101]. Actual identification of these species requires much more sophisticated analysis.

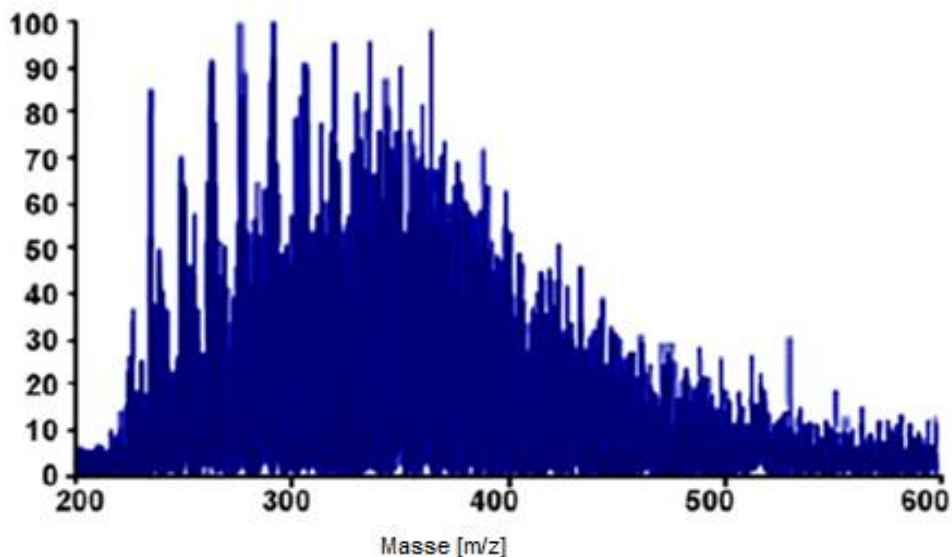


Figure 34: MALDI TOF spectrum of a pyrolysis oil from algal biomass [95]

Figure 34 shows the TOF spectrum of a pyrolysis oil from algal biomass. GC-MS is only useful for analysis of biopolymers up to around 350 g/mol, because larger molecules than this generally decompose in the vaporization stage of the GC. Since TOF spectrometers do not have software for fragment-recognition libraries, this technique can only deliver information about fragment sizes. For analysis of the types of bond present it is mandatory to turn to FTIR (Fourier-Transform Infra-Red) and NMR (nuclear magnetic resonance) spectroscopy. Figure 35 shows the FTIR fingerprint of pyrolysis oil produced from waste from the olive-oil industry. To sum up, it is possible to say that while a basic characterization or fingerprint of a pyrolysis oil can be done with relatively simple methods, a detailed analysis with exact identification of what compounds are present is a very difficult and complex task. Currently intensive efforts are being made to reduce the water content and raise the pH value in order to arrive at a fuel that can be used in diesel engines [102].

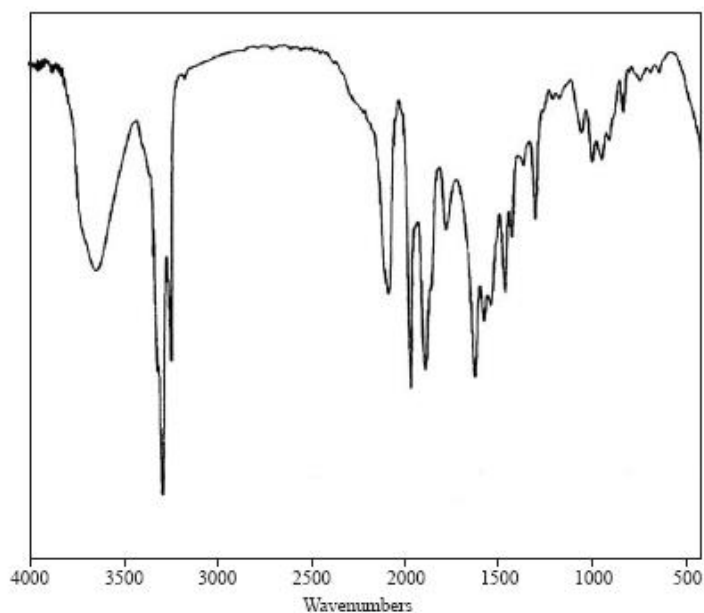


Figure 35: Infra-red spectrum of waste from olive-oil production. Main Peaks are: the O-H bond at 3700 cm^{-1} , C-H bond at 3200 cm^{-1} [103]

Influence of the source of biomass

The fast growing softwood spruce is an easily available regional resource in central Europe. The selection of raw materials for pyrolysis is a simple matter of their availability. Of the three product categories biochar, non-condensable gases (at room temperature) and pyrolysis oil, the influence of the type of biomass used is most evident in the pyrolysis oil [104].

In Figure 36 and Figure 37, the influence of the main components lignin and cellulose on the pyrolysis process is clearly visible in the Py-MS spectra. These form a fingerprint of the pyrolyzable organic components. The results show how different the fingerprints of two of the three main components of lignocellulose can be. Carbohydrates are converted to the expected polyols, acids, aldehydes and ketones, while the products of lignin are derivatives of its monomers, as Figure 36 shows.

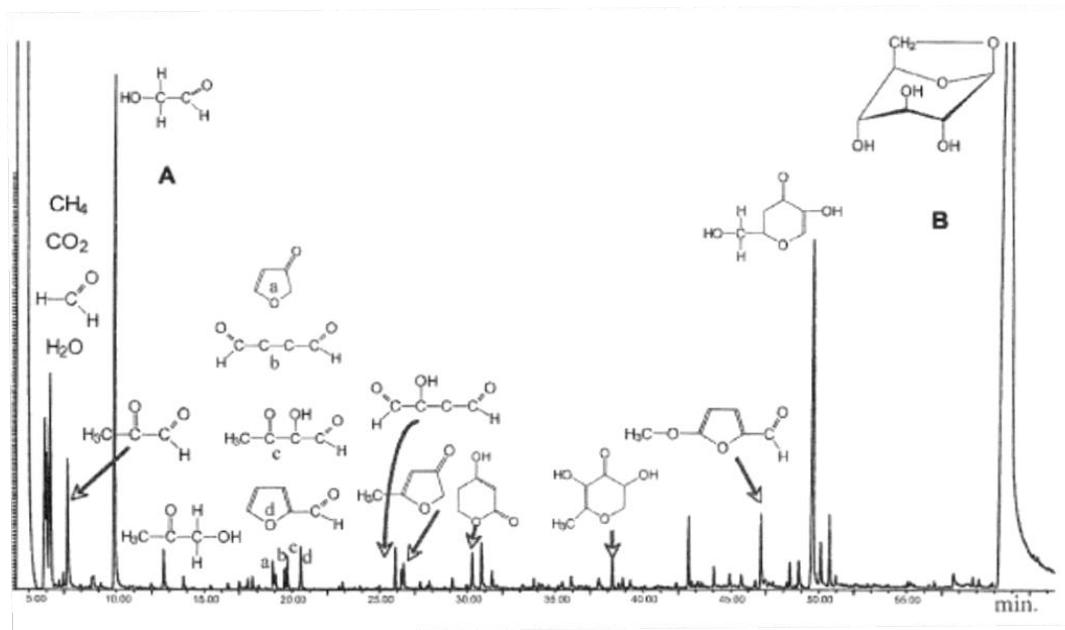


Figure 36: Pyrogram of pure cellulose [105]

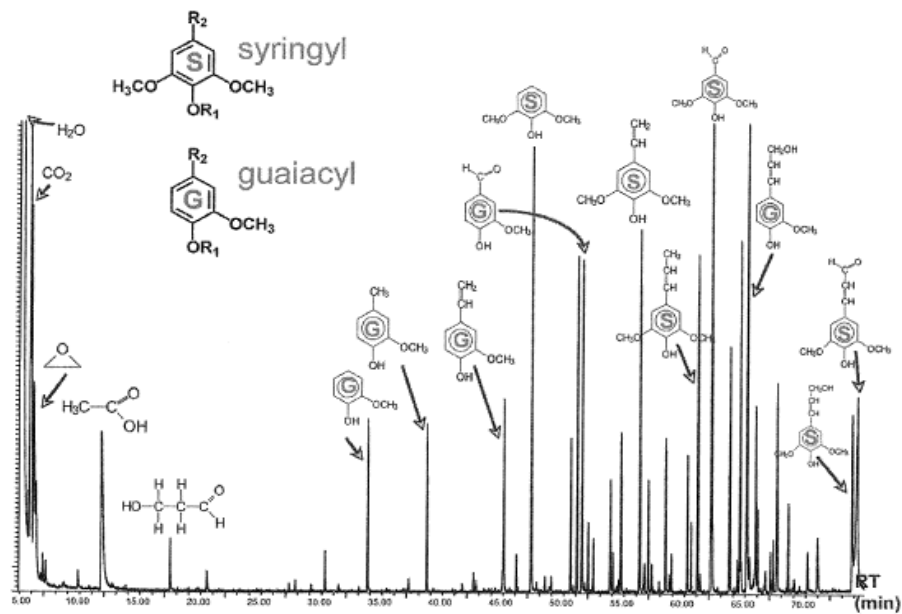


Figure 37: Pyrogram of lignin from beech wood [105]

Apart from the different concentrations of the components lignin, hemicellulose and cellulose, it is needful to bear in mind the wider diversity of types of plant biomass that can be pyrolyzed. For example, pyrolysis of rape-seed oil cake can yield a pyrolysis oil with up to 73% carbon [106], originating in the residual oil in this material. At 433°C, palm kernel shells yield about the same amount of pyrolysis oil as liquid-phase pyrolysis [107]. Bagasse, the fibrous waste from sugarcane processing, can be pyrolyzed alone or with residues from the petrochemical industry under vacuum. With this method, liquefaction yields of 5-85% are reported, depending on the experimental parameters [108]. The pyrolysis of sunflower-seed oil cake at 550°C also yields over 50% of liquid products [109]. Even waste materials from the fishery industry can be pyrolyzed with yields of over 70% at 525°C [110]. [5]

2.2.2.5 Hydrodeoxygenation (HDO) of Pyrolysis Oil to Fuels

As described in Sections 2.2.2.1 to 2.2.2.4, pyrolysis of lignocellulose can be used to produce a liquid fuel intermediate, but with significant disadvantages: it has a high water content, cannot be completely vaporized and, because of the high content of acetic acid, it is corrosive. In order to obtain a diesel fuel from this pyrolysis oil, a hydrodeoxygenation step is needed. The goal is to extract the oxygen from the pyrolysis oil by means of a catalytic hydrogenation, thereby converting the components of the biomass to an apolar fuel phase and water [111]. In this way the pyrolysis of biomass [112–115] and subsequent hydrodeoxygenation can be used to generate a fuel [116] whose oxygen content depends on the degree of hydrodeoxygenation and whose boiling-point profile is comparable to that of conventional diesel fuel [117].

2.2.2.6 Conclusions on Direct Liquefaction of Biomass to Fuel

The direct liquefaction of biomass with subsequent hydrodeoxygenation is a possible route for production of second-generation biofuels. This process requires considerably less complex and smaller production steps than indirect biomass liquefaction. However, direct liquefaction of biomass offers less precise control over the molecular composition of the products than, for example, the synthesis of methanol or poly(oxymethylene) dimethyl ethers.

2.2.3 Pulping Processes for Lignocellulose and Processing of the Products to Fuels

In this section firstly the pulping of the biomass is discussed and secondly the processing of the biomass components is presented. This is a critical division, because in some process types it is difficult to separate the two stages clearly. For example steam explosion processes are mixing the pulping step with de degradation of hemicellulose due to acidic depolymerisation. Despite this, it is possible in principle to mix and match different pulping methods with different workup and refinement processes. For example, the Inbicon process [118] consist of acidic pulping of biomass followed by fermentation of the glucose to ethanol. Fermentation to butanol is also conceivable.

Figure 38 shows a classification of the different pulping processes for lignocellulose, divided into conventional and alternative methods. Briefly the pulping methods used in the paper and pulp industry are presented, where the separation of the components of lignocellulose have a long tradition. Good overviews of these technologies are available in the literature [17, 119–121]. Considering the acidic (bisulphite, acidic sulphate) and alkaline (kraft) pulping methods as the standard processes of the pulp industry, then it is important to note that apart from their high efficiency with which they extract cellulose, these methods have a major disadvantage: they fix functional groups to the lignin scaffold. Figure 39 shows a lignin sulphonate, with a charged sulphonic acid group which is covalently bound to the guaiacol structure of the lignin.

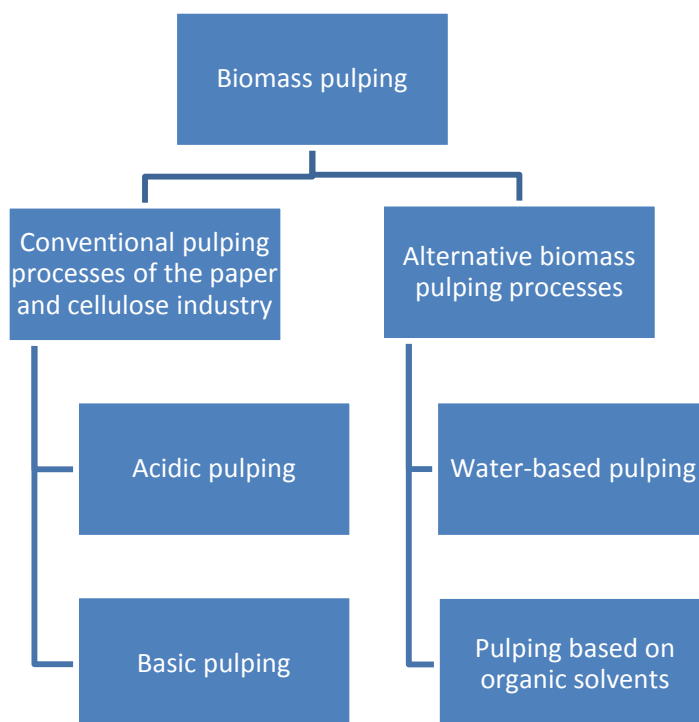


Figure 38: Classification of biomass pulping processes

These chemical modifications maximise the yield of the usable cellulose for the paper industry, and the fibres have properties that play an important role in paper production. But on the one hand, this makes it more difficult to process the lignin [122], and on the other hand it is not possible to regenerate the chemicals used for pulping by physical methods. The chemicals used in a pulp mill are usually regenerated by incinerating the lignin and the hemicellulose.

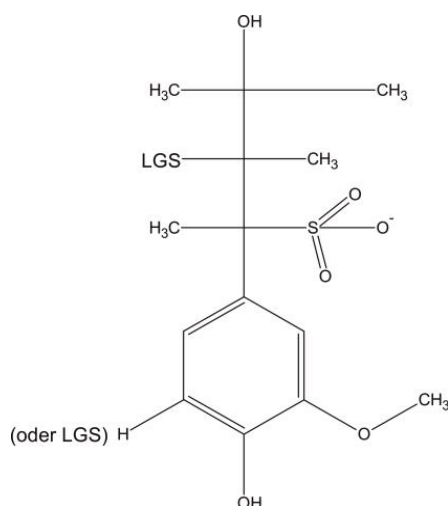


Figure 39: LGS (lignosulphonate) [123]

Partially products such as lignosulphonates, furfural [124, 125] and acetic acid [126] can be extracted and sold. In addition to these methods, the company Chemrec in Sweden converted waste materials from the paper industry to dimethyl ether as described in Section 2.2.1 [127]. Several alternative pulping processes exist, and broadly, they can be divided into two categories. The first category are the water-based processes, such as the steam explosion process of logen [128] or the acidic hydrolysis of straw by Inbicon [129]. The second category also uses water for the pulping of the lignocellulose, but the central role in the pulping process is played by organic compounds. These are intended to separate the components of the biomass 'gently', causing only a minimum of disturbance to their macrostructures. This category includes for example the various organosolv processes [130] and ionic liquid pulping [131]. The goal of this extra effort in the biomass pulping process is to obtain a lignin fraction that is usable for other purposes than combustion.

2.2.3.1 Alternative Water-based Lignocellulose Pulping Processes

This section describes processes that are carried out (more or less) in two stages, the pulping of the biomass and then the production of fuel. In the large plants referred to in this study, the end product is always ethanol, but research is ongoing on production of butanol. The strategy is similar in either case. The biomass is pulped at temperatures of about 180–232°C and pressures of 1 to 40 bar, and the sugars are partially decomposed into monomers [132]. This hydrolysis can be accelerated by adding acids or can be done as autohydrolysis with acetic acid formed in situ [132].

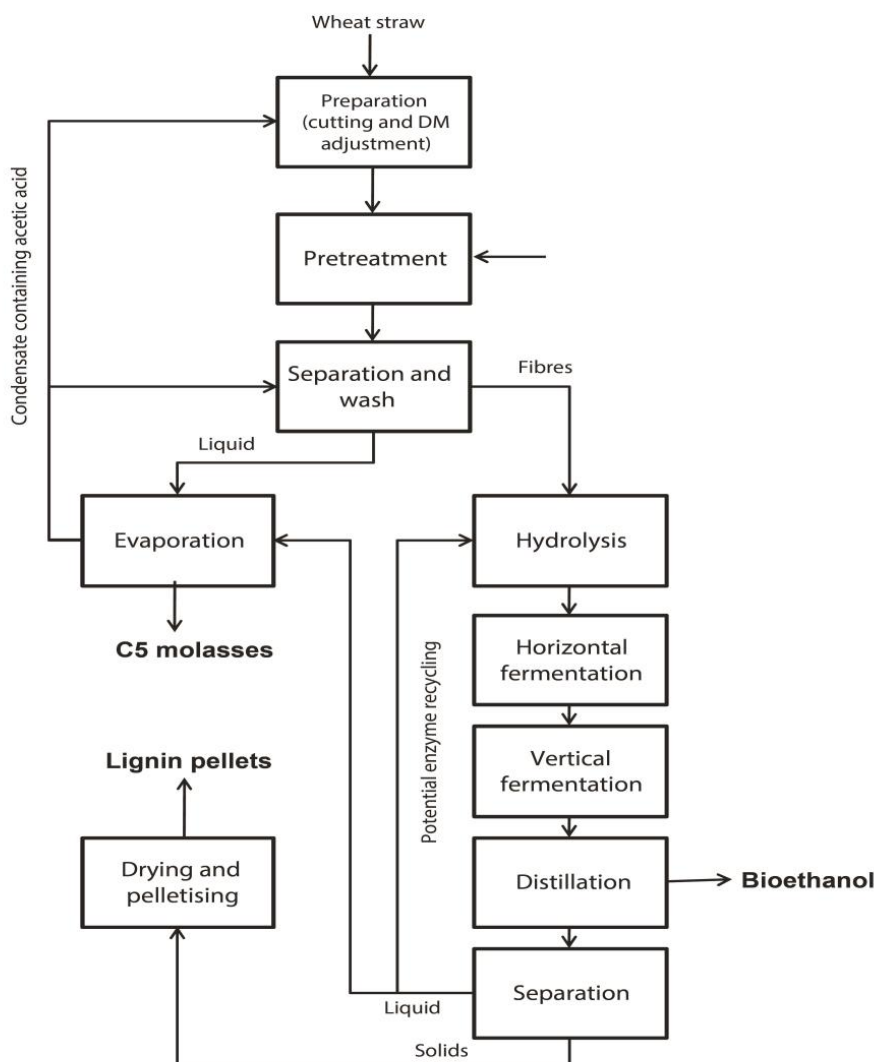


Figure 40: Flow diagram of the Inbicon bioethanol plant [133]

Some of these technologies are already in commercial use or are being used at demonstration scale. The leading companies and plant types in this field are Inbicon [118], Chemtex [134], Iogen [128] and Abengoa [135]. Very little has been published about these processes in scientific journals; an overview is provided by Evans [136].

Figure 40 shows a flow diagram of the Inbicon demonstration plant in Kalundborg. Annually, this plant produces 4262 t of ethanol from 30000 t of wheat straw, a yield of 14.2% by weight. The plant also produces 13100 t of lignin pellets and 11250 t of molasses (sugars from the hemicellulose) per year [118].

These technologies have in common that no separation of the individual macromolecules is done before the biochemical processing (fermentation). The structure of the biomass is broken open and then the sugars are fermented to ethanol or butanol. The remaining materials, mostly lignin, but also hemicellulose, are used for energy production or are sold as animal feed or as other types of fuel. The steps that are critical for the cost efficiency of the

process are usually the enzymes for hydrolysis and the distillation of the product solution to isolate the alcohol.

2.2.3.2 Alternative Processes for Lignocellulose Pulping Based on Organic Solvents

All the methods that use organic substances to pulp biomass have the common goal of separating the macromolecules lignin, cellulose and hemicellulose. This should make it possible to use the lignin fraction for other purposes than burning it directly. Several strategies are used to reach this goal, and are presented in this section.

Ethanol organosolv process

The first processes originated from the work of Kleinert [137]. He was able to demonstrate that wood could be pulped in an ethanol-water mixture without additional chemicals. Kleinert succeeded in pulping diverse types of wood in 30–60 min at 185°C in such a way that the physical properties of the resulting cellulose were comparable to cellulose produced by the bisulphite or kraft processes [138]. Historically, these discoveries were followed by experiments with the ethanol-based organosolv process by the company Lenzing AG. An ethanol-water mixture is mixed with lignocellulose and heated, depending on the process variant, to temperatures of up to 195°C [139]. An unfavourable result of these experiments was the high Kappa number (a measure of the lignin content; Kappa 6 corresponds to 1% lignin) of the resulting cellulose. Despite up to 6 hours of pretreatment with acid, it was not possible to reduce the Kappa number below 31.5. Also, from 160°C upwards in the presence of a too acidic catalyst, conversion of pentoses to furfural increases [19].

At present, under the leadership of Dechema e.V. in Germany, a large-scale biorefinery project is in progress. The central aim is to achieve total utilization of biomass material. For this project, at the University of Hamburg-Harburg, a series of experiments were done on the scale of 6 kg of biomass. The liquor ratio of biomass to the solvent mixture was 1:4. Figure 41 shows the product distribution from experiments at 170°C and different concentrations of sulphuric acid [140]. It can be seen that this procedure is not an effective wood pulping because the lignin content remains higher than 10%.

As with the pulping processes with sodium hydroxide for cellulose production, there are also alkaline organosolv processes investigated. The pH is adjusted with sodium hydroxide. This method is able to reduce the lignin content of wheat straw to 4.2%. Notably, the process is carried out at just 70°C [141].

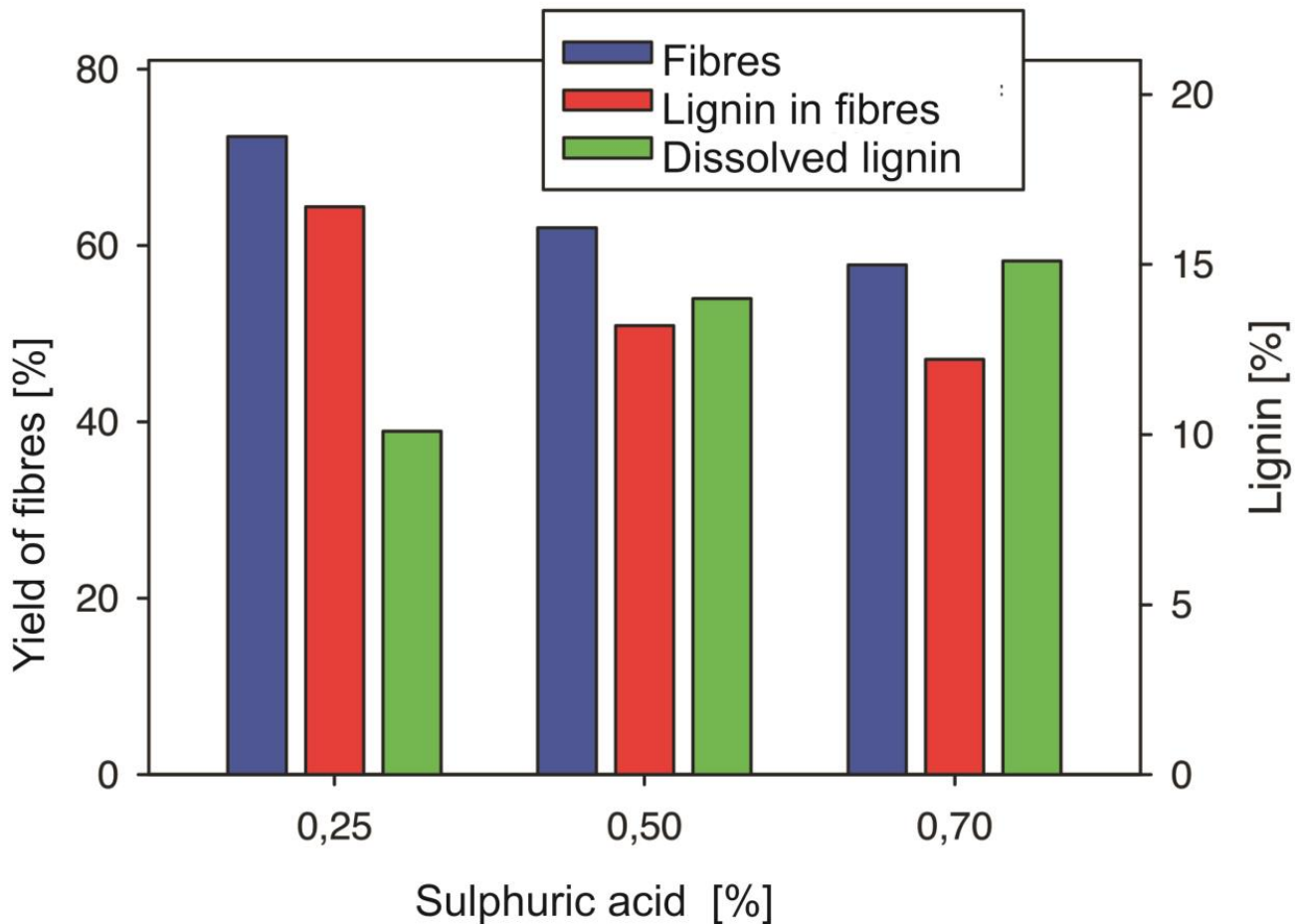


Figure 41: Effect of acid concentration of lignin yield in an organosolv process, data from the University of Hamburg-Harburg [140]

Methanol organosolv process

Muurinen [142] has written a review of the methanol organosolv process. Here, just two of the many variants are presented. The first is a methanol organosolv process that uses only water and methanol. Jiménez et al. [143] have shown in an extensive study that a methanol organosolv process can achieve cellulose yields of almost 40% with a Kappa number of less than 30. The process parameters are shown in Table 15.

Table 15: Process parameters for methanol organosolv pulping [143]

| Temperature range °C | Residence time min | Methanol concentration % |
|-------------------------|-----------------------|-----------------------------|
| 150–200 | 30–120 | 50–80 |

The other variant of this process is alkali methanol anthraquinone pulping (ASAM process). This is an alkaline pulping process. The composition of the liquor is shown in Table 16.

Table 17 presents a comparison of the cellulose yields of the ASAM and Kraft processes. As with all the pulping processes described in this study, the cellulose from the ASAM process has a higher lignin content than from conventional processes.

Table 16: Cooking liquor composition in the ASAM process compared to the Kraft process [144]

| | ASAM | Kraft process |
|---------------------------------------|-------|---------------|
| Initial loading with chemicals % | 19.4 | 15 |
| Na ₂ SO ₃ /NaOH | 80/20 | — |
| Sulfidity | 0 | 30 |
| Methanol (vol % of total liquor) | 25 | — |
| Anthraquinone | 0.1 | — |
| Liquor ratio | 4.0:1 | 4.5:1 |

Table 17: Properties of cellulose produced by the ASAM process and the Kraft process [144]

| | Cellulose yield % | Kappa no. |
|-------|-------------------|-----------|
| ASAM | | |
| 160°C | 74.0 | 41.9 |
| 170°C | 60.4 | 25.1 |
| 180°C | 59.2 | 24.6 |
| Kraft | | |
| 160°C | 55.5 | 18.0 |
| 170°C | 52.2 | 18.0 |
| 180°C | 50.0 | 16.7 |

However, the ASAM process has a higher yield than the Kraft process. According to the authors of the study, for use in the paper industry the ASAM cellulose has the advantages that it is brighter in colour and easier to bleach.

2.2.3.3 Production of Fuels from Pulped Lignocellulose

Two strategies are available for processing pulped lignocellulose to fuel. These strategies are shown in Figure 42. The first strategy is direct fermentation of the material; for this purpose, the material must already be pulped to an extent where hemicellulose and cellulose are accessible to microorganisms and enzymes. The other strategy is to extract the hemicellulose and cellulose, decompose them to free sugars and then use various syntheses to convert these sugars to fuel or to ferment certain fractions.

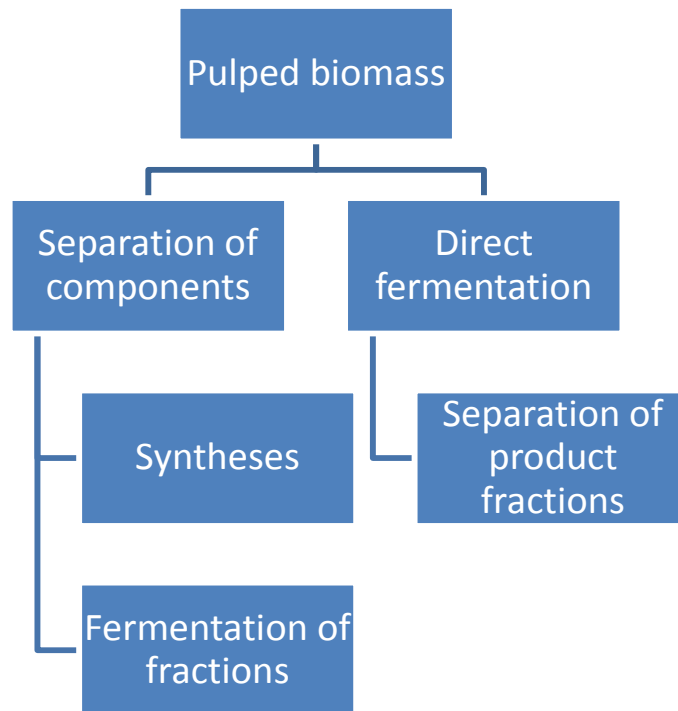


Figure 42: Strategies for processing digested biomass

Fuel production by fermentation

Up to now the only way to produce fuel from lignocellulose at demonstration scale is by fermentation to ethanol. As with fermentation of starch, the digested biomass is first hydrolysed; this can be done enzymatically or using acidic catalysis [145]. Enzymatic catalysis would be preferable except for the throughput rates and the cost of the enzymes, which limit its practicability [146].

The disadvantage of producing ethanol is the low energy content of ethanol; the calorific value of ethanol is 29755 kJ/kg [147]. For this reason, research is now focussing on longer-chain alcohols such as butanol; butanol has a calorific value of 36111kJ/kg [148].

Figure 43 shows possible production pathways for biobutanol, the most interesting of which is the route from biomass. The current state of the art is that starting with a 30 g/l xylan solution, 12.05 g/l butanol and 1.78 g hydrogen can be produced by fermentation [149].

This is remarkable because it shows that a hemicellulose (xylose and arabinose) can be used as a carbohydrate source. On the other hand, it is not clear what the effects of other products of digestion, especially phenols, would have on the fermentation of the hemicellulose.

This means that it is a considerably greater challenge to produce acetone, butanol and ethanol via ABE fermentation [150] than simply to ferment to ethanol. The ABE fermentation usually uses the organisms *Clostridium acetobutylicum*, *Clostridium saccharobutylicum*, *Clostridium beijerinckii* and *Clostridium saccharoperbutylacetonicum* [151].

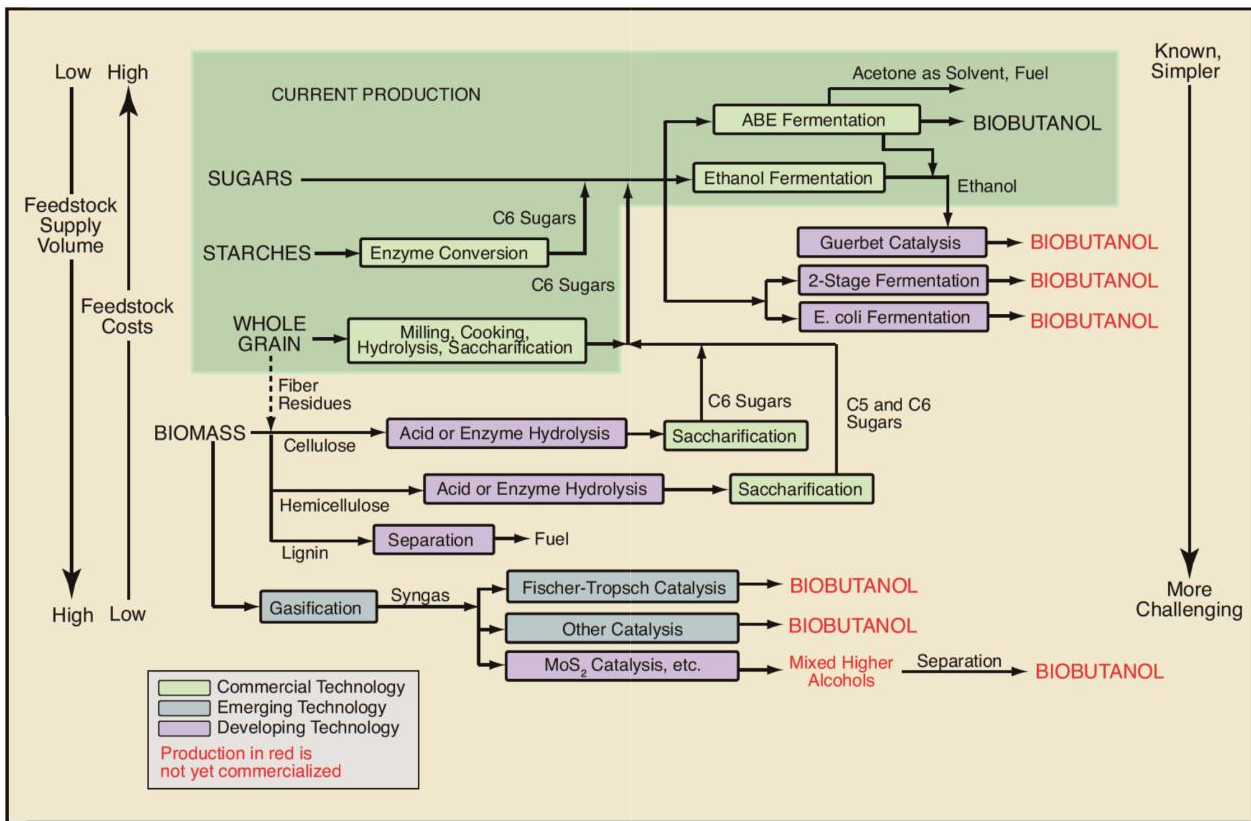


Figure 43: Possible production routes to biobutanol [152]

In the Dechema biorefinery project described in Section 2.2.3.2, ABE fermentation was also done with the hydrolysate from the organosolv process. The authors of that study reported considerable difficulties with the fermentation of a hydrolysate from beech wood to acetone, ethanol and butanol; in particular, the fermentation was inhibited by the high concentration of acetic acid.

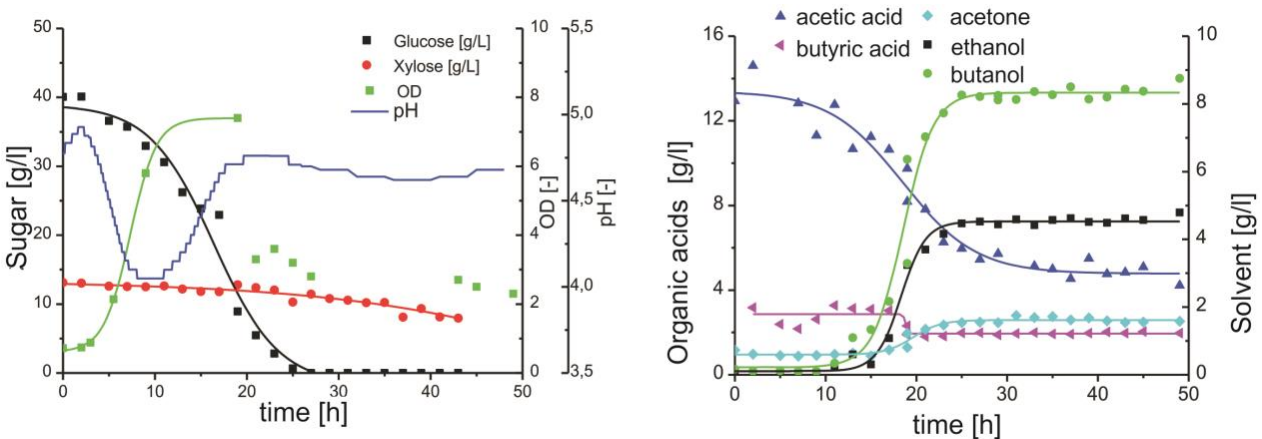


Figure 44: Time course of ABE fermentation of hydrolysate from beech wood [140]

Figure 44 shows time courses of different components in the fermentation of the hydrolysate form beech wood. The low pH concentrations of the products and the fact that there is only a small drop in the xylose concentration both underline quite clearly that this process cannot be

claimed to utilize the whole plant biomass. It is also shown that in this system, the phenolic components do not stop the fermentation.

The problem with butanol production is inhibition of the fermentation by butanol itself, which impairs the function of the cell membrane [153]. However, it was possible to remove butanol by pervaporation, which increased the fermentation yield to 165 g of butanol per litre of fermentation medium [154]. After purification it would be conceivable to convert the butanol to dibutyl ether, which would achieve a further increase in the energy content.

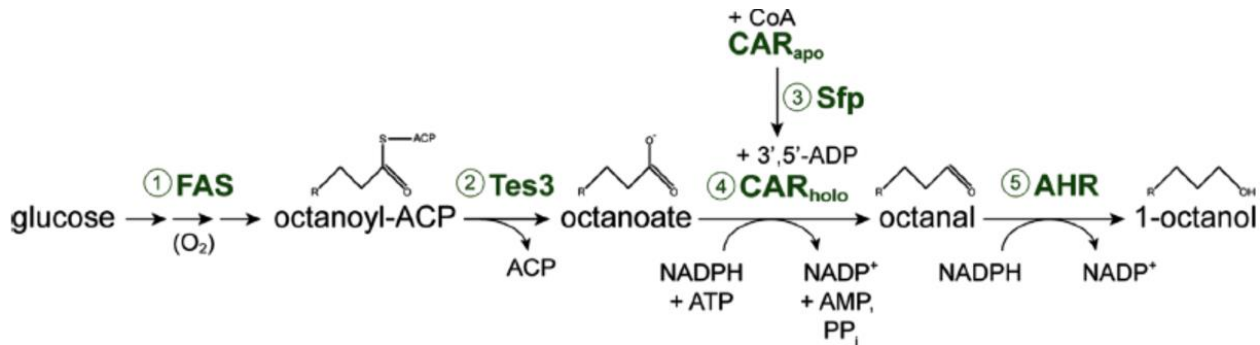


Figure 45: Biochemical pathway for synthesis of octanol [155]

In another development, research is currently being done to produce octanol from glucose. Octanol has an even higher energy content than butanol. However, up to now the yields have been modest. Akthar et al. have reported a formation rate of $4.4 \text{ mg of 1-octanol l}^{-1}\text{h}^{-1}$ using a genetically modified *Escherichia coli* strain [155]. The biosynthesis pathway is shown in Figure 45.

Production of fuels by synthesis from individual components of biomass

In contrast to the fermentation of the pulped biomass, synthetic processing of the individual components can only work with well-defined substances. It is not possible to use a spectrum of molecules resulting from the pulping process; for example a method for converting glucose can only be used with glucose, and will not work with dimers, trimer or other polymers; they would only lead to formation of unwanted side products. A very early synthetic route from glucose to diesel was presented by Huber [156] in 2005.

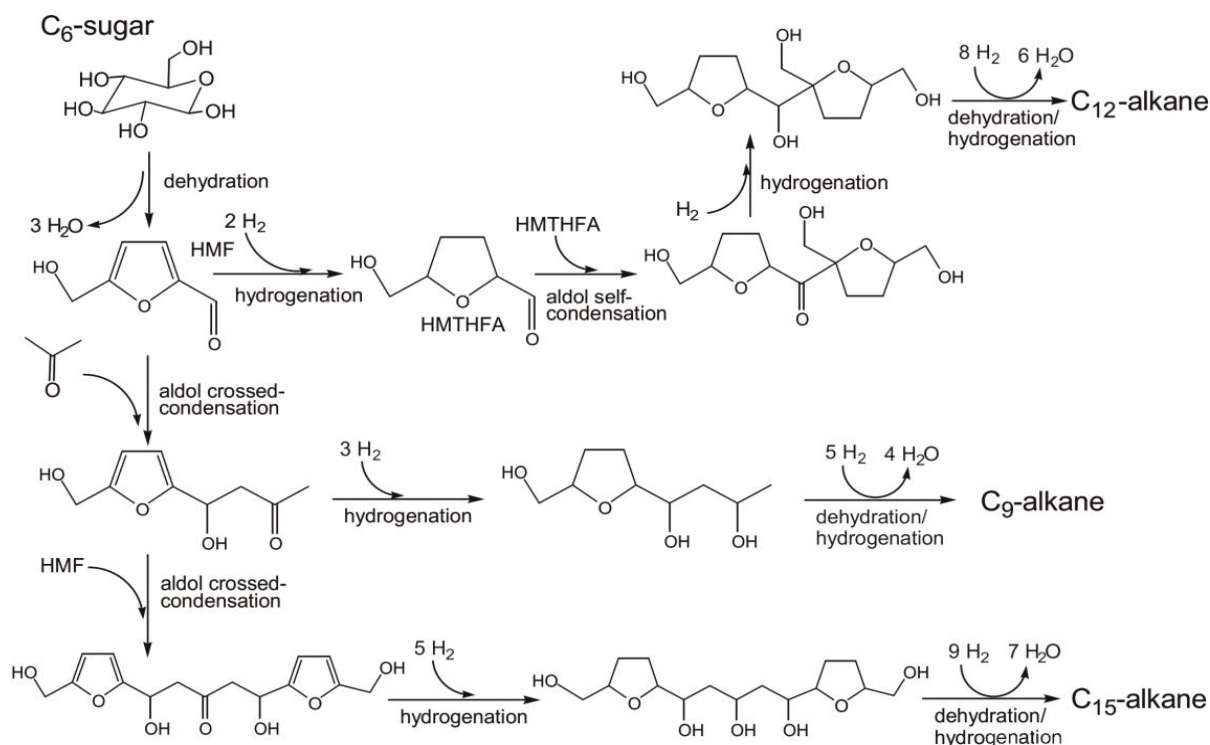


Figure 46: Synthesis of higher alkanes from hexose sugars [156]

Figure 46 shows three routes for synthesis of higher alkanes from hexose sugars. In an initial reaction, the sugar is dehydrated to hydroxymethylfurfural (HMF).

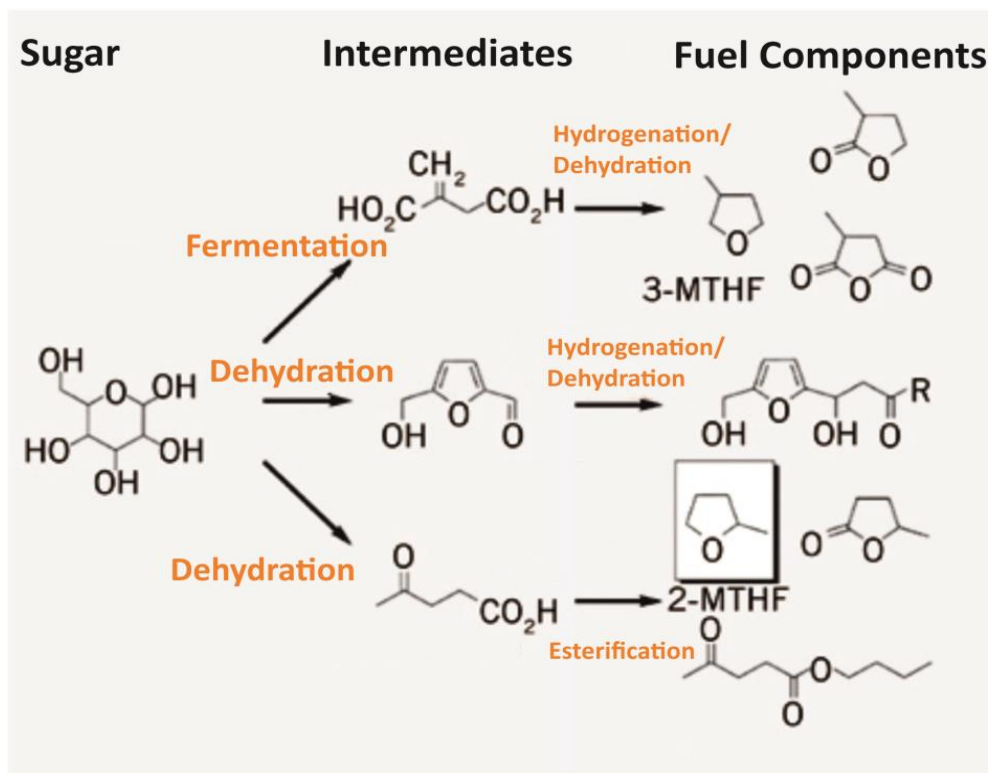


Figure 47: Synthesis of platform chemical from sugar [157]

Then, aldol condensations [8] are used to attach a side chain based on carbon-carbon bonds. To achieve sustainability of the overall process, the acetone needed for these reactions could

be obtained from the ABE fermentation described in this section. Since 2005, numerous other synthetic routes to alkanes and their oxygenated derivatives have been published, all building on Huber's original work. Figure 47 illustrates the diversity of synthesis routes that have been proposed for the different platform chemicals. Jakob und Pischinger [157] have stated their goal of synthesizing methyltetrahydrofuran, γ -valerolactone or butyllaevulinate from laevulinic acid, while Geilen et al. [158] propose 1,4-pentandiol as an additional target molecule. For a discussion of the broad range of research on synthetic transformation of glucose, an article of Thananattananachon [159] is referred. Besides describing other molecules that could be synthesized from laevulinic acid and would be suitable as fuels, this article explains how it is necessary to first convert the starting material to D-fructofuranose in order to increase the yield of hydroxymethylfurfural; this is shown in Figure 48.

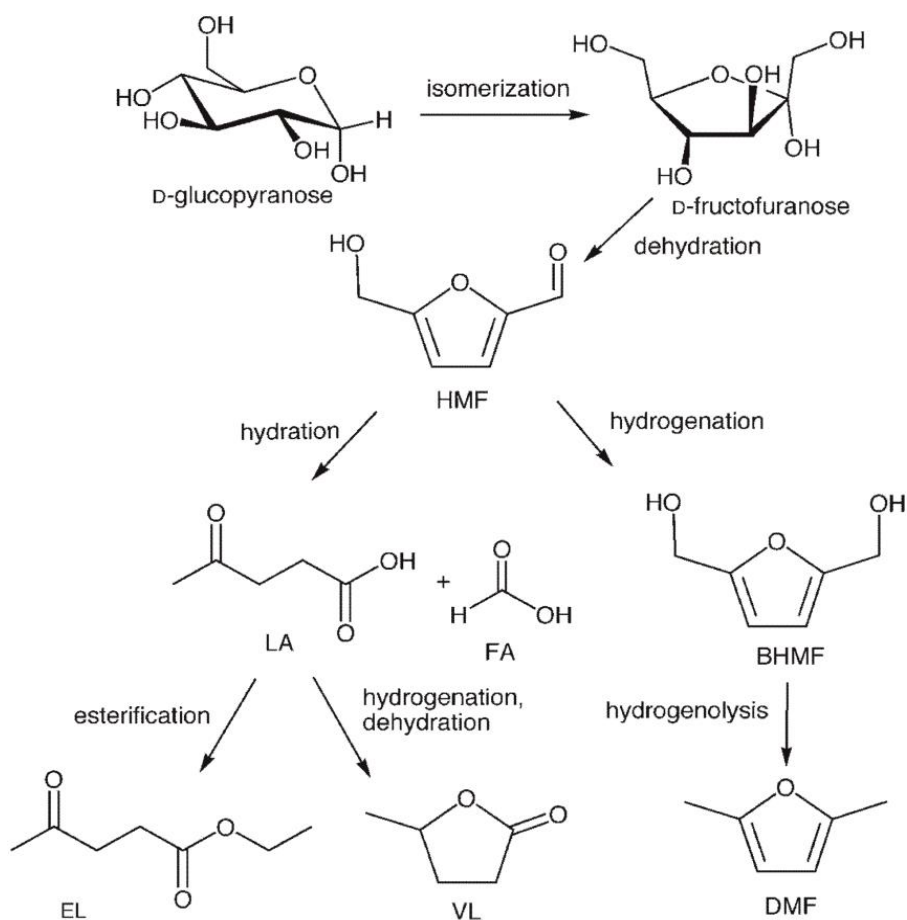


Figure 48: Production of designer fuels via isomerization of D-glucopyranose in D-fructofuranose [159]

The possible uses of hydroxymethylfurfural seem almost inexhaustible. But also crystalline cellulose can be used, which offers a way of avoiding the problems of reactions with oligomers mentioned at the beginning of this section. An in-situ reaction can be used to generate HMF-like products. Chlorination of the hydroxyl group makes the reactive groups of the alkylhalogenides accessible. From these intermediate ethoxymethylfurfural is accessible, as shown in Figure 49 [160]. This is another route for converting glucose to fuels.

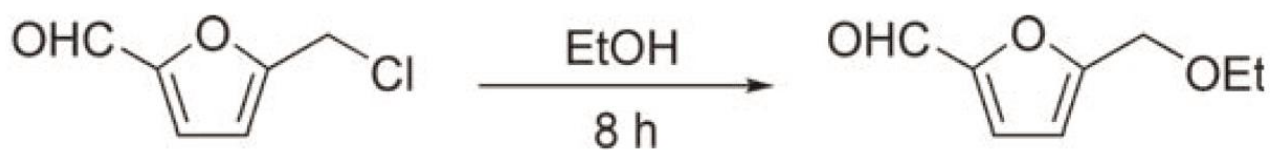


Figure 49: Synthesis of ethoxymethylfurfural from 5-chloromethylfurfural [160]

One essential function of a biorefinery would be to utilize pentose sugars as well as hexose sugars. An example of this is the conversion of xylose to furfural, which is shown in Figure 50. Following an acidic hydrolysis step, furfural is formed from xylose. Xing et. al. [161] have developed a two-phase reaction method in which the furfural is extracted into an apolar phase in order to prevent formation of humins.

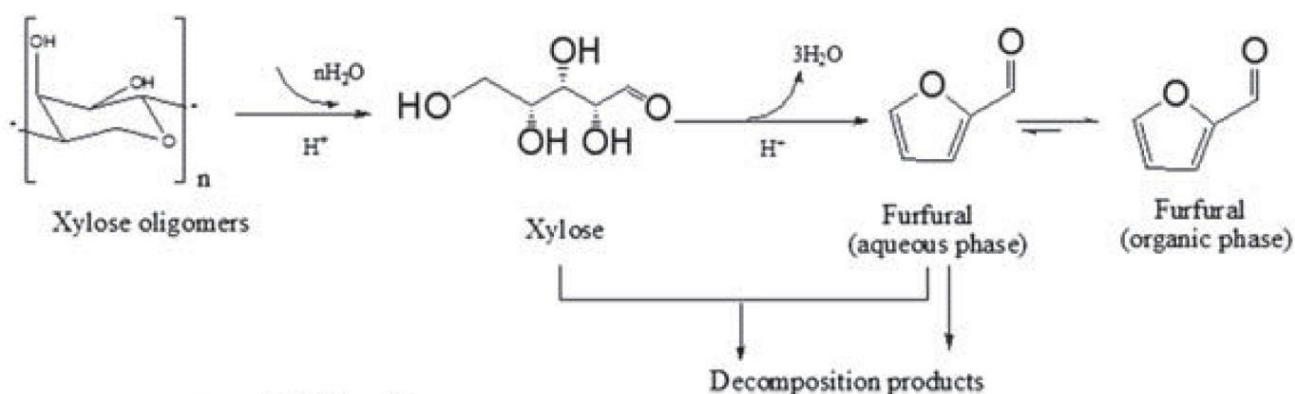


Figure 50: Decomposition of xylan to furfural [161]

Subsequently, a variety of synthetic routes are available, as with the platform chemicals hydroxymethylfurfural and laevulinic acid.

Figure 51 shows a possible strategy [162] for synthesizing straight-chain alkanes. The use of 2-heptanone is questionable, because this compound is difficult to synthesize without using fossil-based precursors. Despite, one could still, for example, oxidize butanol to butanone and then convert it to biofuels via a solvent-free aldol condensation. Octanol could be made in a similar way. An aldol condensation of acetone and furfural with subsequent hydration leads to an oxygenated fuel [163]. Without these detours, it is also possible to transform digested biomass into alkanes via multiple hydrodeoxygenation steps [164].

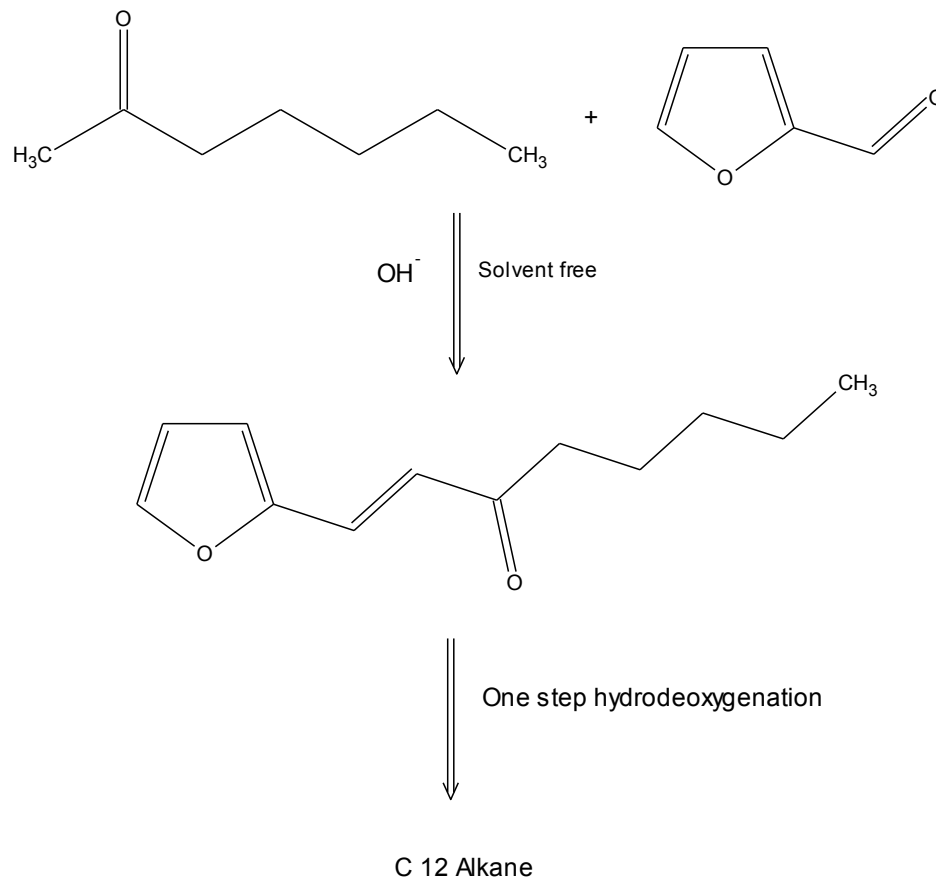


Figure 51: Synthesis route from furfural and 2-heptanone to alkanes [162]

2.2.3.4 Conclusions on Digestion Processes for Biomass and Processing of the products to Fuels

Direct and indirect liquefaction of biomass have advantages and disadvantages. However, the trend of current research seems to be leading towards a sequential and then refinery-like processing of biomass. This would allow individual process steps to be combined, in order to make products that are as sustainable as possible.

2.3 Summary

This chapter describes three strategies for making substitute fuels from lignocellulose. The research activities on these process methods revealed that the scientific literature contains work on a wide variety of fuels. For future investigations, the potential fuels are listed: Methanol, Dimethyl ether, Poly(oxymethylene)dimethylethers, Oxygenated hydrocarbons from direct liquefaction of biomass, Ethanol, Acetone, Butanol, Dibutyl ether, Octanol, 2-methyl-tetrahydrofuran, γ -valerolactone, Dimethylfuran.

This list includes 11 pure substances and two mixtures. The hydrocarbons from the direct liquefaction of biomass are just partially characterized mixture of hydrocarbons and all kinds of structures that carbon can form with hydrogen. In contrast, the poly(oxymethylene) dimethylethers are predominantly mixtures of oxymethylene with its dimers, trimers and tetramers.

2.4 List of Figures

| | |
|---|----|
| FIGURE 1: ATR-IR SPECTRUM OF SPRUCE WOOD [5] | 3 |
| FIGURE 2: B-D-GLUCOPYRANOSE | 5 |
| FIGURE 3: CELLULOSE POLYMER [9]..... | 5 |
| FIGURE 4: INTERMOLECULAR HYDROGEN BONDS IN CELLULOSE [10] | 5 |
| FIGURE 5: THREE-DIMENSIONAL REPRESENTATION OF TWO GLUCOSE DIMERS LINKED BY HYDROGEN BONDS [11] | 6 |
| FIGURE 6: REPRESENTATIVE DETAIL OF AN ARABINO-4-O-METHYLGLUCURONOXYLAN CHAIN [13] | 7 |
| FIGURE 7: DETAIL OF GALACTOGLUCOMANNAN [13] | 7 |
| FIGURE 8: MONOMERS OF LIGNIN WITH NUMBERING/NAMING OF THEIR CARBON CENTRES..... | 8 |
| FIGURE 9: B-O-4 UND 5-5' BONDS IN LIGNIN [10]..... | 9 |
| FIGURE 10: STRUCTURE OF LIGNIN ACCORDING TO FREUDENBERG | 9 |
| FIGURE 11: MODEL OF THE INTERNAL STRUCTURE OF A WOOD CELL WALL A) TRANSVERSE SECTION, B) LONGITUDINAL SECTION [7] . | 10 |
| FIGURE 12: CELL-WALL LAYERS OF A CONIFER TRACHEID [21] | 11 |
| FIGURE 13: IMAGE OF WOOD CELL (SPRUCE) MADE BY UV MICROSPECTROPHOTOMETRY AT 280 NM [14] | 12 |
| FIGURE 14: SCHEME FOR INDIRECT LIQUEFACTION OF BIOMASS [22, 23]..... | 13 |
| FIGURE 15: REACTIONS IN GASIFICATION OF CARBON, OXYGEN AND HYDROGEN [29] | 14 |
| FIGURE 16: COMBUSTION REACTIONS IN BIOMASS GASIFICATION [29] | 14 |
| FIGURE 17: OPERATIONAL MODES OF BIOMASS GASIFICATION [30] | 14 |
| FIGURE 18: AUTOTHERMAL COUNTERFLOW PACKED-BED GASIFIER [31] | 15 |
| FIGURE 19: TWIN CIRCULATING FLUIDIZED BED [34] | 16 |
| FIGURE 20: ENTRAINED-FLOW GASIFIER [38] | 17 |
| FIGURE 21: SIMPLIFIED DIAGRAM OF THE RECTISOL PROCESS [54]..... | 21 |
| FIGURE 22: FLOW DIAGRAM OF THE ASPEN SIMULATION OF A SINGLE-STAGE RECTISOL GAS-WASHING PLANT [55] | 22 |
| FIGURE 23: FUEL PRODUCTION FROM SYNTHESIS GAS [51] | 23 |
| FIGURE 24: RELATIONSHIPS BETWEEN FORMATION OF METHANE AND OTHER HYDROCARBONS (BY CARBON NUMBER) IN A HT FISCHER-TROPSCH SYNTHESIS PROCESS. [58] | 23 |
| FIGURE 25: RELATIONSHIPS BETWEEN THE FORMATION OF HARD WAXES (I.E. COMPOUNDS WITH BOILING POINTS HIGHER THAN 500°C) AND OTHER HYDROCARBONS (BY CARBON NUMBER) IN A LT FISCHER-TROPSCH SYNTHESIS. [58] | 24 |
| FIGURE 26: COAL-BASED HT FISCHER-TROPSCH SYNTHESIS PLANT, WITH A SO-CALLED 'FIXED BED DRY BOTTOM' GASIFIER, SEPARATE FISCHER-TROPSCH SYNTHESIS AND TAR REFINERY (SASOL SYN-FUELS REFINERY 2004, SECUNDA, SOUTH AFRICA). CTN: COAL TAR NAPHTHA; DHT: DISTILLATE HYDROTREATER, HP: HIGH PRESSURE, HT: HYDROTREATER [61] | 25 |
| FIGURE 27: PROCESS DIAGRAM OF THE LPMEOH PLANT OF AIR PRODUCTS LIQUID PHASE CONVERSION COMPANY [68] | 26 |
| FIGURE 28: BLOCK FLOW DIAGRAM OF POMDME PRODUCTION [79]..... | 27 |
| FIGURE 29: INTERACTIONS OF THE MAIN VARIABLES CONTROLLING PYROLYSIS..... | 29 |
| FIGURE 30: REACTORS FOR FLASH PYROLYSIS OF BIOMASS: A) STATIONARY FLUIDIZED-BED REACTOR, B) RECIRCULATING FLUIDIZED-BED REACTOR, C, D, E) ABLATIVE REACTORS, F) REACTOR UNDER VACUUM [88] | 31 |
| FIGURE 31: YIELD OF LIQUID PRODUCTS IN FLASH PYROLYSIS ACCORDING TO BRIDGWATER [85] | 33 |
| FIGURE 32: TEMPERATURE DEPENDENCE OF FORMATION OF GAS AND BIOCHAR [93] | 34 |
| FIGURE 33: TEMPERATURE DEPENDENCE OF FORMATION OF DIFFERENT GAS COMPONENTS [93]..... | 35 |
| FIGURE 34: MALDI TOF SPECTRUM OF A PYROLYSIS OIL FROM ALGAL BIOMASS [95] | 37 |
| FIGURE 35: INFRA-RED SPECTRUM OF WASTE FROM OLIVE-OIL PRODUCTION. MAIN PEAKS ARE: THE O-H BOND AT 3700 CM ⁻¹ , C-H BOND AT 3200 CM ⁻¹ [103] | 38 |
| FIGURE 36: PYROGRAM OF PURE CELLULOSE [105] | 39 |
| FIGURE 37: PYROGRAMM OF LIGNIN FROM BEECH WOOD [105]..... | 39 |
| FIGURE 38: CLASSIFICATION OF BIOMASS PULPING PROCESSES | 41 |
| FIGURE 39: LGS (LIGNOSULFONATE) [123]..... | 42 |
| FIGURE 40: FLOW DIAGRAM OF THE INBICON BIOETHANOL PLANT [133] | 43 |
| FIGURE 41: EFFECT OF ACID CONCENTRATION OF LIGNIN YIELD IN AN ORGANOSOLV PROCESS, DATA FROM THE UNIVERSITY OF HAMBURG-HARBURG [140] | 45 |

| | |
|---|----|
| FIGURE 42: STRATEGIES FOR PROCESSING DIGESTED BIOMASS..... | 47 |
| FIGURE 43: POSSIBLE PRODUCTION ROUTES TO BIOBUTANOL [152] | 48 |
| FIGURE 44: TIME COURSE OF ABE FERMENTATION OF HYDROLYSATE FROM BEECH WOOD [140] | 48 |
| FIGURE 45: BIOCHEMICAL PATHWAY FOR SYNTHESIS OF OCTANOL [155] | 49 |
| FIGURE 46: SYNTHESIS OF HIGHER ALKANES FROM HEXOSE SUGARS [156] | 50 |
| FIGURE 47: SYNTHESIS OF PLATFORM CHEMICAL FROM SUGAR [157] | 50 |
| FIGURE 48: PRODUCTION OF DESIGNER FUELS VIA ISOMERIZATION OF D-GLUCOPYRANOSE IN D-FRUCTOFURANOSE [159]..... | 51 |
| FIGURE 49: SYNTHESIS OF ETHOXYMETHYLFURFURAL FROM 5-CHLOROMETHYLFURFURAL [160] | 52 |
| FIGURE 50: DECOMPOSITION OF XYLAN TO FURFURAL [161]..... | 52 |
| FIGURE 51: SYNTHESIS ROUTE FROM FURFURAL AND 2-HEPTANONE TO ALKANES [162] | 53 |

2.5 List of Tables

| | |
|--|----|
| TABLE 1: ELEMENTAL COMPOSITION OF SPRUCE WOOD WITHOUT INORGANIC COMPONENTS: | 2 |
| TABLE 2: MAIN CONSTITUENTS OF THE ASH OF SPRUCE WOOD [5]..... | 2 |
| TABLE 3: CALORIFIC VALUES OF DIESEL AND WOOD | 3 |
| TABLE 4: TYPES OF BOND FOUND IN ATR-IR OF SPRUCE WOOD [6] | 4 |
| TABLE 5: CATEGORIZATION OF MOLECULAR COMPONENTS IN SPRUCE WOOD [7] | 4 |
| TABLE 6: RELATIVE AMOUNTS OF THE MONOMER RESIDUES COUMARYL ALCOHOL, CONIFERYL ALCOHOL AND SINAPYL ALCOHOL IN DIFFERENT CATEGORIES OF PLANTS: HARD AND SOFT'WOOD AND ANNUAL PLANTS [10]..... | 8 |
| TABLE 7: COMPOSITION OF EUCALYPTUS ASH [44] | 18 |
| TABLE 8: ASH CONTENT OF GASIFICATION RESIDUES OF OLIVE MILL WASTE [45] | 19 |
| TABLE 9: MAXIMUM TAR LEVELS IN THE SYNTHESIS GAS DEPENDING ON THE APPLICATION [47]..... | 19 |
| TABLE 10: SEPARATION OF PARTICULATES AND TAR BY DIFFERENT CLEANING TECHNOLOGIES [49] | 20 |
| TABLE 11: ABSORPTION-BASED GAS CLEANING [53] | 20 |
| TABLE 12: PYROLYSIS PROCESSES AND THEIR VARIABLE PARAMETERS ACCORDING TO HUBER [89] | 32 |
| TABLE 13: ELEMENTAL COMPOSITION OF PYROLYSIS OIL | 36 |
| TABLE 14: PHYSICAL AND CHEMICAL PROPERTIES OF PYROLYSIS OIL..... | 36 |
| TABLE 15: PROCESS PARAMETERS FOR METHANOL ORGANOSOLV PULPING [143]..... | 45 |
| TABLE 16: COOKING LIQUOR COMPOSITION IN THE ASAM PROCESS COMPARED TO THE KRAFT PROCESS [144]..... | 46 |
| TABLE 17: PROPERTIES OF CELLULOSE PRODUCED BY THE ASAM PROCESS AND THE KRAFT PROCESS [144]..... | 46 |

2.6 References

1. Field CB, Barros VR, Dokken DJ, et al. (2014) Climate Change 2014: Impacts, Adaptation, and Vulnerability. Part A: Global and Sectoral Aspects. Contribution of Working Group II to the Fifth Assessment Report of the Intergovernmental Panel on Climate Change. doi: 10.1016/j.renene.2009.11.012
2. Meadows DH, Goldsmith E, Meadow P (1972) The limits to growth.
3. Diesel R (1986) Theorie und Konstruktion eines rationellen Wärmemotors zum Ersatz der Dampfmaschinen und der heute bekannten Verbrennungsmotoren. VDI-Verlag, Düsseldorf
4. Vidal J, Editor E (2010) Nigeria's agony dwarfs the Gulf oil spill. The US and Europe ignore it. *Guard*.
5. Schwaiger N (2011) REAKTIONSTECHNISCHE ANALYSE FÜR DIE OPTIMIERUNG DER FLÜSSIGPHASENPYROLYSE; REAKTIONSMEECHANISMEN DER FLÜSSIGPHASENPYROLYSE VON LIGNOCELLULOSE. Graz University of Technology
6. Atkins P, Höpfner A, Schleitzer A, Bär M (1987) Physikalische chemie.
7. Fengel D, Wegener G (2003) Wood—chemistry, ultrastructure, reactions. *J Polym Sci Polym Lett Ed*. doi: 10.1002/pol.1985.130231112
8. Streitwieser A, Heathcock CH, Kosower EM (1994) Organische Chemie. *Angew Chemie*. doi: 10.1002/ange.19951071230
9. Henriksson G, Lennholm H (2009) 4. Cellulose and Carbohydrate Chemistry. *Wood Chem. Wood Biotechnol. De Gruyter*, pp 71–100
10. Henriksson G (2009) 6. Lignin. *Wood Chem. Wood Biotechnol. De Gruyter*, pp 121–146
11. Bergensträhle M, Wohlert J, Himmel ME, Brady JW (2010) Simulation studies of the insolubility of cellulose. *Carbohydr Res* 345:2060–6. doi: 10.1016/j.carres.2010.06.017
12. Henriksson G, Lennholm H (2009) 3. Wood and Fibre Morphology. *Wood Chem. Wood Biotechnol. De Gruyter*, pp 71–100
13. Teleman A (2009) 5. Hemicelluloses and Pectins. *Wood Chem. Wood Biotechnol. De Gruyter*, pp 101–120
14. Schmitt U, Koch G, Lehnen R (2014) Wood. *Ullmann's Encycl. Ind. Chem.* pp 1–14
15. Saake B, Lehnen R (2012) Lignin. *Ullmann's Encycl Ind Chem*. doi: 10.1002/14356007.a15
16. Eichinger R. (1979) Magnefite Zellstoff der Papiererzeugung.pdf. *Wochenblatt Für Pap* 52–56.
17. Sixta H (2008) Handbook of Pulp. *Handb Pulp*. doi: 10.1002/9783527619887
18. Fredheim GE, Braaten SM, Christensen BE (2002) Molecular weight determination of lignosulfonates by size-exclusion chromatography and multi-angle laser light scattering. *J Chromatogr A* 942:191–199. doi: 10.1016/S0021-9673(01)01377-2
19. Holzinger F (2014) Biomass to Liquid (BtL): Biomasseaufschluss nach dem Organosolv-Verfahren. Technische Universität Graz
20. Lawoko M, Henriksson G, Gellerstedt G (2003) New Method for Quantitative Preparation of Lignin-Carbohydrate Complex from Unbleached Softwood Kraft Pulp: Lignin-Polysaccharide Networks I. *Holzforschung* 57:69–74. doi: 10.1515/HF.2003.011
21. Wagenführ R (1980) Anatomie des Holzes. LinkFachbuchverlag
22. Reaktionstechnik I, Karlsruhe F (2004) Verfahren zur Entschwefelung von flüssigen Brenn- und Kraftstoffen für das Betreiben von Brennstoffzellensystemen Reaktions- und Energietechnik Hydrothermale Wasserstoffherzeugung aus Biomasse ± Einfluss von Inhaltsstoffen und Optimierungsansätze *Unter*. 1266–1267.
23. Fürnsinn S, Hofbauer H (2007) Synthetische Kraftstoffe aus Biomasse: Technik, Entwicklungen, Perspektiven. *Chemie Ing Tech* 79:579–590. doi: 10.1002/cite.200700017
24. Emami Taba L, Irfan MF, Wan Daud WAM, Chakrabarti MH (2012) The effect of temperature on various parameters in coal, biomass and CO-gasification: A review. *Renew Sustain Energy Rev* 16:5584–5596. doi: 10.1016/j.rser.2012.06.015
25. Yang X, Yuan C, Xu J, Zhang W (2014) Co-pyrolysis of Chinese lignite and biomass in a vacuum reactor.

- Bioresour Technol 173:1–5. doi: 10.1016/j.biortech.2014.09.073
26. Kitzler H, Pfeifer C, Hofbauer H (2011) Pressurized gasification of woody biomass-Variation of parameter. *Fuel Process Technol* 92:908–914. doi: 10.1016/j.fuproc.2010.12.009
27. Öhrman OGW, Weiland F, Pettersson E, et al. (2013) Pressurized oxygen blown entrained flow gasification of a biorefinery lignin residue. *Fuel Process Technol* 115:130–138. doi: 10.1016/j.fuproc.2013.04.009
28. Güell B, Sandquist J, Sørnum L (2013) Gasification of biomass to second generation biofuels: a review. *J. ...*
29. Kaneko T (2012) Coal Liquefaction. *Ullmann's Encycl Ind Chem* 1–83. doi: 10.1002/14356007.a07 197
30. Kaltschmitt M, Hartmann H, Hofbauer H (2009) Energie aus Biomasse. *Energ aus Biomasse*. doi: 10.1007/978-3-540-85095-3
31. Biedermann F, Obernberger I (2004) Biomasse-Kwk Auf Basis Stirlingmotor. *Agrar rundschau* 8–10.
32. Marinitsch G (2011) MALL SCALE CHP PLANTS BASED ON STIRLING ENGINES. *Symp. using bioliquids engines turbines CHP Appl.* pp 1–10
33. Martínez JD, Mahkamov K, Andrade R V., Silva Lora EE (2012) Syngas production in downdraft biomass gasifiers and its application using internal combustion engines. *Renew Energy* 38:1–9. doi: 10.1016/j.renene.2011.07.035
34. Penthor S, Mayer K, Kern S, et al. (2014) Chemical-looping combustion of raw syngas from biomass steam gasification - Coupled operation of two dual fluidized bed pilot plants. *Fuel* 127:178–185. doi: 10.1016/j.fuel.2014.01.062
35. Kaushal P, Abedi J, Mahinpey N (2010) A comprehensive mathematical model for biomass gasification in a bubbling fluidized bed reactor. *Fuel* 89:3650–3661. doi: 10.1016/j.fuel.2010.07.036
36. Kirnbauer F, Hofbauer H (2013) The mechanism of bed material coating in dual fluidized bed biomass steam gasification plants and its impact on plant optimization. *Powder Technol* 245:94–104. doi: 10.1016/j.powtec.2013.04.022
37. Feng W, Ji P, Chen B, Zheng D (2011) Analysis of Methanol Production from Biomass Gasification. *Chem Eng Technol* 34:307–317. doi: 10.1002/ceat.201000346
38. Nikoo MB, Mahinpey N (2008) Simulation of biomass gasification in fluidized bed reactor using ASPEN PLUS. *Biomass and Bioenergy* 32:1245–1254. doi: 10.1016/j.biombioe.2008.02.020
39. Jahangiri H, Bennett J, Mahjoubi P, et al. (2014) A review of advanced catalyst development for Fischer–Tropsch synthesis of hydrocarbons from biomass derived syn-gas. *Catal Sci Technol* 4:2210. doi: 10.1039/c4cy00327f
40. Ceccarelli C (2014) bioliq - Startseite. <http://www.bioliq.de/index.php>. Accessed 27 Aug 2014
41. Santo U, Kuhn D, Wiemer HJ, et al. (2007) Erzeugung von Synthesegas aus biomassestämmigen Slurries im Flugstromvergaser. *Chemie-Ingenieur-Technik* 79:651–656. doi: 10.1002/cite.200700037
42. Qin K, Lin W, Jensen PA, Jensen AD (2012) High-temperature entrained flow gasification of biomass. *Fuel* 93:589–600. doi: 10.1016/j.fuel.2011.10.063
43. Dahmen N, Dinjus E (2010) Synthetische chemieprodukte und kraftstoffe aus biomasse. *Chemie-Ingenieur-Technik* 82:1147–1152. doi: 10.1002/cite.201000082
44. Zevenhoven-Onderwater M, Backman R, Skrifvars BJ, et al. (2001) The ash chemistry in fluidised bed gasification of biomass fuels. Part I: Predicting the chemistry of melting ashes and ash-bed material interaction. *Fuel* 80:1489–1502. doi: 10.1016/S0016-2361(01)00026-6
45. Vogel A, Bolhàr-Nordenkampf M, Kaltschmitt M, Hofbauer H (2006) Analyse und Evaluierung der thermochemischen Vergasung von Biomasse, 29th ed. Fachagentur Nachwachsende Rohstoffe e. V. (FNR, Gülzow
46. George A, Morgan TJ, Kandiyoti R (2014) Pyrolytic Reactions of Lignin within Naturally Occurring Plant Matrices: Challenges in Biomass Pyrolysis Modeling Due to Synergistic Effects.
47. Leiva C, Gómez-Barea A, Vilches LF, et al. (2007) Use of Biomass Gasification Fly Ash in Lightweight Plasterboard. *Energy and Fuels* 21:361–367. doi: 10.1021/ef060260n
48. Font Palma C (2013) Modelling of tar formation and evolution for biomass gasification: A review. *Appl Energy* 111:129–141. doi: 10.1016/j.apenergy.2013.04.082

49. Richardson Y, Blin J, Julbe A (2012) A short overview on purification and conditioning of syngas produced by biomass gasification: Catalytic strategies, process intensification and new concepts. *Prog Energy Combust Sci* 38:765–781. doi: 10.1016/j.pecs.2011.12.001
50. Xu C, Donald J, Byambajav E, Ohtsuka Y (2010) Recent advances in catalysts for hot-gas removal of tar and NH₃ from biomass gasification. *Fuel* 89:1784–1795. doi: 10.1016/j.fuel.2010.02.014
51. Han J, Kim H (2008) The reduction and control technology of tar during biomass gasification/pyrolysis: An overview. *Renew Sustain Energy Rev* 12:397–416. doi: 10.1016/j.rser.2006.07.015
52. Nacken M, Ma L, Heidenreich S, Baron G V. (2009) Performance of a catalytically activated ceramic hot gas filter for catalytic tar removal from biomass gasification gas. *Appl Catal B Environ* 88:292–298. doi: 10.1016/j.apcatb.2008.11.011
53. Spath PL, Dayton DC (2003) Preliminary Screening - Technical and Economic Assessment of Synthesis Gas to Fuels and Chemicals with Emphasis on the Potential for Biomass-Derived Syngas. Golden, CO, USA
54. Hamelinck C, Faaij a, Denuil H, Boerrigter H (2004) Production of FT transportation fuels from biomass; technical options, process analysis and optimisation, and development potential. *Energy* 29:1743–1771. doi: 10.1016/j.energy.2004.01.002
55. de Klerk A (2011) Fischer-Tropsch Refining. doi: 10.1002/9783527635603
56. Munder B, Grob S, Fritz PM (2010) Selection of Wash Systems for Sour Gas Removal. 4th Int. Freib. Conf. IGCC Xtl Technol. pp 1–23
57. Sun L, Smith R (2013) Rectisol wash process simulation and analysis. *J Clean Prod* 39:321–328. doi: 10.1016/j.jclepro.2012.05.049
58. Ratnasamy C, Wagner JP (2009) Water Gas Shift Catalysis. *Catal Rev* 51:325–440. doi: 10.1080/01614940903048661
59. Fischer F, Tropsch H (1926) Über die direkte Synthese von Erdöl-Kohlenwasserstoffen bei gewöhnlichem Druck. (Erste Mitteilung). *Berichte der Dtsch Chem Gesellschaft (A B Ser* 59:830–831. doi: 10.1002/cber.19260590442
60. Dry ME (2002) High quality diesel via the Fischer-Tropsch process - A review. *J Chem Technol Biotechnol* 77:43–50. doi: 10.1002/jctb.527
61. (2004) First natural gas from Mozambique arrives in Secunda. 1.
62. Klerk A De (2011) Catalysis. doi: 10.1039/9781849732772
63. Leckel D (2009) Diesel Production from Fischer–Tropsch: The Past, the Present, and New Concepts. *Energy & Fuels* 23:2342–2358. doi: 10.1021/ef900064c
64. Lange J (2001) Methanol synthesis: a short review of technology improvements. *Catal Today* 64:3–8. doi: 10.1016/S0920-5861(00)00503-4
65. Dienes EK (1967) Low temperature shift reaction involving a zinc oxide-copper catalyst. 3.
66. Trimm DL, Wainwright MS (1990) Steam reforming and methanol synthesis. *Catal Today* 6:261–278. doi: 10.1016/0920-5861(90)85005-9
67. Wang T, Wang J, Jin Y (2007) Slurry reactors for gas-to-liquid processes: A review. *Ind Eng Chem Res* 46:5824–5847. doi: 10.1021/ie070330t
68. Kirkland R, Schmetz E, Kornosky R (2004) COMMERCIAL-SCALE DEMONSTRATION OF THE LIQUID PHASE METHANOL (LPMEOH™) Process. Washington D.C.
69. Olah GA et al (2009) Beyond Oil and Gas: The Methanol Economy. Wiley
70. Müller M, Hübsch U (2012) Dimethyl Ether. *Ullmann's Encycl Ind Chem*. doi: 10.1002/14356007.a08
71. Jin E, Zhang Y, He L, et al. (2014) Indirect coal to liquid technologies. *Appl Catal A Gen* 476:158–174. doi: 10.1016/j.apcata.2014.02.035
72. Tan Y, Xie H, Cui H, et al. (2005) Modification of Cu-based methanol synthesis catalyst for dimethyl ether synthesis from syngas in slurry phase. *Catal Today* 104:25–29. doi: 10.1016/j.cattod.2005.03.033
73. Fiedler E, Grossmann G, Keresbohm DB, et al. (2005) Methanol. *Ullman's Encycl. Ind. Chem.*
74. Gmbh T, Specifications Q, Range P (2010) Polyoxymethylenes. *Ullmann's Encycl. Ind. Chem.*

75. Lumpp B, Rothe D, Pastötter C (2011) Oxymethylenether als Dieselkraftstoffzusätze der Zukunft. *Mot ...* 198–203.
76. Burger J, Siegert M, Ströfer E, Hasse H (2010) Poly(oxymethylene) dimethyl ethers as components of tailored diesel fuel: Properties, synthesis and purification concepts. *Fuel* 89:3315–3319. doi: 10.1016/j.fuel.2010.05.014
77. Reuss G, Disteldorf W, Gamer AO, Hilt A (2012) Formaldehyde. *Ullmann's Encycl* 73–198. doi: 10.1002/14356007.a11
78. Prado NT, Nogueira FGE, Nogueira AE, et al. (2010) Modified niobia as a new catalyst for selective production of dimethoxymethane from methanol. *Energy and Fuels* 24:4793–4796. doi: 10.1021/ef100876k
79. Burger J, Hasse H (2013) Multi-objective optimization using reduced models in conceptual design of a fuel additive production process. *Chem Eng Sci* 99:118–126. doi: 10.1016/j.ces.2013.05.049
80. Burger J, Ströfer E, Hasse H (2013) Production process for diesel fuel components poly(oxymethylene) dimethyl ethers from methane-based products by hierarchical optimization with varying model depth. *Chem Eng Res Des* 91:2648–2662. doi: 10.1016/j.cherd.2013.05.023
81. Burger J, Ströfer E, Hasse H (2012) Chemical equilibrium and reaction kinetics of the heterogeneously catalyzed formation of poly(oxymethylene) dimethyl ethers from methylal and trioxane. *Ind Eng Chem Res* 51:12751–12761. doi: 10.1021/ie301490q
82. Xiaolong Fang, Chen J, Ye L, et al. (15AD) Efficient Synthesis of poly(oxymethylene) dimethyl ethers over PVP-stabilized heteropolyacids through self-assembly. *Sci China Chem* 58:131–138.
83. Schwaiger N (2011) Reaktionstechnische Analyse für die Optimierung der Flüssigphasenpyrolyse. Technische Universität Graz
84. Ignatowitz, Eckhard (2015) *Chemietechnik*.
85. Bridgwater AV, Meier D, Radlein D (1999) An overview of fast pyrolysis of biomass. *Org Geochem* 30:1479–1493. doi: 10.1016/S0146-6380(99)00120-5
86. Lédé J, Broust F, Ndiaye F-T, Ferrer M (2007) Properties of bio-oils produced by biomass fast pyrolysis in a cyclone reactor. *Fuel* 86:1800–1810. doi: 10.1016/j.fuel.2006.12.024
87. Fahmi R, Bridgwater A, Donnison I (2008) The effect of lignin and inorganic species in biomass on pyrolysis oil yields, quality and stability. *Fuel* 87:1230–1240. doi: 10.1016/j.fuel.2007.07.026
88. Meier D, Faix O (1999) State of the art of applied fast pyrolysis of lignocellulosic materials—a review. *Bioresour Technol* 68:71–77. doi: 10.1016/S0960-8524(98)00086-8
89. Huber GW, Iborra S, Corma A (2006) Synthesis of transportation fuels from biomass: chemistry, catalysts, and engineering. *Chem Rev* 106:4044–98. doi: 10.1021/cr068360d
90. Shen DK, Gu S, Bridgwater a. V (2010) Study on the pyrolytic behaviour of xylan-based hemicellulose using TG–FTIR and Py–GC–FTIR. *J Anal Appl Pyrolysis* 87:199–206. doi: 10.1016/j.jaap.2009.12.001
91. Yilgin M, Pehlivan D (2004) Poplar wood–water slurry liquefaction in the presence of formic acid catalyst. *Energy Convers Manag* 45:2687–2696. doi: 10.1016/j.enconman.2003.12.010
92. Zhong C, Wei X (2004) A comparative experimental study on the liquefaction of wood. *Energy* 29:1731–1741. doi: 10.1016/j.energy.2004.03.096
93. Scott D, Piskorz J (1982) The flash pyrolysis of aspen-poplar wood. *Can. J. Chem.* ... 60:
94. Glasner C, Robert J, Deerberg G (2010) Prozessanalyse der hydrothermalen Carbonisierung (HTC) zur Optimierung und Effizienzsteigerung. *Chemie Ing Tech* 82:1445–1455. doi: 10.1002/cite.201050302
95. Grierson S, Strezov V, Ellem G, et al. (2009) Thermal characterisation of microalgae under slow pyrolysis conditions. *J Anal Appl Pyrolysis* 85:118–123. doi: 10.1016/j.jaap.2008.10.003
96. Lehmann J, Gaunt J, Rondon M (2006) Bio-char Sequestration in Terrestrial Ecosystems – A Review. *Mitig Adapt Strateg Glob Chang* 11:395–419. doi: 10.1007/s11027-005-9006-5
97. Laird D (2008) The charcoal vision: a win–win–win scenario for simultaneously producing bioenergy, permanently sequestering carbon, while improving soil and water quality. *Agron J.* doi: 10.2134/agronj2007.0161

98. Czernik S, Bridgwater A V (2004) Overview of applications of biomass fast pyrolysis oil. *Energy & Fuels* 18:590–598. doi: Doi 10.1021/Ef034067u
99. Gerdes C (2001) *Pyrolyse von Biomasse-Abfall: Thermochemische Konversion mit dem* Dissertation. Universität Hamburg
100. García-Pérez M, Chaala A, Roy C (2002) Co-pyrolysis of sugarcane bagasse with petroleum residue. Part II. Product yields and properties. *Fuel* 81:
101. Bayerbach R (2006) *Über die Struktur der oligomeren Bestandteile von Flash-Pyrolyseölen aus Biomasse.*
102. Pucher H (2014) *Entwicklung, Design und Modellierung eines Upgrading-Prozesses biobasierter flüssiger Energieträger.* Technische Universität Graz
103. Pütün A, Uzun B, Apaydin E, Pütün E (2005) Bio-oil from olive oil industry wastes: Pyrolysis of olive residue under different conditions. *Fuel Process Technol* 87:25–32. doi: 10.1016/j.fuproc.2005.04.003
104. Zhang J, Toghiani H, Mohan D (2007) Product analysis and thermodynamic simulations from the pyrolysis of several biomass feedstocks. *Energy ...* 2373–2385.
105. Willner T (2008) *Direktverflüssigung von Biomasse am Beispiel der Entwicklungen der HAW Hamburg.* Gülzow
106. Onay O, Kockar OM (2003) Slow, fast and flash pyrolysis of rapeseed. *Renew Energy* 28:2417–2433. doi: 10.1016/S0960-1481(03)00137-X
107. Gómez a., Klose W, Wiest W (2008) Zur Pyrolyse feuchter Ölpalmschalen im indirekt beheizten Drehrohrreaktor. *Chemie Ing Tech* 80:1519–1527. doi: 10.1002/cite.200800092
108. García-Pérez M, Chaala a, Yang J, Roy C (2001) Co-pyrolysis of sugarcane bagasse with petroleum residue. Part I: thermogravimetric analysis. *Fuel* 80:1245–1258. doi: 10.1016/S0016-2361(00)00215-5
109. Yorgun S, Şensöz S, Koçkar Ö (2001) Flash pyrolysis of sunflower oil cake for production of liquid fuels. ... *Anal Appl Pyrolysis* 60:1–12.
110. Wiggers VR, Wisniewski a., Madureira L a. S, et al. (2009) Biofuels from waste fish oil pyrolysis: Continuous production in a pilot plant. *Fuel* 88:2135–2141. doi: 10.1016/j.fuel.2009.02.006
111. Pucher H, Schwaiger N, Feiner R, et al. (2014) Catalytic hydrodeoxygenation of dehydrated liquid phase pyrolysis oil. *Int J Energy Res* 38:1964–1974. doi: 10.1002/er.3205
112. Schwaiger N, Feiner R, Zahel K, et al. (2011) Liquid and Solid Products from Liquid-Phase Pyrolysis of Softwood. *BioEnergy Res* 4:294–302. doi: 10.1007/s12155-011-9132-8
113. Schwaiger N, Witek V, Feiner R, et al. (2012) Formation of liquid and solid products from liquid phase pyrolysis. *Bioresour Technol* 124:90–4. doi: 10.1016/j.biortech.2012.07.115
114. Schwaiger N, Feiner R, Pucher H, et al. (2015) BiomassPyrolysisRefinery - Herstellung von nachhaltigen Treibstoffen. *Chemie Ing Tech* n/a–n/a. doi: 10.1002/cite.201400099
115. Ritzberger J, Pucher P, Schwaiger N, Siebenhofer M (2014) The BioCRACK Process-A Refinery Integrated Biomass-to-Liquid Concept to Produce Diesel from Biogenic Feedstock. *Chem Eng Trans* 39:1189–1194.
116. Schwaiger N, Elliott DC, Ritzberger J, et al. (2015) Hydrocarbon liquid production via the bioCRACK process and catalytic hydroprocessing of the product oil. *Green Chem* 17:2487–2494. doi: 10.1039/C4GC02344G
117. Pucher H, Schwaiger N, Feiner R, et al. (2015) Biofuel production from liquid phase pyrolysis oil: A two-step HDO process. *Green Chem* 17:1291–1298. doi: 10.1039/C4GC01741B
118. Larsen J (2013) Inbicon a flexible cellulosic ethanol process. 3 *Int. Conf. Lignocellul. Ethanol.* p 19
119. Biermann C (1996) *Handbook of Pulping and Papermaking.* Academic Press
120. Ek M, Gellerstedt G, Henriksson G (2009) *Pulp and Paper Chemistry and Technology Volume 2. Pulping Chemistry and Technology.*
121. Kirwan MJ *Handbook of Paper and Paperboard.*
122. Schwaiger N (2014) *VU - Recycling TU Graz.* Graz
123. Shao L, Qiu JH, Feng HX, et al. (2009) Structural investigation of lignosulfonate doped polyaniline. *Synth Met* 159:1761–1766. doi: 10.1016/j.synthmet.2009.05.022

124. AG L (2015) <http://www.lenzing.com/co-products/produkte-lenzing/furfural.html>. Web Page 1.
125. Kanzler W, Schedler J (1983) Method for the recovery of Furfural, acetic acid and formic acid. 5.
126. Sixta H (1986) Zellstoffherstellung und Recycling von Roh- und Hilfsstoffen nach dem Lenzinger Mg-Bisulfitverfahren. Lenzinger Berichte 61:
127. Volvo (2009) The bio-DME Project - From Wood to Wheel. http://www.chemrec.se/admin/UploadFile.aspx?path=/UserUploadFiles/DME Folder_090914 Volvo.pdf.
128. Iogen Corporation (2014) Cellulosic Ethanol Process. <http://www.iogen.ca/technology/cellulosic-ethanol.html>.
129. Harmsen P, Huijgen W, Bermudez L, Bakker R (2010) Literature review of physical and chemical pretreatment processes for Lignocellulosic biomass.
130. Pan X, Arato C, Gilkes N, et al. (2005) Biorefining of softwoods using ethanol organosolv pulping: preliminary evaluation of process streams for manufacture of fuel-grade ethanol and co-products. *Biotechnol Bioeng* 90:473–81. doi: 10.1002/bit.20453
131. Xia S, Baker G a, Li H, et al. (2014) Aqueous Ionic Liquids and Deep Eutectic Solvents for Cellulosic Biomass Pretreatment and Saccharification. *RSC Adv* 4:10586–10596. doi: 10.1039/C3RA46149A
132. Lindorfer J, Steinmüller H, Jäger A, et al. (2010) Untersuchung der Vorhydrolyse von lignocellulosehaltigen Rohstoffen mittels Steam Explosion. *Chemie-Ingenieur-Technik* 82:1169–1176. doi: 10.1002/cite.201000057
133. Larsen J, Haven MØ, Thirup L (2012) Inbicon makes lignocellulosic ethanol a commercial reality. *Biomass and Bioenergy* 46:36–45. doi: 10.1016/j.biombioe.2012.03.033
134. Crescentino (2013) A NEW ERA BEGINS Crescentino World's first advanced biofuels facility. 12.
135. ABENGOA Corporate Presentation (2013) Corporate presentation.
136. Evans G (2007) International Biofuels Strategy Project.
137. Kleinert TN (1971) Organosolv pulping and recovery. US Pat 3,585,104 1–6.
138. Kleinert TN (1974) Der Alkohol-Organosolv-Aufschluss des Holzes. *Das Österreichische Pap* 11:14–19.
139. Peter W, Hoglinger O (1986) Herstellung von Kunstfasern nach dem Organosolv-Aufschlussverfahren. Lenzinger Berichte
140. Michels J (2014) Verbundvorhaben Lignocellulose-Bioraffinerie (Phase 2) - Aufschluss lignocellulosehaltiger Rohstoffe und vollständige stoffliche Nutzung der Komponenten.
141. Fackler K, Ters T, Ertl O (2013) PREPARATION OF LIGNIN. 2611820:2611820.
142. Muurinen ESA (2000) ORGANOSOLV PULPING A review and distillation study related to peroxyacid pulping. ESA MUURINEN
143. Jimenez L, Maestre F, De la Torre M, Perez I (1997) Organosolv pulping of wheat straw by use of methanol water mixtures. *Tappi* 80:148–154.
144. Miranda I, Pereira H (2002) Kinetics of ASAM and kraft pulping of eucalypt wood (eucalyptus globulus). *Holzforschung* 56:85–90. doi: 10.1515/HF.2002.014
145. Brethauer S, Wyman CE (2010) Review: Continuous hydrolysis and fermentation for cellulosic ethanol production. *Bioresour Technol* 101:4862–4874. doi: 10.1016/j.biortech.2009.11.009
146. Singh R, Shukla A, Tiwari S, Srivastava M (2014) A review on delignification of lignocellulosic biomass for enhancement of ethanol production potential. *Renew Sustain Energy Rev* 32:713–728. doi: 10.1016/j.rser.2014.01.051
147. Kosaric N, Duvnjak Z, Farkas A, et al. (2012) Ethanol. *Ullmann's Encyclopedia Ind. Chem.* pp 334–397
148. Hahn H-D, Dämbkes G, Rupprich N, Bahl H (2012) Butanols. *Ullmann's Encyclopedia Ind Chem* 100 C:417–428. doi: 10.1002/14356007.a04_463.pub2
149. Rajagopalan G, He J, Yang KL (2014) Direct fermentation of xylan by *Clostridium* strain BOH3 for the production of butanol and hydrogen using optimized culture medium. *Bioresour Technol* 154:38–43. doi: 10.1016/j.biortech.2013.11.094

150. Ni Y, Sun Z (2009) Recent progress on industrial fermentative production of acetone-butanol-ethanol by *Clostridium acetobutylicum* in China. *Appl Microbiol Biotechnol* 83:415–423. doi: 10.1007/s00253-009-2003-y
151. Kujawska A, Kujawski J, Bryjak M, Kujawski W (2015) ABE fermentation products recovery methods—A review. *Renew Sustain Energy Rev* 48:648–661. doi: 10.1016/j.rser.2015.04.028
152. Cascone R (2008) A Replacement for Bioethanol ? *Chem Eng Prog* 104:4–9.
153. García V, Pääkilä J, Ojamo H, et al. (2011) Challenges in biobutanol production: How to improve the efficiency? *Renew Sustain Energy Rev* 15:964–980. doi: 10.1016/j.rser.2010.11.008
154. Qureshi N, Blaschek HP (2001) Recent advances in ABE fermentation: hyper-butanol producing *Clostridium beijerinckii* BA101. *J Ind Microbiol Biotechnol* 27:287–291. doi: 10.1038/sj.jim.7000114
155. Akhtar MK, Dandapani H, Thiel K, Jones PR (2014) Microbial production of 1-octanol: a naturally excreted biofuel with diesel-like properties. *Metab Eng Commun*. doi: 10.1016/j.meteno.2014.11.001
156. Huber GW, Chheda JN, Barrett CJ, Dumesic J a (2005) Production of liquid alkanes by aqueous-phase processing of biomass-derived carbohydrates. *Science* 308:1446–50. doi: 10.1126/science.1111166
157. Jakob M, Pischinger S (2010) MASSGESCHNEIDERTE KRAFTSTOFFE AUS BIOMASSE – POTENZIAL BIOGENER.
158. Geilen FM a, Engendahl B, Harwardt A, et al. (2010) Selective and flexible transformation of biomass-derived platform chemicals by a multifunctional catalytic system. *Angew Chem Int Ed Engl* 49:5510–4. doi: 10.1002/anie.201002060
159. Thananattananachon T, Rauchfuss TB (2010) Efficient production of the liquid fuel 2,5-dimethylfuran from fructose using formic acid as a reagent. *Angew Chem Int Ed Engl* 49:6616–8. doi: 10.1002/anie.201002267
160. Mascal M, Nikitin EB (2008) Direct, high-yield conversion of cellulose into biofuel. *Angew Chem Int Ed Engl* 47:7924–6. doi: 10.1002/anie.200801594
161. Xing R, Qi W, Huber GW (2011) Production of furfural and carboxylic acids from waste aqueous hemicellulose solutions from the pulp and paper and cellulosic ethanol industries. *Energy Environ Sci* 4:2193. doi: 10.1039/c1ee01022k
162. Yang J, Li N, Li S, et al. (2015) Synthesis of diesel and jet fuel range alkanes with furfural and ketones from lignocellulose under solvent free conditions. *Green Chem*. doi: 10.1039/C4GC01314J
163. Heuser B, Kremer F, Pischinger S, et al. (2013) Optimization of Diesel Combustion and Emissions with Newly Derived Biogenic Alcohols. *SAE Int*. doi: 10.4271/2013-01-2690
164. Kunkes E, Simonetti D, West R (2008) Catalytic conversion of biomass to monofunctional hydrocarbons and targeted liquid-fuel classes. *Science (80-)* 1322381:417–421.

Chapter 3

Liquid and Solid Products from Liquid-Phase Pyrolysis of Softwood

Liquid and Solid Products from Liquid-Phase Pyrolysis of Softwood

Nikolaus Schwaiger · Roland Feiner · Kerstin Zahel · Angela Pieber · Verena Witek · Peter Pucher · Edgar Ahn · Peter Wilhelm · Boril Chernev · Hartmuth Schröttner · Matthäus Siebenhofer

© Springer Science+Business Media, LLC. 2011

Abstract Lignocellulosic feed is expected to contribute significantly to production of liquified and solid combustibles in future, because of the quantity and the variety of feed material. The aim of the project is the production of high-quality biochar and a liquid energy carrier in a non-aqueous hydrocarbon-based pyrolysis system. Therefore, the pyrolytic degradation properties of wood and its building blocks glucose, cellulose, hemicellulose, and lignin were investigated during liquid-phase pyrolysis conditions. The process was carried out in a semibatch reaction vessel under isothermal conditions at various temperatures between $T=350^{\circ}\text{C}$ and $T=390^{\circ}\text{C}$. Process pressure was ambient. For optimum heat transfer, pyrolysis was carried out in a liquid heat carrier phase which provides sufficient heat capacity and high heat conductivity for isothermal operation. The interaction between heat carrier, biomass, and biomass products in the liquid and vapor phases was investigated. Liquid-phase pyrolysis is an exothermic process which produces 25–28% liquid CHO

products. The heat of reaction is -864 ± 25 kJ/kg at $T=350^{\circ}\text{C}$. To quantify products of biogenous and fossil origin, liquid products were analyzed by elemental analysis, gas chromatography, and accelerated mass spectroscopy. Solid products were analyzed by elemental analysis, electron microscopy, and accelerated mass spectroscopy.

Keywords Biochar · Biomass to liquid · Liquid heat carrier · Liquid-phase pyrolysis

Abbreviations

| | |
|---------|---|
| GC | Gas chromatograph |
| FID | Flame ionization detector |
| MS | Mass spectrometer |
| BtL | Biomass to liquid |
| SimDis | Simulated distillation with GC |
| EDX | Energy-dispersive X-ray spectroscopy |
| AMS-C14 | Accelerator mass spectroscopy to detect ^{14}C Atoms |
| IR | Infrared spectroscopy |
| SEM | Scanning electron microscopy |
| BDI | BDI-BioEnergy International AG |
| GPC | Gel permeation chromatography |
| ICP-OES | Inductively coupled plasma-optical emission spectroscopy |

Introduction

Thirty percent of European Union energy consumption is needed for traffic and mobility, and 98% of these fuels are from fossil sources [1]. The European Union wants to reduce greenhouse gas emissions due to the European Directive 2009/28/EC by 20% and raise the percentage of renewable fuels up to 10% [2]. This policy and the strategies for sustainability open a wide range of possibilities for renewable resource fuels and combustibles all over

N. Schwaiger (✉) · A. Pieber · M. Siebenhofer
Institute of Chemical Engineering, Graz University of Technology,
8010 Graz, Austria
e-mail: nikolaus.schwaiger@tugraz.at

P. Wilhelm · B. Chernev · H. Schröttner
Institute for Electron Microscopy and Graz Centre
for Electron Microscopy, Graz University of Technology,
Steyrergasse 17,
A-8010 Graz, Austria

H. Schröttner
e-mail: hartmuth.schroettner@felmi-zfe.at

R. Feiner · K. Zahel · V. Witek · P. Pucher · E. Ahn
BDI-BioEnergy International AG,
8074 Grambach/Graz, Austria

P. Pucher
e-mail: peter.pucher@bdi-bioenergy.com

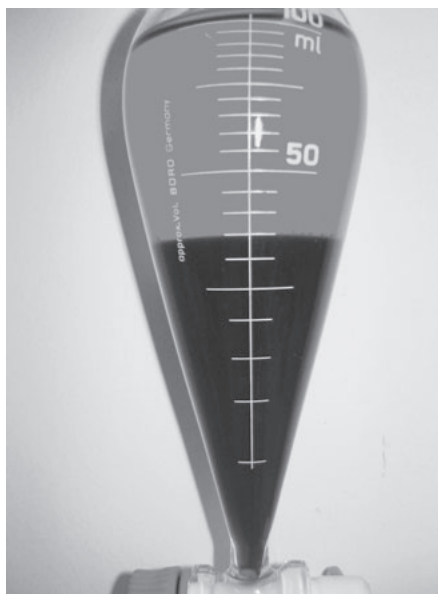


Fig. 1 Entrained heat carrier (*upper phase*) and biocrude oil (*lower phase*)

the world. BtL (biomass to liquid) can play a big role in conversion of biomass to fuels and energy carriers. Thermo-chemical conversion of biomass provides many applications in the value chain of fuels, electricity, and chemicals [3]. The number of different implementations

of BtL processes in Germany [4] and all over the world [3] is comparable with the variety of applications of BtL products [5]. Different systems concerning biomass pre-treatment, product conditioning and collecting, and reactor configuration are reported; different reactor systems have been investigated and proposed [6]. To avoid dust formation in the vapor phase and to provide high heat transfer during operation, the pyrolysis process was carried out in liquid phase. Neither does liquid-phase pyrolysis need high technical vapor biochar separation systems like in fluidized bed pyrolysis [7] nor does it demand high pressure reaction atmosphere like in hydrothermal carbonization reactors [8]. Liquid-phase pyrolysis is a KISS principle (keep it smart and simple) enabling high potential in production of biochar and biocrude oil [9].

Methods

Biomass Preparation

Feedstock for this study was bone-dry spruce wood to avoid formation of heterogeneous azeotropic mixtures of excess water and heat carrier biomass was dried for 24 h at 105°C. Pyrolysis of wood chips of different particle size of

Fig. 2 Schematic of the fed batch reactor

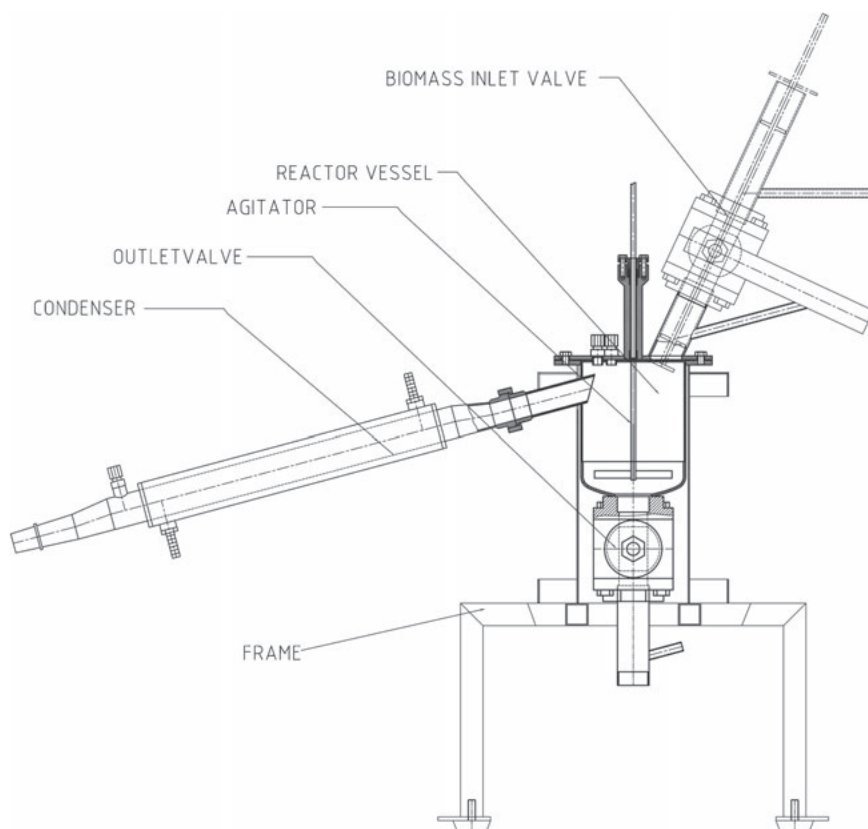
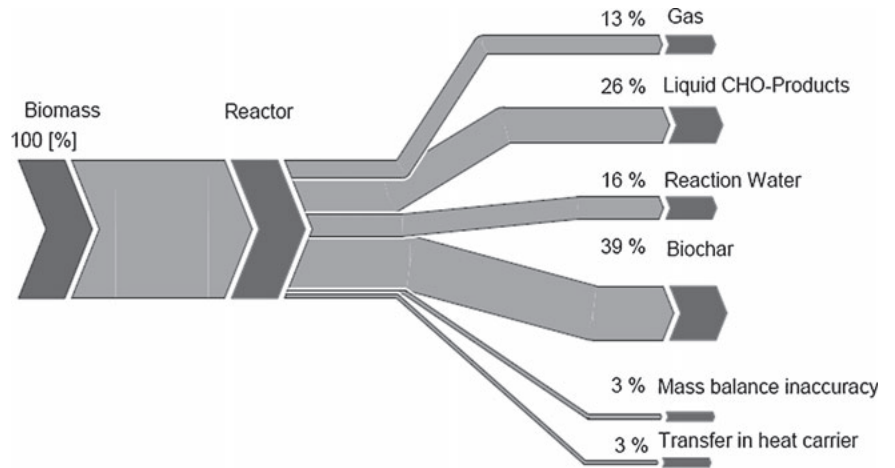


Fig. 3 Mass balance at T=350°C



10×10×10 mm, 5×5×5 mm and dust of 1–2 mm as well as dust of less than 630 μm was investigated.

System

Biomass was pyrolyzed in a liquid heat carrier at ambient pressure. The mass ratio was five parts of heat carrier to one part of biomass. Liquid heat carrier provides sufficient heat conductivity ~0.100 W/mK at T=350°C and high heat capacity of ~2.4 kJ/kgK at T=350°C for isothermal operation of semibatch pyrolysis. Heat carrier is a mixture of *n*-alkanes, with a boiling range between 410°C and 440°C. The total amount of heat carrier in the reaction vessel was 500 g. After 1 h and 20 min of preheating, the reactor temperature (350–390°C) was obtained. The 16.6 g of biomass was then added six times every 5 min under nearly isothermal operation conditions. The temperature fluctuated ±2°C during metering of biomass. Products of liquid-phase pyrolysis are non-condensibles, biocrude oil, and biochar. During pyrolysis, the biocrude oil is entrained with heat carrier because of formation of heterogeneous azeotropes due to limited

miscibility of biocrude oil, water, and heat carrier, as shown in Fig. 1.

Reactor Design

The reactor was designed according to the needs of semibatch operation. The schematic is shown in Fig. 2. Biomass was added through a 40-mm ball-type inlet valve. The heat carrier was agitated by a stirrer at 150 rpm. All condensables were condensed in a water-cooled heat exchanger. Vapor temperature at the condenser outlet was set at T~15°C. Inert atmosphere was provided by two nitrogen purge lines. The temperature was controlled in the liquid heat carrier phase, in the vapor phase above the heat carrier at the condenser inlet, and at the end of the condenser, the temperature was recorded.

Analytics

The gas amount was measured by a red-y gas flow meter (Vögtlin). Gas composition was measured with a Hartmann+ Braun advance Optima infrared and thermal conductivity

Fig. 4 Heat carrier mass balance at T=350°C

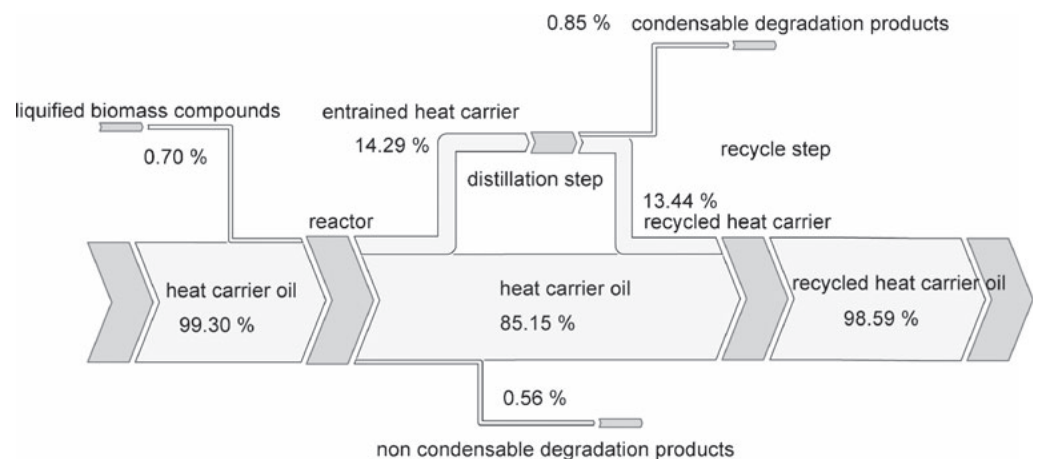
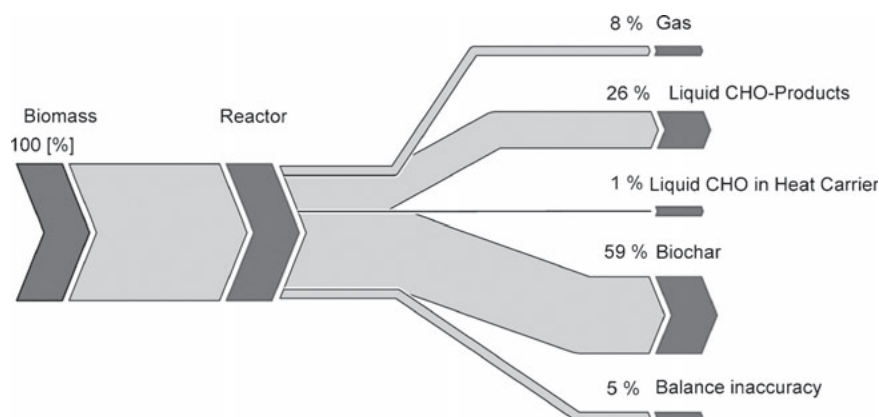


Fig. 5 Carbon balance at T=350°C

measurement system and an AC Hi-Speed RGA GC (gas chromatograph) system (DIN 51666 approved), supplied by ASG Analytik-Service Gesellschaft.

All liquid and solid products and educts were characterized by elemental analysis with a Vario macro from Elementar Analysensysteme in Carbon, Nitrogen and Hydrogen mode. Liquid products were measured by gas chromatography-mass spectroscopy (GC-MS) 5890 Series from Hewlett Packard with a WCOT fused silica 30 m low bleed column. Heat carrier and entrained heat carrier were determined with a gas chromatograph-SimDis MXT 2887, 10 m column from Restek and Agilent 7890A GC. Water was measured with Titro Line Karl Fischer system from Schott. Molecule size distribution in biocrude oil was determined with gel permeation chromatography (GPC) on three separation columns with 500, 100, and 50 Å pore size from Polymer Standards Service (5 µm, 8×300 mm columns); signals were detected with a refractometer/viscometer from Viscotek. The pH was measured with a pH-meter from Orion. Heat carrier and biochar were separated by filtration in a first step and in a second step solid/liquid extraction with hexane in a Soxhlett apparatus for 24 h. Transfer of fossil carbon between the heat carrier and Biomass products was controlled with an AMS, following the ASTM-D6866 method supported by Beta Analytic Inc. Biochar was IR (infrared) characterized with a Bruker Hyperion by Graz

Center of Electron Microscopy. EDX (energy-dispersive X-ray spectroscopy) and SEM (scanning electron microscopy) photos were done with a FEI Quanta 200 ESEM and an EDAX Genesis EDX System by Graz Center of Electron microscopy. Element screening with ICP-OES and microwave-assisted sample decomposition was done by TU Graz Institute of Analytical Chemistry and Food Chemistry with a Spectro Ciros Vision EOP.

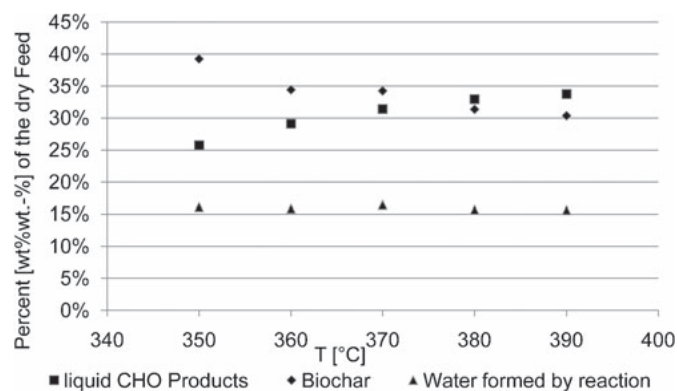
Results

Balances

During liquid-phase pyrolysis, lignocellulosic biomass is transferred into biocrude oil, which consists of water and liquid CHO products. Due to its polar nature, biocrude oil is nearly fully separable into its two main compounds, water and organics, by distillation. Biochar is the solid residue of liquid-phase pyrolysis. Figure 3 shows the mass balance of liquid-phase pyrolysis. The balance inaccuracy of 3 wt.% is mainly caused by dissolution of liquid-CHO products in the heat carrier which is evaporated. The heat carrier cycle is shown in

Table 1 Comparison between torrefaction, slow pyrolysis, and liquid-phase pyrolysis

| | Torrefaction [16] | Slow pyrolysis [17] | Liquid phase pyrolysis |
|---------------------|-------------------|---------------------|------------------------|
| Temperature | 300°C | 300°C | 350°C |
| Char [wt.%] | 60.8 | 66.8 | 39 |
| Liquid yield [wt.%] | 28 | 28 | 42 |
| Gas [wt.%] | 11.2 | 5.2 | 13 |

**Fig. 6** Effect of temperature on liquid-phase pyrolysis

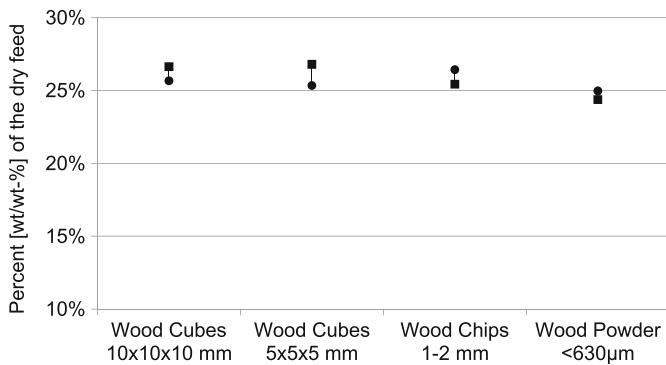


Fig. 7 Liquid CHO-product formation depending on particle size at T=350°C

Fig. 4. The first step of the cycle is liquid-phase pyrolysis. During this process, about 3 wt.% of the biomass is dissolved in the heat carrier. Some heat carrier is evaporated because of formation of a heterogeneous azeotrope with water. About 1.4 wt.% of the heat carrier is cleaved to form non-condensable hydrocarbon volatiles and condensable hydrocarbons. These condensables mainly consist of alkanes and alkenes.

Degradation products dissolved in the heat carrier were identified to mainly consist of 2-methyl-furan, 2,5-dimethylfuran, 2-methoxyphenol, 2-methoxy-4-methylphenol, 4-ethyl-2-methoxyphenol, 2-methoxy-4-(2-propenyl)-phenol, 2-methoxy-4-propylphenol, 2-methoxy-4-(1-propenyl)-phenol. While 2-methyl-furan and 2,5-dimethylfuran originates in degradation carbohydrates, the majority of substances are formed through degradation of lignin sources like conyferyl alcohol.

Within the selected range of operation temperature, most carbon remains in the biochar, which is the target product of liquid-phase pyrolysis below T=400°C. Based on the hydrocarbon balance, the transfer of biomass into the heat carrier does not exceed 3 wt.%. The carbon balance of biogeneus carbon in Fig. 5, deduced from C¹⁴-analysis, confirms that, at least 1 wt.% of biogeneus carbon feed dissolves in the heat carrier.

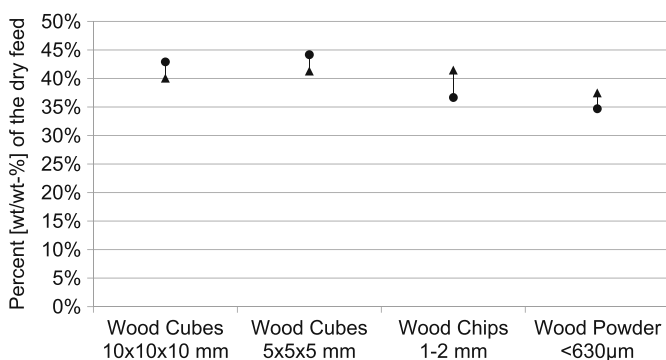


Fig. 8 Biochar formation depending on particle size at T=350°C

Table 2 Composition of liquid-phase pyrolysis gas

| Gas | [Vol. %] |
|----------------------------------|----------|
| Carbon dioxide | 46 |
| Carbon monoxide | 33 |
| Nitrogen | 14 |
| Methane | 2 |
| Oxygen | 2 |
| Hydrogen | 0.5 |
| Other volatile organic compounds | 2 |

The transfer of biogeneus carbon into biochar makes liquid-phase pyrolysis more comparable with low-temperature processes like torrefaction and slow pyrolysis rather than fast or flash pyrolysis. Table 1 shows the product distribution of different pyrolysis processes.

Influence of Operation Temperature on Product Distribution

As expected [5], elevated temperature in the temperature range between 350°C and 390°C leads to rising liquefaction and decreasing amount of biochar as shown in Fig. 6. The carbon content of biochar as well as the amount of biocrude oil increases. Formation of water is not affected. Unfortunately, the heat carrier is not stable at temperatures above 350°C. The rate of carrier oil degradation rises exponentially with rising temperatures. The degradation mechanism follows strictly Arrhenius law with an activation energy=171 kJ/mol and a frequency factor of $1.02 \times 10^9 (g < C_{20}) / (gHC \cdot s)$.

Influence of Particle Size on Liquid-Phase Pyrolysis

Particle size of less than 10 mm shows a weak influence on formation of biochar and biocrude oil as well as on the composition of products. The effect of particle size on product distribution is shown in Figs. 7 and 8. Neither biocrude oil formation nor biochar formation

Table 3 Comparison of liquid-phase pyrolysis biocrude composition with literature [10]

| Parameter | Liquid-phase pyrolysis | Fluidized bed reactor [10] |
|----------------------------|------------------------|----------------------------|
| Yield (wt.%) | 42 | 75 |
| Water (%) | 39 | 20 |
| C (wt.%) | 31.5 | 55 |
| H (wt.%) | 8.5 | 7 |
| High heating value (MJ/kg) | 11.6 | 20 |

Table 4 Inorganic load of biocrude

| Element | [g/kg] |
|---------|--------|
| Ca | <0.15 |
| K | <0.06 |
| Na | <0.05 |
| S | <0.15 |
| Si | <0.13 |

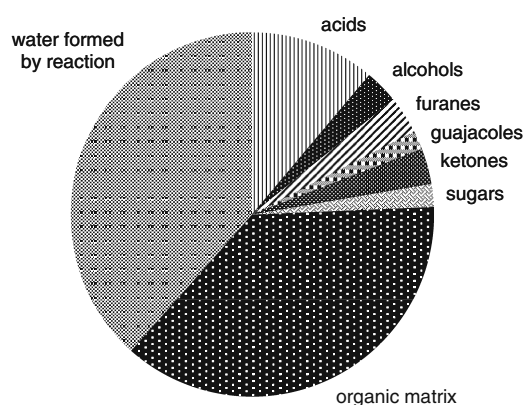
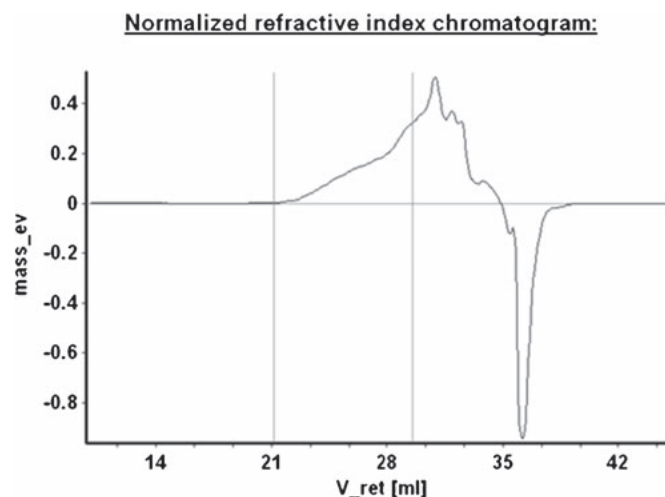
shows a significant dependence of the particle size. From these findings, one may conclude that the penetration length of the feed does not have an effect on the quality of products. Less biochar formation from small particles was rather caused by solid/liquid separation than by particle size.

Gaseous Products

Main components of the pyrolysis gas (the gaseous phase after separation of condensibles at $T=15^{\circ}\text{C}$) are carbon dioxide, carbon monoxide, nitrogen, and methane. A detailed list of the gas mixture is shown in Table 2. The source of nitrogen and oxygen in the system is biomass, which was deaerated with nitrogen before metering. The gas contains 2% of volatile organics with 0.5 vol.% of hydrocarbons with more than six carbon atoms, mainly from degradation of the heat carrier.

Liquid Products

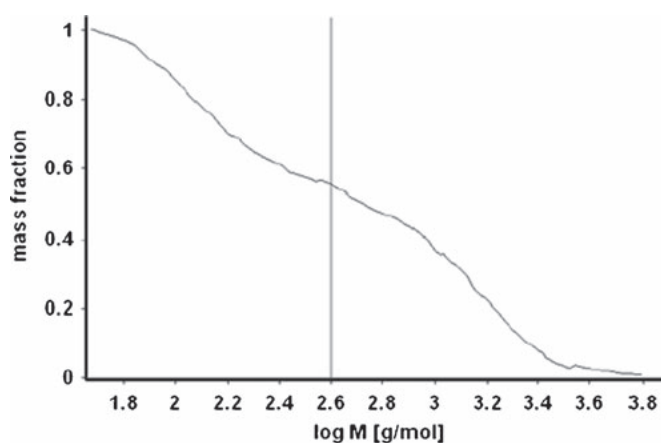
Liquid-phase pyrolysis biocrude oil is “light biocrude oil” compared with flash pyrolysis biocrude oil [10] in Table 3. As a result of preferred biochar formation, less biomass is transferred into liquid products, explaining elevated water content and low carbon contents.

**Fig. 9** Biocrude oil main substance classes**Fig. 10** GPC chromatogram of liquid-phase pyrolysis-based biocrude oil

Biocrude oil from fluidized bed reactor pyrolysis is particle-loaded [11], a major disadvantage which is not observed in liquid-phase pyrolysis. All liquid products are completely ethanol-soluble. Without separation steps for ash and char particles, biocrude oil from flash pyrolysis can carry up to 500 ppm sodium and potassium and up to 600 ppm calcium [12]. In liquid-phase pyrolysis particulate matter is trapped in the liquid heat carrier inside the reactor, the reason for low inorganic compounds in the unfiltered and untreated biocrude oil, shown in Table 4.

Figure 9 shows the main constituent classes of biocrude oil, including the organic matrix, which is made up of oligomers [13]. GPC gives the approximate size of non GC-MS detectables. The molar mass of $M_w=400$ g/M compares well with carbohydrate di- and trimers, as shown in Figs. 10 and 11.

As shown in Fig. 7, biomass particle size does not affect formation of biocrude oil nor does it affect the composition

**Fig. 11** Detail of GPC chromatogram with a M_w of 400 g/M

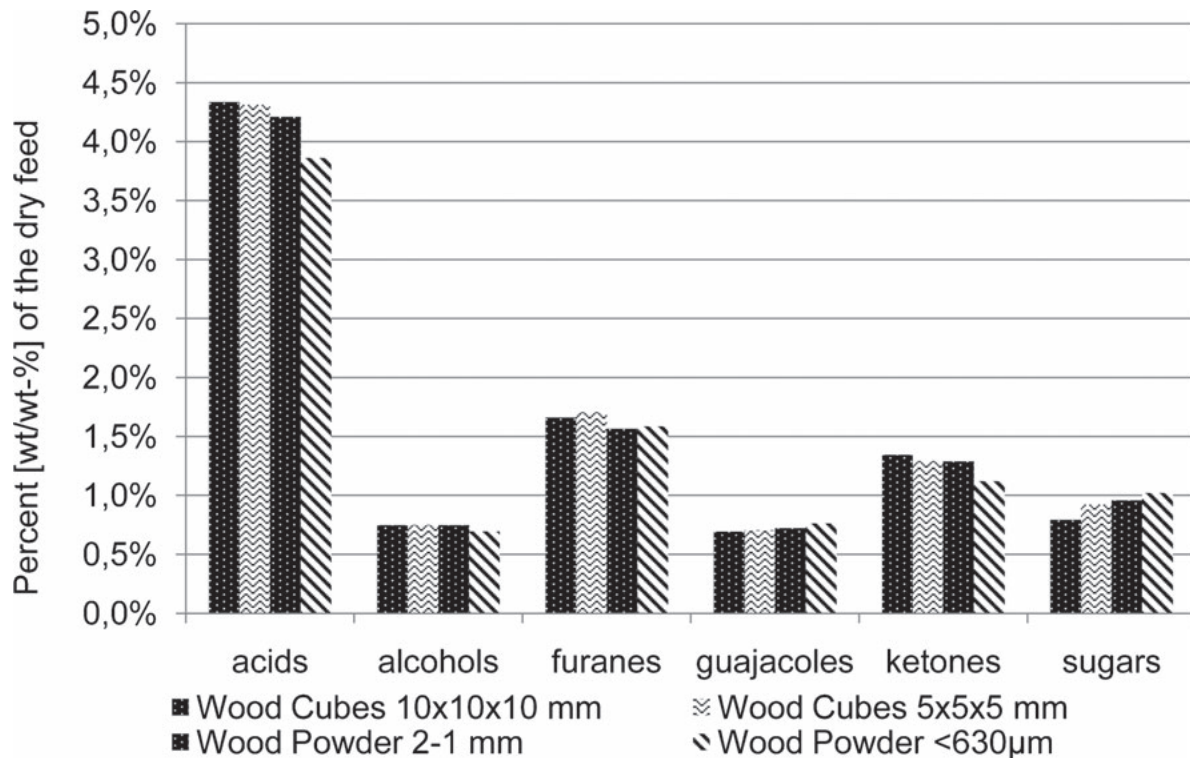


Fig. 12 Effect of particle size on composition of biocrude oil

of biocrude oil, as shown in Fig. 12. The total amount of acids decreases while the residual amount of sugar is observed when particle size is decreased.

Solid Product

As shown in Fig. 5, carbon is mainly transferred into biochar during liquid-phase pyrolysis. Table 5 shows the transfer of elements from feed to the solid residue during liquid-phase pyrolysis. An increase in temperature from $T=350^{\circ}\text{C}$ to $T=390^{\circ}\text{C}$ does not increase the relative amount of carbon in the residue. The total amount of biochar decreases with increasing temperature. During liquid-phase pyrolysis, the upper heating value of solids rises from 18.9 MJ/kg (biomass) to 27.3 MJ/kg (biochar) at

Table 5 Elemental analysis of biomass and biochar

| Compound | Biomass [wt.%] | Biochar [wt.%] |
|----------|----------------|----------------|
| Carbon | 49.5 | 75.3 |
| Hydrogen | 6.5 | 5.2 |
| Nitrogen | 0.1 | 0.5 |
| Oxygen | 43.8 | 18.5 |
| Ash | 0.2 | 0.6 |

$T=350^{\circ}\text{C}$. The calorific value of biochar is comparable with the calorific value of bituminous coal [14].

The IR-spectrum of biochar and lignite tar pitch are well comparable. As shown in Fig. 13, structures and functional groups compare well with lignite tar pitch. Lower sulfur content improves significantly to mean quality of fossil coal. Bituminous coal has 1.5 wt.% sulfur, whereas the sulfur content of biochar is <0.02 wt.%.

SEM photographs in Figs. 14 and 15 show the structure of biochar from softwood after liquid-phase pyrolysis. While hemicelluloses and celluloses seemingly got pyrolyzed, the high-temperature-resistant lignin frame keeps almost stable. Toledano et al. showed that ultrafiltered lignin degrades at about 400°C during thermogravimetric analysis [15]. Below 400°C , lignin does not undergo liquefaction; shrinking and carbonization processes are observed. EDX analysis through the whole longitudinal section, shown in Fig. 16, showed the same C-to-O ratio at every point in the two-dimensional framework. From constant C-to-O ratio, constant pyrolysis of the whole particle is concluded.

Discussion

Liquid-phase pyrolysis is an adequate technology to produce high-value biochar and biocrude oil within a

Fig. 13 IR spectroscopy of biochar (black lower line) and lignite [18]

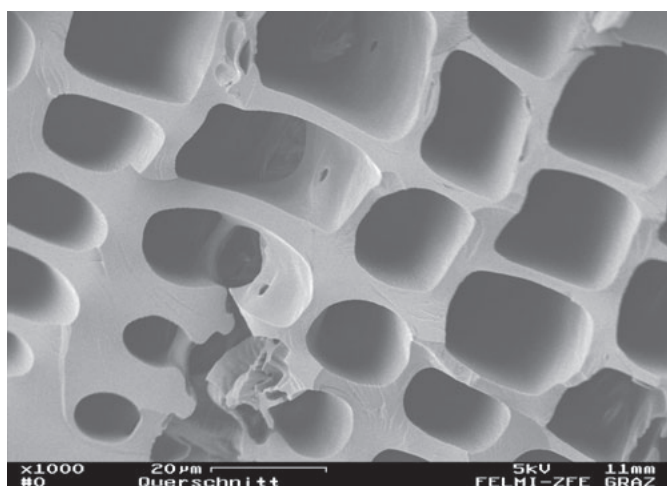
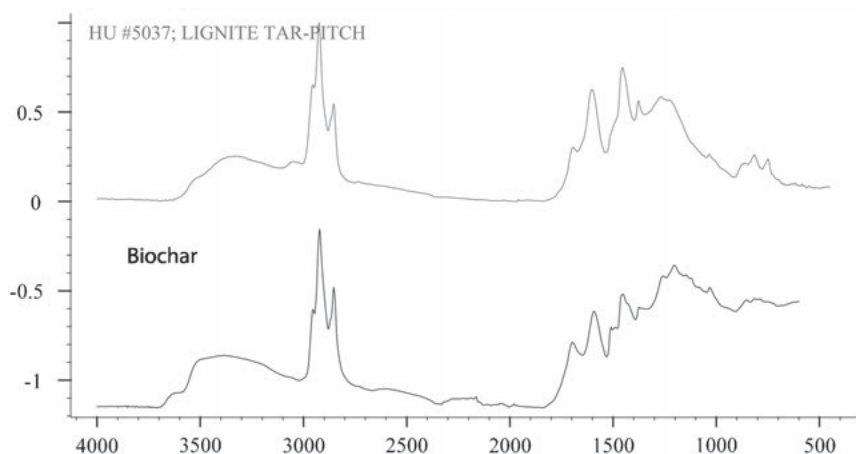


Fig. 14 Biochar cross section

short contact time and therefore cost of operation. Biochar formed through liquid-phase pyrolysis is a high-quality product with a broad field of industrial applications, including gasification, metallurgical applications, as well as production of value-added products in the chemical industry. Biocrude oil can be easily processed to obtain ready-for-market product quality. A major advantage of liquid-phase pyrolysis compared with fluidized bed processes is the simple energy management due to liquid-phase heat transfer, and dust-free operation. In comparison with high-temperature pyrolysis, the limitation of solids conversion according to the temperature limit of approximately $T=400^{\circ}\text{C}$ has to be mentioned.

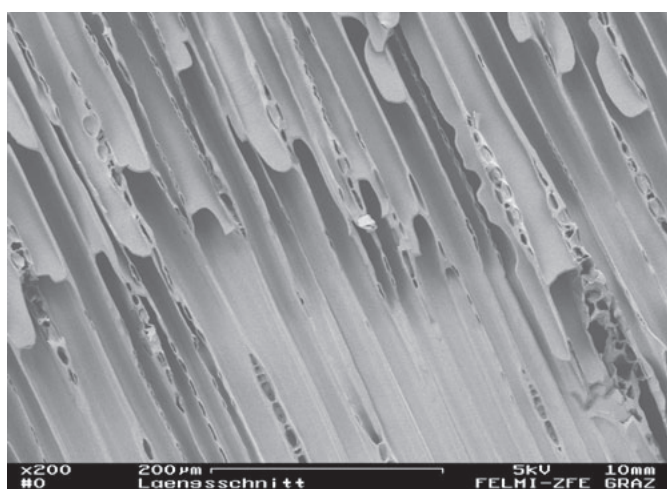


Fig. 15 Biochar longitudinal section structure

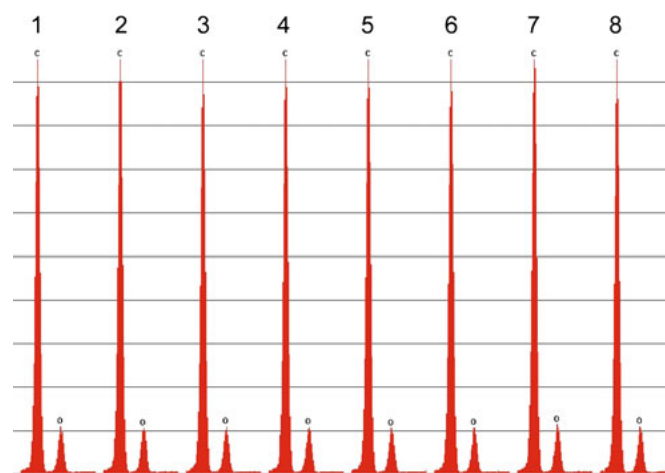


Fig. 16 EDX of liquid-phase pyrolysis biochar in a longitudinal section

Acknowledgment This project is supported by the Austrian climate- and-energy funds within the “Energy of the Future” program.

References

1. DG Research, EUR 22066, Biofuels in the EU, a vision for 2030 and beyond. (2006) Final draft report of the Biofuels Research Advisory
2. EU-Directive 2009/28/EC (2009) Promotion of the use of energy from renewable sources. Official Journal of the EU, L140/1
3. Bridgwater AV, Peacocke GVC (2000) Fast pyrolysis processes for biomass. *Renew Sustain Energy Rev* 4:1–73
4. Behrendt F et al (2006) Direktverflüssigung von Biomasse-Reaktionsmechanismen und Produktverteilung 114-50-10-0337/05-B. Bundesanstalt für Landwirtschaft und Ernährung, Berlin
5. Bridgwater A et al (1999) An overview of fast pyrolysis of biomass. *Org Geochem*, S. 1479–1493
6. Kaminsky W (1989) Pyrolyse von biomasse. *Chem Ing Tech* 61 (10):775–782
7. Mohan D et al (2006) Pyrolysis of wood/biomass for bio-oil: a critical review. *Energy Fuels* 20(3):848–889
8. Bockhorn H et al (2010) Hydrothermale carbonisierung von biomassen. *Chemie Ingenieur Technik* 82(9):1314
9. Witek V (2009) Process design data for liquid phase pyrolysis of biogenic feedstock. AIChE Annual Meeting. Nashville
10. Meier D et al (1999) State of the art of applied fast pyrolysis of lignocellulosic materials—review. *Bioresour Technol* 68:71–77
11. Lédé J et al (2007) Properties of bio-oils produced by biomass fast pyrolysis in a cyclone reactor. *Fuel* 86(12–13):1800–1810
12. Oasmaa A, Czernik S (1999) Fuel oil quality of biomass pyrolysis oil state of the art for the end users. *Energy Fuels* 13(4):914–921
13. Bayerbach B (2006) Über die Struktur der oligomeren Bestandteile von Flash-Pyrolyseölen aus Biomasse. Dissertation. Hamburg
14. Crelling J et al (2010) Ullmann’s Encyclopedia of Industrial Chemistry. Wiley-VCH Verlag GmbH & Co, KGaA
15. Toledano A et al (2010) Lignocellulosic biorefinery approach: a challenge for a new world. Prague Pres 2010 Poster Presentation
16. Prins MJ, Ptasinski KJ, Janssen FJJG (2006) More efficient biomass gasification via torrefaction. *Energy* 31(15):3458–3470
17. Williams PT, Besler S (1996) The influence of temperature and heating rate on the slow pyrolysis of biomass. *Renew Energy* 7 (3):233–250
18. Hummel et al. (1969) Infrared analysis of polymers, resins and additives. An Atlas, vol. 1

Chapter 4

Formation of liquid and
solid products from liquid
phase pyrolysis



Formation of liquid and solid products from liquid phase pyrolysis

N. Schwaiger^{a,*}, V. Witek^b, R. Feiner^a, H. Pucher^a, K. Zahel^b, A. Pieber^b, P. Pucher^b, E. Ahn^b, B. Chernev^c, H. Schroettner^c, P. Wilhelm^c, M. Siebenhofer^a

^aInstitute of Chemical Engineering, Graz University of Technology, Inffeldgasse 25/C, 8010 Graz, Austria

^bBDI-BioEnergy International AG, Parkring 18, 8074 Grambach/Graz, Austria

^cInstitute for Electron Microscopy, Graz University of Technology, Steyrergasse 17, 8010 Graz, Austria

HIGHLIGHTS

- ▶ Liquid phase pyrolysis is a process dedicated to biochar and biocrudeoil production.
- ▶ The process is not very sensitive to particle size.
- ▶ During pyrolysis the lignin frame stays almost substantially stable.
- ▶ Lignin frame undergoes just sintering and shrinking.
- ▶ Liquid and solid product formation is almost finished after 800 s.

ARTICLE INFO

Article history:

Received 4 May 2012

Received in revised form 25 July 2012

Accepted 26 July 2012

Available online 17 August 2012

Keywords:

Biochar

Biomass to liquid

Liquid heat carrier

Liquid phase pyrolysis

ABSTRACT

The aim of the present work was to improve the C:O ratio in biomass by preserving the lignin macrostructure of lignocellulosic feed. The intention of liquid phase pyrolysis is to liquefy biomass and prepare biomass for further upgrading steps like hydrogenation and deoxygenation. Pyrolysis was carried out in a non-aqueous liquid phase heat carrier. The process was carried out in a semi-batch reaction vessel under isothermal conditions at $T = 350\text{ }^{\circ}\text{C}$, supported by a quench to stop reactions instantaneously in order to observe formation of solid intermediates. This pyrolysis system enables the observation of liquid and solid product formation. Transformation of biomass into biochar was analyzed by infrared spectroscopy and elemental analysis. Stable lignin structure throughout the whole transformation was confirmed. It was shown that the lignin frame in wood remains without substantial loss, while the major amount of carbohydrates is pyrolyzed during liquid phase pyrolysis at $T = 350\text{ }^{\circ}\text{C}$.

© 2012 Elsevier Ltd. All rights reserved.

1. Introduction

Despite of improved exploring and production methods, fossil fuels are obviously vanishing. OPEC (2008, 2011) discloses at the end of the year 2011 1.2 billion barrels of proven crude oil reserves, compared to 1.7 billion barrels of reserves at the end of the 1980s. This demonstrates a strong decrease of reserves and this is just a result of retarding peak oil with highly developed exploration techniques. Even though nowadays exploration is coupled with higher risks, as the Deepwater Horizon disaster showed in April 2010. Parallel to decreasing crude oil resources climate change is a global threat. To avoid rising world average temperature and to become independent of overseas energy imports the European Union (EU-Directive, 2008) wants to reduce greenhouse gas emissions according to the European Directive (2009) by 20% and raise the

percentage of renewable fuels up to 10%. To limit imports of crude oil and reduce greenhouse gasses, biofuels are a promising alternative. First generation biofuels like biodiesel and bioethanol are ready to market technologies, but with a limited range of feasibility, caused by the specific needs of energy crops. Moreover first generation biofuels are affected by negative food versus fuel discussion in mass media. To avoid this discussion biodiesel industry tries to turn feedstock from edible plants to non-edible feedstock like algae biodiesel. Open or closed pond systems for algae production are probably feasible alternatives (Tredici and Zittelli, 1998; Richmond, 2000) but at the moment there are still many obstacles to face (Früwirth, 2010).

A serious alternative to these routes to liquid fuels is the thermo-chemical conversion of lignocellulosic material. The most important reason is the availability, by ecologic treatment of this resource. "It is estimated that the total phytomass of earth is 1.24×10^{12} metric tons and 80% of which is attributed to wood. The potentially utilizable annual wood growth is 1.1×10^{10} ton"

* Corresponding author.

E-mail address: nikolaus.schwaiger@tugraz.at (N. Schwaiger).

(Nimz et al., 2000). There are two major pathways to apply liquefaction of lignocellulose. First the Fischer–Tropsch technology, which was used by “Choren GmbH” or the “Karlsruhe Institut für Technologie”. This technology is based on first step gasification of biomass to synthesis gas (Choren, 2007) or indirect biomass gasification of pyrolysis oil and biochar slurry to synthesis gas (Dinjus, 2010), coupled with Fischer–Tropsch reaction in a second step. On the one hand gasification combined with Fischer–Tropsch reaction is, with respect to the biomass feed, a highly flexible path for production of high level quality fuels (Rauch, 2010). On the other hand this technology needs enormous cost of investment.

The second path is the direct Biomass liquefaction which is well described in literature (Bridgwater et al., 1999; Meier and Faix, 1999; Carlson et al., 2008; Demirbas, 2001; Di Blasi et al., 1999; Mohan et al., 2006). There are various applications like fixed bed reactors, entrained flow reactors, rotating cone reactors mentioned in literature. The range of reaction temperature for optimum liquid product yield is between 450 and 600 °C (Huber et al., 2006). Highest liquefaction output of 75–80% is obtained with fast pyrolysis between 450 and 550 °C and a very short residence time (Bridgwater and Peacocke, 2000).

1.1. Liquid phase pyrolysis

In addition to fast pyrolysis and Fischer–Tropsch synthesis liquid phase pyrolysis is dedicated to form solid and liquid products. Products of liquid phase pyrolysis are noncondensibles, biocrude oil, and biochar. Liquid phase pyrolysis improves the C:O ratio of lignocellulose during biomass conversion, leaving the lignin frame unaffected. Liquid phase pyrolysis generates water and pyrolysis oil with low inorganics load. Operation temperature and product yield classify liquid phase pyrolysis between fast pyrolysis and torrefaction as shown in Table 1: Comparison of several pyrolysis systems; torrefaction (Prins et al., 2006), slow pyrolysis (Williams and Besler, 1996), fast pyrolysis (Gerdes, 2001) and liquid phase pyrolysis. Detailed information about liquid phase pyrolysis is reported elsewhere (Schwaiger et al., 2011).

2. Methods

2.1. Reactor design

The reactor was designed according to the needs of fed batch operation. The schematic is shown in Fig. 1. Biomass was fed through a 40 mm ball type inlet valve. Heat carrier was agitated with 150 rpm. All condensibles were condensed in a water cooled heat exchanger tube. Set point of vapor temperature at the condenser outlet was 15 °C. Inert atmosphere was provided by two nitrogen feed lines. The temperature was controlled in the liquid heat carrier phase, in the vapor phase above the heat carrier, at the condenser inlet and at the end of the condenser. For determination of kinetics a second cask was fixed at the biomass outlet valve. This cask was separately purged with nitrogen to provide inert atmosphere and it was cooled with ice water.

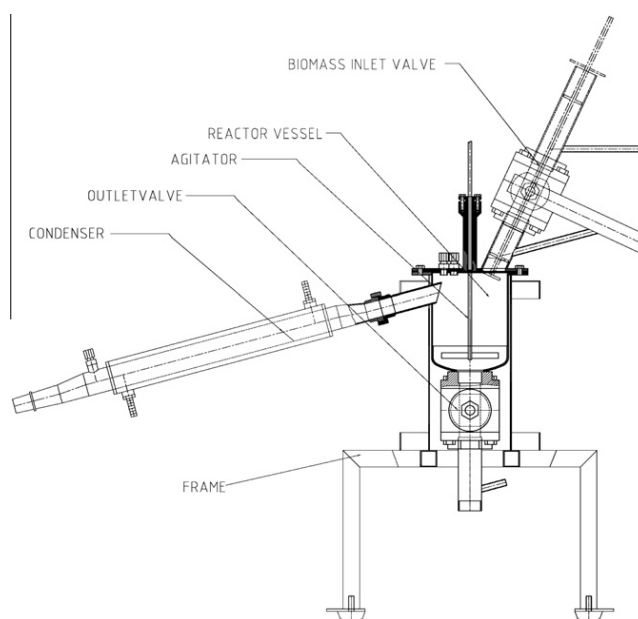


Fig. 1. Schematic of the reactor.

2.2. System

Biomass was pyrolyzed in liquid heat carrier at ambient pressure. The heat carrier was a highly hydrogenated mixture of straight long chain alkanes. Elemental composition of the heat carrier was 86% carbon and 14% hydrogen. The liquid heat carrier provided sufficient heat conductivity (~ 0.100 W/m K at $T = 350$ °C) and high heat capacity of ~ 2.4 kJ/kg K at $T = 350$ °C for isothermal operation of semibatch pyrolysis. The heat carrier was a mixture of *n*-alkanes, with a boiling range between 410 and 440 °C. The total amount of heat carrier in the reaction vessel was 500 g. After 1 h and 20 min of preheating, the reactor temperature of 350 °C was reached.

For kinetic experiments 17 g of biomass was then added under nearly isothermal operation conditions. The temperature change was ± 2 °C during metering of biomass. Due to the limited influence of particle size on liquid phase pyrolysis, wood-cubes with a diameter of 10 mm were used and the wood-cubes were cut with a band saw. Formation of liquid products was monitored by weight.

Biochar formation in the heat carrier was stopped by quenching in the ice cooled cask. An immediate drop of temperature to less than 150 °C was obtained by mixing the product with precooled heat carrier in excess.

Feedstock for kinetic experiments for this study was bone-dry spruce wood, to avoid formation of heterogeneous azeotropic mixtures of excess water and the heat carrier. Biomass, spruce wood cubes with a particle size of $10 \times 10 \times 10$ mm, was dried for 24 h at 105 °C. In a first series of experiments lignin, hemicellulose and cellulose were separately pyrolyzed. 100 g of each compound was pyrolyzed in 500 g of heat carrier. The lignin (alkali lignin

Table 1
Comparison between several pyrolysis systems.

| Parameter | Torrefaction (Prins, 2006) | Slow pyrolysis (Williams, 1996) | Fast pyrolysis in a fluidized bed reactor (Gerder, 2001) | Liquid phase pyrolysis |
|--------------------|----------------------------|---------------------------------|--|------------------------|
| Temperature [°C] | 300 | 300 | 476 | 350 |
| Liquid yield [wt%] | 28 | 28 | 67.4 | 40–44 |
| Char [wt%] | 60.8 | 66.8 | 16 | 37–40 |
| Gas [wt%] | 11.2 | 5.2 | 16.6 | 13–16 |

CAS 8068-05-1, M_w : 28000 g/mol from Sigma–Aldrich), hemicellulose (birchwoodxylan $M_{(132)_n}$ from Carl Roth GmbH) and cellulose powder (CAS 9004-34-6 from Sigma–Aldrich) were also dried for 24 h at 105 °C. The Biomass was added in six portions of 16.6 g every 5 min under nearly isothermal operation conditions. The temperature change was ± 2 °C during metering of biomass compounds. During pyrolysis biocrude oil was entrained with heat carrier because of formation of heterogeneous azeotropes due to limited miscibility of biocrude oil, water, and heat carrier.

2.3. Analytics

The gas flow rate was recorded by red-y gas flow meter (Vögtlin). Gas composition was analyzed by a Madur Photon II infrared gas analyzer for CH₄, O₂, CO and CO₂.

All liquid and solid products and educts were characterized by elemental analysis with a Vario macro CHNO-analyzer, from Elementar Analysensysteme, in CHN mode. In addition the liquid products were analyzed by GC–MS¹ 5890 Series, Hewlett Packard, with a WCOT fused silica 30 m low bleed column. The heat carrier and entrained heat carrier composition were determined with a GC–SimDis² MXT 2887, 10 m column from Restek and Agilent 7890A GC. Water was measured with GC–TCD³. After the experiment the heat carrier and biochar were separated by filtration in a first step and afterwards biochar was refined in a second step by solid/liquid extraction with hexane for 24 h in a Soxhlet apparatus. ATR–FTIR⁴ measurements of Biochar were performed by Graz Center of Electron microscopy with an Equinox 55 FTIR spectrometer, connected to a Hyperion 3000 IR microscope. The used objective was an $\times 20$ ATR-objective with germanium crystal with flattened tip (approx. 100 μ m width). ESEM⁵ Photos were taken with a FEI Quanta 200 ESEM by Graz Center of Electron microscopy.

3. Results and discussion

At 350 °C Liquid phase pyrolysis of lignocellulose provided two mayor products; pyrolysis oil and biochar. The overall mass balance was 40–44% liquids, 37–40% biochar and 13–16% gaseous products at $T = 350$ °C. At maximum 3% of liquid yield was dissolved in the liquid heat carrier. Biochar yield of liquid phase pyrolysis was rather comparable with intermediate pyrolysis reactor systems than with fast pyrolysis (Enders et al., 2012).

3.1. Formation of liquid and solid products

A first test of liquid phase pyrolysis without admixture of biomass gave a constant condensed heat carrier flow due to evaporation as shown in Fig. 2 marked as line a. The flow rate was dependent upon the ambient pressure being between 0.002 and 0.004 g_{Heat carrier}/s.

During pyrolysis, evaporable reaction products like water and liquid CHO-products formed heterogeneous azeotropes with the heat carrier. The overall liquid product stream consisted of evaporated heat carrier, azeotropic entrained heat carrier, water and liquid CHO-products. Kinetics of overall condensibles is shown in Fig. 2 line b.

By subtracting the evaporated heat carrier stream (Fig. 2 line a from Fig. 2 line b), the reaction dependent flow of azeotropic en-

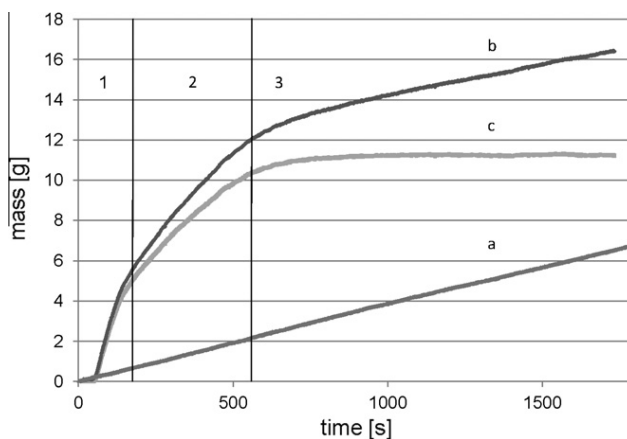


Fig. 2. Liquid product formation.

trained heat carrier, water and liquid CHO-products was isolated. Fig. 2 line c shows the kinetics of liquid product formation. From these results a three step process is proposed:

1. Dewatering in a first phase.
2. Liquid product formation in a second phase.
3. Stagnation of conversion without any further liquid product formation in a third phase.

Investigation of pyrolysis kinetics of spruce wood considered different particle size of the feed between 630 μ m and wood cubes with a lateral length of 10 mm. Rate of formation of condensibles did not show any dependency of product formation and particle size. Seemingly heat transfer to the core of particles and diffusion of degradation products from particle core to the surface was not rate limiting. Compared with other pyrolysis systems, which need smaller average particle size (DuPont et al., 2009), these results were surprising and may be explained with rate control by the transport of constituents in the heat carrier phase and the phase transfer step.

Solid product formation was monitored via elemental analysis of the carbon to oxygen ratio in biochar. Biomass carburization is shown in Fig. 3. Similar to liquid product formation, three steps of biochar formation were observed:

1. Initial phase of water discharge.
2. Carbonization and formation of condensibles.

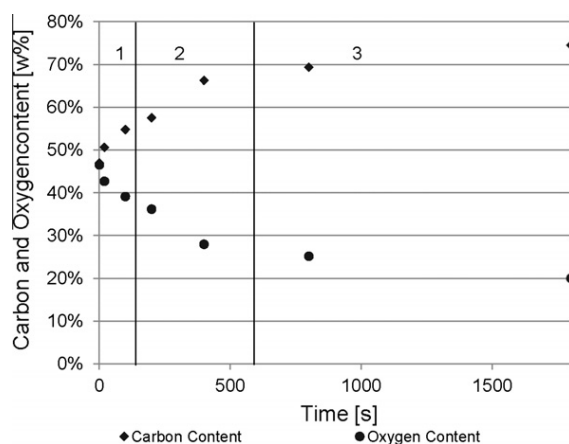


Fig. 3. Solid product formation.

¹ Thermal conductivity detector. Gas chromatography–mass spectrometry.

² Simulated distillation with GC.

³ Thermal conductivity detector.

⁴ Attenuated Total Reflection Fourier Transform Infrared Spectroscopy.

⁵ Environmental Scanning electron microscope, works on higher pressures (80–100 pa) then conventional Scanning electron microscopes, coating of samples is not necessary

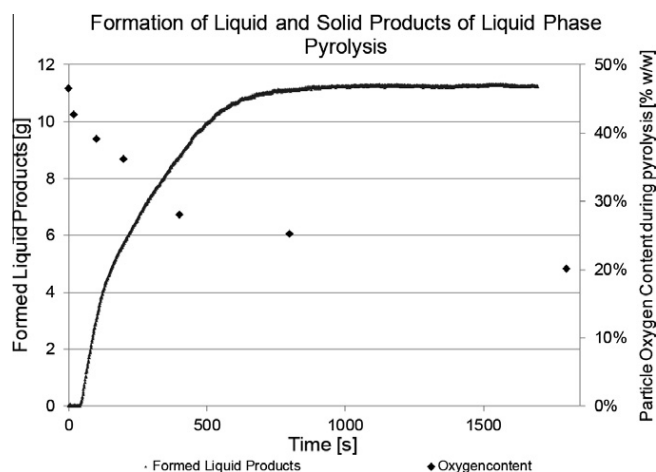


Fig. 4. Comparison of liquid and solid product formation.

3. Stagnant carbonization and formation of gaseous constituents.

While formation of condensibles was limited to phase 1 and phase 2, formation of gaseous products, preferably CO_2 , dropped but did not stop. A clear view on the process was enabled by comparing liquid and solid product formation. Fig. 4 shows a comparison of liquid and solid products. The data showed correlation of formation of biocrudeoil and oxygen decline in biomass particles, indicating, that in liquid phase pyrolysis at $T = 350^\circ\text{C}$ just oxygen rich biomass fractions were liquefied. As a consequence hemicellulose and cellulose were tending to be liquefied to a much larger extent than lignin.

To validate the proposed concept of favored carbohydrate liquefaction, ATR-IR spectra of biomass particles after distinct sequences of pyrolysis were compared. The ATR-IR spectra of native wood and after 400 s of pyrolysis do not differ significantly. As long as C–O bonds at a wavenumber of 1100 cm^{-1} (Lin-Vien, 1991) were detectable, condensibles were formed. With vanishing C–O absorption liquefaction stopped and gas formation, caused by carburetion, was the driving process. It was possible to show the isochronous decrease of the C–O stretching vibration with termination of liquid product formation. The transformation of spruce wood into biochar was observed by SEM. During the first 400 s of pyrolysis the fiber like structures of native spruce wood were identifiable. After 400 s a structural change of the surface of biomass and a breakdown of the fibrous structure was monitored. Any rough fiber-like structures were observable and the overall image was similar to the final biochar structures. The remaining wood cell structure is finally sintered with partly melted middle lamella and primary wall. During this phase of pyrolysis lignin was highly enriched (Wagenführ, 1999; Saake and Lehnen, 2000). It indicated that lignin was almost stable in native wood structures and not split into oligomer and monomer fractions under liquid phase pyrolysis conditions.

Table 2
Massbalances of compounds.

| | Liquid CHO-products (%) | Solid residua (%) | Gas (%) | Water formed by reaction (%) |
|---------------|-------------------------|-------------------|---------|------------------------------|
| Cellulose | 34 | 29 | 16 | 21 |
| Ligin | 6 | 79 | 9 | 6 |
| Hemicellulose | 16 | 44 | 21 | 19 |
| Sprucewood | 26 | 40 | 17 | 17 |

Table 3
Simulation of overall pyrolysis.

| | Liquid CHO-products (%) | Solid residua (%) | Gas (%) | Water formed by reaction (%) |
|------------------|-------------------------|-------------------|---------|------------------------------|
| Simulated spruce | 21 | 47 | 16 | 16 |
| Spruce | 26 | 40 | 17 | 17 |

Table 2 shows the comparison of products for different feed, underlining the different role of constituents under thermal charge at $T = 350^\circ\text{C}$ during liquid phase pyrolysis. Lignin was only sparingly liquefied, which matches with literature. Saikrishna et al. (2012) showed that 23% of lignin was liquefied at 500°C . TGA records showed that more than 80% of lignin was left in the solid residue at 350°C (Melligan et al., 2012).

With the results presented in Table 2 it was possible to simulate overall pyrolysis, enabling “construction” of product constituents of spruce wood. Therefore spruce wood was categorized, well specified according to literature (Nimz et al., 2000) by the three main components, lignin, hemicellulose and cellulose. Table 3 shows good accordance between simulation and experiments for water formed by reaction and the amount of gas formed during pyrolysis. These product streams originate in carbohydrate degradation as shown in Table 3. Simulation of liquid CHO-products and solid residues did not match with experiments because of minor lignin liquefaction. Seemingly lignin samples, isolated from kraft process, differ strongly from native lignin. Because of the interaction of lignin and carbohydrates in wood lignin rather tends to liquefaction than isolated lignin.

4. Conclusion

Liquid phase pyrolysis of spruce soft wood is an intermediate process, established between fast pyrolysis and torrefaction. The process is not very sensitive to particle size. Therefore intensive grinding and milling pre-treatment are not necessary for feed preparation.

During pyrolysis the lignin frame stayed almost substantially stable, sintering and shrinking was observed during carburetion.

References

- Bridgwater, A.V., Peacocke, G.V.C., 2000. Fast pyrolysis processes for biomass. *Renew. Sustain. Energy Rev.* 4, 1–73.
- Bridgwater, A.V., Meier, D., Radlein, D., 1999. An overview of fast pyrolysis of biomass. *Org. Geochem.* 30, 1479–1493.
- Carlson, T.R., Vispute, T.P., Huber, G.W., 2008. Green gasoline by catalytic fast pyrolysis of solid biomass derived compounds. *ChemSusChem* 1, 397–400.
- Choren, 2007. Choren Industries BTL-Anlage Freiberg. C.I. GmbH.
- Demirbas, A., 2001. Biomass resource facilities and biomass conversion processing for fuels and chemicals. *Energy Convers. Manage.* 42, 1357–1378.
- Di Blasi, C., Signorelli, G., Di Russo, C., Rea, G., 1999. Product distribution from pyrolysis of wood and agricultural residues. *Ind. Eng. Chem. Res.* 38, 2216–2224.
- Dinjus, E., 2010. Entwicklungs und Forschungsstand des Karlsruher bioliq-Prozesses. 4 BtL-Kongress: Berlin.
- Dupont, C., Chen, L., Cances, J., Commandre, J., Cuoci, A., Pierucci, S., Ranzi, E., 2009. Biomass pyrolysis: kinetic modelling and experimental validation under high temperature and flash heating rate conditions. *J. Anal. Appl. Pyrol.* 85, 260–267.
- Enders, A., Hanley, K., Whitman, T., Joseph, S., Lehmann, J., 2012. Characterization of biochars to evaluate recalcitrance and agronomic performance. *Bioresour. Technol.* 114, 644–653.
- EU-Directive 2009/28/EC, 2009. Promotion of the use of energy from renewable sources. Official Journal of the EU, L140/16, 23.April.
- Früwirth, H., 2010. Biodiesel Production from Algae – Obstacles and Challenges. AIChE Annual Meeting, Salt Lake City.
- Gerdes, C., 2001. Pyrolyse von Biomasse-Abfall: thermochemische Konversion mit dem Hamburger-Wirbelschichtverfahren. Dissertation. Universität Hamburg, p. 266.
- Huber, G.W., Iborra, S., Corma, A., 2006. Synthesis of transportation fuels from biomass: chemistry, catalysts, and engineering. *Chem. Rev.* 106, 4044–4098.

- Lin-Vien, D., 1991. *The Handbook of Infrared and Raman Characteristic of Frequencies of Organic Molecules*. Academic Press, San Diego.
- Meier, D., Faix, O., 1999. State of the art of applied fast pyrolysis of lignocellulosic materials – a review. *Bioresour. Technol.* 68, 71–77.
- Melligan, F., Dussan, K., Auccaise, R., Novotny, E.H., Leahy, J.J., Hayes, M.H.B., Kwapinski, W., 2012. Characterisation of the products from pyrolysis of residues after acid hydrolysis of *Miscanthus*. *Bioresour. Technol.* 108, 258–263.
- Mohan, D., Pittman, C.U., Steele, P.H., 2006. Pyrolysis of wood/biomass for bio-oil: a critical review. *Energy Fuels* 20, 848–889.
- Nimz, H.H., Schmitt, U., Schwab, E., Wittmann, O., Wolf, F., 2000. Wood. *Ullmanns Encykl. Tech. Chem.*
- OPEC, 2008. *World Oil Outlook*, 36.
- OPEC, 2011. *The Oil Industry*, 2011.12.28; http://www.opec.org/opec_web/en/press_room/179.htm.
- Prins, M.J., Ptasiński, K.J., Janssen, F.J.J.G., 2006. More efficient biomass gasification via torrefaction. *Energy* 31, 3458–3470.
- Rauch, R., 2010. Status of R&D of Synthetic Biofuels in Güssing, vol. 4. BtL Kongress, Berlin.
- Richmond, A., 2000. Microalgal biotechnology at the turn of the millennium: a personal view. *J. Appl. Phycol.* 12, 441–451.
- Saake, B., Lehnen, R., 2000. Lignin. *Ullmanns Encykl. Tech. Chem.*
- Clayton Saikrishna, M., Wheeler, M., van Heiningen, A.R.P., DeSisto, W.J., 2012. Formate-assisted fast pyrolysis of lignin. *Energy Fuels* 26, 1353–1362.
- Schwaiger, N., Feiner, R., Zahel, K., Pieber, A., Witek, V., Pucher, P., Ahn, E., Wilhelm, P., Chernev, B., Schröttner, H., Siebenhofer, M., 2011. Liquid and solid products from liquid-phase pyrolysis of softwood. *Bioenerg. Res.* 4, 294–302.
- Tredici, M.R., Zittelli, G.C., 1998. Efficiency of sunlight utilization: tubular versus flat photobioreactors. *Biotechnol. Bioeng.* 57, 187–197.
- Wagenführ, R., 1999. *Anatomie des Holzes; Anatomie-Chemie -Physik*, vol. 5.
- Williams, P.T., Besler, S., 1996. The influence of temperature and heating rate on the slow pyrolysis of biomass. *Renew. Energy* 7, 233–250.

Chapter 5

The BioCRACK Process- A Refinery Integrated Biomass-to-Liquid Concept to Produce Diesel from Biogenic Feedstock

The BioCRACK Process - A Refinery Integrated Biomass-to-Liquid Concept to Produce Diesel from Biogenic Feedstock

Jürgen Ritzberger^{*a}, Peter Pucher^a, Nikolaus Schwaiger^b,
Matthäus Siebenhofer^b

^aBDI - BioEnergy International AG, Parkring 18, 8042 Grambach, Austria

^bGraz University of Technology, Institute of Chemical Engineering and Environmental Technology, Inffeldgasse 25/C/II, 8010 Graz, Austria
juergen.ritzberger@bdi-bioenergy.com

Second generation biofuels, especially fuels from lignocellulose biomass, which are manufactured from non-food feedstock play a key role to reduce greenhouse gas emissions and the dependency on fossil oil. The bioCRACK process represents a new biomass-to-liquid concept to generate advanced biofuel by liquid-phase pyrolysis. As liquid heat carrier vacuum gas oil (VGO), an intermediate heavy oil product from the vacuum distillation, is used.

Since autumn 2012 a fully integrated pilot plant at the refinery in Schwechat/Austria with a nominal biomass capacity of 100 kg/h is in continuous operation and generates data for up-scaling the technology to an industrial scale.

This paper reports the results of the continuous operation. The influence of various reaction parameters, such as the reaction temperature, on yield and composition of the reaction products were investigated. As expected from previous results with a semi batch lab-scale reactor, within the selected range of temperature (350 °C to 400 °C), elevated temperature leads to decreasing amount of biochar and rising liquefaction. Based on the results could be shown that 10 to 20 % of the biogenic carbon can be transferred directly into raw fuels with the bioCRACK concept. Additionally 11 to 18 % of the bio-carbon merges into the remaining heat carrier.

1. Introduction

Transportation represents about 27 % of the total primary energy demand and is almost exclusively fuelled by mineral oil. The share may increase by 38 % from 2010 to 2035 (IEA, 2012). Therefore, and not least because of the fact that the global transportation sector is responsible for 22 % of the global greenhouse gas emissions (Olivier et al., 2012), the transport sector is challenged to play a key role to achieve the global targets relating to greenhouse gas emissions. The European Union has the ambitious aim to achieve at least ten percent of renewable energy share in the transport fuel sector until the year 2020. Furthermore the greenhouse gas emissions should be reduced by 20 % until 2020 (EU, 2009).

A few main routes can be distinguished to produce biofuels: extraction of vegetable oils, fermentation of sugars to alcohol, gasification and chemical synthesis and direct liquefaction (Hamelinck and Faaij, 2006). Due to the characteristic of their manufacture, commercially available biofuels employ almost uniquely food crops as their feedstock - predominantly sugar cane and sugar-beet, corn and oil seeds (Sorda et al., 2010). In comparison, second generation biofuels, also called advanced biofuels, are manufactured from non-food feedstock. The IEA (2011) assumes that especially the demand of advanced biodiesel is increasing in the foreseeable future. For this reason, intensive research and developing activities for advanced biofuel technologies are required to achieve the global targets.

BDI-BioEnergy International AG and OMV have been jointly involved in the bioCRACK pilot plant project to develop a new biomass-to-liquid concept to generate second generation biofuel. The process bases on the liquid phase pyrolysis (LPP) of lignocelluloses feedstock. In addition to fast pyrolysis and Fischer-Tropsch synthesis liquid phase pyrolysis is dedicated to form solid and liquid products. Mertlitz (2010) and

Please cite this article as: Ritzberger J., Pucher P., Schwaiger N., Siebenhofer M., 2014, The BioCRACK process - a refinery integrated biomass-to-liquid concept to produce diesel from biogenic feedstock, Chemical Engineering Transactions, 39, 1189-1194 DOI:10.3303/CET1439199

Schwaiger (2011) investigated the formation of liquid and solid products during liquid phase pyrolysis of wood with a semi-batch lab scale reactor. With rising reaction temperature the formation of biochar decreases, while formation of liquid CHO-products linearly correlates with the operation temperature. Schwaiger et al. (2012) reported additionally that the lignin frame in wood remains without substantial loss, while the major amount of carbohydrates is pyrolysed during liquid phase pyrolysis at $T = 350\text{ }^{\circ}\text{C}$. Building on the experiences with the semi-batch lab scale reactor a fully integrated pilot plant at the refinery in Schwechat/Austria with a biomass capacity of nominal 100 kg/h was established. This paper reports the results of the experimental tests performed on the continuous pilot-scale plant. The influence of various reaction parameters, such as the reaction temperature, on yield and composition of the reaction products was investigated.

2. Experimental

2.1 bioCRACK process

The bioCRACK concept is shown in Figure 1. To allocate high heat transfer and to avoid dust formation during the reaction, the pyrolysis process was carried out in liquid-phase. Feedstock for the experiments was lignocellulosic biomass (spruce wood and wheat straw). As liquid heat carrier vacuum gas oil (VGO), an intermediate heavy oil product from the vacuum distillation, which can be transformed into gasoline and diesel fuel by means of fluid catalytic cracking (FCC), is used. The biomass and the vacuum gas oil join the reaction by temperatures from $350\text{ }^{\circ}\text{C}$ to $400\text{ }^{\circ}\text{C}$. Reaction products of the bioCRACK liquid-phase pyrolysis are condensable liquid products (pyrolysis oil, reaction water, raw fuel), non-condensable products and biochar as solid residue.

On account of the fact, that the bioCRACK process is based on the liquid phase pyrolysis (LPP) and uses as heat carrier a heavy oil fraction from the refinery it is obvious that the integration of the process in an already existing refinery is conducive. Figure 1 shows a feasible way of integration for the bioCRACK technology in a refinery. Apart from the using of the heavy oil fraction there are further synergies arising from the fact that the process will be integrated in an existing refinery. The already in the refinery existing utilities (steam, power, cooling water, nitrogen) are also required for the bioCRACK process. Moreover, the reaction products can be upgraded with the already existing facilities in the refinery. For example the raw fuel is upgradeable via hydrogenation to diesel fuel with renewable content, according to the EN590 standard. Other refinery facilities like the FCC (Fluid Catalytic Cracker) can be used for upgrading the bioCRACK products as well.

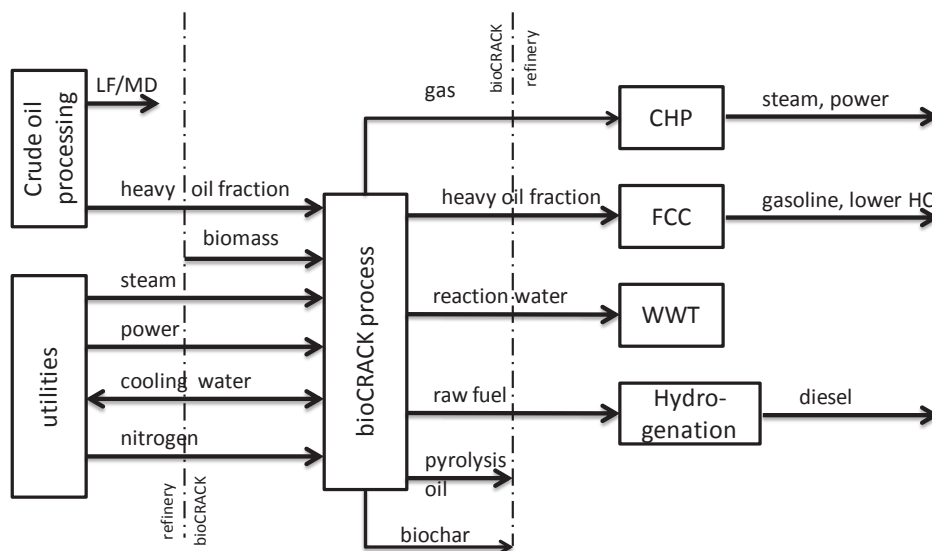


Figure 1: Possible integration of the bioCRACK process in a refinery

Table 1: Test parameter

| Parameter | | Range |
|----------------------|------|-----------|
| Biomass-Feed | kg/h | 60 - 100 |
| Reaction Temperature | °C | 350 - 400 |
| VGO / Biomass ratio | - | 3 - 6 |

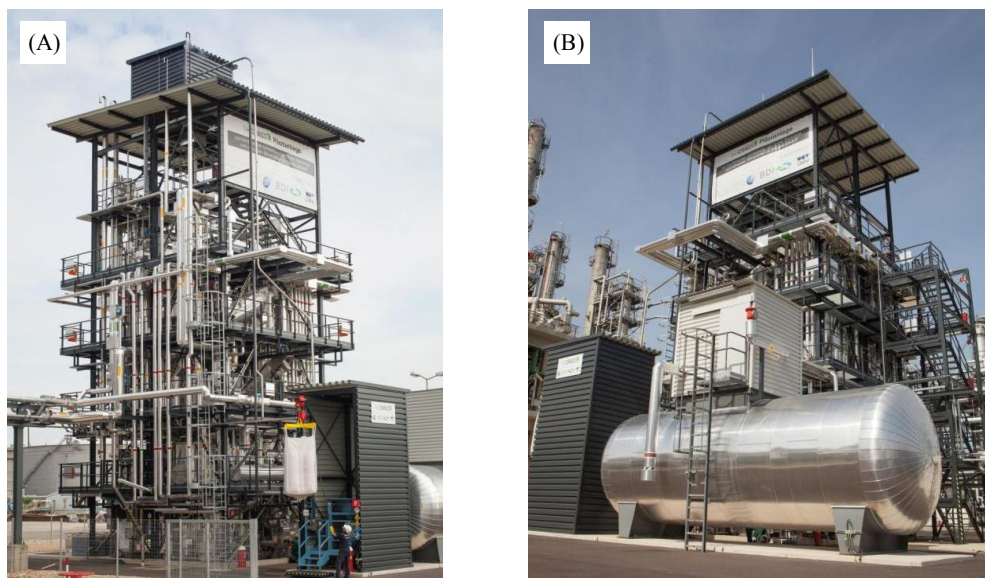


Figure 2: (A) Pilot plant at the refinery Schwechat/Austria, (B) Heat carrier oil vessel

2.2 Pilot plant and experimental procedure

The bioCRACK concept will be tested in a fully integrated pilot plant at the refinery Schwechat/Austria. Since autumn 2012 the pilot plant is under continuous operation for upscaling purposes to a demo plant. Figure 2 shows the bioCRACK plant. The nominal biomass capacity is 100 kg/h. The mass ratio varies between three to six parts of VGO to one part of biomass and the reaction temperature is altered between 350 °C and 400 °C. Table 1 shows an overview of the used test parameter.

3. Results

The influence of different test parameter (Table 1) on distribution and chemical composition of the reaction products were investigated. During liquid phase pyrolysis (LPP) the lignocellulosic biomass is transferred into hydrocarbons (mixed oil, carrier oil), liquid CHO-products, reaction water, biochar and gaseous products. Figure 3 shows the carbon balance of biogenic carbon, deduced from ^{14}C -analysis, at 375 °C. In this case 16 % of the biomass were directly transferred into fuel fractions. In general, the experiments have shown that with the bioCRACK concept about 10 to 20 % of bio-carbon can converted directly into raw fuels. Additionally 11 to 18 % of the biogenic carbon merges into the remaining carrier. During the LPP of spruce at 375 °C, see Figure 3, 15 % of bio-carbon transfers into the remaining heat carrier (heat carrier oil - after treatment).

The used heat carrier oil - vacuum gas oil (VGO) - also degrades during the bioCRACK process into reaction products. The conversion of the carrier oil in relation to the carrier oil to biomass ratio shows Figure 4. Particularly the conversion into gasoil decreases with increasing VGO to biomass ratio. The total conversion rate of the VGO with carrier oil to biomass ratio of three is 20 %. While with increasing carrier oil to biomass ratio the conversion rate decreases. With a VGO to biomass ratio of about six the total conversion rate declined below 12 %.

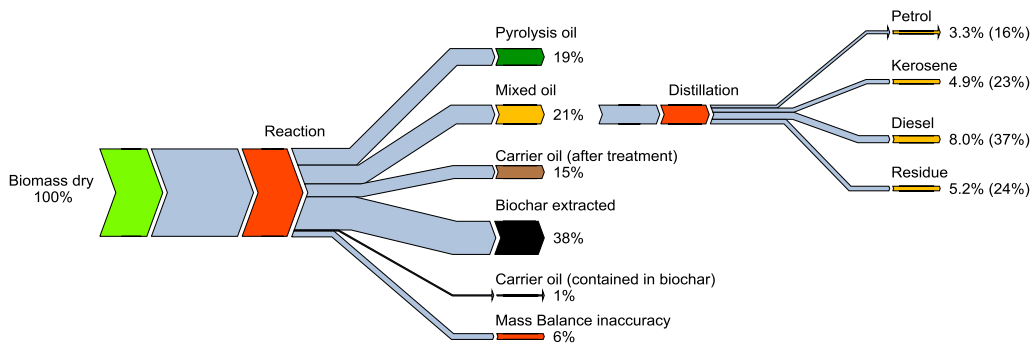


Figure 3: Carbon balance at $T = 375\text{ }^{\circ}\text{C}$, spruce wood

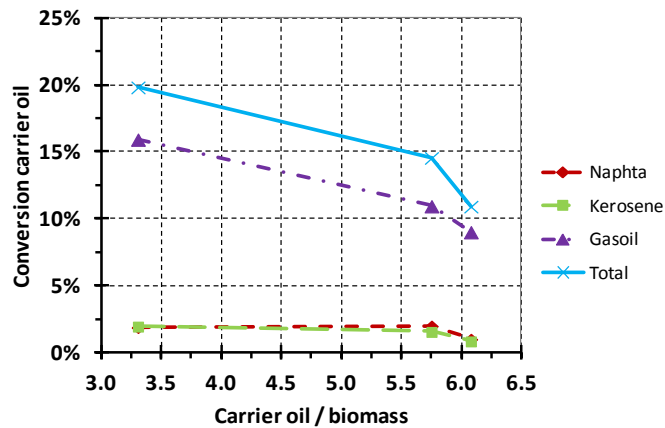


Figure 4: Conversion of the carrier oil

As expected from previous results with a semi batch lab-scale reactor (Mertlitz, 2010) and more recently (Schwaiger, 2011), within the selected range of temperature (350 °C to 400 °C), elevated temperature leads to decreasing amount of biochar and rising liquefaction as shown in Figure 5 and Table 2. At temperatures below 385 °C biochar is the dominant reaction product. The ratio of biochar formed during the liquid-phase pyrolysis decreases linearly, while the formation of liquid CHO-products and hydrocarbons increase with rising temperature.

Table 2: Distribution of the reaction products dependent on the reaction temperature

| | | 350 °C | 375 °C | 390 °C |
|---------------------|--------|--------|--------|--------|
| Hydrocarbons | [wt.%] | 11 | 19 | 20 |
| Liquid CHO-products | [wt.%] | 18 | 20 | 23 |
| Reaction water | [wt.%] | 20 | 20 | 24 |
| Biochar | [wt.%] | 36 | 28 | 22 |

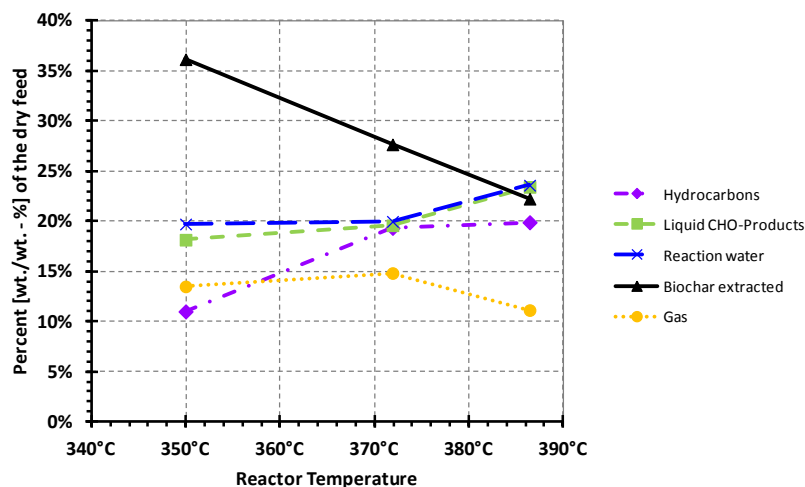


Figure 5: Effect of temperature on the mass conversion of spruce wood, 60 kg/h

The carbon balance of biogenic carbon dependent on the reaction temperature, illustrate in Figure 6, exhibits the same results. With increasing temperature the biochar yield sinks and the transfer of the biogenic carbon, deduced from ^{14}C -analysis, into liquid fractions (pyrolysis oil, hydrocarbons - mixed oil and carrier oil) rises.

As already mentioned, bio-carbon is mainly converted into biochar during the liquid-phase pyrolysis (Figure 3). Table 3 shows the transfer of elements from lignocelluloses biomass to biochar during the bioCRACK process. Due to the elevated carbon content biochar is a considerable feedstock for direct liquefaction in order to produce biofuels (Feiner et al., 2013).

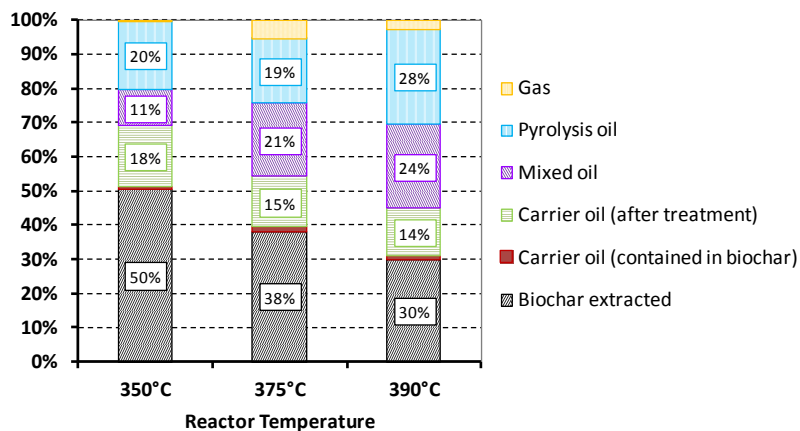


Figure 6: Effect of temperature on bio-carbon transfer of spruce wood, 60 kg/h

Table 3: Ultimate analysis of biomass and biochar

| Compound | | Biomass | Biochar |
|---------------------|--------|---------|---------|
| Carbon | [wt.%] | 49.6 | 80.9 |
| Hydrogen | [wt.%] | 6.3 | 5.4 |
| Nitrogen | [wt.%] | 0.0 | 0.3 |
| Rest (Oxygen + Ash) | [wt.%] | 44.2 | 13.4 |

4. Conclusion

Liquid-phase pyrolysis experiments are carried out in an innovative biomass-to-liquid pilot plant to generate advanced biogenic diesel. The results show, that the up-scaling from a semi batch lab-scale reactor to a pilot plant was successful. Comparable results were obtained under the various operation conditions. The bioCRACK process thus represents a new opportunity to manufacture advanced biofuel from lignocellulose biomass.

Further investigations will be conducted to optimize the bioCRACK concept and to generate data for up-scaling the technology to a demo plant.

Acknowledgement

This project is funded by the Austrian Climate and Energy Fund as part of the 'New Energies 2020' research and technology program. The authors thank for the support by our project partner OMV Refining and Marketing GmbH.

References

- EU (European Union), 2009, EU-Directive 2009/28/EC on promotion of the use of energy from renewable sources, Official Journal of the EU, L140/1.
- Feiner R., Schwaiger N., Pucher H., Ellmaier L., Pucher P., Siebenhofer M., 2013, Liquefaction of pyrolysis derived biochar: a new step towards biofuel from renewable resources, *RSC Advances*, 3, 17898-17903.
- Hamelinck C.N., Faaij A.P.C., 2006, Outlook for advanced biofuels, *Energy Policy*, 34, 3268-3283.
- IEA (International Energy Agency), 2011, Technology Roadmap: Biofuels for Transport, France.
- IEA (International Energy Agency), 2012, World Energy Outlook 2012 <www.iea.org> accessed 12.03.2014.
- Mertlitz V., 2010, Liquid phase pyrolysis of biogenic feedstock, PhD Thesis, Graz University of Technology, Austria.
- Olivier J.G.J., Janssens-Maenhout G., Muntean M., Peters J.A.H.W., 2013, Trends in global CO2 emissions 2013 report, The Hague: PBL Netherlands Environmental Assessment Agency, Ispra: Joint Research Centre.
- Schwaiger N., 2011, Reaction Mechanisms of Liquid-Phase Pyrolysis of Lignocellulosic Feed, PhD Thesis, Graz University of Technology, Austria.
- Schwaiger N., Witek V., Feiner R., Pucher H., Zahel K., Pieber A., Pucher P., Ahn E., Chernev B., Schroettner H., Wilhelm P., Siebenhofer M., 2012, Formation of liquid and solid products from liquid phase pyrolysis, *Bioresource technology*, 124, pp.90-94.
- Sorda G., Banse M., Kemfert C., 2010, An overview of biofuel policies across the world, *Energy Policy*, 38, 6977-6988.

Chapter 6

Catalytic hydrodeoxygenation of dehydrated liquid phase pyrolysis oil



Catalytic hydrodeoxygenation of dehydrated liquid phase pyrolysis oil

Hannes Pucher^{1,*}, Nikolaus Schwaiger^{1,2}, Roland Feiner^{1,2}, Peter Pucher², Lisa Ellmaier² and Matthäus Siebenhofer¹

¹Institute of Chemical Engineering and Environmental Technology, Graz University of Technology, Graz, Austria

²BDI – BioEnergy International AG, Grambach, Austria

SUMMARY

Biomass has been considered as promising energy source that should be able to suffice the increasing energy demand in the future. Therefore, new biomass utilization technologies and concepts are highly desirable. This paper contributes to the understanding of liquid phase pyrolysis oil upgrading that differs from the intensively investigated fast pyrolysis oil. Two new approaches, which were never reported in literature before, were investigated in this paper. At first, the liquid phase pyrolysis oil was dehydrated to lower transportation costs and increase energy density and efficiency of further upgrading steps. At second, a catalyst screening for hydrodeoxygenation (HDO) of dehydrated liquid phase pyrolysis oil was conducted in a batch reactor. Neither the dehydration nor the HDO of dehydrated liquid phase pyrolysis oil were reported in literature by now. The activity of the HDO catalysts Ru/C, Pt/C, and Pd/C as well as a Ni-based catalyst was compared. HDO was investigated at 250 °C and 100 bar and at 300 °C and 150 bar. HDO of dehydrated liquid phase pyrolysis oil was observed with all catalysts. The Pt/C catalyst was found to be most promising with respect to the oil yield (56 wt.%), the deoxygenation ratio (65%), and hydrogen content (8.6 wt.%). Copyright © 2014 John Wiley & Sons, Ltd.

KEY WORDS

biomass; liquid phase pyrolysis; hydrodeoxygenation; biofuels; hydrogenation; dehydration

Correspondence

*Hannes Pucher, Institute of Chemical Engineering and Environmental Technology, Graz University of Technology, Graz, Austria.

†E-mail: hannes.pucher@tugraz.at

Received 22 October 2013; Revised 3 March 2014; Accepted 4 April 2014

1. INTRODUCTION

Because of increasing world population and increasing living standards, energy consumption has never been higher [1]. As a consequence, the energy crises of the 20th century have shown that nonrenewable energy sources, such as oil and coal, will not suffice the increasing demand for energy in the future. According to the Organization of the Petroleum Exporting Countries reports [2,3], the proven crude oil reserves decreased from 1700 billion barrels in the year 1980 to 1200 billion barrels at the end of the year 2011. This indicates that despite of improved exploring and production methods fossil oil resources are decreasing continuously. Additionally, environmental concerns and the climate change are a global threat.

To solve these problems, substantial research is carried out to develop alternative bio-based fuels, which are similar to fossil fuel but renewable, can retard greenhouse gas emissions, and can be integrated into the conventional infrastructure [4]. Recapitulating these biofuels should be able to substitute a certain amount of the fossil fuels. It is assumed that biofuels are

part of the solution, because they have several advantages [5,6]. The greenhouse gasses, for example CO₂, which are produced during the utilization of biomass, can be reabsorbed. This cycle can help to lower the consequences, such as rising temperature, caused by climate change. Because of the wide availability of biomass, energy security can be improved, and fossil fuel dependence can be decreased.

First-generation biofuels such as biodiesel and bio-ethanol are already on the market. However, these technologies may need edible (food grade) biomass, such as arable crops, sugar cane, and vegetable oils, as a feedstock. For this reason, first-generation biofuels are afflicted with the negative food *versus* fuel discussion.

Second-generation biofuels, such as pyrolysis oil-based fuels, use nonedible ('nonfood') lignocellulosic biomass, such as wood or straw, as a feedstock. Different conversion concepts, for example, Fischer–Tropsch synthesis, ethanol fermentation, and pyrolysis are currently investigated [7]. A potentially economically interesting route for the production of second-generation biofuel is hydrodeoxygenation (HDO) of pyrolysis oil [1].

The two-step concept for the production of second-generation biofuels, which is developed and investigated in this project, is shown in Figure 1.

In the first step of the concept (bioCRACK), any kind of nonedible lignocellulosic biomass is converted into pyrolysis oil, pyrolysis char, and gas through liquid phase pyrolysis (LPP). In addition, up to 20 wt.% of the biomass is directly transferred into the fossil liquid energy carrier (e.g., vacuum gas oil). This upgraded liquid fossil energy carrier (vacuum gas oil+) can be further upgraded to biofuels in a conventional refinery without any additional pretreatment step. Technology and process design of LPP were investigated and published [8,9]. In 2012, a pilot scale LPP plant at OMV refinery in Vienna with a capacity of 100 kg of biomass per hour went into operation.

In the second step of the concept (bioBOOST), the LPP products are upgraded through HDO of the LPP oil and hydrogenation of the LPP char [10].

Because of the decomposition of cellulose, hemicellulose, and lignin, the LPP oil is a mixture of a variety of different degradation products [6]. It has a high water content of 40–60 wt.% and contains a large amount of oxygenated constituents such as low molecular weight acids, aldehydes, and alcohols. Limited stability of pyrolysis oil, especially during storage, is a major constraint. The stability of LPP oil is currently subject of investigation. Improvement of product quality and stability of pyrolysis oil is therefore a high priority issue [11].

The upgrading of pyrolysis oil from fast pyrolysis through HDO has been reported [12–16]. Little information is available about HDO of LPP oil. The main differences between (shown in Table I) fast pyrolysis and LPP oil are the following: (i) the higher water content (50–30 wt.%); (ii) the lower carbon content (47.4–51.1 wt.%); (iii) the higher oxygen content (44.1–41.6 wt.%); (iv) the lower density (1070–1200 kg/m³); and (v) the lower load with inorganics [8].

In this project, a catalyst screening study in a batch reactor setup, on the basis of literature data about HDO of pyrolysis oil from fast pyrolysis [12–16], with dehydrated LPP oil was carried out. The HDO catalysts Ru/C, Pt/C, and Pd/C (shown in Table II) as well as a Ni-based catalyst were screened [12] on the basis of their performance in the fast pyrolysis oil HDO. HDO was investigated at 250 °C and 100 bar hydrogen pressure and 300 °C and 150 bar hydrogen pressure [12,14–16]. Investigation focused on the activity of catalysts with respect to yield, deoxygenation level, and molecular size.

2. MATERIALS

The noble metal catalysts Ru/C, Pt/, and Pd/C (5 wt.% active metal) were obtained as powders from Sigma-Aldrich. Relevant properties are reported in Table II.

The LPP oil used for investigation was produced from spruce wood chips. Details of the process have been published [8,9].

Prior to HDO, the pyrolysis oil was dehydrated to decrease the amount of unwanted low molecular weight constituents such as hydroxyacetone and water. Through dehydration, two phases were produced, a dark brown oil dehydrated LPP oil and a slightly yellow wastewater phase. This wastewater phase was additionally fed into a continuous lab scale biogas plant. Thereby, 100 wt.% of this phase could be converted into biogas and wastewater to normal feed ratios of 7:3 were achieved. The relevant properties of the different products are presented in Table III.

It is important to mention that through this dehydration step, the water content was reduced by 86 wt.%, and the energy density can be more than doubled. Thus, the transportation costs can be lowered, and the efficiency of further upgrading process is increased.

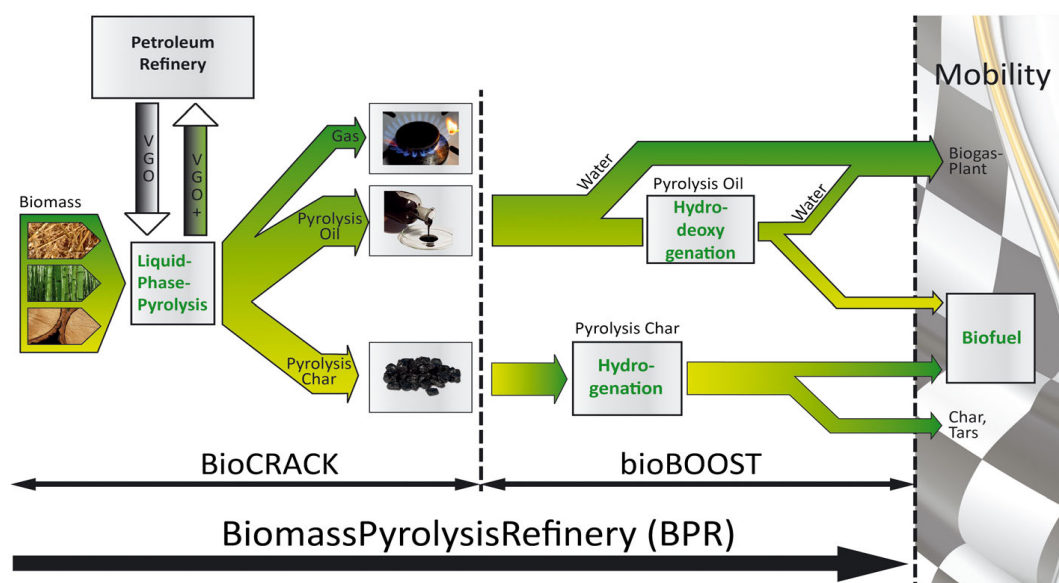


Figure 1. BiomassPyrolysisRefinery [25].

Table I. Comparison of pyrolysis oil quality from fast pyrolysis [12], liquid phase pyrolysis (LPP), and liquid phase pyrolysis oil after dehydration.

| | Fast pyrolysis oil | LPP oil | Dehydrated LPP oil |
|---------------------------------|--------------------|-----------|--------------------|
| Water content (wt.%) | 30 | 50 | 7 |
| Lower calorific value (kJ/kg) | 15,030 | 8,670 | 20,530 |
| Density (kg/m ³) | 1,200 | 1,070 | 1,230 |
| Viscosity (cP) | 40–40 °C | <10–20 °C | — |
| Elemental analysis on dry basis | | | |
| Carbon content (wt.%) | 51.1 | 47.4 | 55.5 |
| Hydrogen content (wt.%) | 7.3 | 7.9 | 6.9 |
| Oxygen content (wt.%) | 41.6 | 44.1 | 37.3 |
| Nitrogen content (wt.%) | <1 | <1 | <1 |

Table II. Catalyst details.

| Catalyst | Ru/C | Pd/C | Pt/C |
|------------------------|---------------|---------------|---------------|
| Supplier | Sigma-Aldrich | Sigma-Aldrich | Sigma-Aldrich |
| Catalog number | 206180 | 205680 | 205931 |
| APS (μm) | 19 | 44 | 19 |
| SA (m ² /g) | 900 | 900–1000 | 950 |

The dehydrated LPP oil was analyzed and then stored in a refrigerator (6 °C) to avoid aging. Selected properties of the LPP oil are shown in Table I. Further information can be found elsewhere [8,9].

3. EXPERIMENTAL SETUP AND PROCEDURE

Dehydrated LPP oil was hydrotreated in a 450 ml batch autoclave setup, type limbo from Büchi Glas Uster AG. The autoclave can be operated up to 500 °C and 350 bar. The temperature was controlled with an electric heating jacket. The reactor content was stirred at 500 rpm with a magnetically driven gas-inducing Rushton type impeller. Temperature and pressure were continuously monitored. A schematic is shown in Figure 2.

The reactor was filled with dehydrated LPP oil (100 g) and the catalyst (5 wt.% on the basis of wet dehydrated LPP oil). Afterwards, the reactor was pressurized with 50 bar of hydrogen at ambient temperature. The reactor was heated with a heating rate of 10 °C/min to the reaction

temperature. The reaction temperature was kept constant 2 h long for all experiments. The pressure at reaction temperature was preset to 100 bar at 250 °C (mild HDO) and 150 bar at 300 °C (deep HDO) and kept constant over the reaction time by continuously metering hydrogen gas to the reactor. After the experiment, the reactor was cooled to ambient temperature.

For mass balance calculations, the weight of the reactor was measured before and after the gaseous/liquid product was relieved. Then, the reactor was depressurized. The gas composition was determined with a Mardur Photon II infrared gas analyzer. The solid and liquid reaction products were recovered and separated in a separating funnel. The combined oil and solid phase were diluted with acetone and filtered. After filtration, the filter was dried and weighed. Then, the net amount of solids formed during HDO was determined.

4. APPARATUS AND METHODS

The gas composition was analyzed for CH₄, O₂, CO₂, and CO with a Mardur Photon II infrared gas analyzer.

The liquid products were characterized with a Vario Macro CHNO-analyzer, from Elementar Analysensysteme, in CHN mode.

The molecular size measurements were carried out with a Shimadzu RID-10A refractive index detector and a Merck HITACHI L-6000A Pump using a SDV 5 μm 8 × 50 column and two SDC 1000 Å 8 × 300 columns from polymer standard service. Size-exclusion chromatography was calibrated against polystyrene.

Table III. Comparison of liquid phase pyrolysis (LPP) oil, dehydrated liquid phase pyrolysis oil, and wastewater.

| | LPP oil | Dehydrated LPP oil | Wastewater |
|-------------------------------|---------|--------------------|------------|
| Product yield (%) | 100 | 28.2 | 71.8 |
| Lower calorific value (kJ/kg) | 8,670 | 20,530 | 2,290 |
| Water content (wt.%) | 50 | 7 | 80 |
| Carbon content (wt.%) | 23.6 | 51.8 | 10.1 |
| Hydrogen content (wt.%) | 9.5 | 7.1 | 10.5 |
| Oxygen content (wt.%) | 66.5 | 40.8 | 79.2 |
| Nitrogen content (wt.%) | <1 | <1 | <1 |

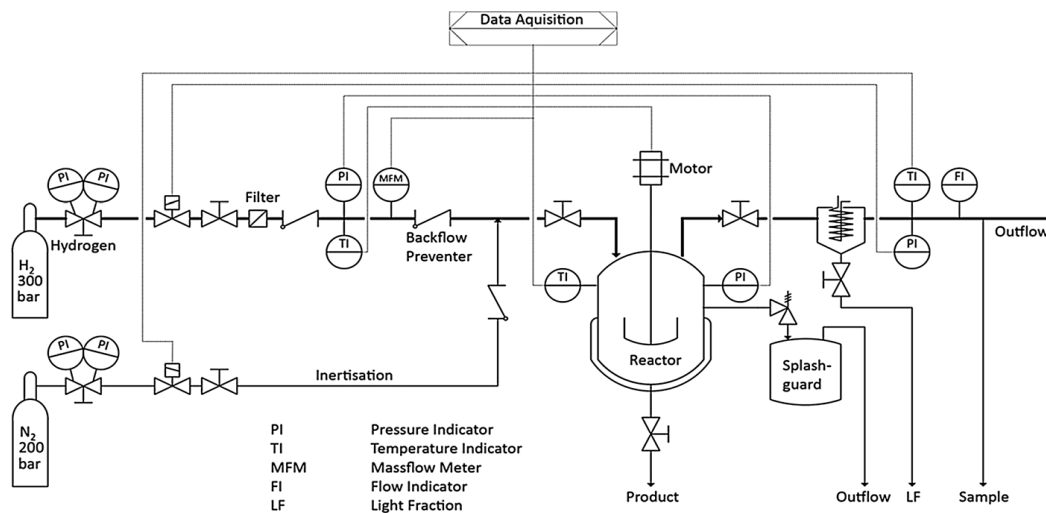


Figure 2. Scheme of the autoclave setup.

The water content of the liquid products was determined with gas chromatography thermal conductivity detector from Agilent Technologies using a column from HP-Innowax.

Furthermore, the dehydrated LPP oil and the oil PHASE were fractionated by a solvents fraction technique (Figure 3) as proposed by Oasmaa *et al.* [17,18].

5. RESULTS AND DISCUSSION

5.1. Catalysts and screening conditions

The noble metal catalysts (Ru/C, Pt/C, and Pd/C 5 wt.% active metal on carbon support) and the Ni-based catalyst were investigated. The HDO experiments were conducted at 250 °C and 100 bar (mild HDO) and 300 °C and 150 bar (deep HDO). Catalyst selection and HDO conditions were based on literature data about HDO of pyrolysis oil from fast pyrolysis [12–16]. The reaction time at reaction temperature was 2 h, and the pressure during each experiment was kept constant by continuously metering hydrogen gas to the reactor.

5.2. Key figures

For a better understanding, different key figures were defined.

The deoxygenation rate is calculated from Equation (1) [19].

$$\text{Deoxygenation Rate} = 1 - \frac{\text{Oxygen Content}_{\text{Product,dry}}}{\text{Oxygen Content}_{\text{Feed,dry}}} \quad (1)$$

The lower calorific value is calculated from Equation (2) [20].

$$\text{LCV} = 34,0 \cdot w_C + 101,6 \cdot w_H + 6,3 \cdot w_N + 19,1 \cdot w_S - 9,8 \cdot w_O - 2,5 \cdot w_{H_2O} \quad (2)$$

5.3. Mild hydrodeoxygenation of dehydrated liquid phase pyrolysis oil

After mild HDO, conducted at 250 °C and 100 bar H₂, four product phases were found: (i) one clear slightly brown water phase (which could be further processed in a biogas plant); (ii) a dark brown oil phase; (iii) a solid phase; and (iv) a gas phase. Density and viscosity of the oil phase were higher than the density and viscosity of the water phase.

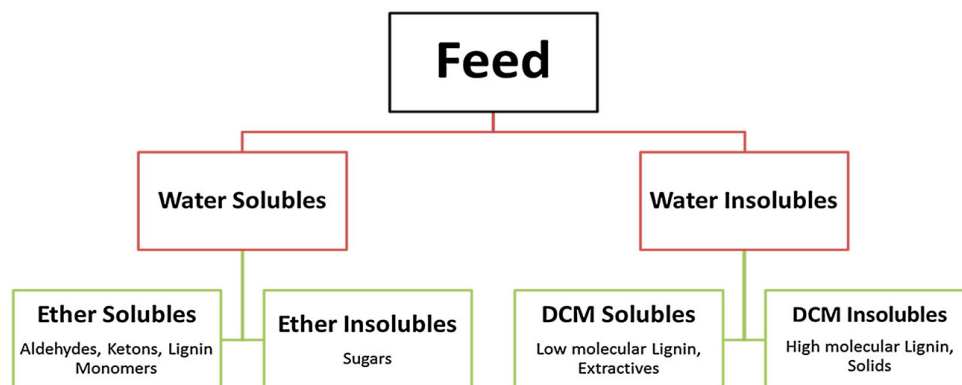


Figure 3. Solvents fractionation technique proposed by Oasmaa *et al.* [17,18].

The product and energy yield of the different phases on dry basis is presented in Figure 4. The elemental composition of the oil, the aqueous phase, and the feed on dry basis is shown in Table IV. In general, the mass balance closure varied between 91% and 96%. The most likely reasons for this inaccuracy were the complicated product workup because of its high viscosity and stickiness.

In all experiments, the oxygen content was decreased, and the hydrogen content was increased. With a final oxygen content of 24.9 wt.% and an oil yield of 64 wt.%, the Pd/C catalyst performed best in mild HDO. The hydrogen content in the oil phase was highest (8.6 wt.%) when the Pt/C catalyst was used. This indicates that the Pt/C

catalyst is capable of hydrogenating the dehydrated LPP oil under mild HDO conditions best. The highest oil yield (66 wt.%) was obtained when the Ru/C catalyst was used; on the other hand, the oxygen content was high (27.1 wt.%). The Ni-based catalyst resulted in a high oil yield (64 wt.%) and low oxygen content (25.4 wt.%), indicating that for mild HDO conditions, the catalyst is nearly as active as the noble metal catalysts.

Mild HDO of dehydrated pyrolysis oil from LPP results in formation of less than 2 wt.% solids, compared with a solid content of up to 10 wt.% from HDO of pyrolysis oil from fast pyrolysis under same conditions [12].

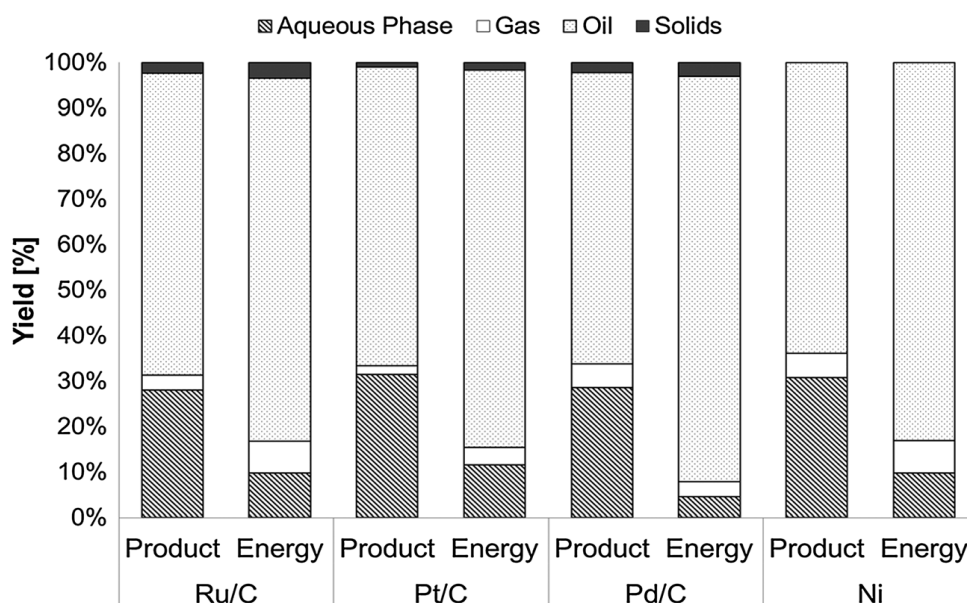


Figure 4. Product and energy yield for mild hydrodeoxygenation (250 °C, 100 bar, 2 h) of dehydrated liquid phase pyrolysis oil with different catalysts.

Table IV. Elemental composition of the mild hydrodeoxygenation oils, the aqueous phase, the feed on dry basis, and the gas composition (250 °C, 100 bar, 2 h).

| Catalyst | Phase | LCV (kJ/kg) | C (wt.%) | H (wt.%) | O (wt.%) | N (wt.%) | CO ₂ (vol.%) | CH ₄ (vol.%) | CO (vol.%) | H ₂ (vol.%) |
|----------|---------|-------------|----------|----------|----------|----------|-------------------------|-------------------------|------------|------------------------|
| None | Feed | 20,530 | 55.5 | 6.9 | 37.3 | <1 | — | — | — | — |
| Ru/C | Oil | 24,800 | 64.4 | 7.9 | 27.1 | <1 | — | — | — | — |
| | Aqueous | 10,050 | 26.9 | 9.3 | 63.4 | <1 | — | — | — | — |
| | Gas | — | — | — | — | — | 8.1 | 0.0 | 0.0 | 91.9 |
| Pt/C | Oil | 23,600 | 63.8 | 8.6 | 27.2 | <1 | — | — | — | — |
| | Aqueous | 12,000 | 30.2 | 9.6 | 59.7 | <1 | — | — | — | — |
| | Gas | — | — | — | — | — | 6.8 | 0.1 | 0.2 | 92.9 |
| Pd/C | Oil | 24,200 | 67.1 | 7.6 | 24.9 | <1 | — | — | — | — |
| | Aqueous | 5,900 | 27.2 | 9.2 | 63.3 | <1 | — | — | — | — |
| | Gas | — | — | — | — | — | 17.8 | 1.0 | 0.0 | 81.2 |
| Ni | Oil | 24,500 | 66.7 | 7.6 | 25.4 | <1 | — | — | — | — |
| | Aqueous | 9,200 | 25.5 | 9.1 | 65.1 | <1 | — | — | — | — |
| | Gas | — | — | — | — | — | 12.3 | 0.1 | 0.7 | 86.9 |

LCV, lower calorific value.

The gas yield ranged between 2 and 6 wt.%. The main gaseous components, presented in Table IV, were unreacted hydrogen and carbon dioxide. Carbon dioxide (7–18 mol%) can be formed through the decarboxylation of organic acids, such as acetic and formic acid, common constituents in dehydrated LPP oils (8–10 wt.%) [21–23]. This gas could be recycled or burned directly to produce heat.

5.4. Deep hydrodeoxygenation of dehydrated liquid phase pyrolysis oil

The purpose of deep HDO experiments (300 °C and 150 bar H₂) was to decrease the final oxygen content. In general, deep HDO led to formation of four phases: (i) a clear slightly brown water phase (which could be further processed in a biogas plant); (ii) a dark brown oil phase; (iii) a solid phase; and (iv) a gas phase. Density and the viscosity of the oil phase from deep HDO experiments were comparable with the results from mild HDO experiments.

The product and energy yield is presented in Figure 5. Mass balance closure varied between 94% and 96%. The most likely reasons for this inaccuracy were the complicated product workup because of its high viscosity and stickiness. The elemental composition of the oil, aqueous phase, and the feed on dry basis is shown in Table V.

It is obvious that under harsh conditions (300 °C and 150 bar), more oxygen can be removed from dehydrated LPP oil. However, the oil yield of 51–58 wt.% is lower compared with an oil yield of 64–66 wt.% from mild HDO. This decrease can be explained by the fact that with increasing deoxygenation ratio, more oxygen is removed from the oil phase by forming water and carbon dioxide [12,14].

To obtain an oil phase with the lowest oxygen content (13 wt.%) and high yield (56 wt.%), Pt/C seems to be the best catalyst choice for deep HDO conditions. The highest hydrogen content (8.8 wt.%) was obtained when the Pd/C was used. Under deep HDO conditions, the Ru/C catalyst is capable of lowering the oxygen content (17.9 wt.%) and increasing the hydrogen content (8.5 wt.%). The Ni-based catalyst gives the highest oil yield (58 wt.%). However, the obtained oil phase had the highest oxygen content (19.4 wt.%) and a low hydrogen content (7.8 wt.%).

These results indicate that under deep HDO conditions, on the one hand, all catalysts are capable of hydrodeoxygenating and hydrogenating the dehydrated liquid phase to a higher extent. On the other hand, the oil yield is lower.

The amount of solid phase obtained under deep HDO conditions is 1–5 wt.% and comparable with mild HDO conditions (0–2 wt.%).

Under the deep HDO conditions, more gas was produced (7–10 wt.%). The main gaseous products, presented in Table V, were unreacted hydrogen and carbon dioxide (16–27 mol%). This indicated that harsh conditions lead to a higher decarboxylation rate of organic acids, such as acetic and formic acid [21–23]. This gas could be recycled or burned directly to produce heat.

5.5. Deoxygenation rate

For a better understanding of the process in Figure 6, the hydrogen consumption over the deoxygenation rate is shown, and two separate areas are visible for mild and deep HDO. Under deep HDO conditions, the deoxygenation ratio is higher than under mild HDO conditions. The oxygen content in the oil phase can be lowered to a higher extent under harsh conditions. The deoxygenation ratio was 27–35% for mild HDO conditions and 48–65% for

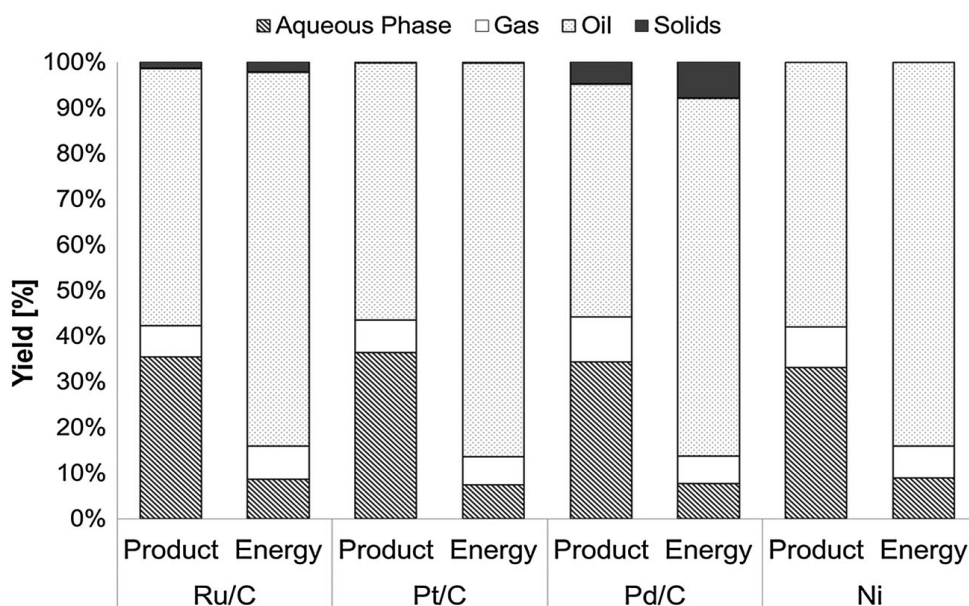


Figure 5. Product and energy yield for deep hydrodeoxygenation (300 °C, 150 bar, 2 h) of dehydrated liquid phase pyrolysis oil with different catalysts.

Table V. Elemental composition of the deep hydrodeoxygenation oils, the aqueous phase, the feed on dry basis, and the gas composition (300 °C, 150 bar, 2 h).

| Catalyst | Phase | LCV (kJ/kg) | C (wt.%) | H (wt.%) | O (wt.%) | N (wt.%) | CO ₂ (vol.%) | CH ₄ (vol.%) | CO (vol.%) | H ₂ (vol.%) |
|----------|---------|-------------|----------|----------|----------|----------|-------------------------|-------------------------|------------|------------------------|
| None | Feed | 20,530 | 55.5 | 6.9 | 37.3 | <1 | — | — | — | — |
| Ru/C | Oil | 29,900 | 72.9 | 8.5 | 17.9 | <1 | — | — | — | — |
| | Aqueous | 5,900 | 17.7 | 9.9 | 72.1 | <1 | — | — | — | — |
| | Gas | — | — | — | — | — | 16.0 | 0.3 | 0.9 | 82.8 |
| Pt/C | Oil | 31,300 | 77.8 | 8.6 | 13.0 | <1 | — | — | — | — |
| | Aqueous | 5,200 | 15.7 | 10.2 | 73.8 | <1 | — | — | — | — |
| | Gas | — | — | — | — | — | 19.4 | 0.5 | 0.4 | 79.7 |
| Pd/C | Oil | 29,800 | 72.6 | 8.8 | 18.1 | <1 | — | — | — | — |
| | Aqueous | 5,100 | 16.2 | 9.9 | 73.5 | <1 | — | — | — | — |
| | Gas | — | — | — | — | — | 27.4 | 0.7 | 1.8 | 70.1 |
| Ni | Oil | 28,100 | 72.2 | 7.8 | 19.4 | <1 | — | — | — | — |
| | Aqueous | 6,600 | 19.7 | 9.6 | 70.4 | <1 | — | — | — | — |
| | Gas | — | — | — | — | — | 21.5 | 0.5 | 1.5 | 76.5 |

LCV, lower calorific value.

deep HDO conditions. Under deep HDO conditions, more hydrogen is consumed. These results indicate that harsh conditions promote the HDO and hydrogenation reactions.

The highest deoxygenation ratio of 65% was achieved with Pt/C catalyst under deep HDO conditions. For mild HDO conditions, the Pt/C resulted in low deoxygenation ratio of 27%. With the Pt/C catalyst, the highest hydrogen consumption of 12.1 mol/kgFeed for deep HDO conditions and 10.8 mol/kgFeed for mild HDO conditions was observed.

The Pd/C catalyst performed similar. Under mild HDO conditions, the deoxygenation ratio was 33%, and under deep HDO conditions, it was 51%. In both experiments, a hydrogen consumption of 8.7 mol/kgFeed under mild HDO conditions and 11.2 mol/kgFeed under deep HDO conditions was monitored. Pt/C and the Pd/C catalyst are hydrogenation catalysts under mild HDO conditions and HDO catalyst under deep HDO conditions.

The deoxygenation ratio of Ru/C catalyst was 35% under mild HDO condition and 52% under deep HDO

conditions. The hydrogen consumption under mild HDO conditions was 7.5 mol/kgFeed and under deep HDO conditions, it was 8.7 mol/kgFeed. The results show that the Ru/C catalyst was also very active under mild HDO conditions and that its activity increased under harsh conditions.

The observations made for the Ni-based catalyst indicate that it is able to deoxygenate the dehydrated LPP oil but does not perform as good as the noble metal catalysts. The deoxygenation ratio under mild HDO conditions was 32% and under deep HDO conditions 48%. The hydrogen consumption was 5.4 mol/kgFeed under mild HDO conditions and 5.3 mol/kgFeed under deep HDO conditions.

5.6. Van Krevelen plot

Effects of process conditions and catalyst on the elemental composition of the hydrodeoxygenated dehydrated LPP oil are shown in Figure 7, and two separate areas for deep

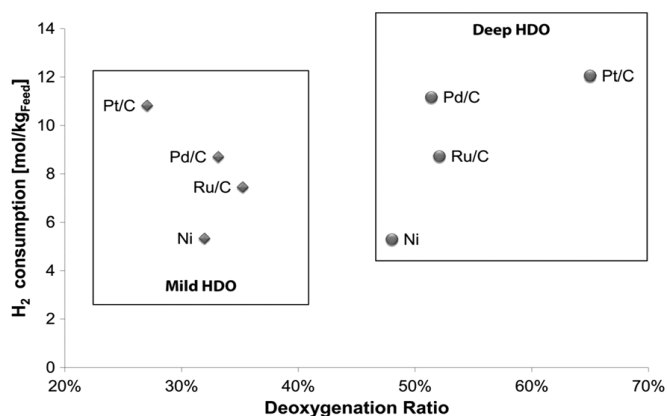


Figure 6. Hydrogen consumption over deoxygenation ratio for mild (250 °C, 100 bar, 2 h) and deep (300 °C, 150 bar, 2 h) hydrodeoxygenation (HDO).

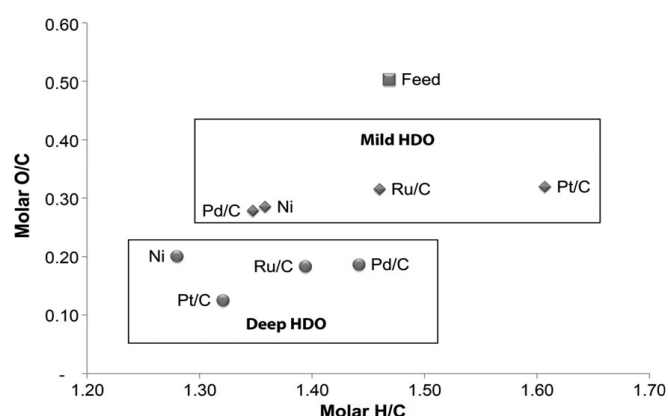


Figure 7. Van Krevelen plot for the elemental composition for mild (250 °C, 100 bar, 2 h) and deep (300 °C, 150 bar, 2 h) hydrodeoxygenation (HDO).

HDO conditions and mild HDO conditions clearly point out the different effects [24].

The best molar H/C ratio of 1.61 was achieved with the Pt/C catalyst under mild HDO conditions. This result indicates that the Pt/C catalyst is able to hydrogenate the dehydrated LPP oil under mild HDO conditions.

The best molar O/C ratio of 0.13 was achieved with the Pt/C catalyst under deep HDO conditions.

A molar H/C ratio of 1.46 and a molar O/C ratio of 0.32 were obtained when the Ru/C catalyst was used under mild conditions.

Under mild HDO condition, nearly similar molar H/C ratios of 1.35 and 1.36 and molar O/C ratios of 0.28 and 0.29 were observed for the Pd/C and the Ni-based catalyst. These results indicate that under mild conditions, the influence of catalysts on the properties of the oil phase is not as significant as under deep HDO condition.

On the one hand, the molar H/C ratios varied between 1.44 for the Pd/C catalyst, 1.39 for the Ru/C catalyst, and

1.28 for the Ni-based catalyst. On the other hand, the molar O/C ratio was similar for all three catalysts with 0.19 for Pd/C, 0.18 for Ru/C, and 0.20 for Ni-based catalyst. These findings allow the conclusion that the Pd/C catalyst is able to hydrogenate the dehydrated LPP oil to a higher extent than Ru/C and the Ni-based catalyst.

5.7. Solvents fraction technique

The results of the solvents fraction technique proposed by Oasmaa *et al.* [17,18] are shown in Table VI for the mild and deep HDO oils.

These figures show that under harsh conditions, the water-insoluble (WIS) content increases, and the water-soluble and WIS/DCMIS (high molecular lignin, solids) content decreases. In addition, the WIS/DCMS content, which consist of low molecular lignins and extractives, ranged in the mild HDO

Table VI. Results of solvents fraction technique applied to the results of mild (250 °C, 100 bar, 2 h) and deep (300 °C, 150 bar, 2 h) HDO of dehydrated liquid phase pyrolysis oil.

| | WIS/DCMIS (wt.%) | WIS/DCMS (wt.%) | WS/EIS (wt.%) | WS/ES (wt.%) | WC (wt.%) |
|----------|------------------|-----------------|---------------|--------------|-----------|
| Feed | 6 | 11 | 51 | 25 | 7 |
| Mild HDO | | | | | |
| Ru/C | 13 | 47 | 2 | 30 | 8 |
| Pt/C | 11 | 53 | 15 | 7 | 14 |
| Pd/C | 11 | 56 | 12 | 8 | 13 |
| Ni | 26 | 53 | 10 | 0 | 11 |
| Deep HDO | | | | | |
| Ru/C | 7 | 71 | 5 | 12 | 5 |
| Pt/C | 13 | 61 | 4 | 15 | 7 |
| Pd/C | 1 | 76 | 1 | 16 | 6 |
| Ni | 3 | 84 | 4 | 2 | 7 |

HDO, hydrodeoxygenation; WIS/DCMIS, water-insoluble/dichloromethane insoluble; WIS/DCMS, water-insoluble/dichloromethane soluble; WS/ES, water-soluble/ether soluble; WC, water content.

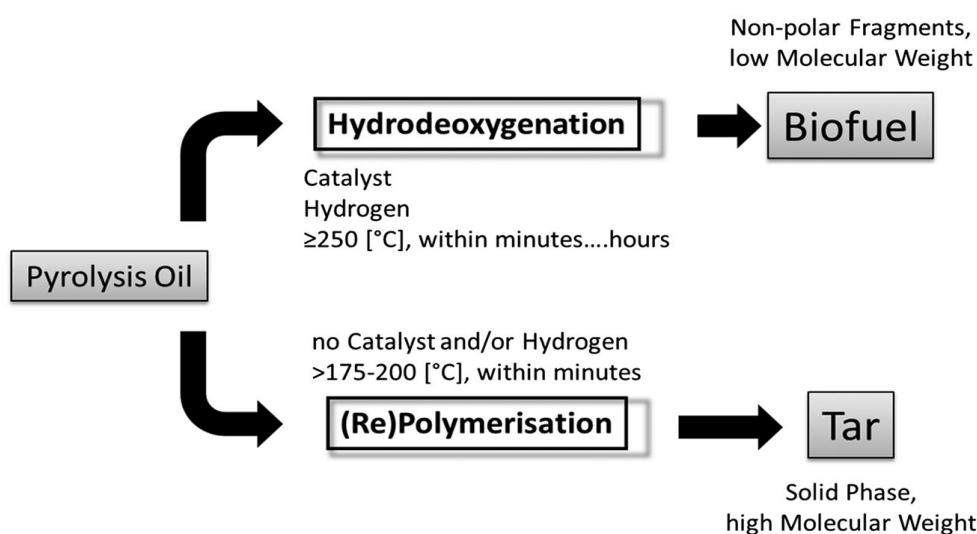


Figure 8. Reaction pathway [15,16].

experiments from 47 to 56 wt.% and in the deep HDO experiments from 61 to 84 wt.%. These results indicate that the harsh operation conditions led to a higher degree of HDO.

5.8. Molecular size measurements

A schematic HDO reaction pathway, proposed by Venderbosch and Mercader, is presented in Figure 8 [15,16]. Thereby, it is important to mention that during the HDO, the hydrotreating reactions are in competition with the polymerization reaction that leads to a solid phase with high molecular weight [16].

As presented in Figure 9, all mild HDO oils have a slightly higher molecular weight distribution (MWD) than the dehydrated pyrolysis oil (feed AVM: 500 g/mol). This indicates that polymerization reactions are taking place during the HDO. The lowest AVM (700 g/mol) was obtained when the Pt/C catalyst was used. These findings allow the conclusion that a catalyst that is capable of hydrogenating the dehydrated pyrolysis oil to the highest degree also hinders the polymerization reactions best. The Pd/C has the highest deoxygenation activity and is also capable of preventing extensive polymerization

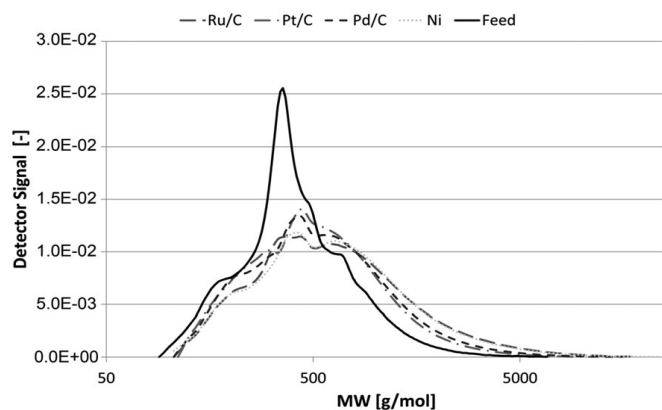


Figure 9. Molecular weight distribution of the mild hydrodeoxygenation oils (250 °C, 100 bar, 2 h).

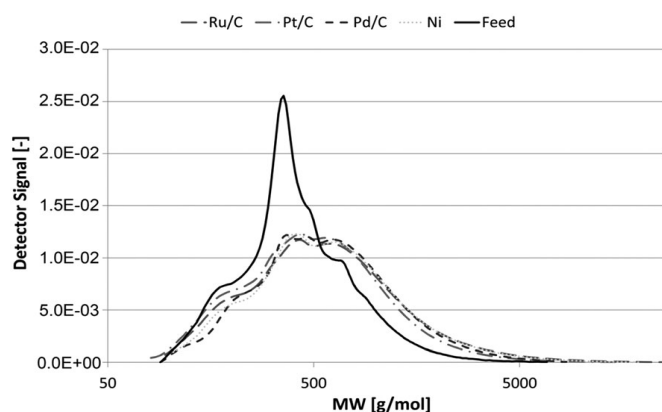


Figure 10. Molecular weight distribution of the deep hydrodeoxygenation oils (300 °C, 150 bar, 2 h).

(AVM 740 g/mol). The MWD of the mild oils produced by using the Ru/C (AVM 850 g/mol) and the Ni-based catalyst (AVM 860 g/mol) are very similar.

The MWD of the deep HDO oils is presented in Figure 10. It is obvious that the tested catalysts are not capable to suppress the polymerization reactions, and so the AVM of the obtained oils (Pt/C: 700 g/mol, Ru/C: 800 g/mol, Ni: 800 g/mol, and Pd/C 830 g/mol) is higher than from the dehydrated pyrolysis oil (feed AVM: 500 g/mol). It is worth mentioning that under harsh condition, polymerization reactions occur only to the same extent than under mild ones.

6. CONCLUSION

The HDO and dehydration of LPP oil, which were never reported in literature before, were investigated in this study. By this means this paper contributes to the understanding of LPP oil upgrading that differs from the intensively investigated fast pyrolysis oil. The HDO experiments were conducted under two operation conditions: 250 °C/100 bar (mild HDO) and under 300 °C/150 bar (deep HDO) with three noble metal catalysts and a Ni-based catalyst.

The main results of this study indicate the following:

1. Through dehydration, the water content of the LPP oil can be reduced by 86%. Thereby, the energy density and the efficiency of further process steps are increased, and the transportation costs are lowered.
2. HDO of dehydrated LPP oil is possible.
3. Under harsh conditions, deoxygenation ratio of 65% can be achieved.
4. The amount of solid phase obtained in the dehydrated LPP oils HDO experiments is much lower compared with the fast pyrolysis oils HDO experiments.
5. The investigated catalysts successfully applied for HDO of fast pyrolysis oil are able to hydrodeoxygenate dehydrated LPP oil.
6. Pt/C catalyst seems to be the most promising catalyst for HDO of LPP oil.
7. A total of 73–90% of the energy is transferred into fuel fraction/oil phase.

NOMENCLATURE

| | |
|--------|--|
| AMW | = average molecular weight |
| APS | = average particle size |
| GC-TCD | = gas chromatography thermal conductivity detector |
| GPC | = gel permeation chromatography |
| HDO | = hydrodeoxygenation |
| LCV | = lower calorific value |
| LPP | = liquid phase pyrolysis |
| MWD | = molecular weight distribution |

| | |
|-----------|---|
| SA | = surface area |
| VGO | = vacuum gas oil |
| WIS/DCMIS | = water-insoluble/dichloromethane insoluble |
| WIS/DCMS | = water-insoluble/dichloromethane soluble |
| WS/EIS | = water-soluble/ether insoluble |
| WS/ES | = water-soluble/ether soluble |
| WC | = water content |

ACKNOWLEDGEMENTS

We thank M. Derntl, T. Glatz, L. Steiner, J. Redlinger-Pohn, A. Toth, and A. Prettnner for assistance. This work was funded by the Austrian Research Promotion Agency (FFG) under the scope of A3 Plus Program.

REFERENCES

- Mortensen PM, Grunwaldt JD, Jensen PA, Knudsen KG, Jensen AD. A review of catalytic upgrading of bio-oil to engine fuels. *Applied Catalysis A: General* 2011; **407**:1–19.
- OPEC. World oil outlook 2008.
- OPEC. The oil industry. [Online]. Available: http://www.opec.org/opec_web/en/press_room/179.htm. [Accessed: 28-Dec-2011].
- Bernstein L, Bosch P, Canziani O, Chen Z, Christ R, Davidson O, Hare W, Huq S, Karoly D, Kattsov V, Kundzewicz Z, Liu J, Lohmann U, Manning M, Matsuno T, Menne B, Metz B, Mirza M, Nicholls N, Nurse L, Pachauri R, Palutikof J, Parry M, Qin D, Ravindranath N, Reisinger A, Renv J, Riahi K, Rosenzweig C, Rusticucci M, Schneider S, Sokona Y, Solomon S, Stott P, Stouffer R, Sugiyama T, Swart R, Tirpak D, Vogel C, Yohe G. IPCC: climate change 2007: Synthesis Report 2007; **21**.
- Bull T. Biomass in the energy picture. *Science* 1999; **285**(80):1209.
- Mercader FM, Groeneveld MJ, Kersten SRA, Venderbosch RH, Hogendoorn JA. Pyrolysis oil upgrading by high pressure thermal treatment. *Fuel* 2010; **89**:2829–2837.
- Bridgwater A, Double J. Production costs of liquid fuels from biomass. *International Journal of Energy Research* 1994; **18**:79–95.
- Schwaiger N, Feiner R, Zahel K, Pieber A, Witek V, Pucher P, Ahn E, Wilhelm P, Chernev B, Schrottner H, Siebenhofer M. Liquid and solid products from liquid-phase pyrolysis of softwood. *Bioenergy Research* 2011; **4**:294–302.
- Schwaiger N, Witek V, Feiner R, Pucher H, Zahel K, Pieber A, Pucher P, Ahn E, Chernev B, Schrottner H, Wilhelm P, Siebenhofer M. Formation of liquid and solid products from liquid phase pyrolysis. *Bioresource Technology* 2012; **124**:90–94.
- Feiner R, Schwaiger N, Pucher H, Ellmaier L, Pucher P, Siebenhofer M. Liquefaction of pyrolysis derived biochar: a new step towards biofuel from renewable resource. *RSC Advances* 2013; **3**:17898–17903.
- Vamvuka D. Bio-oil, solid and gaseous biofuels from biomass pyrolysis processes – an overview. *International Journal of Energy Research* 2011; **35**:835–862.
- Wildschut J, Mahfud FH, Venderbosch RH, Heeres HJ. Hydrotreatment of fast pyrolysis oil using heterogeneous noble-metal catalysts. *Industrial and Engineering Chemistry Research* 2009; **48**:10324–10334.
- Wildschut J, Iqbal M, Mahfud FH, Cabrera IM, Venderbosch RH, Heeres HJ. Insights in the hydrotreatment of fast pyrolysis oil using a ruthenium on carbon catalyst. *Energy and Environmental Science* 2010; **3**:962–970.
- Mercader FM, Groeneveld MJ, Kersten SRA, Geantet C, Toussaint G, Way NWJ, Schaverien CJ, Hogendoorn KJA. Hydrodeoxygenation of pyrolysis oil fractions: process understanding and quality assessment through co-processing in refinery units. *Energy and Environmental Science* 2011; **4**:985–997.
- Venderbosch RH, Ardiyanti AR, Wildschut J, Oasmaa A, Heeres HJ. Stabilization of biomass-derived pyrolysis oils. *Journal of Chemical Technology and Biotechnology* 2010; **85**:674–686.
- Mercader FM. Competition between hydrotreating and polymerization reactions during pyrolysis oil hydrodeoxygenation. *AIChE Journal* 2011; **57**:3160–3170.
- Oasmaa A, Kuoppala E. Fast pyrolysis of forestry residue. 3. Storage stability of liquid fuel. *Energy & Fuels* 2003; **17**:1075–1084.
- Oasmaa A, Kuoppala E, Solantausta Y. Fast pyrolysis of forestry residue. 2. Physicochemical composition of product liquid. *Energy & Fuels* 2003; **17**:433–443.
- Baldauf W, Balfanz U, Rupp M. Upgrading of flash pyrolysis oil and utilization in refineries. *Biomass and Bioenergy* 1994; **7**:237–244.
- Dubbel: Taschenbuch für den Maschinenbau*. Springer Verlag: Berlin Heidelberg, 1981.
- Laurent E, Delmon B. Influence of water in the deactivation of a sulfided NiMo/γ³-Al₂O₃ catalyst during

- hydrodeoxygenation. *Journal of Catalysis* 1994; **146**:281–291.
22. Masende ZPG, Kuster BFM, Ptasinski KJ, Janssen FJJG, Katima JHY, Schouten JC. Kinetics of malonic acid degradation in aqueous phase over Pt/graphite catalyst. *Applied Catalysis, B: Environmental* 2005; **56**:189–199.
23. Kubičková I, Snåre M, Eränen K, Mäki-Arvela P, Dmitry YM. Hydrocarbons for diesel fuel via decarboxylation of vegetable oils. *Catalysis Today* 2005; **106**:197–200.
24. Krevelen DW. Graphical-statistical method for the study of structure and reaction processes of coal. *Fuel* 1950; **29**:269–284.
25. Feiner R, Schwaiger N, Pucher H, Siebenhofer M. Biorefinery: a two step approach for producing liquid energy carriers based on lignocellulosic feed. *Achema* 2012.

Chapter 7

Lignocellulosic Biofuels:
Phase Separation during
Catalytic Hydrodeoxygenation of Liquid
Phase Pyrolysis Oil

Lignocellulosic Biofuels: Phase Separation during Catalytic Hydrodeoxygenation of Liquid Phase Pyrolysis Oil

H. Pucher,¹ N. Schwaiger,^{1,2} R. Feiner,^{1,2} L. Ellmaier,² P. Pucher,² B. S. Chernev,³ and M. Siebenhofer¹

¹Institute of Chemical Engineering and Environmental Technology, Graz University of Technology, Graz, Austria

²BDI-BioEnergy International AG, Grambach/Graz, Austria

³Institute for Electron Microscopy and Nanoanalysis, Graz, Steyrergasse, Austria

This paper contributes to the understanding of liquid phase pyrolysis (LPP) oil upgrading. The subject of discussion is hydrodeoxygenation (HDO). A three-stage hydrotreatment of liquid phase pyrolysis oil is described. It was found that during the initial heating stage conditions no HDO oil was produced. The HDO oil was formed during the main heating stage. During the initial heating stage, the oxygen content and the average molecular weight remained relatively constant. In the main heating stage the oxygen content decreased from 40 wt.% to 24 wt.% and the average molecular weight also decreases from 630 to 570 g/mol. Finally in the isothermal stage HDO oil was formed, indicated by a drop in oxygen content.

Keywords biomass to liquid; hydrodeoxygenation; liquid phase pyrolysis; phase separation; kinetic study (KS); pyrolysis oil upgrading

INTRODUCTION

It is generally assumed that only renewable resources are able to close the gap in the world's future energy availability. Biomass is particularly noteworthy because it is considered the renewable energy source in the next century (1). It provides a nearly immeasurable hydrocarbon resource, every year 3300 million m³ round wood (2) are consumed. Due to this fact it is a sufficient feedstock for chemical conversion to biofuels and basic stock chemicals (3, 4). However, there are still obstacles to overcome to make this biomass to liquid (BtL)-process economically and ecologically feasible. Standard refinery processes are currently not prepared for converting biomass to biofuels. The high transportation costs and low economic value of biomass necessitates a cheap liquefaction method to facilitate the conversion process into bio-fuels. In this project

pyrolysis is applied to convert biomass at elevated temperature and oxygen exclusion to liquid and solid intermediates. This paper provides a contribution to the understanding of liquid phase pyrolysis oil upgrading. The upgrading of LPP oil is a major issue of LPP. The influence of the temperature and reaction time on HDO of LPP oil was investigated.

Liquid Phase Pyrolysis

Different to fast pyrolysis (5–7) where sand is used, LPP uses a liquid heat carrier as heat transfer medium. Therefore, the process temperature of LPP is limited to the boiling point of the heat carrier. LPP, as applied in this project, converts any type of lignocellulosic biomass into pyrolysis oil, pyrolysis char (8–10) and lean gas as shown in Fig. 1. Unfortunately liquid CHO products and water form one phase, the so called LPP oil, and need HDO upgrading for water separation and H/C ratio improvement. Technology and process design of LPP were previously investigated (11–13). In 2012, a pilot scale LPP plant (bioCRACK) at OMV refinery in Vienna with a capacity of 100 kg of biomass per hour started operation.

Due to the decomposition of holocellulose and lignin this LPP oil is a mixture of different degradation products (14). It contains a large amount of oxygenated constituents like low molecular weight acids, aldehydes, and alcohols. It has high water content. These properties lead to limited stability of LPP oil, especially during storage, which is a major constraint. As far as biofuel production is concerned, improvement of product properties like water content, hydrogen and carbon content, molecule size, acidity, and stability of LPP oil is therefore a high priority issue.

Hydrodeoxygenation (HDO)

Hydrodeoxygenation (HDO) of Fast Pyrolysis (FP) oils has been reported (15–19). Only little information is available regarding HDO of LPP oil (20, 21). Main differences in composition and properties between FP oil and LPP oil are caused

Received 5 November 2014; accepted 4 August 2015.

Address correspondence to N. Schwaiger, Institute of Chemical Engineering and Environmental Technology, Graz University of Technology, Inffeldgasse 25/C, 8010 Graz, Austria.
E-mail: nikolaus.schwaiger@tugraz.at

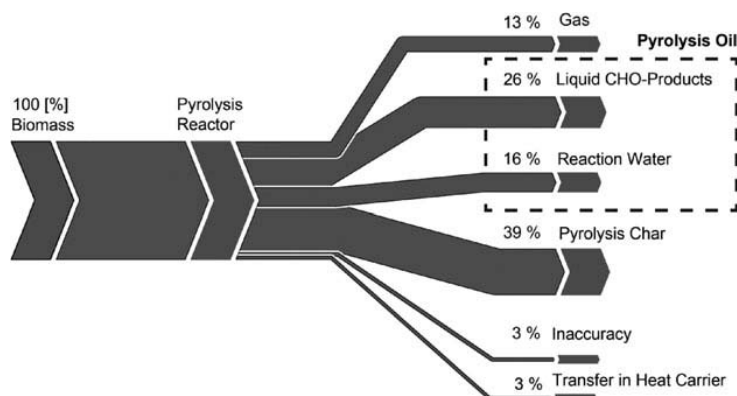


FIG. 1 Mass balance of LPP at $T=350^{\circ}\text{C}$ (11).

TABLE 1

Comparison of pyrolysis oil quality from FP (15) and LPP oil

| | FP oil | LPP oil |
|------------------------------------|----------------------------|-----------------------------|
| Water Content (wt.%) | 30 | 50 |
| Lower Calorific Value (MJ/kg) | 15.0 | 8.7 |
| Density (kg/m^3) | 1200 | 1070 |
| Viscosity (cP) | 40 at 40°C | <10 at 20°C |
| Elemental analysis on dry basis | | |
| Carbon Content (wt.%) | 51.1 | 47.4 |
| Hydrogen Content (wt.%) | 7.3 | 7.9 |
| Oxygen Content (wt.%) | 41.6 | 44.1 |
| Nitrogen Content (wt.%) | <1 | <1 |

by operation conditions during biomass liquefaction. Due to lower operation temperature, the liquefaction rate of LPP is lower. Opposite to FP inorganics and ash are trapped in the heat carrier oil while LPP. As shown in Table 1 LPP oil has (1) a higher water content (50 wt.% to 30 wt.%), (2) a lower carbon content (47.4 wt.% to 51.1 wt.%), (3) a higher oxygen content (44.1 wt.% to 41.6wt.%) (4) a lower density ($1070 \text{ kg}/\text{m}^3$ to $1200 \text{ kg}/\text{m}^3$) and (5) a lower load with inorganics (11) than FP oil.

During HDO different reactions occur in parallel (18). To achieve an insight into the HDO process and determine the influence of the temperature and reaction time different experiments were conducted. Investigations focused on the yield, the elemental composition, the molecular weight distribution (MWD), and the average molecular weight (AMW).

MATERIAL AND METHODS

Materials

The catalyst used in these experiments was Ni-based and it was obtained from Merck Millipore.

The LPP oil used for investigation was obtained from the pilot scale LPP plant (bioCRACK) at the OMV refinery in Vienna. It was produced from spruce wood chips (11, 12).

The LPP oil was analyzed and then stored in a refrigerator (6°C) to avoid aging. Selected properties of the LPP oil are shown in Table 1.

Experimental Set-Up and Procedure

LPP oil was hydrotreated in a 450 mL batch autoclave, type limbo from Büchi Glas Uster AG. The reactor content was stirred with a magnetically driven, gas-inducing, Rushton type impeller. The stirring speed was set to 500 rpm during the experiment as well as the cooling phase.

For each batch 100 g of LPP oil was fed to the reactor together with the catalyst. The catalyst to oil ratio on wet basis was 0.05. The reactor was pressurized with 50 bar of hydrogen at ambient temperature. Afterwards, the reactor was heated with a heating rate of $10^{\circ}\text{C}/\text{min}$ to the isothermal reaction temperature (300°C) or a preset time (see Table 2). During the isothermal stage hydrogen was continuously metered at 150 bar.

After the experiment was finished the reactor was immediately cooled to ambient temperature.

For mass balance calculations the weight of the reactor was measured before and after the gaseous/liquid product was relieved. Then the reactor was depressurized. The gas composition was determined. The solid and liquid reaction products were recovered and separated in a separating funnel.

Apparatus and Methods

The gas composition was analyzed for CH_4 , O_2 , CO_2 , and CO with a Mardur Photon II infrared gas analyzer.

The liquid products were characterized with a Vario Macro CHNO-analyzer, from Elementar Analysensysteme, in CHN Mode.

The determination of the molecular weight distribution was carried out with a Shimadzu RID – 10A Refractive Index

Detector and a Merck HITACHI L-6000A Pump and a SDV 5 μm 8 x 50 pre-column and two SDC 1000 \AA 8 x 300 columns from Polymer Standard Service. Size exclusion chromatography was calibrated against polystyrene. The MWD determination was carried out according to Hoekstra et al. (22).

The water content of the liquid products was determined with Gas Chromatograph with Thermal Conductivity Detector (GC-TCD) from Agilent Technologies and a column from HP-Innowax.

To identify specific components a gas chromatograph (GC) equipped with a mass spectrometer (Shimadzu GCMS-QP2010Plus + DB-1701) was used.

RESULTS AND DISCUSSION

To determine the influence of the temperature and the reaction time different experiments were conducted. Detailed experimental data are illustrated in Table 2. Table 2 shows the effect of time and temperature on phase separation of LPP oil. The results show that in the initial heating stage (0-9 min, 25-136°C) two different product phases were found after the experiment. In the heating stage (16-33 min, 225-300°C) as well as in the isothermal stage (33-273 min, 300°C) three product phases were found after the experiment. The yields of the different phases remained nearly constant in the isothermal stage. Despite this the deoxygenation rate (DOR) still increased and the AMW decreased with ongoing reaction time and temperature (23). The mass balance closure varied between 95% and 99%. The most likely reasons for inaccuracy were the complicated separations due to the high viscosity and stickiness of LPP oil.

Initial Heating Stage

At the end of the initial heating stage of the HDO process two product phases were found—a brown water phase and a gas phase. The density and viscosity of the water phase were

TABLE 2
Product distribution during experiments of the HDO of LPP oil

| | Time (min) | Temp. (°C) | Water Phase (wt.%) | Oil Phase (wt.%) | Gas Phase (wt.%) |
|-----------------------|------------|------------|--------------------|------------------|------------------|
| Initial heating stage | | | | | |
| | 0 | 25 | 100.0 | 0.0 | 0.0 |
| KS_5 | 5 | 73 | 98.4 | 0.0 | 1.6 |
| KS_9 | 9 | 136 | 98.5 | 0.0 | 1.5 |
| Main heating stage | | | | | |
| KS_16 | 16 | 225 | 88.0 | 10.1 | 1.9 |
| KS_19 | 19 | 264 | 83.0 | 15.0 | 2.1 |
| KS_23 | 23 | 277 | 80.5 | 17.4 | 2.1 |
| KS_33 | 33 | 300 | 80.7 | 17.3 | 2.1 |
| Isothermal stage | | | | | |
| KS_153 | 153 | 300 | 75.5 | 21.0 | 3.4 |
| KS_273 | 273 | 300 | 74.7 | 21.3 | 4.0 |

equal to the density and viscosity of the LPP oil. The gas yield ranged between 0 and 2 wt.%. The main gaseous component was unreacted hydrogen. This gas could potentially be recycled or burned directly to produce heat.

Heating Stage and Isothermal Stage

After the heating stage and the isothermal stage of the HDO process three product phases were found: a clear slightly brown water phase; a dark brown oil phase and a gas phase. Density and viscosity of the oil phase were higher than the density and viscosity of the water phase. The gas yield ranged between 2 and 4 wt.%. The main gaseous components were unreacted hydrogen and carbon dioxide. Carbon dioxide (3-6 mol%) can be formed through the decarboxylation of organic acids, like acetic and formic acid, common constituents in LPP oils (8-10 wt.%) (24-26). This gas could be potentially recycled or burned directly to produce heat.

Elemental Composition

As shown in Fig. 2, it is obvious that in the initial heating stage the elemental composition of the aqueous phase was similar to the feed, suggesting no HDO of the feed. The first oil phase was produced between 136 and 225°C. After that the oxygen content on dry basis was reduced from 40 to 25 wt.%. It is apparent that the composition of the oil phase was improved with ongoing reaction time and temperature, indicated by the drop of oxygen and increase of hydrogen. Comparison of products after 33, 153, and 273 minutes underlines the advantage of elevated temperature and reaction time. The oxygen content of the oil phase was lowered from 24.4 wt.% after 33 min to 19.4 wt.% after 153 min and 18.5 wt.% after 273 min.

Van Krevelen Plot

The effects of process conditions and catalyst on the elemental composition of the hydrodeoxygenated LPP oil is shown in

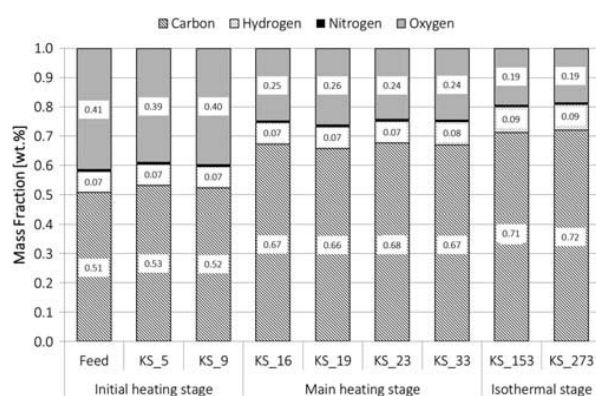


FIG. 2 Elemental composition on dry basis of the aqueous phase and oil phase during HDO according to phase formation as shown in Table 2.

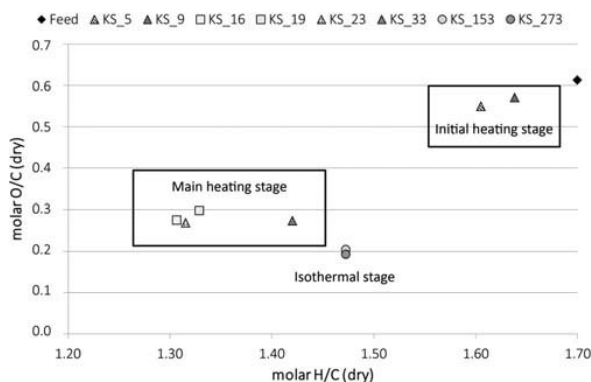


FIG. 3 Van Krevelen Plot on dry basis.

Fig. 3 (27). The molar oxygen to carbon (O/C) ratio was decreasing and the molar hydrogen to carbon (H/C) ratio was increasing with reaction time. In the initial heating stage the molar composition was similar to the feed (see section titled “Elemental Composition”). In the heating stage the molar O/C ratio was lowered from 0.28 at 16 minutes to 0.27 at 33 minutes. The molar H/C ratio was increased from 1.31 at 16 minutes to 1.42 at 33 minutes. In the isothermal stage HDO reaction was continued and the molar O/C ratio was lowered to 0.19 after 273 minutes. The molar H/C ratio was 1.47 after the same time.

Molecular Weight Distribution (MWD) Based on Gel Permeation Chromatography (GPC)

A schematic HDO reaction pathway was proposed by Venderbosch and Mercader (18, 19). It is important to mention that during HDO, the hydrotreating reactions are in competition

with polymerization reactions which can lead to the formation of a solid or liquid tar phase with high molecular weight (19).

As presented in Fig. 4, it is obvious that the reaction time as well as the temperature had an impact on the MWD. It seems that all product phases have a slightly higher MWD than the LPP oil (Feed AMW: 420 g/mol). In the initial heating stage the aqueous phases were similar to the feed (KS_5 AMW: 430 g/mol, KS_9 AMW: 440 g/mol).

After phase separation the MWD and the AMW was increased by 50% because of accumulation of oligomers in the product phase (KS_16 AMW 630 g/mol, KS_19 AMW: 660 g/mol, KS_23 AMW 640 g/mol, KS_33 AMW: 570 g/mol). Due to hydrodeoxygenation the polarity of the LPP oil components change. The polar, low molecular weight, and oxygen rich components are separated and a nonpolar oil phase is produced. Due to this fact and the normalization of the detector signal, the oil phase seemingly shifted to an increased molecular weight. This increase in MW suggests polymerisation reactions. While actually the oil phase was cracked (see experiments; KS_153 AMW: 510 g/mol, KS_273 AMW: 510 g/mol).

GC-MS Results

The product phases were analyzed by GC-MS to better understand the specific composition. The quantities shown in Table 3 approximate (+/- 50%) the actual situation, because components were not specifically quantified. Due to the fact that the chromatograms were quite complex, only a representative standard, according to Elliott et al. (28), was used for each chemical compound.

The amount of “Unknowns” increased from 31 to 77% due to phase separation. This indicates, as shown in section titled “Molecular Weight Distribution (MWD) Based on Gel

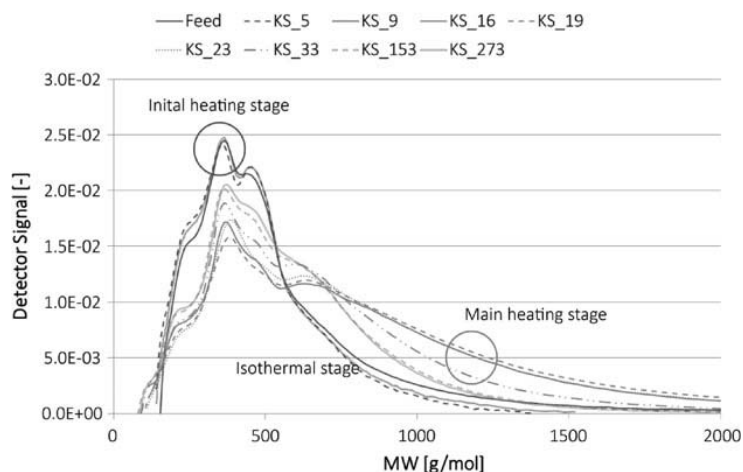


FIG. 4 Molecular weight distribution (MWD).

TABLE 3
Chemical compounds found by gas chromatography (GC-TCD
and GC-MS) in the LPP oil (Feed) and the oil phases of
KS_16, KS_33 and KS_153

| | Feed | KS_16 | KS_33 | KS_153 |
|------------------|------|-------|-------|--------|
| Oil Phase (wt.%) | 0 | 10.1 | 17.3 | 21.0 |
| Unknowns (wt.%) | 31 | 64 | 77 | 65 |
| Water [wt.%] | 50 | 22 | 12 | 8 |
| Ketones [wt.%] | 7 | 10 | 2 | 13 |
| Diketones [wt.%] | 1 | 0 | 0 | 1 |
| Phenols [wt.%] | 0 | 3 | 0 | 4 |
| Ester [wt.%] | 0 | 0 | 0 | 2 |
| Acids [wt.%] | 9 | 8 | 8 | 8 |
| Aldehydes [wt.%] | 2 | 0 | 0 | 0 |
| Sugars (wt.%) | 1 | 0 | 0 | 0 |

Permeation Chromatography (GPC),” that low molecular weight, GC-MS detectable and oxygen rich compounds, and the water were separated from the initial mixture. Due to the polarity change of components triggered by hydrogenation, phase separation between 136 and 225°C occurred. The non polar oil phase contained the high molecular weight components of the LPP oil with low oxygen content. With increasing time and temperature, these high molecular weight compounds are cracked and increase the amount of identifiable components.

Attenuated Total Reflectance Infrared Spectroscopy (ATR-IR)

As shown in Fig. 5 the C-H peak at 3000cm⁻¹ is almost completely superimposed by the O-H peak at 3000-3500 cm⁻¹. The C=O peak at about 1700 cm⁻¹ represents the carbohydrate

degradation products such as formaldehyde, hydroxy propanone, acetone, and furancarboxaldehyde in general substances with carbonyl groups. The stretching vibrations decrease from the range of 1000 cm⁻¹, because only few hemiacetals and alcohols, as expected in carbohydrates, are present in the LPP oil. (3)

In Fig. 6 the ATR-IR spectrum of the oil phase of the KS_23 and KS_153 are shown. It is apparent that the OH peak between 3000 and 3500 cm⁻¹ depleted with increasing temperature and time indicating conversion and loss of hydroxyl groups due to phase separation.

The C-H peak at 3000 cm⁻¹ and the characteristic peaks for aromatics continuously increase with rising temperature and time.

CONCLUSIONS

HDO of LPP oil was carried out at a temperature of 300°C and a hydrogen pressure of 150 bar. Several experiments were conducted to investigate the influence of the temperature and reaction time on HDO of LPP oil.

The results of these investigations show that:

1. HDO of LPP oil from spruce wood is possible.
2. The influence of the initial heating stage as well as the main heating stage is significant. The oxygen content of the oil phase during both stages is depleted by 41%.
3. In the initial heating stage hydrodeoxygenation reactions partially lower the oxygen content of organic components of LPP oil and phase separation between aqueous constituents and low oxygenated hydrocarbons (CHO) is observed within the temperature range from 136°C and 225°C.
4. Because of phase separation the MWD/AMW seemingly increases.
5. Actually advancing DOR does decrease the AMW and MWD of the oil phase with increasing temperature and reaction time.

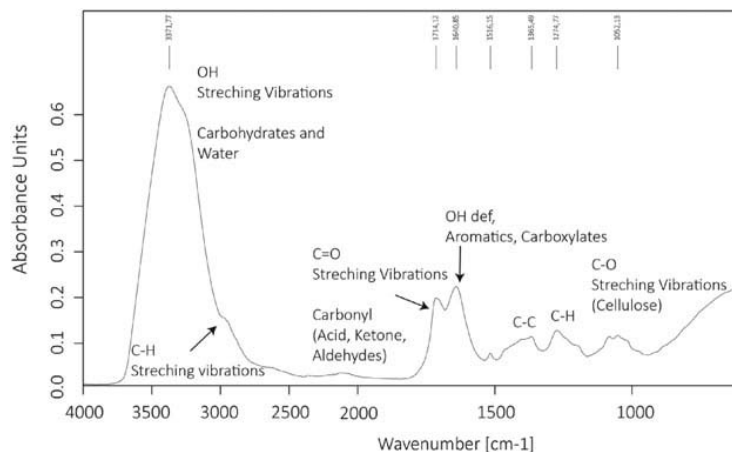


FIG. 5 ATR-IR spectrum of LPP oil (21).

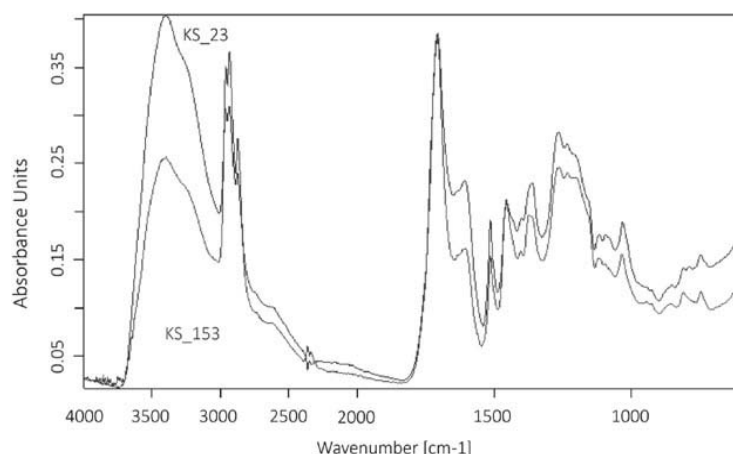


FIG. 6 ATR-IR spectrum of the oil phase of the KS_23 and KS_153.

ACKNOWLEDGEMENTS

We thank A. Rollett, M. Aitken, R. Pichler, H. Kindermann, J. Binder, R. Fellner, S. Krainer, J. Drack, A. Toth, and M. Tandler for assistance.

FUNDING

This work was funded by the Austrian Research Promotion Agency (FFG) under the scope of A3 Plus Program.

REFERENCES

- Bull, T. (1999) Biomass in the energy picture. *Science*, 80(285):1209.
- Gellerstedt, G. (2009) *The Worldwide Wood Resource*. Wood Chem. Wood Biotechnol.; De Gruyter, Amsterdam, pp. 1–12.
- Schwaiger, N. (2011) Reaktionstechnische Analyse für die Optimierung der Flüssigphasenpyrolyse. pp. 1–70.
- Nimz, H. H., Schmitt, U., Schwab, E. (2000) *Wood*. Ullmann's Encycl. Ind. Chem.; Wiley: Weinheim, Germany, pp. 454–503.
- Bridgwater, A. V., Meier, D., Radlein, D. (1999) An overview of fast pyrolysis of biomass. *Org Geochem.*, 30:1479–1493.
- Meier, D., Faix, O. (1999) State of the art of applied fast pyrolysis of lignocellulosic materials: A review. *Bioresour Technol.*, 68:71–77.
- Mohan, D., Pittman, C. U, Steele, P. H. (2006) Pyrolysis of wood/biomass for bio-oil: A critical review. *Energy & Fuels*, 20:848–889.
- Feiner, R., Schwaiger, N., Pucher, H. (2013) Liquefaction of pyrolysis derived biochar: A new step towards biofuel from renewable resources. *RSC Adv.*, 3:17898–17903.
- Feiner, R., Schwaiger, N., Pucher, H. (2014) Chemical loop systems for biochar liquefaction: Hydrogenation of naphthalene. *RSC Adv.*, 4:34955.
- Feiner, R., Schwaiger, N., Pucher, H. (2014) Kinetics of biochar liquefaction. *BioEnergy Res.*, 7:1343–1350.
- Schwaiger, N., Feiner, R., Zahel, K. (2011) Liquid and solid products from liquid-phase pyrolysis of softwood. *BioEnergy Res.*, 4:294–302.
- Schwaiger, N., Witek, V., Feiner, R. (2012) Formation of liquid and solid products from liquid phase pyrolysis. *Bioresour Technol.*, 124:90–94.
- Ritzberger, J., Pucher, P., Schwaiger, N., Siebenhofer, M. (2014) The BioCRACK Process: A refinery integrated biomass-to-liquid concept to produce diesel from biogenic feedstock. *Chem Eng Trans.*, 39:1189–1194.
- Mercader, F. M., Groeneveld, M. J., Kersten, S. R. A. (2010) Pyrolysis oil upgrading by high pressure thermal treatment. *Fuel*, 89:2829–2837.
- Wildschut, J., Mahfud, F. H., Venderbosch, R. H., Heeres, H. J. (2009) Hydrotreatment of fast pyrolysis oil using heterogeneous noble-metal catalysts. *Ind Eng Chem Res.*, 48:10324–10334.
- Wildschut, J., Iqbal, M., Mahfud, F. H. (2010) Insights in the hydrotreatment of fast pyrolysis oil using a ruthenium on carbon catalyst. *Energy Environ Sci.*, 3:962–970.
- De Miguel Mercader, F, Groeneveld, M. J., Kersten, S. R. A. (2011) Hydrodeoxygenation of pyrolysis oil fractions: Process understanding and quality assessment through co-processing in refinery units. *Energy Environ Sci*, 4:985.
- Venderbosch, R. H., Ardiyanti, A. R., Wildschut, J. (2010) Stabilization of biomass-derived pyrolysis oils. *J Chem Technol Biotechnol.*, 85:674–686.
- Mercader, F. D. M. (2011) Competition between hydrotreating and polymerization reactions during pyrolysis oil hydrodeoxygenation. *AIChE J*, 57:3160–3170.
- Pucher, H., Schwaiger, N., Feiner, R. (2014) Catalytic hydrodeoxygenation of dehydrated liquid phase pyrolysis oil. *Int J Energy Res.*, 38:1964–1974.
- Pucher, H., Schwaiger, N., Feiner, R. (2014) Biofuels from liquid phase pyrolysis oil: a two-step hydrodeoxygenation (HDO) process. *Green Chem.*, doi:10.1039/C4GC01741B
- Hoekstra, E., Kersten, S. R. A., Tudos, A. (2011) Possibilities and pitfalls in analyzing (upgraded) pyrolysis oil by size exclusion chromatography (SEC). *J Anal Appl Pyrolysis*, 91:76–88.
- Baldauf, W., Balfanz, U., Rupp, M. (1994) Upgrading of flash pyrolysis oil and utilization in refineries. *Biomass and Bioenergy*, 7:237–244.
- Laurent, E., Delmon, B. (1994) Influence of water in the deactivation of a sulfided NiMo/ γ -Al₂O₃ catalyst during hydrodeoxygenation. *J Catal.*, 146:281–291.
- Masende, Z. P. G., Kuster, B. F. M., Ptasinski, K. J. (2005) Kinetics of malonic acid degradation in aqueous phase over Pt/graphite catalyst. *Appl Catal B Environ* 56:189–199.
- Kubičková, I., Snáre, M., Eränen, K. (2005) Hydrocarbons for diesel fuel via decarboxylation of vegetable oils. *Catal Today* 106:197–200.
- Krevelen, D. W. (1950) Graphical-statistical method for the study of structure and reaction processes of coal. *Fuel* 29: 269–284.
- Elliott, D. C., Hart, T. R., Neuenschwander, G. G. (2012) Catalytic hydroprocessing of fast pyrolysis bio-oil from pine sawdust. *Energy & Fuels* 26:3891–3896.

Chapter 8

Biofuels from liquid
phase pyrolysis oil:
a two-step hydrodeoxygenation (HDO) process



Cite this: *Green Chem.*, 2015, **17**, 1291

Biofuels from liquid phase pyrolysis oil: a two-step hydrodeoxygenation (HDO) process

Hannes Pucher,^a Nikolaus Schwaiger,^{*a,b} Roland Feiner,^{a,b} Lisa Ellmaier,^b Peter Pucher,^b Boril. S. Chernev^c and Matthäus Siebenhofer^a

New biomass utilization technologies and concepts are needed to suffice future increasing energy demand. This paper contributes to the understanding of liquid phase pyrolysis (LPP) oil upgrading, which significantly differs from fast pyrolysis (FP) oil upgrading processes. A two-step hydrodeoxygenation (HDO) process was established to convert the LPP oil into a biofuel with diesel fuel-like properties. In the first HDO step (250 °C, 85 bar), the bulk of the water and most of the highly-oxygenated water-soluble carbonaceous constituents were removed, to lower hydrogen consumption in the second HDO step. In addition, the highly reactive compounds were stabilized in the first step. In the second HDO step (400 °C, 150/170 bar), the product specification was improved. This paper shows a proof-of-principle for a two-step HDO process for converting LPP oil to a diesel-like biofuel.

Received 8th September 2014,
Accepted 29th October 2014

DOI: 10.1039/c4gc01741b

www.rsc.org/greenchem

Introduction

This work addresses the production of LPP oil, to help increase efficiency of LPP oil upgrading technology. A two-step HDO process was established to convert LPP oil into a biofuel with diesel fuel-like properties.

It is expected that energy from renewable resources will close the rising gap in the world's future energy demand. Biomass has high potential as a renewable resource because it provides a nearly immeasurable quantity of renewable biologically-fixed carbon (1.24×10^{12} tons).¹⁻³

However, there are still obstacles to be overcome in order to make biomass to liquid (BTL)-processes economically and ecologically feasible. Standard refinery processes are currently not applicable for converting biomass to biofuels. The high transportation costs and low energy density of biomass, mean that there is a demand for cheap pretreatment, to facilitate the conversion process. In this project, LPP is used to convert the biomass to liquid intermediates.

Liquid phase pyrolysis (LPP)

The LPP process applied for this project converts any type of non-edible lignocellulosic biomass into bioCRACK oil (BCO), LPP oil, pyrolysis char and pyrolysis gas. The technology and

process design of the LPP and the upgrading of the pyrolysis char have been previously reported.⁴⁻⁷ In 2012, a pilot scale LPP plant (bioCRACK plant) with a capacity of 100 kg of biomass per hour started operation at OMV refinery in Vienna. This pilot plant uses VGO as a liquid heat carrier. VGO has a high boiling range, between 320 °C and 580 °C, and an elemental composition of 86 wt% carbon and 12 wt% hydrogen. As shown in Fig. 1, 20 wt% of the biogenous carbon in the biomass is converted into LPP oil.

Due to the decomposition of holocellulose and lignin, LPP oil is a mixture of different degradation products.⁸ It contains a large amount of oxygenated constituents, such as low molecular weight acids, aldehydes and alcohols. It has a high water content and limited stability, especially during storage, which is a major drawback. Therefore, improvement of the product quality and stability of LPP oils is highly desirable.

The produced BCO is a mixture of VGO and biogenous constituents (10 wt%). Table 1 shows selected properties of LPP oil, BCO and conventional diesel. BCO has almost diesel fuel-like properties and can be directly refined in a conventional refinery.

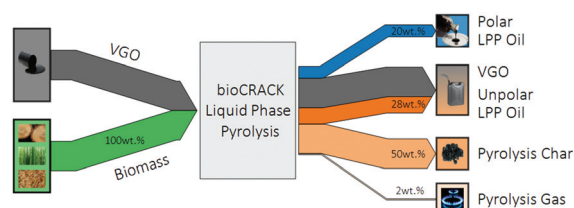


Fig. 1 Biogenous carbon balance for LPP at $T = 350$ °C (mass balance inaccuracy is 5%).

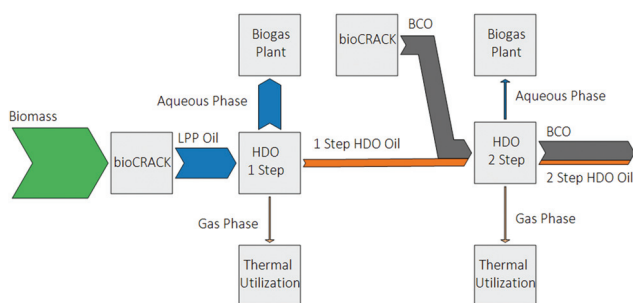
^aInstitute of Chemical Engineering and Environmental Technology, NAWI Graz, Central Lab Biobased Products, Graz University of Technology, Inffeldgasse 25/C, 8010 Graz, Austria. E-mail: nikolaus.schwaiger@tugraz.at

^bBDI-BioEnergy International AG, Parkring 18, 8074 Grambach/Graz, Austria

^cAustrian Centre for Electron Microscopy and Nanoanalysis, Steyrergasse 17/III, 8010 Graz, Austria

Table 1 Comparison of LPP oil, BCO and conventional diesel

| | LPP oil | BCO | Diesel |
|-----------------------------------|---------|------|--------|
| Water content (wt%) | 50 | 0.04 | 0.02 |
| LCV (MJ kg ⁻¹) | 8.7 | 40.1 | 42.5 |
| Density (kg m ⁻³) | 1070 | 890 | 835 |
| Viscosity (mPa s) | 4 | 8 | 4 |
| Biogenous carbon (wt%) | 100 | 10 | <7 |
| Elemental analysis on a wet basis | | | |
| Carbon content (wt%) | 25.6 | 83.6 | 85.9 |
| Hydrogen content (wt%) | 9.2 | 11.8 | 13.3 |
| Oxygen content (wt%) | 64.9 | 4.2 | <1 |
| Nitrogen content (wt%) | <1 | <1 | <1 |

**Fig. 2** Scheme of the two-step HDO process.

Hydrodeoxygenation (HDO)

Hydrodeoxygenation (HDO) of FP oil has been previously reported.^{9–13} Only a little information is available regarding the HDO of LPP oil.¹⁴ Compared to FP oils,⁹ LPP oils have (1) a higher water content (50 wt% vs. 30 wt%), (2) a lower carbon content (47.4 wt% vs. 51.1 wt%), (3) a higher oxygen content (44.1 wt% vs. 41.6 wt%), (4) a lower density (1070 kg m⁻³ vs. 1200 kg m⁻³) and (5) a lower content of inorganics and char.⁴

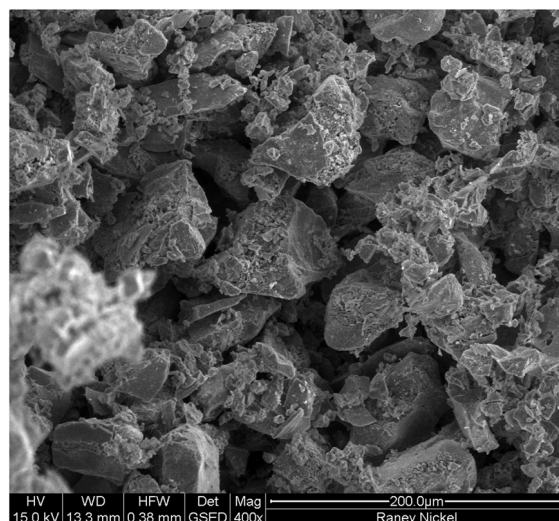
During HDO, different reactions occur in parallel.¹² To achieve an insight into the HDO process and to determine the influence of the temperature and reaction time, studies were conducted and the results were published elsewhere.¹⁴ Based on these results, a two-step HDO process, see Fig. 2, was established to convert LPP oil into a biofuel with diesel fuel-like properties. Investigations focused on the mass/energy yield, the elemental composition, the density, the viscosity, the distillation characteristics and the biogenous carbon content.

Material and methods

Materials

RANEY® nickel as a pre-activated catalyst (CAS: 7440-02-0, Merck 8208760250) consisting of 90% Ni and 10% Al (by weight, on a dry basis), was obtained from Merck Millipore and used for the hydrodeoxygenation in the form shown in Fig. 3.

The LPP oil used for the investigations was obtained from the pilot scale LPP plant (bioCRACK plant) at the OMV refinery in Vienna. It had been produced from spruce wood pellets.^{4,5}

**Fig. 3** RANEY® nickel as used for the hydrodeoxygenation.

The LPP oil was analyzed and then stored in a refrigerator (6 °C) to avoid aging. Select properties of the LPP oil are shown in Table 1.

Experimental set-up and procedure

The LPP oil was hydrotreated in a 450 ml batch reactor, of type limbo, from Büchi Glas Uster AG. The reactor was equipped with a magnetically driven, gas-inducing, Rushton type impeller. The stirring speed was set to 500 rpm during the experiment.

First HDO step – procedure

For each batch, 100 g of LPP oil and the catalyst were fed into the reactor. The catalyst to oil ratio, on a wet basis, was 0.05 : 1. The reactor was pressurized with 50 bar of hydrogen at ambient temperature. Afterwards, the reactor was heated, at a heating rate of 10 °C min⁻¹, to the isothermal reaction temperature of 250 °C. During the isothermal stage, the hydrogen pressure was continuously kept at 85 bar.

Second HDO step – procedure

For each batch, 100 g of a mixture of LPP oil, BCO and catalyst were fed into the reactor. Two different BCO to LPP oil ratios were investigated (2.5 : 1 and 4 : 1). The catalyst to feed ratio, on a wet basis, was 0.10 : 1 in both experiments. The reactor was pressurized with 50 bar of hydrogen at ambient temperature. Afterwards, the reactor was heated, at a heating rate of 10 °C min⁻¹, to the isothermal reaction temperature of 400 °C. During the isothermal stage, the hydrogen pressure was continuously kept at 150/170 bar.

Cooling procedure

After the experiment was finished, the reactor was rapidly cooled to ambient temperature. Then, the reactor was depressurized and the gas composition was determined. The solid

and liquid reaction products were recovered and separated using a separating funnel.

Apparatus and methods

The gas obtained was analyzed for its composition of CH₄, O₂, CO₂ and CO, using a Mardur Photon II infrared gas analyzer.

The liquid products were characterized using a Vario Macro CHNO-analyzer from Elementar Analysensysteme, in the CHN mode.

The water content of the liquid products was determined using a gas chromatograph with a thermal conductivity detector (GC-TCD) from Agilent Technologies and a HP-Innowax column.

The biogenous carbon content of the liquid samples was determined by Beta Analytic according to the standard EN 15440.

The distillation characteristics of the BCO and the HDO oil from the 2nd step were determined using a Gas Chromatograph-SimDist MXT 2887 with a 10 m column from Restek and Agilent 7890A GC.

The IR-ATR spectra of the liquid products were recorded using a Tensor 37 spectrometer from Bruker. The samples were measured by attenuated total reflection (ATR) using a MIRacle® unit with a diamond crystal. The spectra were accumulated with a spectral resolution of 4 cm⁻¹.

GC-MS analyses were performed using a GCMS-QP 2010 Plus from Shimadzu with a 60 m DB-1701 column. Data comparison was performed using the peak area units.

GPC of the liquid product was carried out with a Shimadzu RID-10A Refractive Index Detector and a Merck HITACHI L-6000A Pump. A SDV 5 μm 8 × 50 mm precolumn and two SDC 1000 Å 5 μm 8 × 300 mm columns from PSS were used. The GPC was calibrated against polystyrene samples of 163 g mol⁻¹ and 1890 g mol⁻¹ molar masses.

Results and discussion

According to Fig. 2, a two-step process was established to convert the LPP oil into biofuel with diesel fuel-like properties.

In a first HDO step, the LPP oil was stabilized at 250 °C and 85 bar hydrogen pressure. The bulk of the water and the highly oxygenated carbonaceous constituents were removed.

In the second HDO step, the 1st step HDO oil was mixed with the BCO from the bioCRACK plant and then treated at 400 °C, to improve the product specification. The 2nd step HDO oil has nearly similar properties to conventional diesel. The experimental matrix is illustrated in Table 2. The reaction

time for the preheating and the isothermal operation have been discussed separately.

The mass balance closure varied from 97% to 99%. The most likely reasons for the inaccuracy were the complicated separations, due to the high viscosity and stickiness of the 1st step HDO oil.

Key figures

For a better understanding, some key figures are defined here.

The mass yield (MY_{Phase}), which is the fraction of a single product phase (*m*_{Phase, dry}) within the total mass of all the product phases ($\sum m_{\text{Phase, dry}}$) on a dry basis, is calculated according to eqn (1).

In order to calculate the energy yield (EY_{Phase}) of a single phase, the lower calorific value (*H*_{i, Phase}) is calculated according to eqn (2).¹⁵ The energy yield of each phase (EY_{Phase}) is calculated by dividing the energy content of each phase (*m*_{Phase}·*H*_{i, Phase}) by the sum of the energy contents for all phases (see eqn (3)).

$$MY_{\text{Phase}} = \frac{m_{\text{Phase, dry}}}{\sum m_{\text{Phase, dry}}} \quad (1)$$

$$H_{i, \text{Phase}} = 34.0w_{\text{C}} + 101.6w_{\text{H}} + 6.3w_{\text{N}} + 19.1w_{\text{S}} - 9.8w_{\text{O}} - 2.5w_{\text{H}_2\text{O}} \quad (2)$$

$$EY_{\text{Phase}} = \frac{m_{\text{Phase}} H_{i, \text{Phase}}}{\sum m_{\text{Phase}} H_{i, \text{Phase}}} \quad (3)$$

First HDO step

After the first HDO step, the formation of three product phases was observed: a clear slightly brown water phase which could be processed further in a biogas plant; a dark brown oil phase (1st step HDO oil) and a gas phase. It is important to mention that no solid phase was produced in the first HDO step. The density and viscosity of the 1st step HDO oils were higher than the density and viscosity of the aqueous phase and the LPP oil (feedstock). The gas yield was between 1 and 2 wt%. The main gaseous components were unreacted hydrogen and carbon dioxide. Carbon dioxide was formed through the decarboxylation of organic acids, such as acetic and formic acid, which are common constituents in pyrolysis oils (8–10 wt%).^{16–18} This gas could potentially be recycled or burned directly to produce heat.

Second HDO step

After the second HDO step, three product phases were also found: an almost transparent aqueous phase which can be

Table 2 Experimental matrix

| | Step | BCO/1 st step HDO oil Ratio | Catalyst amount [wt%] | Temperature [°C] | Pressure [bar] | Time [min] |
|-----------|------|--|-----------------------|------------------|----------------|------------|
| HDO_1_4 | 1 | — | 5 | 250 | 85 | 240 |
| HDO_2_4 | 2 | 4 : 1 | 10 | 400 | 170 | 120 |
| HDO_1_2.5 | 1 | — | 5 | 250 | 85 | 120 |
| HDO_2_2.5 | 2 | 2.5 : 1 | 10 | 400 | 150 | 120 |

processed further in a biogas plant; a clear slightly brown oil phase (2nd step HDO oil) and a gas phase. It has to be mentioned that even at the high temperatures of the second HDO step no solid phase was produced. This indicates that the constituents of the LPP oil were stabilized in the first HDO step. Dilution of the 1st step HDO oil with BCO retards polymerization at high temperatures. The density and viscosity of the 2nd step HDO oils were lower than the density and viscosity of the LPP oil and the BCO (feed). The gas yield was between 5 and 10 wt%. The main gaseous components were unreacted hydrogen, carbon dioxide and methane. This gas can be recycled or incinerated.

Mass and energy yield

In Fig. 4, the corresponding MY_{Phase} and EY_{Phase} for each experiment and each phase are shown. The elemental composition of the 1st/2nd step HDO oil on a dry basis can be found in Fig. 5.

In the first HDO step (experiments HDO_1_4 and HDO_1_2.5), 19 and 22 wt% of the LPP oil was converted into an oil phase (1st step HDO oil), which accumulated 67 and 70% of the energy content of the feed, respectively. On a dry basis, the 1st step HDO oils contained 70 wt% carbon and

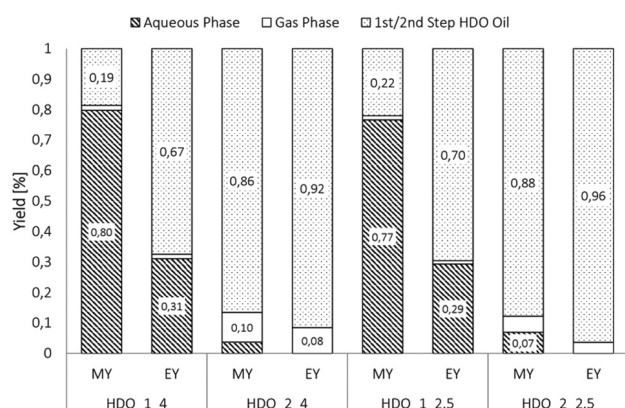


Fig. 4 Mass (MY_{Phase}) and energy (EY_{Phase}) yields for each experiment.

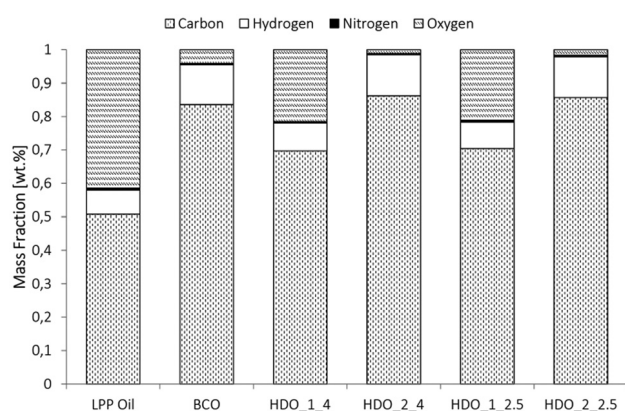


Fig. 5 The elemental compositions of the 1st/2nd step HDO oil, on a dry basis.

8.0 wt% hydrogen. Compared to the LPP oil, on a dry basis, the amount of oxygen was reduced, to 21 wt%.

In the second HDO step (experiments HDO_2_4 and HDO_2_2), 87% (on average) of the feed (the 1st step HDO oil and BCO) was converted into an oil phase (2nd step HDO oil). This phase contained 92 to 96% of the accumulated energy of the feed. The 2nd step HDO oils contained less oxygen and more hydrogen and carbon than BCO. It can be concluded, that through the second HDO step the elemental composition of the oil is improved, despite the accumulation of the biogenous carbon content. 62 to 67% of the energy content in terms of the LCV was present in the 2nd step HDO oil.

van Krevelen plot

To quantify the effect of HDO on the quality of the LPP oil, the molar ratios of oxygen to carbon (O/C) and hydrogen to carbon (H/C) were plotted in a van Krevelen plot (see Fig. 6).¹⁹

In order to obtain a biofuel with diesel fuel-like properties, the molar O/C ratio must be reduced and the molar H/C ratio must be increased. By decreasing the oxygen content, the chemical stability, lower heating value (LCV) and energy density of the fuel can be improved.

In the first HDO step (experiments HDO_1_4 and HDO_1_2.5), the molar O/C ratio was reduced by 63% (on average) to 0.23 and 0.22. At the same time, the molar H/C ratio decreased significantly (HDO_1_4: decreased by 16% to 1.43, HDO_1_2.5: decreased by 21% to 1.35). These results indicate that neither the reaction temperature (250 °C) nor the reaction pressure (85 bar) was sufficient to permit hydrogenation of the LPP oil in the first HDO step.

The molar H/C ratio of 2nd step HDO oil was very similar to that of BCO. It was possible to reduce the molar O/C ratio of the 2nd step HDO oil by 75% in comparison to the 1st step HDO oil.

Density and viscosity

Density and viscosity are key fuel properties. Especially in diesel engines, where viscosity plays a crucial role during injection. It determines the size of the droplets and the quality of

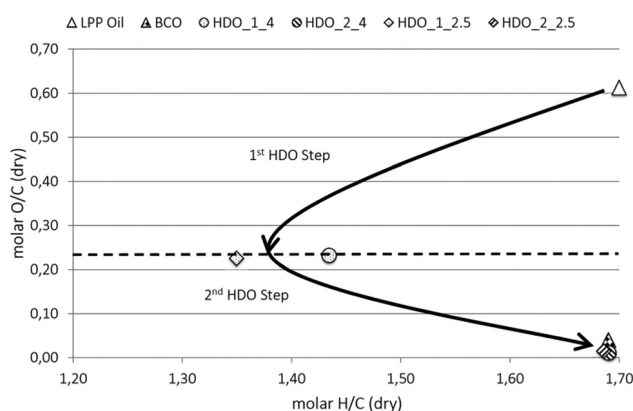


Fig. 6 A van Krevelen plot for the elemental compositions of the 1st step and 2nd step HDO oils on a dry basis.

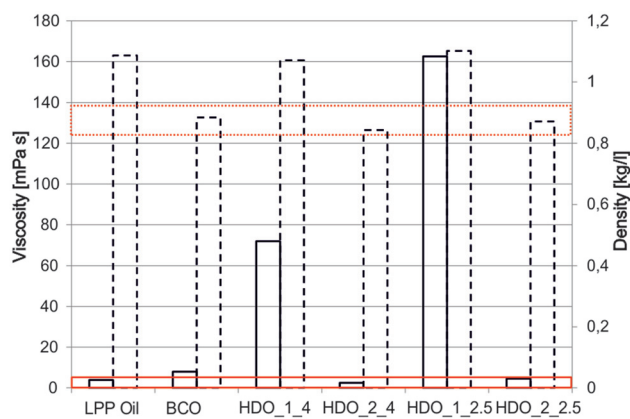


Fig. 7 The density and viscosity of the LPP oil, BCO and the 1st and 2nd step HDO oils.

the atomization of the fuel. Too highly viscous oils result in a higher energy consumption with respect to the pump performance and the wear of the injector equipment.

Reference values from standard EN 590²⁰ diesel for density at 15 °C (0.82 to 0.845 g cm⁻³) and for dynamic viscosity at 40 °C (2.44 to 5.33 mPa s) are marked in Fig. 7.

As can be seen from Fig. 7, it is obvious that in the first HDO step the viscosity of the LPP oil increased significantly. For HDO_1_4, the viscosity increased by 1749% to 71.9 mPa s, and for HDO_1_2.5 it increased by 4079% to 162.6 mPa s. The density of the 1st step HDO oil, however, was very similar to that of the LPP oil (HDO_1_4: 1.07 kg m⁻³ and HDO_1_2.5: 1.10 kg m⁻³).

In the first HDO step, viscosity was increased enormously through a water reduction of 80% and the low degree of hydrodeoxygenation. Density, however, was not significantly altered by the first HDO step. In order to produce a biofuel that meets with the standard specification, the 1st step HDO oil had to be further processed.

As previously mentioned, the 1st step HDO oil was processed along with BCO in the second HDO step. From Fig. 7, it can be clearly seen that the 2nd step HDO oils were much improved regarding density and viscosity. Despite the increased biogenous carbon content, both the density and viscosity specifications were lower than the specifications of BCO.

Compared to the 1st step HDO oil, the density for both second step HDO experiments was reduced by 21%. The viscosity was decreased significantly by 96%.

It can be concluded that the two-step HDO process can convert LPP oil into a 2nd step HDO oil that has an almost diesel-like density and viscosity. It was possible to improve the properties of the BCO used, despite the increase in the biogenous carbon content.

GC-MS analysis

Fig. 8 shows the GC-MS chromatograms of LPP, HDO_1_2.5, and HDO_2_2.5. All three chromatograms show a gap between the retention times of 4.75 min and 6 min. This is the solvent gap, where the detector was switched off. It is hard to determine

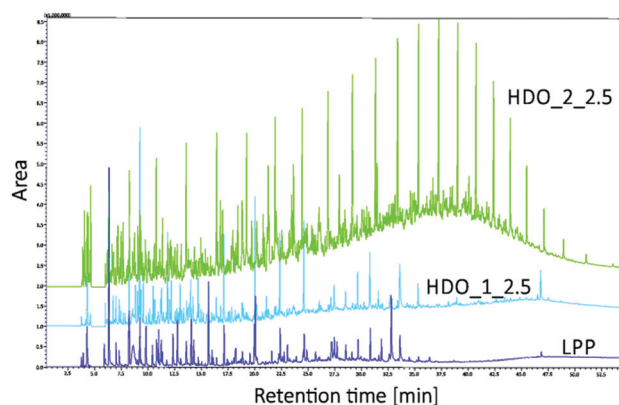


Fig. 8 GC chromatograms of LPP, HDO_1_2.5 and HDO_2_2.5.

the chemical transformations undergone by the liquids, due to the huge number of constituents which show up in the GC-MS chromatograms. Besides, the GC-MS technique is limited by the boiling points of the compounds. GC-MS analysis seemingly suggests that only molecules with a retention time below 35 min or a molecule size smaller than *n*-nonadecane are present in the LPP oil or 1st step HDO liquid. To reveal the whole range of compounds present, GPC analysis was additionally performed (see below section). Fig. 8 and Table 3 show the influence of the BCO carrier on the oil composition, which introduces fossil fuel-based long chain non-branched alkanes into the fuel fraction at the second HDO step.

The effect of hydrodeoxygenation is well demonstrated by the disappearance of highly oxygenated compounds such as levoglucosane (retention time 32.8 min) and 2-hydroxy-3-methyl-2-cyclopenten-1-one (retention time 15.8 min) during

Table 3 The major constituents of LPP, HDO_1_2.5 and HDO_2_2.5

| LPP Compound name | Retention time [min] | Concentration [area%] |
|--|----------------------------|--------------------------|
| Hydroxypropanone | 6.3 | 15.3 |
| Levoglucosane | 32.8 | 7.6 |
| 2-Hydroxy-3-methyl-2-cyclopenten-1-one | 15.7 | 7.4 |
| 2-Methoxy-4-methylphenol | 20.1 | 5.2 |
| Methoxyphenol | 17.1 | 2.9 |
| HDO_1_2.5 | | |
| Compound name | [min] | [area%] |
| 2-Methylcyclopentanone | 9.2 | 10.3 |
| 2-Methoxy-4-methylphenol | 20.0 | 8.3 |
| 2-Methoxyphenol | 17.1 | 6.1 |
| 2-Methoxy-4-propylphenol | 24.6 | 4.9 |
| 4-Ethyl-2-methoxyphenol | 22.3 | 4.7 |
| HDO_2_2.5 | | |
| Compound name | [min] | [area%] |
| Heneicosane | 37.2 | 2.3 |
| Nonadecane | 33.4 | 2.2 |
| Eicosane | 35.3 | 2.1 |
| Hexadecane | 26.8 | 2.1 |
| Docosane | 39.0 | 2.0 |

the first HDO step. 2-Methylcyclopentanone, which shows the highest peak in the HDO_1_2.5 chromatogram at 9.2 min, is a major product of hydrodeoxygenation. This compound partly resists the second HDO step, and so this is one of the sources of the oxygen content of the final HDO fuel.

GPC analysis

The GPC chromatograms in Fig. 9 show the different size ranges of the molecules present in LPP and the HDO products. Compared to FP oil, LPP oil contains few compounds with an average molar mass of 2000 g mol^{-1} .

During the first HDO step, the LPP oil is hydrophobized through the loss of small highly oxygenated compounds and water into the aqueous fraction, suggesting that increased polymerization would be detected in the GPC chromatogram. This effect is also the reason for the viscosity and density, as presented in Fig. 7. Actually, phase separation during the first HDO step, separating the water from the nonaqueous phase, increases the amount of polymers in the nonaqueous phase. Hydrogenation and cracking govern the second HDO step, to produce the final fuel; whereas the first HDO step is mainly required for deoxygenation and chemical dehydration.

Simulated distillation

To quantify the volatility of the BCO and the 2nd step HDO oil, simulated distillation experiments were performed. Fig. 10 shows that the biogenous carbon content obtained in the 2nd HDO step does not have a “negative” effect on the distillation characteristics.

The quality of the 2nd step HDO oils was closer to that of diesel than BCO, as the distillation curves for the 2nd step HDO oils were closer to and partly above the reference curve for the diesel fuel.

Attenuated total reflection Fourier transform infrared (ATR-IR) spectroscopy

As shown in Fig. 11, for LPP oil the C–H peak at 3000 cm^{-1} is almost completely superimposed by the O–H peak at $3000\text{--}3500 \text{ cm}^{-1}$. The C=O peak at about 1700 cm^{-1} re-

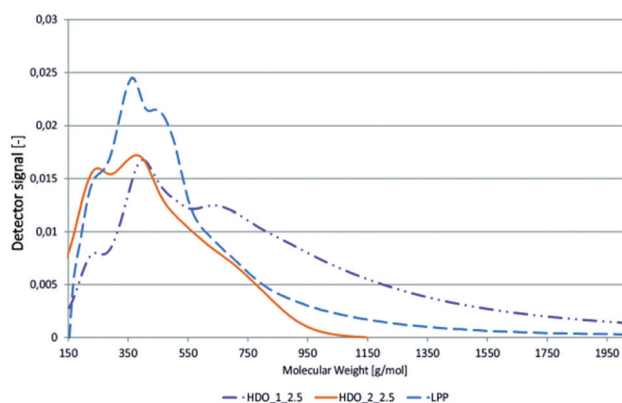


Fig. 9 GPC chromatograms of LPP, HDO_1_2.5 and HDO_2_2.5 (calibrated against polystyrene).

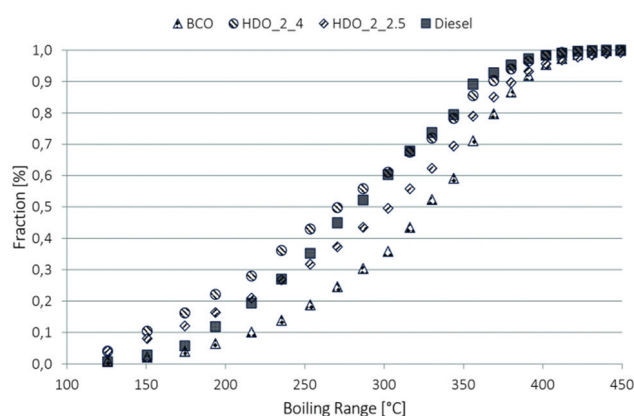


Fig. 10 The distillation characteristics of BCO, diesel and the 2nd step HDO oils.

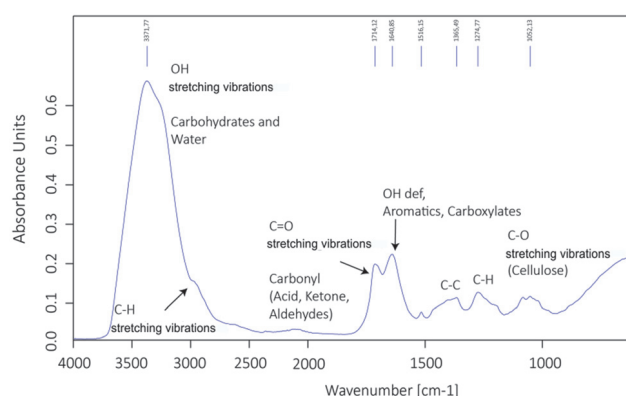


Fig. 11 ATR-IR spectrum of the LPP oil.

presents the carbohydrate degradation products, such as formaldehyde, hydroxypropanone, acetone and furancarboxaldehyde, and in general substances with carbonyl groups. The stretching vibrations below 1000 cm^{-1} are depleted in comparison to biomass, because only a few hemiacetals and alcohols, which are expected to be present in carbohydrates, are present in the LPP oil.

In Fig. 12–14, the ATR-IR spectra of selected samples are shown. The interpretation of the different spectra is as explained in Fig. 11.

It is evident that for the 1st step HDO oil (HDO_1_4), the water and oxygen content decreased and the fraction of aromatic carbon constituents increased in comparison to the LPP oil.

1st step HDO (HDO_1_4) oil is converted into a biofuel through the second HDO step. In the 2nd step HDO oil (HDO_2_4 and HDO_2.5), CH absorption (3000 cm^{-1}) and the characteristic absorption for the aromatics ($1500\text{--}1700 \text{ cm}^{-1}$) are clearly confirmed through ATR-IR.

Biogenous carbon content

In comparison to BCO, the biogenous carbon content in the 2nd step HDO oil had increased, as shown in Table 4. These results show that using the two-step HDO process the LPP oil

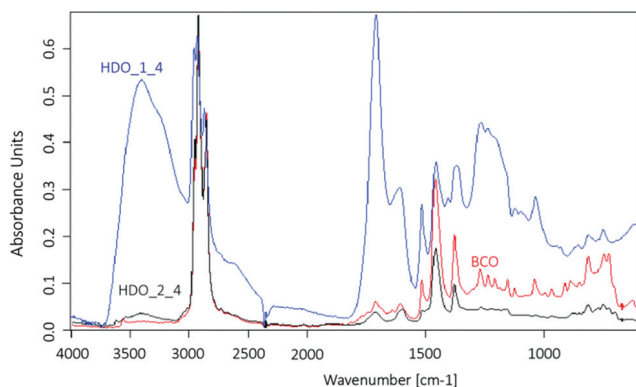


Fig. 12 ATR-IR spectra of BCO and 1st/2nd step HDO oils.

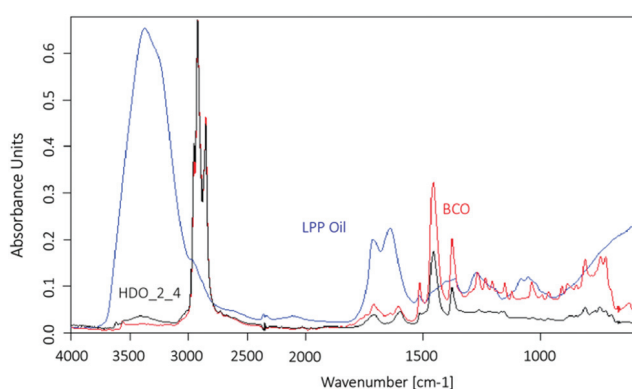


Fig. 13 ATR-IR spectra of BCO, the LPP oil and a 2nd step HDO oil.

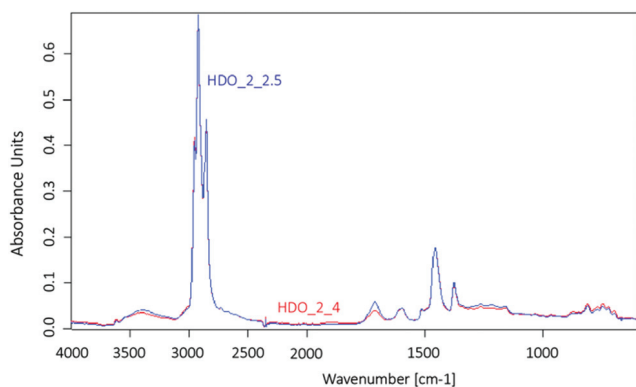


Fig. 14 ATR-IR spectra of the 2nd step HDO oils.

Table 4 Radiocarbon monitoring of the 2nd step HDO oil and the BCO

| | Biogenous carbon Content [wt%] | Difference [%] |
|-----------|--------------------------------|----------------|
| BCO | 10 | — |
| HDO_2_4 | 22.0 | 125 |
| HDO_2_2.5 | 28.0 | 186 |

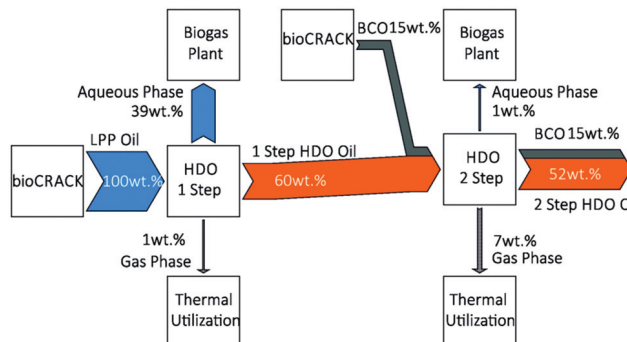


Fig. 15 The mass balance of the biogenous carbon content for the two-step HDO process.

can be converted into a 2nd step HDO oil with diesel-like properties and a high biogenous carbon content.

Mass balance of biogenous carbon

In Fig. 15, the mass balance of the biogenous carbon content is shown for the two-step HDO process. It is apparent that 52 wt% of the biogenous carbon of the LPP oil can be converted into a biofuel with diesel fuel-like properties.

Most of the biogenous carbon content was “lost” during the first HDO step into the aqueous phase, since most of the unwanted highly oxygenated water soluble carbonaceous constituents such as hydroxypropanone, glycolaldehyde, acetic acid and formic acid were removed, in order to enable less hydrogen consumption in the second HDO step. As shown in Fig. 15, these aqueous phases can be further processed in a biogas plant.

In the second HDO step, 87% of the biogenous carbon content from the feed (the 1st step HDO oil) was recovered. BCO was not converted into gaseous or aqueous products.

Conclusion

In this paper, a two-step HDO process which is able to convert LPP oil into a biofuel with diesel fuel-like properties has been discussed. In Table 5, the key properties of the discussed substances are summarized and compared.

Table 5 A comparison of LPP oil, the 1st and 2nd step HDO oils, and conventional diesel

| | LPP oil | HDO_1_2.5 | HDO_2_2.5 | Diesel |
|-----------------------------------|---------|-----------|-----------|--------|
| Water content (wt%) | 50 | 11 | 0.2 | 0.02 |
| LCV (MJ kg ⁻¹) | 8.7 | 26.4 | 41.2 | 42.5 |
| Density (kg m ⁻³) | 1070 | 1100 | 870 | 835 |
| Viscosity (mPa s) | 4 | 163 | 4.5 | 4 |
| Biogenous carbon (wt%) | 100 | 100 | 28 | <7 |
| Elemental analysis on a wet basis | | | | |
| Carbon content (wt%) | 25.6 | 62.5 | 85.5 | 85.9 |
| Hydrogen content (wt%) | 9.2 | 8.3 | 12.1 | 13.3 |
| Oxygen content (wt%) | 64.9 | 28.7 | 1.9 | <1 |
| Nitrogen content (wt%) | <1 | <1 | <1 | <1 |

It is apparent that, on going from the LPP oil to the 2nd step HDO oil:

- the water content was lowered by 99.6%
- the LCV was increased by 470% to 41.2 MJ kg⁻¹
- the density and viscosity were lowered
- the carbon content of the product phase was increased by 330%
- the hydrogen content was increased by 30% and
- the oxygen content was lowered by 97%

A proof-of-principle for a two-step HDO process to convert LPP oil into a diesel-like biofuel was successfully investigated. The 2nd step HDO oil contained 52 wt% biogenous carbon and 67% of the chemically fixed combustion energy.

Abbreviations

| | |
|-----------------------|---|
| ATR-IR | Attenuated total reflection Fourier transform infrared spectroscopy |
| BCO | bioCRACK oil |
| BtL | Biomass to liquid |
| EY _{phase} | Energy yield |
| FP | Fast pyrolysis |
| GC-MS | Gas chromatography with mass spectrometry |
| GC-TCDD | Gas chromatography with thermal conductivity detector |
| GPC | Gel permeation chromatography |
| H/C | Hydrogen to carbon |
| HDO | Hydrodeoxygenation |
| H _{i, phase} | Heating value |
| LCV | Lower calorific value |
| LPP | Liquid phase pyrolysis |
| MY _{phase} | Mass yield |
| O/C | Oxygen to carbon |
| VGO | Vacuum gas oil |
| wt% | Weight percent |

Acknowledgements

We thank A. Rollett, H. Kindermann, S. Krainer and A. Toth for assistance. This work was funded by the Austrian Research Promotion Agency (FFG) under the scope of the A3 Plus Program.

References

- 1 H. H. Nimz, U. Schmitt, E. Schwab, O. Wittmann and F. Wolf, in *Ullmann's Encyclopedia of Industrial Chemistry 2000*, Wiley-VCH Verlag GmbH & Co. KGaA., 2000, pp. 454–503.
- 2 T. Bull, *Science*, 1999, **285**, 1209.
- 3 T. Kaneko, F. Derbyshire, M. Eiichiro, D. Gray and M. Tamura, in *Ullmann's Encyclopedia of Industrial Chemistry*, Wiley-VCH, 2005, p. 37.
- 4 N. Schwaiger, R. Feiner, K. Zahel, A. Pieber, V. Witek, P. Pucher, E. Ahn, P. Wilhelm, B. Chernev, H. Schröttner and M. Siebenhofer, *BioEnergy Res.*, 2011, **4**, 294–302.
- 5 N. Schwaiger, V. Witek, R. Feiner, H. Pucher, K. Zahel, a Pieber, P. Pucher, E. Ahn, B. Chernev, H. Schroettner, P. Wilhelm and M. Siebenhofer, *Bioresour. Technol.*, 2012, **124**, 90–94.
- 6 R. Feiner, N. Schwaiger, H. Pucher, L. Ellmaier, P. Pucher and M. Siebenhofer, *RSC Adv.*, 2013, **3**, 17898–17903.
- 7 R. Feiner, N. Schwaiger, H. Pucher, L. Ellmaier, A. Reiter, M. Derntl, T. Glatz, P. Pucher and M. Siebenhofer, *BioEnergy Res.*, 2014, **7**, 1343–1350.
- 8 F. M. Mercader, M. J. Groeneveld, S. R. A. Kersten, R. H. Venderbosch and J. A. Hogendoorn, *Fuel*, 2010, **89**, 2829–2837.
- 9 J. Wildschut, F. H. Mahfud, R. H. Venderbosch and H. J. Heeres, *Ind. Eng. Chem. Res.*, 2009, **48**, 10324–10334.
- 10 J. Wildschut, M. Iqbal, F. H. Mahfud, I. M. Cabrera, R. H. Venderbosch and H. J. Heeres, *Energy Environ. Sci.*, 2010, **3**, 962–970.
- 11 F. de Miguel Mercader, M. J. Groeneveld, S. R. a. Kersten, C. Geantet, G. Toussaint, N. W. J. Way, C. J. Schaverien and K. J. a. Hogendoorn, *Energy Environ. Sci.*, 2011, **4**, 985.
- 12 R. H. Venderbosch, a. R. Ardiyanti, J. Wildschut, a. Oasmaa and H. J. Heeres, *J. Chem. Technol. Biotechnol.*, 2010, **85**, 674–686.
- 13 F. D. M. Mercader, *AIChE J.*, 2011, **57**, 3160–3170.
- 14 H. Pucher, N. Schwaiger, R. Feiner, P. Pucher, L. Ellmaier and M. Siebenhofer, *Int. J. Energy Res.*, 2014, **38**, 1964–1974.
- 15 *DUBBEL Taschenbuch für den Maschinenbau*, ed. K. Grote and J. Feldhusen, Springer Verlag, Berlin, Heidelberg, 24th edn, 2014.
- 16 E. Laurent and B. Delmon, *J. Catal.*, 1994, **146**, 281–291.
- 17 Z. P. G. Masende, B. F. M. Kuster, K. J. Ptasiński, F. J. J. G. Janssen, J. H. Y. Katima and J. C. Schouten, *Appl. Catal., B*, 2005, **56**, 189–199.
- 18 I. Kubičková, M. Snåre, K. Eränen, P. Mäki-Arvela and M. Dmitry Yu, *Catal. Today*, 2005, **106**, 197–200.
- 19 D. W. Krevelen, *Fuel*, 1950, **29**, 269–284.
- 20 Austrian Standards Institute, *Kraftstoffe für Kraftfahrzeuge - Dieselkraftstoff - Anforderungen und Prüfverfahren*, 2010.

Chapter 9

Liquefaction of pyrolysis
derived biochar:

a new step towards biofuel
from renewable resources

Liquefaction of pyrolysis derived biochar: a new step towards biofuel from renewable resources

Cite this: DOI: 10.1039/c3ra43516d

Roland Feiner,^{*ab} Nikolaus Schwaiger,^{ab} Hannes Pucher,^a Lisa Ellmaier,^b Peter Pucher^b and Matthäus Siebenhofer^a

There are several ways to produce the renewable resource biochar, such as pyrolysis or hydrothermal carbonization. Technologies for the conversion of biochar to biofuels could contribute to suffice the growing demand for fuel. Liquid-phase pyrolysis produces about 40 wt% of biochar. Direct liquefaction of biochar is a conceivable way of producing biofuels but has not been considered yet. Direct liquefaction of biochar is carried out in a 450 ml batch reactor at the temperature of 425 °C using tetralin as a hydrogen donor solvent. Several experiments were conducted to investigate the influence of an initial heating and an isothermal stage on the conversion of biochar to biofuel. The isothermal stage was investigated at two pressure levels. Reaction time was limited to 30 min. Biochar conversion of 84% and an oil yield of 72% were observed.

Received 17th May 2013,
Accepted 23rd July 2013

DOI: 10.1039/c3ra43516d

www.rsc.org/advances

Introduction

This work is intended to address producers of biochar to discuss alternatives to combustion of this renewable energy source. Biochar has the potential to be converted to a value-added product like biofuel. The influence of two process stages on the conversion of biochar was investigated. The hydrogen donor tetralin acts as a solvent for biochar liquefaction. The feasibility of biochar liquefaction has been confirmed.

Lignocellulosic biomass is the most abundant renewable material¹ in the world. Roughly 80% of the total planet's phytomass is assigned to wood.² This abundance makes it a feasible feedstock for chemical conversion to biofuels. As far as biofuel is concerned there are still obstacles to overcome for fossil fuel substitution. Most of the processes developed by the petrochemical and chemical industry are not suitable for converting biomass to biofuels. This is due to the fact that biomass is a highly oxygenated raw material.³ Behrendt *et al.* specifies the chemical composition of dry wood as $\text{CH}_{1.4}\text{O}_{0.7}$ ⁴ so there is nearly one atom of oxygen on each carbon atom. This shows the indispensable need for hydrogen when converting lignocellulosic biomass directly to biofuels. By these means a simple and cheap pre-treatment is needed to eliminate oxygen in the feedstock. Liquid-phase pyrolysis is a feasible route for thermo-chemical elimination of oxygen from biomass and formation of liquid and solid intermediates.

Liquid-phase-pyrolysis

The formation of liquid-phase pyrolysis products was investigated and has been reported elsewhere (Fig. 1).^{5,6} C^{14} -Analysis shows that biochar contains roughly 60 wt% of the biogenous carbon, originating in the biomass feed.⁵ The elemental composition of biomass is very different to biochar. Due to liquid-phase pyrolysis the oxygen content in the biomass is reduced from 47 wt% to 20 wt% while the carbon content is increased from 47 wt% to 75 wt% (Table 1). This makes biochar a considerable feedstock for direct liquefaction in order to produce biofuels. Biochar is a major product of pyrolysis processes, torrefaction and hydrothermal carbonization.^{7,8} Despite high availability of biochar and its potential to contribute to soil melioration, direct liquefaction of biochar has not been considered in literature yet, while direct liquefaction of fossil coal (DCL) is well reported.

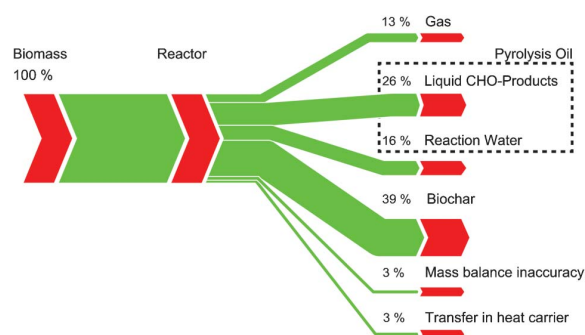


Fig. 1 Mass balance for liquid-phase pyrolysis at 350 °C.

^aGraz University of Technology, Institute of Chemical Engineering and Environmental Technology, Graz, Austria. E-mail: roland.feiner@tugraz.at;

Fax: +43 (0)316 873-7469

^bBDI – BioEnergy International AG, Grambach, Austria

Table 1 Fuel analysis of biomass and biochar

| | Ultimate Analysis (wt%) | | | |
|------------------|---------------------------------------|---------------------|-------------------|-----------------------|
| | C | H | O | N |
| Biomass (Spruce) | 47.0 | 6.4 | 46.5 | 0.1 |
| Biochar | 74.5 | 5.2 | 20.1 | 0.2 |
| | Proximate Analysis (wt%) ^a | | | |
| | M | Ash _{d.b.} | V _{d.b.} | C _{fix d.b.} |
| Biochar | 0.5 | 1.7 | 40.7 | 57.6 |

^a Moisture (M), Volatiles (V), Fixed Carbon (C_{fix}), dry basis (d.b).

Direct liquefaction of fossil coal

When utilizing direct liquefaction, coal reacts at elevated temperature and pressure with hydrogen gas and or a hydrogen donor solvent. The products of direct coal liquefaction are highly aromatic and suitable for usage as high-octane gasoline or feedstock for aromatic chemicals.⁹

Bergius was the first researcher who did investigate liquefaction of coal as early as 1911. He demonstrated the conversion of coal to heavy oil by using a solvent and hydrogen pressure.¹⁰ The Royal Swedish Academy of Sciences awarded him for this achievement with the Nobel Prize for chemistry in 1931. A lot of research has been undertaken to investigate the formation of products during coal liquefaction. Weller *et al.*^{11–13} proposed that the conversion of coal to oil occurs *via* intermediate formation of asphaltenes. Pre-asphaltenes as further intermediate were isolated later on. At present product formation from coal *via* pre-asphaltenes and asphaltenes to oil is an accepted mechanism.^{9,14,15}

The liquefaction of fossil coal as well as the liquefaction of biochar is a combination of (1) *hydrodeoxygenation*, (2) *hydrogenation* and (3) *hydrocracking*.

During coal liquefaction, while thermal decomposition ruptures the coal bonds, hydrogen from the gaseous phase or a hydrogen donor solvent stabilizes the fragments and eliminates heteroatoms like oxygen. The stabilization ensures the breakdown of macromolecules into smaller hydrocarbons. At low hydrogen availability fragments are not stabilized and will undergo re-polymerization reactions to form tar.¹⁵

Materials and methods

Used materials

Biochar was obtained from pilot scale liquid-phase pyrolysis plant from BDI (OMV refinery, Vienna). Biochar portions of 300 g were extracted with n-hexane in a Soxhlet apparatus. The extracted, dried biochar was milled in a centrifugal mill to <200 μm and dried in a vacuum oven at 100 mbar pressure and 105 °C for 24 h to remove solvent residues. The biochar was sealed in air tight bottles and stored for further use. Ultimate and proximate analysis of biochar are shown in Table 1.

Reagent-grade tetralin (1,2,3,4-tetrahydronaphthalene) with a purity of 98% was used as hydrogen donor solvent.

Experimental procedure

Liquefaction of biochar was investigated in a stirred, 450 ml batch reactor between 370 °C and 425 °C. For each experiment 30 g of dried biochar was added to the reactor together with tetralin. The solvent to coal ratio on weight basis was 3. The reactor was then pressurized with 50 bar of hydrogen. The reactor was heated to 425 °C within 30 min. The stirring speed was set to 500 rpm during the experiment as well as the cooling phase.

In order to distinguish between the contribution of different process phases on conversion and product formation the *heating stage* was investigated separately prior to investigation of the *isothermal stage*. During investigation of the *initial heating stage* the experiment was stopped when 370 °C reactor temperature was reached. This temperature was assumed to be the start temperature of the fossil coal liquefaction reaction.^{16,17} In the following series of experiments the heating phase was stopped at 390, 405, 415 and 425 °C, respectively. At 425 °C the final temperature and starting point of the *isothermal stage* was reached. Isothermal experiments were stopped after 5, 10, 20 and 30 min at 425 °C, respectively.

Experiments were conducted at two pressure levels. A first series (1) with an initial pressure of 50 bar hydrogen without hydrogen metering during the *isothermal stage*, hereinafter referred to as (50/-) series and a second series (2) with initial pressure of 50 bar and hydrogen metering at 180 bar during the *isothermal stage*, hereinafter referred to as (50/180) series.

Upon completion of the experiment the heating jacket was removed and the reactor was cooled to below 200 °C within 5 min with compressed air. When the temperature in the reactor reached 50 °C the pressure was relieved and the reactor was opened. Gas amount as well as the gas composition were determined.

Product characterization

For the liquefaction of biochar two options for product characterization are conceivable. On the one hand the characterization by boiling points and on the other hand the characterization by lumped parameters¹⁸ are recommended. In this project the lumped parameters gas (G), oil (O), asphaltenes (A), pre-asphaltenes (PA) and residue (R) were chosen to evaluate the progress of liquefaction. The parameters are calculated from the results of extraction experiments as shown in the following section.

Solids (extraction)

Extraction experiments are carried out in a fluidized bed extraction apparatus (fex-IKA 200). After finishing the reaction the liquid/solid mixture was filtered. The wet cake was subjected to sequential extraction, as illustrated in Fig. 2.

As illustrated in Fig. 2 the liquefaction products were separated into (1) oil (hexane soluble), (2) asphaltenes (hexane insoluble but toluene soluble), (3) pre-asphaltenes (toluene insoluble but THF soluble) and (4) residue (THF insoluble).

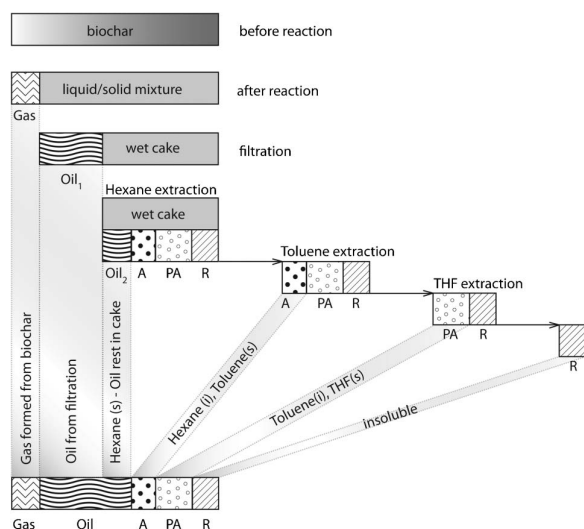


Fig. 2 Product characterization by extraction.[†]

The lumped parameters are calculated according to following formulas.[‡]

$$\text{Gas (G)} = \frac{m_{\text{Gas}}}{m_{\text{Biochar}_{\text{d.a.f.}}}}$$

$$\text{Asphaltenes (A)} = \frac{m_{\text{Hexane(i)}} - m_{\text{Toluene(s)}}}{m_{\text{Biochar}_{\text{d.a.f.}}}}$$

$$\text{Pre-asphaltenes (PA)} = \frac{m_{\text{Toluene(i)}} - m_{\text{THF(s)}}}{m_{\text{Biochar}_{\text{d.a.f.}}}}$$

$$\text{Residue (R)} = \frac{m_{\text{THF(i)}}}{m_{\text{Biochar}_{\text{d.a.f.}}}}$$

$$\text{Conversion (C)} = 1 - R$$

$$\text{Oil (O)} = C - G - A - PA$$

Liquids

The liquid product from filtration, containing the solvent as well as the liquefied biochar, was subjected to GC-FID analysis in order to determine the tetralin and naphthalene content.

While tetralin is acting as a hydrogen donor and provides hydrogen, the molecule itself is converted into naphthalene. Beside the intended dehydrogenation of tetralin unwanted breakdown of the molecule, depending on the temperature and exposure time, occurs.¹⁹ Exposing tetralin to a temperature of 450 °C leads to mainly naphthalene formation as well as significant amounts of 1-methylindan, n-butylbenzene and minor amounts of indene, decalin, toluene and ethylbenzene.²⁰ The elevated cleaving probability of tetralin at 450 °C

[‡] Dry ash free (d.a.f.).

[†] Insoluble (i), soluble (s).

was a major reason to conduct experiments at a reaction temperature of 425 °C.

The liquid product was also subjected to size exclusion chromatography in order to compare the molecular size of the liquefied biochar for different reaction times.

Analytics

The gas composition was analyzed for CH₄, O₂, CO, CO₂. While CH₄, CO, CO₂ concentration were measured by infrared gas analysis, the O₂ concentration in the gas was determined with an electrochemical sensor.

All liquid and solid products as well as the feed were characterized by elemental analysis with a Vario macro CHNO-analyzer, (Elementar Analysensysteme) in CHN mode.

The liquid product from filtration was analyzed with a GC-FID. A MXT 2887, 10 m column from Restek and a Agilent 7890A GC were used.

Size exclusion chromatography of the liquid product was carried out with a Shimadzu RID - 10A Refractive Index Detector and a Merck HITACHI L-6000A Pump. A SDV 5 μm 8 × 50 column and two SDC 1000 Å 8 × 300 columns from PSS were used. SEC was calibrated against polystyrene.

Results and discussion

Detailed experimental data of the *initial heating stage* as well as the *isothermal stage* are illustrated in Table 2. The results show that the *initial heating stage* contributes to biochar conversion (C) to an extent of 36.5%. The highest conversion (C) of 84.1% was observed for the (50/-) series and 30 min isothermal reaction and 83.8% respectively for the (50/180) series. The highest oil yield of 72.4% was recorded for the (50/-) series and 72.0% respectively for the (50/180) series.

Two assumptions were made for the interpretation of the experiments: (1) Water, produced during liquefaction, is included in the oil phase and (2) CO and CO₂ are assumed to be produced from biochar and CH₄ is assumed to be formed due to degradation of the solvent.

Initial heating stage

The influence of the initial heating stage was investigated. The experimental data are valid for both series (50/-) and (50/180) because the heating procedure was the same.

The first data point of the initial stage (370 °C) shows conversion of about 10%. Therefore the initiation temperature for liquefaction of biochar with the solvent tetralin is below the temperature of 370 °C. This result is in agreement with literature where the initiation temperature for fossil coal liquefaction is mentioned to be between 350 °C to 370 °C.^{17,16}

With rising temperature a rising amount of pre-asphaltenes (PA) and gas (G) is recorded while the amount of asphaltenes (A) is decreasing (see Fig. 3). Between 415 °C and 425 °C a rapid increase of (PA), accompanied by decreasing gas (G) formation was recorded. Taking the reaction scheme of section *Direct Liquefaction of fossil Coal* into account the reaction of (PA) to (A) is the limiting step for the conversion of biochar to oil in the initial heating stage.

Table 2 Experimental data

| Time (min) | <i>T</i> (°C) | Gas (wt%) | Oil (wt%) | Asphaltenes (wt%) | Pre-Asphaltenes (wt%) | Conversion (wt%) |
|---|---------------|-----------|-----------|-------------------|-----------------------|------------------|
| Initial Heating Stage | | | | | | |
| -4.5 | 370 | 2.8 | 2.3 | 3.6 | 1.6 | 10.3 |
| -3.5 | 390 | 3.0 | 10.7 | 2.0 | 3.1 | 18.8 |
| -2.5 | 405 | 4.5 | 15.1 | 1.3 | 4.4 | 25.3 |
| -1.0 | 415 | 5.1 | 19.8 | 0.5 | 5.6 | 31.0 |
| 0.0 | 425 | 2.5 | 23.8 | 0.0 | 10.2 | 36.5 |
| Isothermal Stage (50/0) series | | | | | | |
| 0.0 | 425 | 2.5 | 23.8 | 0.0 | 10.2 | 36.5 |
| 5.0 | 425 | 3.4 | 45.1 | 0.0 | 12.8 | 61.3 |
| 10.0 | 425 | 3.8 | 54.4 | 0.9 | 10.1 | 69.2 |
| 20.0 | 425 | 3.9 | 62.1 | 2.3 | 8.4 | 76.7 |
| 30.0 | 425 | 7.8 | 72.4 | 0.4 | 3.5 | 84.1 |
| Isothermal Stage (50/180) series | | | | | | |
| 0.0 | 425 | 2.5 | 23.8 | 0.0 | 10.2 | 36.5 |
| 5.0 | 425 | 3.7 | 41.8 | 1.5 | 9.0 | 56.0 |
| 10.0 | 425 | 8.4 | 54.4 | 3.4 | 1.7 | 67.9 |
| 20.0 | 425 | 9.6 | 64.5 | 2.5 | 2.2 | 78.8 |
| 30.0 | 425 | 10.3 | 72.0 | 1.5 | 0.1 | 83.9 |

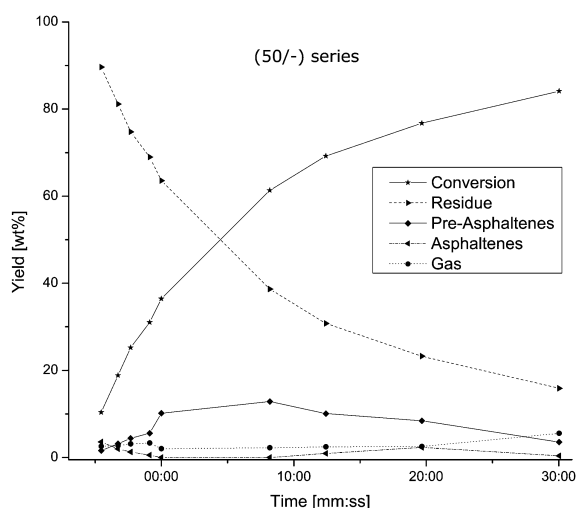
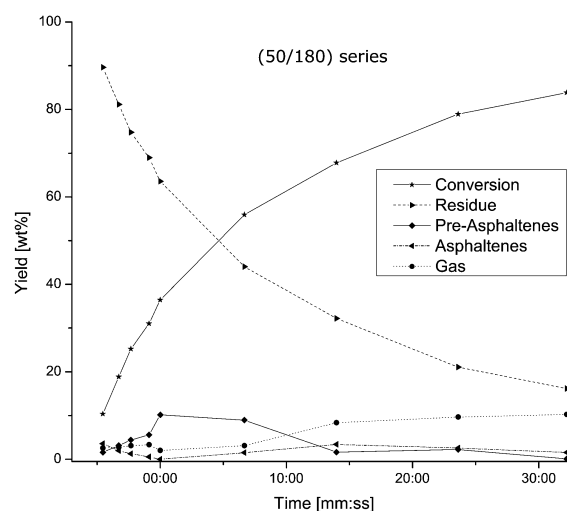
Isothermal phase (50/-)bar

The isothermal phase of the (50/-) series shows a small increase of the (PA) followed by a steady decrease with reaction time. The amount of asphaltenes (A) remains very low while gas formation (G) rises after 20 min. These observations indicate that at higher temperatures the C-C bond cleavage occurs more easily and large (PA) molecules can be cracked and stabilized faster while conversion of (PA) to (A) is the limiting step.

Isothermal phase (50/180)bar

In this series of experiments the reactor was further pressurized to 180 bar after reaching the isothermal temperature level of 425 °C. Compared to the (50/-) series a rapid decrease of (PA) was observed and a final content of 1.7 wt% was obtained after 10 min. Gas formation accelerated to reach a plateau at 10.3% (Fig. 4).

It can be concluded from comparison of results that the surplus hydrogen promotes the breakdown of (PA). Similar oil yields were observed for both series. The balances of the experiments indicates that surplus hydrogen consumption is negligible, indicating that hydrogen for stabilization is mainly provided from the hydrogen donor solvent tetralin. This is in agreement with the findings for fossil coal.²¹ Bcaud *et al.* found that with non-donor solvents, direct incorporation of gaseous hydrogen is predominant. When tetralin is used without catalyst the molecule itself donates most of the hydrogen. The idea of a so called shuttle mechanism is widely accepted today.^{21,19,22,9} Tetralin donates hydrogen and stabilizes the cleaved fragments, and it does fix hydrogen from the gaseous phase. Gaseous hydrogen is transferred to the coal fragments with the hydrogen shuttle tetralin. This effect is promoted with catalysts.^{21,22}

**Fig. 3** Liquefaction without additional metering of hydrogen (50/- bar).**Fig. 4** Liquefaction with hydrogen metering during isothermal reaction (50/180 bar).

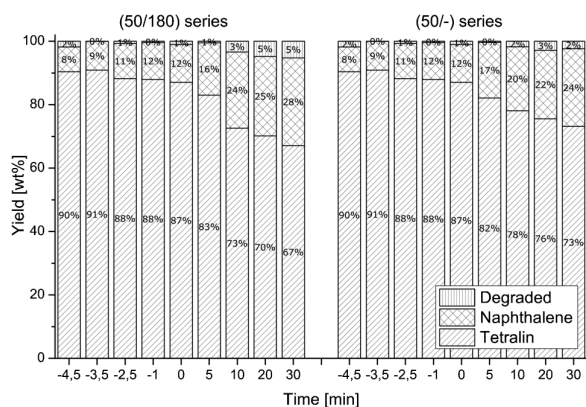


Fig. 5 Hydrogen transfer from tetralin, naphthalene formation and degradation products; (50/-) experiment right, (50/180) experiment left.

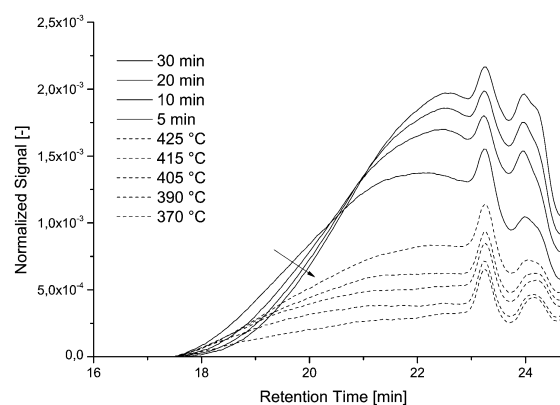


Fig. 6 Size exclusion chromatography data of the (50/180) bar series. The legend shows the order of appearance.

Hydrogen transfer from tetralin

The hydrogen transfer from tetralin was determined by GC-FID. The percentage of tetralin, naphthalene as well as the percentage of degradation based on the amount of tetralin in the feed is illustrated in Fig. 5.

The *initial heating stage* is equal for both series. The first data point at 370 °C of the *initial heating stage* shows that already 8% of tetralin converted to naphthalene (Fig. 5). This is different from earlier findings of reference 20. Mushrush *et al.* observed naphthalene in the magnitude of 3.8% when exposing tetralin for 60 min at 450 °C without coal. The higher consumption of hydrogen in the present project is seemingly consumed for stabilization of intermediates.

For the (50/-) series a smooth accumulation of naphthalene can be observed to finally reach a plateau at 24%. Only 2% of the tetralin feed were degraded at 425 °C and 30 min exposure. The (50/180) series shows a different behavior. After pressurizing the reactor the naphthalene content rose quickly from 16% to 24%. This may be due to the system pressure. Although the higher hydrogen pressure did not improve the shuttle activity the amount of hydrogen donated by tetralin was promoted. Only 5% of the tetralin feed degraded at 425 °C and 30 min exposure.

The highest amounts of hydrogen transfer for the (50/0) series and the (50/180) series was 0.35 mol (11.7 mol kg⁻¹ feed) and 0.39 mol (13.0 mol kg⁻¹ feed), respectively.

Size exclusion chromatography

Additional information about the quality of liquefied biochar can be derived from size exclusion chromatography (SEC). The SEC provides information of the relative molecule size and makes the liquid products of different experiments comparable.

Fig. 6 shows the SEC of two stages: the (1) *initial heating state* in dashed lines and the (2) *isothermal state* (50/180) in solid lines. The first data point of the *initial heating state* at 370 °C leads to a conversion of 10 wt% (Table 2). Heating from 370 °C to 425 °C requires roughly five minutes. Within this time the conversion of biochar increases rapidly with a rate of about 6 [wt%/min] to reach a conversion of 36.5 wt% at the end of the

initial stage. These observations suggest that the liquefaction reaction may start at about 350 °C (already 10 wt% conversion at 370 °C) but significant and rapid liquefaction starts at 370 °C. With increase of the reaction time the amount of liquefied biochar increases slower while the relative molecular size decreases Fig. 6. The decrease of the relative molecular size is indicated through a shift of the peaks from left to right marked with an arrow in Fig. 6.

Conclusion

Liquefaction of biochar from liquid-phase pyrolysis was carried out with the solvent tetralin at the temperature of 425 °C. Several experiments were conducted to investigate the influence of an initial heating period from 370 °C to 425 °C and an isothermal period at 425 °C on the conversion of biochar.

The results of this study indicate that:

- (1) Liquefaction of biochar is possible
- (2) Liquefaction of biochar at greater extent starts at 370 °C.
- (3) The influence of the initial heating period is significant. The conversion during this heating period is rapid and reaches 36 wt%.
- (4) Additional hydrogen metering has only a small influence on the conversion of biochar

Notes and references

- 1 X. Zhao, K. Cheng and D. Liu, *Appl. Microbiol. Biotechnol.*, 2009, **82**, 815–27.
- 2 H. H. Nimz, U. Schmitt, E. Schwab, O. Wittmann and F. Wolf, in *Ullmann's Encyclopedia of Industrial Chemistry*, Wiley-VCH Verlag GmbH, 2000.
- 3 R. Rinaldi and F. Schüth, *Energy Environ. Sci.*, 2009, **2**, 610.
- 4 F. Behrendt, Y. Neubauer, M. Oevermann, B. Wilmes and N. Zobel, *Chem. Eng. Technol.*, 2008, **31**, 667–677.

- 5 N. Schwaiger, R. Feiner, K. Zahel, A. Pieber, V. Witek, P. Pucher, E. Ahn, P. Wilhelm, B. Chernev, H. Schröttner and M. Siebenhofer, *BioEnergy Res.*, 2011, **4**, 294–302.
- 6 N. Schwaiger, V. Witek, R. Feiner, H. Pucher, K. Zahel, A. Pieber, P. Pucher, E. Ahn, B. Chernev, H. Schroettner, P. Wilhelm and M. Siebenhofer, *Bioresour. Technol.*, 2012, **124**, 90–94.
- 7 D. Ciolkosz and R. Wallace, *Biofuels, Bioprod. Biorefin.*, 2011, **5**, 317–329.
- 8 A. Funke and F. Ziegler, *Biofuels, Bioprod. Biorefin.*, 2010, **4**, 160–177.
- 9 T. Kaneko, F. Derbyshire, E. Makino, D. Gray and M. Tamura, in *Ullmann's Encyclopedia of Industrial Chemistry*, Wiley-VCH Verlag GmbH, 2005, pp. 1–83.
- 10 R. Haul, *Chem. Unserer Zeit*, 1985, **19**, 59–67.
- 11 S. Weller, M. Pelipetz and S. Friedman, *Ind. Eng. Chem.*, 1951, **43**, 1575–1579.
- 12 S. Weller, M. Pelipetz and S. Friedman, *Ind. Eng. Chem.*, 1951, **43**, 1572–1575.
- 13 S. Weller, E. L. Clark and M. G. Pelipetz, *Ind. Eng. Chem.*, 1950, **42**, 334–336.
- 14 S. Vasireddy, B. Morreale and A. Cugini, *Energy Environ. Sci.*, 2011, **4**, 311–345.
- 15 M. W. Haenel, in *Handbook of Heterogeneous Catalysis*, Wiley-VCH Verlag GmbH, 2008, pp. 3023–3036.
- 16 X. Li, H. Hu, S. Zhu, S. Hu, B. Wu and M. Meng, *Fuel*, 2008, **87**, 508–513.
- 17 W.-Y. Li, J. Feng, K.-C. Xie and R. Kandiyoti, *Fuel Process. Technol.*, 2004, **85**, 1671–1687.
- 18 W. Ding, J. Liang and L. L. Anderson, *Ind. Eng. Chem. Res.*, 1997, **36**, 1444–1452.
- 19 M. Godo, M. Umemura, A. Ishihara and T. Kabe, *AIChE J.*, 1997, **43**, 3105–3110.
- 20 G. Mushrush and W. Stalick, *J. Anal. Appl. Pyrolysis*, 1988, **14**, 17–23.
- 21 R. Bacaud, *Appl. Catal.*, 1991, **75**, 105–117.
- 22 M. Godo, M. Saito, A. Ishihara and T. Kabe, *Fuel*, 1998, **77**, 947–952.

Chapter 10

Kinetics of Biochar Liquefaction

Kinetics of Biochar Liquefaction

Roland Feiner · Nikolaus Schwaiger · Hannes Pucher ·
Lisa Ellmaier · Anton Reiter · Michael Derntl ·
Thomas Glatz · Peter Pucher · Matthäus Siebenhofer

© Springer Science+Business Media New York 2014

Abstract The renewable resource pyrolysis char hereinafter often referred to as biochar, produced by pyrolysis or hydrothermal carbonization, has promising properties for advanced upgrade. Technologies for the conversion of biochar to biofuels may therefore contribute to suffice the growing demand for fuel. Direct liquefaction of biochar is a conceivable way of producing biofuels. Direct liquefaction of biochar was carried out in a 450 ml batch reactor at a temperature of 425 °C with the hydrogen donor solvent tetralin. Biochar conversion of 84 % and an oil yield of 72 % were observed after 33 min of reaction time. Compared to fossil coal liquefaction, the hydrogenation of biochar leads to a diverse product distribution with more oil products and less intermediates. In process modeling, intermediates as well as products and residues of similar product properties according to their solubility in different organic solvents were identified. These product classes formed the basis for investigation of kinetics of biochar liquefaction. The reaction route network resulting from the reaction scheme was solved with a FORTRAN algorithm.

Keywords Pyrolysis char · Biochar · Kinetics · Biofuel · Noncatalytic

R. Feiner (✉) · N. Schwaiger · H. Pucher · A. Reiter · M. Derntl ·
T. Glatz · M. Siebenhofer
Institute of Chemical Engineering and Environmental Technology,
Graz University of Technology, Inffeldgasse 25/C/II, 8010 Graz,
Austria
e-mail: roland.feiner@tugraz.at

R. Feiner · N. Schwaiger · L. Ellmaier · P. Pucher
BDI-BioEnergy International AG, Parkring 18, 8074, Grambach
Graz, Austria

Introduction

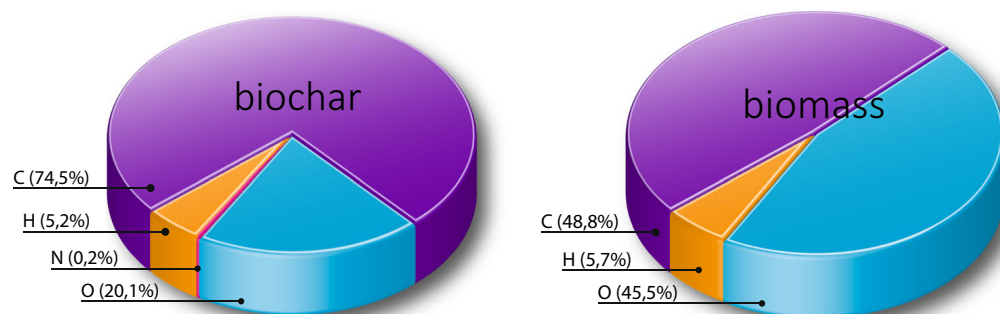
Nowadays, there is a great effort to commercialize pyrolysis of biomass for biofuel production. Pyrolysis of biomass produces significant amounts of biochar up to 40 %, depending on the pyrolysis process and the type of biogenous feedstock. Except combustion, there is still a lack of high-end products for utilization of biochar. Pyrolysis oil as well as biochar have the potential to be converted to value-added products like biofuel [1, 2].

Lignocellulosic phytomass is the most abundant renewable material in the world [3]. Roughly 80 % of the total planet's phytomass is assigned to lignocellulose, such as wood [4]. This abundance makes it a feasible feedstock for chemical conversion to second-generation biofuels. The obstacle which arises with the use of biomass is a high amount of oxygen in the feedstocks [5] and a highly complex chemical composition based on different monomers. The high amount of oxygen in the feedstock indicates an indispensable need of hydrogen when converting lignocellulosic biomass directly to biofuels.

From the perspective of biochar, properties and composition pyrolysis of biomass is a pretreatment step. Due to pyrolysis, the oxygen content is lowered by 57 from 46 % in spruce biomass to 20 % in the biochar, as shown in Fig. 1. Biochar is comparable with sub-bituminous coal, except sulfur which is negligible in biochar. The coal-like composition makes it a conceivable feedstock for direct liquefaction to biofuels.

Fossil coal liquefaction has been well investigated. Weller et al. [6–8] proposed that the conversion of fossil coal to oil occurs via intermediate formation of asphaltenes (A). Asphaltenes are polycondensed aromatic structures consisting of five to seven rings and aliphatic chains with a total of up to 80 carbon atoms [9]. An example for asphaltenes is the shiny black amorphous solid which can be extracted from crude oil with light hydrocarbons. Another class of intermediates, pre-

Fig. 1 Elemental composition of biochar and spruce biomass



asphaltenes (PA), an order of magnitude bigger in size than asphaltenes (A) were isolated in a later state. At present, product formation from coal via (PA) and (A) to oil (O) and gas (G) is an accepted mechanism [10–12].

Due to thermal decomposition of the coal particle, molecule cluster fragments break out of the structure. These fragments need to be stabilized with hydrogen. Stabilized clusters can be cleaved to smaller molecules, which need to be stabilized with hydrogen again, as shown in Fig. 2. The size of molecules categorize the classes residue (R), (PA), (A), (O), or

(G). At low hydrogen availability, fragments are not stabilized and will undergo repolymerization reactions to form tar [12].

It is reasonably assumed that the formation of oil from biochar acts in the same manner although fossil coal and biochar differ in the chemical composition. Due to high sulfur contents of fossil coal C-S (259 kJ/mol) and C=S (536 kJ/mol) bonds will also be addressed because of low decomposition demand. C-C (349 kJ/mol) and C-O (335 kJ/mol) bonds as well as C=O (707 kJ/mol) bonds which are likely to occur in biochar, are more difficult to rupture.

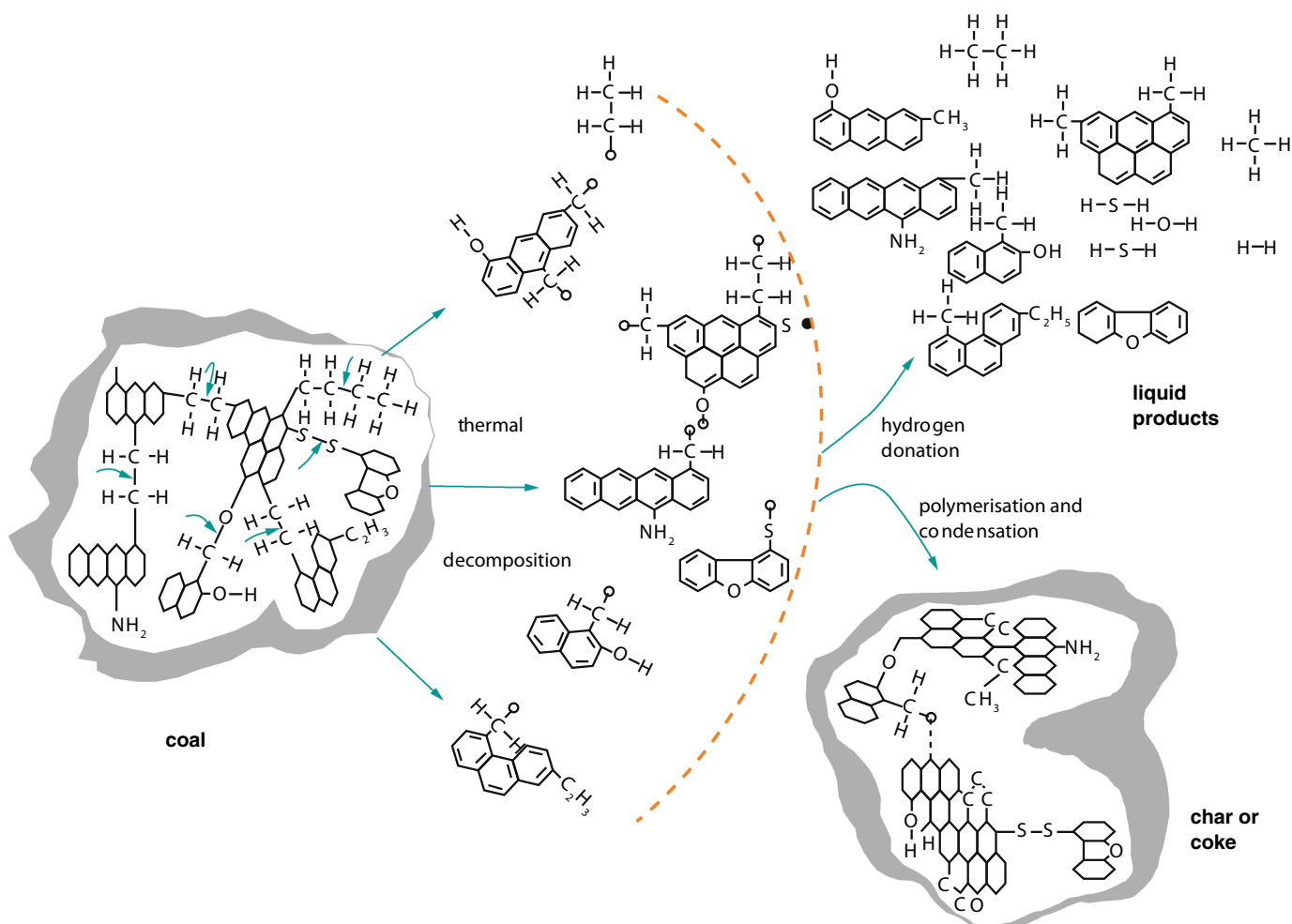


Fig. 2 Product formation during coal liquefaction [10]

When utilizing direct liquefaction, biochar reacts at elevated temperatures and pressures with hydrogen gas and or a hydrogen donor solvent. The products of direct coal liquefaction are highly aromatic and suitable for usage as high-octane gasoline or feedstock for aromatic chemicals [10]. While direct liquefaction of fossil coal is well developed, the direct liquefaction of biochar to produce biofuels is a scarcely investigated approach. The kinetics of the liquefaction of biochar provides crucial information for process design. Due to the formation of various compounds, kinetics of biochar liquefaction is complex. For modeling liquefaction kinetics, there is a need to lump compounds to classes of similar properties. The classes can be defined either by boiling point distributions, by size exclusion chromatography (SEC) or by elutropic properties. Kinetics of different substance classes is a promising approach for modeling the overall liquefaction process.

Materials and Methods

Materials

Biochar was obtained from pilot scale liquid-phase pyrolysis plant “bioCRACK” from BDI-Bioenergy International AG at the OMV refinery in Schwechat, Vienna. The liquid-phase pyrolysis was performed between 350 and 400 °C using spruce wood as a feedstock producing 20–50 wt.% biochar. The biochar has an ash content of 1.45 wt.% on a dry basis. Liquid-phase pyrolysis and the formation of liquid-phase pyrolysis products were investigated and has been reported elsewhere [13, 14].

Biochar samples of 300 g were extracted with *n*-hexane in a Soxhlet apparatus to remove residual heat carrier oil used for the liquid-phase pyrolysis. The extracted, dried biochar was milled in a centrifugal mill to <200 μm and dried in a vacuum dryer at 100 mbar pressure and 105 °C for 24 h to remove solvent residues. The biochar was sealed in air-tight bottles and stored for further use. Ultimate and proximate analysis of biochar was illustrated in previous work [1]. Reagent-grade tetralin (1,2,3,4-tetrahydronaphthalene) with a purity of 98 % was used as the hydrogen donor solvent.

Experimental Procedure

Liquefaction of biochar was investigated in a stirred, 450 ml batch reactor between 370 and 425 °C. For each experiment, 30 g of dried biochar was added to the reactor together with tetralin. A solvent to char ratio of 3 on weight basis was used. The reactor was then pressurized with 50 bar of hydrogen followed by heating to 425 °C within 30 min. The stirring speed was set to 500 rpm during the experiment as well as the cooling phase.

In order to distinguish between the contribution of different process phases on conversion and product formation, the heating stage was investigated separately prior to investigation of the isothermal stage. During investigation of the initial heating stage, the experiment was stopped when 370 °C reactor temperature was reached. This temperature was reported to be the start temperature of fossil coal depolymerisation [15, 16]. In the following series of experiments, the heating phase was stopped at 390, 405, 415, and 425 °C, respectively. At 425 °C, the final temperature and starting point of the isothermal stage was obtained. Isothermal experiments were stopped after 5, 10, 20, and 30 min at 425 °C, respectively.

Experiments were also conducted with an initial pressure of 50 bar hydrogen and additional hydrogen feed for consumption during the isothermal stage at an operation pressure of 180 bar.

Upon completion of the experiment, the heating jacket was removed and the reactor was cooled to below 200 °C within 5 min. When the temperature in the reactor reached 50 °C, the pressure was relieved and the reactor was opened. Volume and composition of product gas were determined.

The experiments for this study were performed earlier and are published in [1]. The kinetics of the liquefaction are intended to be investigated in this work.

Product Characterization

In this work, the kinetically similar compounds are defined as classes: (PA), (A), (O), and (G). The unreacted residual biochar was presumed not to be changed in structure or chemical composition and is defined as (R). Sequential extraction with *n*-hexane, toluene, and THF was employed for determining the amount of product in each class. The procedure is reported elsewhere [1]. The lumped parameters are calculated according to following formulas (d.a.f. is dry, ash free; soluble (s), insoluble (i)):

$$\text{Gas}(G) = \frac{m_{\text{Gas}}}{m_{\text{Char}_{d.a.f.}}}$$

$$\text{Asphaltenes}(A) = \frac{m_{\text{Hexane}(i)} - m_{\text{Toluene}(s)}}{m_{\text{Char}_{d.a.f.}}}$$

$$\text{Pre-asphaltenes}(PA) = \frac{m_{\text{Toluene}(i)} - m_{\text{THF}(s)}}{m_{\text{Char}_{d.a.f.}}}$$

Table 1 Experimental data

| Time (min) | Temperature (°C) | Gas (%) | Oil (%) | Asphaltenes (%) | Pre-asphaltenes (%) | Conversion (%) |
|-----------------------|------------------|---------|---------|-----------------|---------------------|----------------|
| Initial heating stage | | | | | | |
| -3.76 | 370 | 2.8 | 2.3 | 3.6 | 1.6 | 10.3 |
| -2.22 | 390 | 3.0 | 10.7 | 2.0 | 3.1 | 18.8 |
| -1.27 | 405 | 4.5 | 15.1 | 1.3 | 4.4 | 25.3 |
| 0.00 | 415 | 5.1 | 19.8 | 0.5 | 5.6 | 31.0 |
| Isothermal stage | | | | | | |
| 0.00 | 425 | 5.1 | 19.8 | 0.5 | 5.6 | 31.0 |
| 1.13 | 425 | 2.5 | 23.8 | 0.0 | 10.2 | 36.5 |
| 7.80 | 425 | 3.7 | 41.8 | 1.5 | 9.0 | 56.0 |
| 15.10 | 425 | 8.4 | 54.4 | 3.4 | 1.7 | 67.9 |
| 24.75 | 425 | 9.6 | 64.5 | 2.5 | 2.2 | 78.8 |
| 33.35 | 425 | 10.3 | 72.0 | 1.5 | 0.1 | 83.9 |

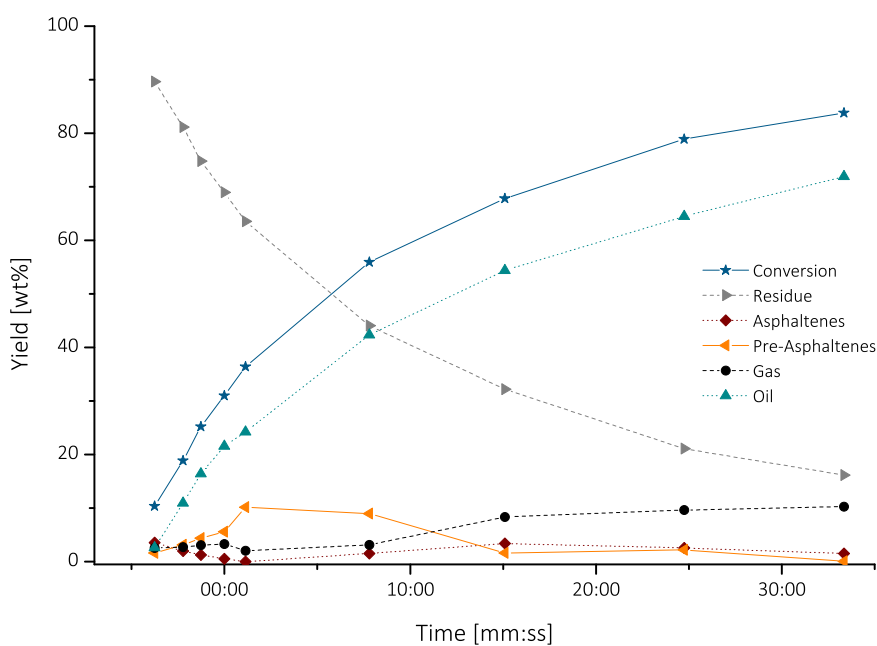
$$\text{Residue}(R) = \frac{m_{\text{THF}(i)}}{m_{\text{Char}_{d.a.f.}}}$$

$$\text{Conversion}(C) = 1 - R$$

$$\text{Oil}(O) = C - G - A - \text{PA}$$

Results and Discussion

Detailed experimental data of the initial heating stage as well as the isothermal stage are illustrated in Table 1. The results show that the initial heating stage contributes to biochar conversion (C) to an extent of 36.5 %. The highest C of 83.8 % was observed for 30 min isothermal reaction with an oil yield of 72.0 %. The high conversion of biochar in the initial heating stage suggests that the initial stage should also be modeled.

Fig. 3 Product formation with respect to time

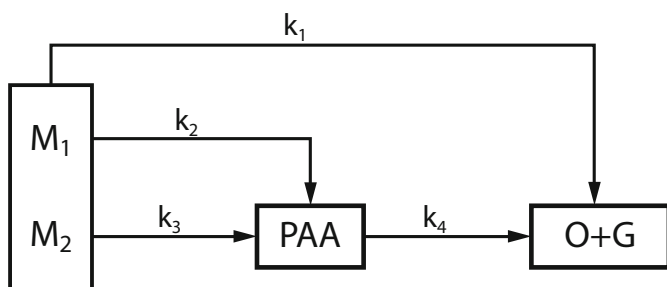


Fig. 4 Kinetic network

Initial Heating Stage

The first data point of the initial stage (370 °C) shows conversion of about 10 %. Therefore, the initiation temperature for liquefaction of biochar with the solvent tetralin is below the temperature of 370 °C. This result is in agreement with literature where the initiation temperature for fossil coal liquefaction is reported to be between 350 and 370 °C [16, 17]. With rising temperature, a rising amount of (PA) and (G) is recorded while the amount of (A) decreases (see Fig. 3). Between 415 and 425 °C, a rapid increase of (PA), accompanied by decreasing (G) formation was recorded. Taking the reaction scheme of biochar→(PA)→(A)→(O) and (G) into account, the reaction of (PA) to (A) is the limiting step for the conversion of biochar to oil in the initial heating stage.

Isothermal Stage

After reaching the isothermal temperature of 425 °C, the reactor was further pressurized to 180 bar with hydrogen. The amount of (PA) was observed to deplete, reaching a final content of 1.7 % after 15 min. Gas formation accelerated to finally reach a plateau at 10.3 %. It can be concluded that surplus hydrogen, as well as high temperature promote the breakdown of (PA) so that the reaction of biochar to (PA) is the limiting step after 15 min of isothermal reaction time at 425 °C.

Kinetic Model

Several kinetic models investigated for the liquefaction of fossil coal have been reported. The works of Ding [18], Gioia

[19], and Li [17] provide a good overview about excellent attempts. For this project, a reaction network slightly different to Li [17] was chosen and adopted for the liquefaction of biochar. Four assumptions were made for the interpretation of experiments: (1) water, produced during liquefaction, is included in the oil phase; (2) CO and CO₂ present in the gas phase are assumed to be produced from biochar while CH₄ is assumed to be formed due to degradation of the solvent; (3) biochar consists of two parts—an easy accessible part (M₁) and a hardly reactive part (M₂); and (4) (PA) and (A) as well as (O) and (G) were grouped together as intermediates (PAA) respectively products (O + G).

The non-isothermal temperature profile (370–415 °C) in the initial heating stage was not taken into account. In the initial heating stage, small activation energy is presumed. According to Arrhenius-Law, small activation energy leads to a gradual slope in the Arrhenius plot. Therefore, an independency of temperature in this stage can be presumed with adequate accuracy. The works of [20] and [21] support this suggestion (Fig. 4).

The equations for solving the reaction network are shown below as vectors.

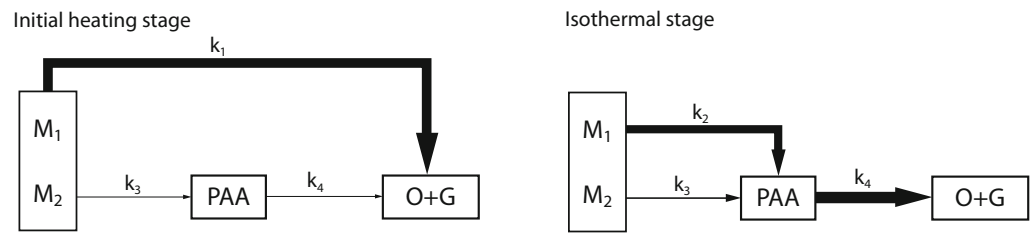
$$\begin{aligned} \frac{d\vec{\alpha}}{dt} &= K\vec{\alpha} \\ \vec{\alpha} &= \vec{\alpha}_0 \quad \text{for } t = 0 \\ \vec{\alpha} &= \begin{Bmatrix} M_1 \\ M_2 \\ (PAA) \\ (O + G) \end{Bmatrix} \\ \vec{\alpha}_0 &= \begin{Bmatrix} M_{10} \\ M_{20} \\ (PAA)_0 \\ (O + G)_0 \end{Bmatrix} \end{aligned}$$

$$K = \begin{Bmatrix} -(k_1 + k_2) & 0 & 0 & 0 \\ 0 & -k_3 & 0 & 0 \\ k_2 & k_3 & -k_4 & 0 \\ k_1 & 0 & k_4 & 0 \end{Bmatrix}$$

Table 2 Kinetic parameters of biochar liquefaction

| | Rate constant (min ⁻¹) | | | | Components (% <i>d.a.f.</i>) | |
|-----------------------|------------------------------------|-----------------------|-----------------------|-----------------------|-------------------------------|------------------------|
| | <i>k</i> ₁ | <i>k</i> ₂ | <i>k</i> ₃ | <i>k</i> ₄ | <i>M</i> ₁₀ | <i>M</i> ₂₀ |
| Initial heating stage | 0.224 | 0.000 | 0.004 | 0.002 | 35.46 | 54.17 |
| Isothermal stage | 0.000 | 0.190 | 0.037 | 0.265 | 15.58 | 53.32 |

Fig. 5 True to scale size arrows of the rate constants for different stages



Solving the first-order kinetic equations led to:

$$M_1 = M_{10}e^{-(k_1+k_2)t} \tag{1}$$

$$M_2 = M_{20}e^{-k_3t} \tag{2}$$

$$(PAA) = \left((PAA)_0 + \frac{k_2M_{10}}{k_1+k_2-k_4} + \frac{k_3M_{20}}{k_3-k_4} \right) e^{-k_4t} - \frac{k_2M_{10}}{k_1+k_2-k_4} e^{-(k_1+k_2)t} - \frac{k_3M_{20}}{k_3-k_4} e^{-k_3t} \tag{3}$$

$$(O + G) = M_{10} + M_{20} + (PAA)_0 + (O + G)_0$$

$$- \left((PAA)_0 + \frac{k_2M_{10}}{k_1+k_2-k_4} + \frac{k_3M_{20}}{k_3-k_4} \right) e^{-k_4t}$$

$$+ \left(-M_{10} + \frac{k_2M_{10}}{k_1+k_2-k_4} \right) e^{-(k_1+k_2)t}$$

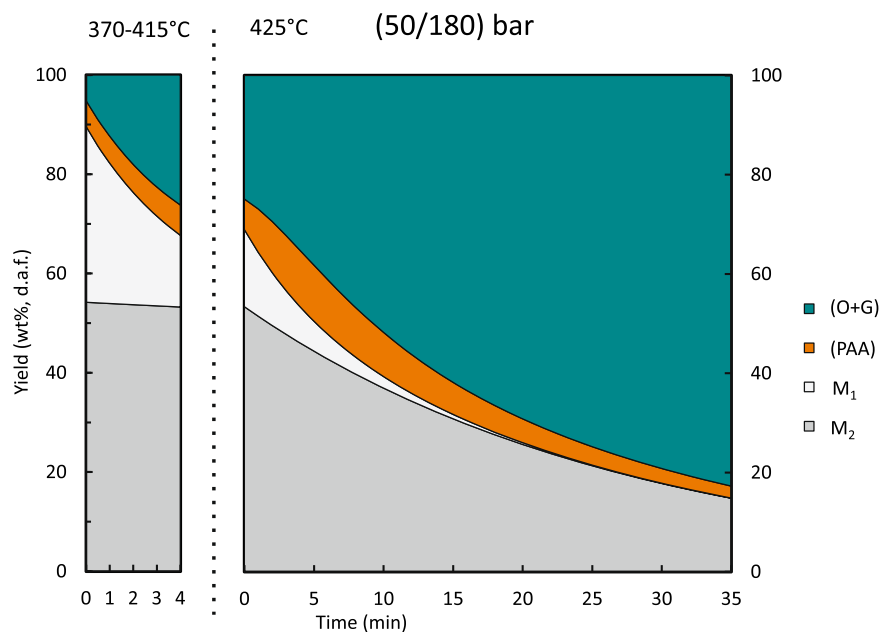
$$+ \left(-M_{20} + \frac{k_3M_{20}}{k_3-k_4} \right) e^{-k_3t}$$

(4)

R is calculated from a balance equation:

$$(R) = 100\% - (PAA) - (O + G) = M_1 + M_2$$

Fig. 6 Product formation with respect to time, model



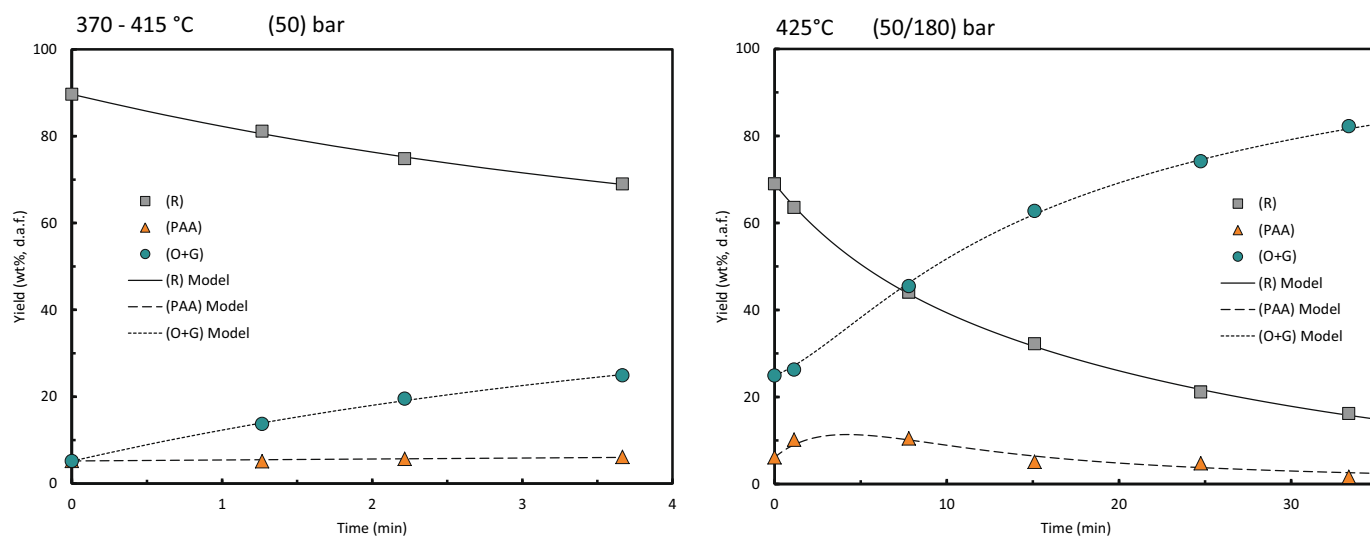


Fig. 7 Liquefaction of biochar; experimental data compared with the model

Balances are calculated according to:

$$\begin{aligned}
 100\% &= (\text{PAA}) + (\text{O} + \text{G}) + M_1 + M_2 \\
 100\% &= (\text{PAA})_0 + (\text{O} + \text{G})_0 + M_{10} + M_{20}
 \end{aligned}
 \tag{5}$$

Despite the fact that the reaction network applied in this work is slightly different to that used by Li [17], the resulting equations should be similar. Deviation of results was identified in an algebraic sign error in the work of Li.

The reaction network equations consist of several constants k_1, k_2, k_3, M_{10} , and M_{20} which need to be solved. In this work, the FORTRAN algorithm “Simulated annealing” [22] was utilized for solving the problem. The algorithm uses the experimental data points of (R), pre-asphaltenes and (PAA) and (O+G) as well as the four analytically solved function Eqs. (1) to (4) and the balance Eq. (5). A target function of the deviation of all data points with the corresponding functions is minimized. “Simulated annealing” is able to overcome unsteady function values, as well as local minima, to find the global minimum of the target function. The values for the rate constants as well as M_{10} and M_{20} are illustrated in Table 2.

The kinetic parameters suggest that the ratio of easy accessible amount to hardly reactive amount of biochar M_{10}/M_{20} is 0.65 for the initial heating stage and 0.29 for the isothermal stage, respectively. These rates suggest that the easy accessible part is liquefied in the first stage which is in agreement with all presumptions made previously. For the initial heating stage, a high rate constant k_1 is observed while all other rate constants are negligible. At the lower temperature in the heating stage, easily accessible and small molecules are breaking fast and form products. The hardly reactive part is not affected in this stage.

For the isothermal stage, direct reaction of biochar to (O+G) is not relevant. At the starting point of the isothermal stage, it is observed that half of the amount M_1 is already liquefied in the initial heating stage while M_2 remains unaffected. In the isothermal stage, the kinetic parameters suggest that residual M_1 reacts fast via (PAA) to (O+G). The rate constant for M_2 conversion to (PAA) increased by a factor of 9 compared to the initial heating stage, but is still 2 orders of magnitude lower than the reaction of the easily reactive portion. This is in agreement with the fact that the hardly reactive part, which consists of a three-dimensional crosslinked molecular network, is more difficult to rupture. The differing size of the rate constants in the two stages are shown in Fig. 5.

The product formation with respect to time is shown in Fig. 6. It can be observed that in the initial heating stage, only small amounts of M_2 are consumed. The product distribution at 370 °C (0 min) heating stage is indicated on the left hand side of Fig. 6 and consists of $M_{10}, M_{20}, (\text{PAA})_0$, and $(\text{O}+\text{G})_0$. New values of $M_{10}, M_{20}, (\text{PAA})_0$, and $(\text{O}+\text{G})_0$ can be indicated at the start of the isothermal stage (0 min) on the right hand side of Figs. 6 and 7.

The comparison of the experimental data with the model shows excellent agreement in the heating stage as well as the isothermal stage. Additionally, the local maximum for the intermediate products (PAA) for the isothermal stage is described well.

Conclusion

Liquefaction of biochar from liquid-phase pyrolysis was carried out with the solvent tetralin at a temperature of 425 °C. Several experiments were conducted to investigate the

influence of an initial heating period from 370 to 415 °C and an isothermal stage at 425 °C on the conversion of biochar. A kinetic network was solved to describe the liquefaction properties of biochar. The biochar was assumed to consist of two portions, an easily reactive and a hardly reactive portion.

The results of this study indicate that:

1. The model is valid for both stages, the initial heating stage and the isothermal stage
2. Liquefaction of biochar is very fast in the initial heating stage and directly forms oil and gas products.
3. The kinetic schemes for both stages are different. While most of the easily accessible portion reacts in the first stage directly to products, the hardly reactive part reacted to intermediates and afterwards to products.
4. Rate constant of the easily reactive portion is 2 orders of magnitudes higher than the reaction of the hardly reactive part due to the highly cross-linked molecular network of the hardly reactive part of biochar.
5. The applied model fits the experimental data well.

Liquefaction of biochar showed a conversion of 84 % and an oil yield of 72 % at 425 °C after 33 min isothermal reaction time. Biochar liquefaction performed even superior than catalytic fossil coal liquefaction, carried out by [17], who reported conversion of 81 % and an oil yield of 42 % after 30 min, respectively.

Acknowledgments This work was supported with funding by the FFG - Austrian Research Promotion Agency within the A3Plus task [Nr.: 835804].

References

1. Feiner R, Schwaiger N, Pucher H et al (2013) Liquefaction of pyrolysis derived biochar: a new step towards biofuel from renewable resources. *RSC Adv* 3:17898–17903. doi:10.1039/c3ra43516d
2. Pucher H, Schwaiger N, Feiner R et al (2014) Catalytic hydrodeoxygenation of dehydrated liquid phase pyrolysis oil. *Int J Energy Res* (in press)
3. Zhao X, Cheng K, Liu D (2009) Organosolv pretreatment of lignocellulosic biomass for enzymatic hydrolysis. *Appl Microbiol Biotechnol* 82:815–827. doi:10.1007/s00253-009-1883-1
4. Nimz HH, Schmitt U, Schwab E et al (2000) Wood. *Ullmann's Encycl Ind Chem*. doi:10.1002/14356007.a28_305
5. Rinaldi R, Schüth F (2009) Design of solid catalysts for the conversion of biomass. *Energy Environ Sci* 2:610. doi:10.1039/b902668a
6. Weller S, Pelipetz MG, Friedman S (1951) Kinetics of coal hydrogenation conversion of asphalt. *Ind Eng Chem* 43:1572–1575
7. Weller S, Clark EL, Pelipetz MG (1950) Mechanism of coal hydrogenation. *Ind Eng Chem* 42:334–336. doi:10.1021/ie50482a033
8. Weller S, Pelipetz MG (1951) Coal hydrogenation catalysts studies of catalyst distribution. *Ind Eng Chem* 43:1243–1246
9. Ancheya J, Trejo F, Rana MS (2009) Asphaltenes: chemical transformation during hydroprocessing of heavy oils. 441
10. Kaneko T, Derbyshire F, Makino E et al (2005) Coal liquefaction. *Ullmann's Encycl Ind Chem*. Wiley, New York. pp 1–83
11. Vasireddy S, Morreale B, Cugini A (2011) Clean liquid fuels from direct coal liquefaction: chemistry, catalysis, technological status and challenges. *Energy Environ Sci* 4:311–345
12. Haenel MW (2008) Catalysis in direct coal liquefaction. *Handb. Heterog. Catal.* Wiley, New York. pp 3023–3036
13. Schwaiger N, Feiner R, Zahel K et al (2011) Liquid and solid products from liquid-phase pyrolysis of softwood. *BioEnergy Res* 4:294–302. doi:10.1007/s12155-011-9132-8
14. Schwaiger N, Witek V, Feiner R et al (2012) Formation of liquid and solid products from liquid phase pyrolysis. *Bioresour Technol* 124:90–94. doi:10.1016/j.biortech.2012.07.115
15. Li X, Hu H, Jin L et al (2008) Approach for promoting liquid yield in direct liquefaction of Shenhua coal. *Fuel Process Technol* 89:1090–1095. doi:10.1016/j.fuproc.2008.05.003
16. Li W-Y, Feng J, Xie K-C, Kandiyoti R (2004) Analysis of solvent extracts from coal liquefaction in a flowing solvent reactor. *Fuel Process Technol* 85:1671–1687. doi:10.1016/j.fuproc.2003.12.012
17. Li X, Hu H, Zhu S et al (2008) Kinetics of coal liquefaction during heating-up and isothermal stages. *Fuel* 87:508–513. doi:10.1016/j.fuel.2007.03.041
18. Ding W, Liang J, Anderson LL (1997) Kinetics of thermal and catalytic coal liquefaction with plastic-derived liquids as solvent. *Ind Eng Chem Res* 36:1444–1452
19. Gioia F, Murena F (1988) Kinetics of hydrogen donation in the liquefaction of coal. *Ind Eng Chem Res* 27:1978–1983
20. Pradhan VR, Holder GD, Wender I, Tierney JW (1992) Kinetic modeling of direct liquefaction of Wyodak coal catalyzed by sulfated iron oxides. *Ind Eng Chem Res* 31:2051–2056
21. Ramdoss PK, Tarrer AR (1997) Kinetic model development for single-stage coal coprocessing with petroleum waste. *Fuel Process Technol* 51:83–100. doi:10.1016/S0378-3820(97)00002-7
22. Corana A, Marchesi M, Martini C, Ridella S (1987) Minimizing multimodal functions of continuous variables with the “simulated annealing” algorithm. *ACM Trans Math Softw* 13:262–280

Chapter 11

Chemical loop systems for biochar liquefaction: hydrogenation of Naphthalene

Cite this: *RSC Adv.*, 2014, 4, 34955

Chemical loop systems for biochar liquefaction: hydrogenation of Naphthalene

 Roland Feiner,^{*ab} Nikolaus Schwaiger,^{ab} Hannes Pucher,^a Lisa Ellmaier,^b Michael Derntl,^a Peter Pucher^b and Matthäus Siebenhofer^a

Liquefaction of biochar from liquid-phase pyrolysis was carried out in the solvent Tetralin. Tetralin is able to act as hydrogen donor during liquefaction of biochar and is itself rearranged into Naphthalene. Naphthalene must be re-hydrogenated to Tetralin to allow for further use in the liquefaction reaction (chemical loop system). Therefore Naphthalene hydrogenation was investigated, applying a full factorial design of experiments approach. The yield of Tetralin was chosen as response variable, while two-level-factors for temperature (150 °C and 200 °C), pressure (20 bar and 50 bar) and Raney-Nickel catalyst load (5 wt% and 10 wt%) were selected. The Design of Experiments approach showed a rising influence of all three factors in the order: temperature < pressure < catalyst load. The reaction kinetics of the hydrogenation of Naphthalene to Tetralin and Decalin was then investigated at 150 °C and 200 °C. The reaction proceeds stepwise and not in consecutive steps. In a first step Naphthalene reacts selectively with 96% yield to Tetralin, while the reaction of Tetralin to Decalin does not start until all Naphthalene is consumed. The rate-constant of the reaction of Naphthalene to Tetralin is one magnitude higher than that for the reaction of Naphthalene to Decalin. This is in agreement with the findings from the design of experiments approach. The results of these investigations indicate that the chemical-loop system Naphthalene–Tetralin is suitable for usage in the liquefaction of biochar.

Received 17th April 2014
Accepted 30th July 2014

DOI: 10.1039/c4ra03487b

www.rsc.org/advances

1. Introduction

Liquefaction of renewable solid carbon sources is a promising route for production of second generation biofuels. Due to rising acceptance of pyrolysis in biofuel production, a significant amount of the by-product biochar is available.^{1–3} This biochar can be liquefied in the presence of Tetralin.^{4,5} Tetralin acts as a carrier for the biochar particles, as a heat transfer agent and most importantly as a hydrogen donor solvent.^{4,6} The biochar particles are thermally decomposed and the radicals of the breaking fragments need to be saturated instantaneously with hydrogen. If the availability of hydrogen is low, breaking fragments will fall into repolymerisation reactions to form unwanted tars.⁷ The solvent Tetralin provides 2 moles of H₂ by rearranging to Naphthalene. Therefore hydrogenation of Naphthalene to Tetralin is needed for usage in a chemical loop system.

A common way to produce Tetralin is to partially hydrogenate Naphthalene with 2 moles of H₂.⁸ Further hydrogenation with 3 moles of H₂ leads to formation of fully saturated Decalin,

according to the overall balance shown in Fig. 1. Decalin does form two stereoisomeric molecules, *trans*-Decalin and *cis*-Decalin. Although Decalin has a higher H/C-value than Tetralin it is unfavourable because it does not have the ability to act as a hydrogen donor.⁹ This is due to a higher molecular stability of Decalin compared with Tetralin. The hydrogenation products of Naphthalene, dihydro-, hexahydro- and octahydronaphthalene, are not of technical relevance.⁸

Naphthalene consists of two aromatic rings and belongs to the group of polyaromatic hydrocarbons (PAHs). Naphthalene is found in coal tars and crude oil,⁸ beside PAHs consisting of three to five aromatic rings, like pyrene, anthracene, phenanthrene and fluoranthene *etc.*, Naphthalene at ambient conditions is a crystalline/waxy white solid product with a melting point of 80 °C, while Tetralin and Decalin are liquids. The

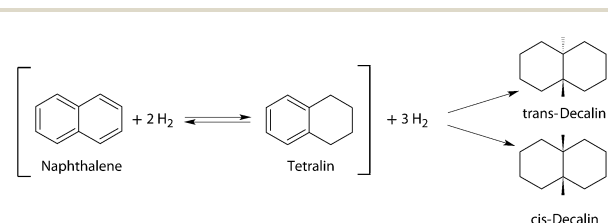


Fig. 1 Hydrogenation of Naphthalene to Tetralin and to Decalin.

^aGraz University of Technology, Institute of Chemical Engineering and Environmental Technology, NAWI Graz Central Lab Biobased Products, Inffeldgasse 25/C/II, 8010 Graz, Austria

^bBDI-BioEnergy International AG, Parkring 18, 8074 Grambach/Graz, Austria

partial hydrogenation of Naphthalene to Tetralin can be conducted in the liquid-phase and the vapour-phase. Selectivity of Tetralin over Decalin is higher for liquid-phase reactions.¹⁰ Noble metal catalysts like platinum and ruthenium but also nickel are proposed to have a high selectivity towards the products.^{8,11,12} The catalyst Red Mud, a by-product of the alumina production was investigated with minor success.¹³ Sulphur compounds¹⁴ may act as sulphided catalysts. The mechanisms of the catalytic hydrogenation of Naphthalene was investigated in ref. 15 and 16.

Several authors¹⁷ propose the hydrogenation of Naphthalene in a liquid carrier at temperatures between 150 °C and 200 °C and a hydrogen pressures of 1 to 20 atm. Cyclohexane, methylcyclohexane, dimethylcyclohexane, ethylcyclohexane, cyclopentane and methylcyclopentane are preferred liquid carriers. As the reaction temperature is as low as 260 °C,⁸ decomposition of Naphthalene, Tetralin, Decalin or the carrier is not to be expected. Under biochar liquefaction conditions above 400 °C partial degradation of Tetralin and Naphthalene is observed.

Hydrogenation of Naphthalene to Tetralin was investigated by applying design of experiments with the program JMP for data analysis. The aim of design of experiments is to obtain an accurate mathematical prediction model with as few as possible physical experiments. A full factorial design was applied to investigate the hydrogenation for a reaction time of 5 minutes. Design of experiments needs two sorts of variables: (1) response variables and (2) factor variables. The yield of the desired product Tetralin was chosen as the response variable. The temperature, hydrogen pressure and Raney-Nickel catalyst load (with respect to Naphthalene feed) were used as factor variables. All independent factor variables that influence the response variable need to be taken into account. Factor constraints were defined. In the physical experiments a temperature of either 150 °C or 200 °C, a pressure of either 20 bar or 50 bar and a Raney-Nickel catalyst load of either 5 wt% or 10 wt% were used.

Design of experiment proposes that all combinations of factor variables should be investigated, which leads to a lower experimental effort. The number of experiments for the design of experiments approach is calculated as follows: With two steps for all factor variables (temperature of either 150 °C or 200 °C) and three different factors (k) the number of experiments $n = 2^k$, resulting in 8 experiments. For improved accuracy a replica is recommended.

From design of experiments the optimum combination of operation conditions for investigation of the kinetics of the hydrogenation of Naphthalene to Tetralin were deduced.

2. Materials and methods

Materials

Reagent-grade Naphthalene (CAS: 91-20-3) with a purity of 99%, the carrier methylcyclohexane (MCH) (CAS: 108-87-2) with a purity of 99%, Raney-Nickel as pre-activated catalyst (CAS: 7440-02-0 from Merck) consisting of 90% Ni and 10% Al on weight dry basis (SEM image, see Fig. 2) and high grade hydrogen were used for the experiments.

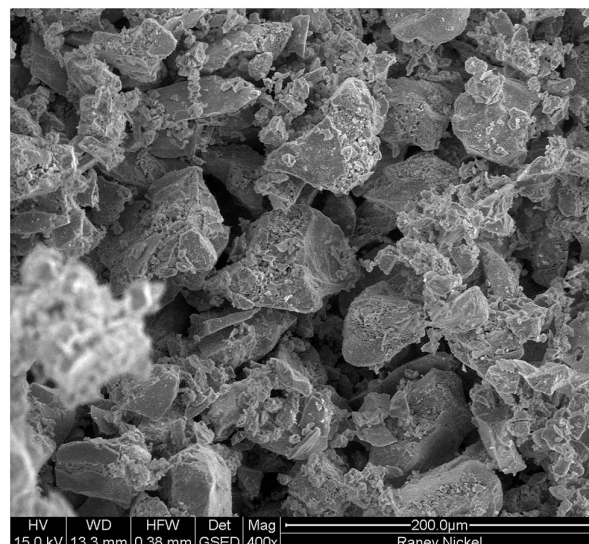


Fig. 2 SEM Image of Raney-Nickel catalyst.

Experimental procedure

All design of experiments investigations were performed in a stirred 450 ml batch reactor. For each experiment 20 g of Naphthalene was added to the reactor together with 80 g of MCH and 5 wt% or 10 wt% Raney-Nickel catalyst (with respect to Naphthalene). The Naphthalene to MCH ratio was 1/4. The reactor was then sealed tightly. The stirring speed was set to 500 rpm during the experiment as well as the cooling phase. The reactor was heated with an electric heating jacket to the desired temperature. When the operation temperature was reached hydrogen was supplied, pre-set to the desired pressure by an expansion valve. The exothermic reaction started immediately and the reactor was cooled during the experiment (5 minutes of reaction time) in order to keep the reaction isothermal. Upon completion of the experiment the hydrogen valve was closed, the heating jacket removed and the reactor was cooled to below 100 °C within 3 minutes. When the temperature in the reactor reached 30 °C the pressure was relieved and the reactor was opened. The liquid product obtained was filtered through a syringe filter and analysed.

Reaction kinetics were studied in a 1100 ml reactor at two temperatures 150 °C and 200 °C over a 60 minutes reaction period. This bigger reactor allows for taking samples while the reactor is in operation at elevated temperature and pressure conditions. The hydrogen pressure applied was 20 bar. For each experiment 93 g of Naphthalene was added to the reactor together with 187 g of MCH and 5 wt% Raney-Nickel catalyst (with respect to Naphthalene). The Naphthalene to MCH ratio was 1/2. Hydrogenation of Naphthalene to Tetralin is a fast reaction. After loading, the reactor was sealed tightly. The stirring speed was set to 500 rpm during the experiment. The reactor was heated with an electric heating jacket to the desired temperature. When the desired temperature was reached the reactor was supplied with hydrogen, pre-set to the desired

pressure by an expansion valve. The exothermic reaction started immediately. The reactor was cooled during the 60 minutes of reaction time to keep the reaction isothermal. Samples of the reaction mixture were taken every minute in the first 10 minutes and thereafter every 5 minutes. The samples taken were filtered through a syringe filter and subjected to analysis.

The generic reaction rate equations can be expressed according to:

$$\begin{aligned}r_{\text{N}} &= -k_1 c_{\text{N}}^n \\r_{\text{T}} &= k_1 c_{\text{N}}^n - k_2 c_{\text{T}}^n \\r_{\text{D}} &= k_2 c_{\text{T}}^n\end{aligned}$$

where r is for the reaction rate, subscript N is for Naphthalene, T for Tetralin and D for Decalin (*cis*- and *trans*-), k is for the rate-constants, c is for the concentration and superscript n is for the order of reaction.

Analytics

The liquid product from filtration was analysed with a GC-FID. A MXT 2887, 10 m column from Restek and a gas chromatograph, type Agilent 7890A, was used. All substances are detectable between 80 °C and 150 °C. Therefore the heating-rate was set to 10 °C per minute in this section and to 20 °C per minute in all other sections. The injection method was “cool on-column”. The final temperature was 360 °C.

3. Results and discussion

Design of experiments

Detailed experimental data of the conducted experiments are illustrated in Table 1. The highest yields of Tetralin (96 mol% and 95 mol%) were observed after 5 minutes of reaction for 200 °C, 50 bar, 10 wt% catalyst. Decalin production was observed at the upper temperature level. Experiments marked grey in Table 1 were not considered in the statistics. These are

Table 1 Design of experiments data after 5 minutes of reaction

| Pattern | Temperature [°C] | Pressure [bar] | Catalyst [wt%] | Yield Tetralin [mol%] |
|---------|------------------|----------------|----------------|-----------------------|
| --- | 150 | 20 | 5 | 37 |
| +- | 150 | 50 | 5 | 49 |
| ++ | 200 | 20 | 5 | 39 |
| ++ | 150 | 20 | 10 | 23 |
| ++ | 150 | 50 | 5 | 2 |
| +++ | 200 | 20 | 10 | 85 |
| +++ | 200 | 20 | 10 | 82 |
| +++ | 200 | 50 | 5 | 82 |
| +++ | 150 | 50 | 10 | 75 |
| +++ | 200 | 50 | 10 | 96 |
| +++ | 150 | 50 | 10 | 53 |
| +++ | 200 | 50 | 10 | 95 |
| +++ | 200 | 50 | 5 | 77 |
| +++ | 150 | 20 | 10 | 62 |
| +++ | 200 | 20 | 5 | 30 |
| --- | 150 | 20 | 5 | 32 |

experimental values which do not fit the 95% confidence interval.

The results in Table 1 were subjected to an effect screening through JMP software. During this effect screening the influence of the three factors (temperature, pressure, catalyst amount) as well as two-fold combinations (the combination of pressure and temperature has an effect) and three-fold combination of factors on the response were determined. As a result of the effect screening the factors temperature, pressure and catalyst amount have a significant influence on the yield of Tetralin. Two-fold and three-fold interactions showed no significance. With the essential effects in mind the mathematical model can be built. Results of the linear regression model are shown in Fig. 3.

Fig. 3A shows the experimental Tetralin yields on the y-axis and the predicted Tetralin yields on the x-axis. If the model would predict perfectly performed experiments, all data points would lie on the 45 degree line. The 95% probability confidence interval is plotted in red dotted lines. The RSME (Root Mean Square Error) describes the average deviation of the experimental data from the model with 9.4, which is within limits. Fig. 3B–D show the influence of the factor variables on the yield of Tetralin. The impact is increasing in the following order: temperature < pressure < catalyst amount, and can be read from the slope of the solid red line. The x-axis is not scaled like the observed regressors (temperature, pressure, catalyst load) because the model doesn't consist of a simple regression of one regressor but a multiple regression. Therefore the values of the x-axis are no longer corresponding to actual data values. Points on the x-axis farther out (+1.5 and -1.5) pull on the line of fit with greater leverage than the points near the middle (0.0). The influential points in all leverage plots are the ones far out on the x-axis. This makes it possible to judge if the line of fit (red line) on the effect's leverage plot carries the points significantly better than the horizontal line (blue line) does.

The estimated regression parameters and the mean yields lead to the empirical model equation for the hydrogenation of Naphthalene to Tetralin (eqn (1)) calculated with JMP.

Empirical model equation.

$$\begin{aligned}\text{Yield} &= 64.74 + 8.62 \left(\frac{\text{Temperature} - 175}{25} \right) \\ &+ 11.54 \left(\frac{\text{Pressure} - 35}{15} \right) + 15.04 \left(\frac{\text{Catalyst} - 7.5}{2.5} \right) \quad (1)\end{aligned}$$

The graphical display of the model equation is the prediction variance surface plot, shown in Fig. 4. By setting one factor constant (temperature, pressure or catalyst load) a surface is formed in the three-dimensional space. The Tetralin yield is displayed on the z-axis.

Design of experiment shows that a combination of 200 °C, 50 bar and 10 wt% catalyst lead to the best result for the hydrogenation of Naphthalene to Tetralin. Fig. 4A and B both show a significant effect of the pressure on the prediction variance surface. Fig. 4C and D (catalyst) both show the most

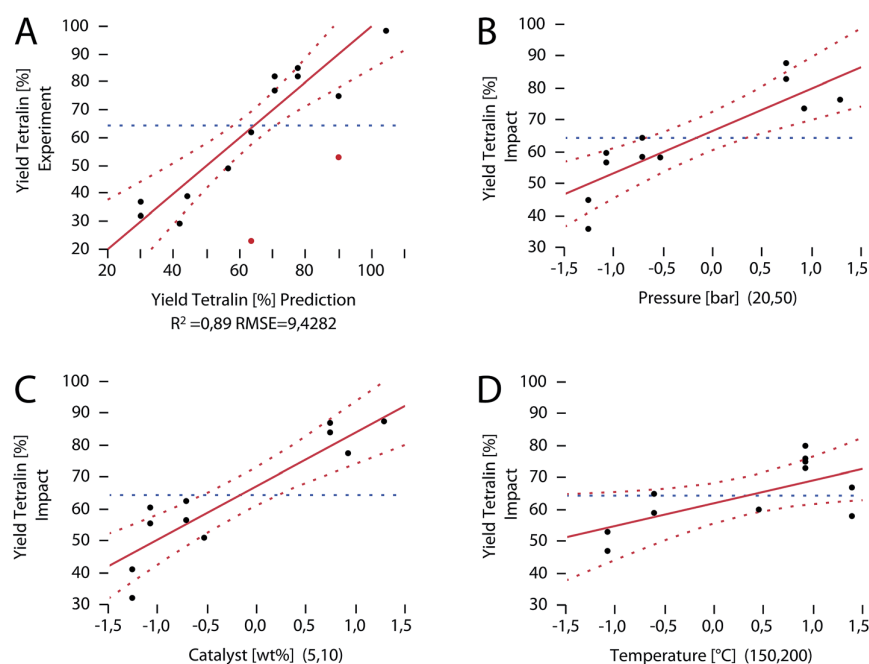


Fig. 3 Influence of factor variables on the response variable.

significant shift of the prediction variance surface to higher values of Tetralin yield and Fig. 4E and F (temperature) the least.

Investigation of reaction kinetics

Results of the kinetic experiments at 150 °C, 20 bar and 5% catalyst are shown in Fig. 5 and at 200 °C, 20 bar and 5% catalyst in Fig. 6. Both figures indicate that the reaction of Naphthalene (N) to Tetralin (T) to Decalin (D) is not classically consecutive but rather occurs stepwise. In the first step Naphthalene reacts selectively to Tetralin without the formation of Decalin until 96% of the Naphthalene is consumed. A small amount of Naphthalene remains in the reaction mixture. After this first step the Tetralin is hydrogenated to Decalin, but an order of magnitude slower than the reaction of Naphthalene to Tetralin. Compared to 150 °C the reaction of Naphthalene to Tetralin is faster at 200 °C, which can be seen by comparing Fig. 5 and 6 or from the rate-constants. This agrees to the findings of the temperature dependency through design of experiments. The reaction of Tetralin to Decalin is slower at 200 °C than at 150 °C which can be seen from the rate-constants.

In Fig. 5 and 6 no concentration dependency can be observed. The reactions are therefore zero-order reactions. The start concentration of Naphthalene is 2.6 mmol per gram reaction mixture. When Naphthalene reacts to Tetralin very fast, there is a time where only a small amount of Naphthalene is left in the reaction mixture, which is practically zero. The time where the Naphthalene concentration is zero is herein-after defined as t_N . After the time t_N the reaction of Tetralin to Decalin starts with the rate-constant k_2 , see Table 2. For the

kinetic experiment at 150 °C, 20 bar and 5% catalyst the time t_N is 9.76 min for the experiment at 200 °C, 20 bar and 5% catalyst the time t_N is 7.92 min. As proposed through design of experiments the higher reaction temperature increases the reaction rate from Naphthalene to Tetralin. Kirumakki¹⁸ investigated continuous hydrogenation of Naphthalene and found 200 °C to be the temperature for highest conversions to Tetralin while further increase of temperature above 200 °C lead to decrease in conversion because of the exothermic nature of the reaction.

The stepwise reaction leads to the following kinetic equations:

The calculated rate-constants correspond to:

$$t_{N|150^{\circ}\text{C}} = 9.76 \text{ [min]}$$

$$k_1' |_{150^{\circ}\text{C}} = 5.71 \times 10^{-5} \left[\frac{\text{mmol}}{\text{g} \times \text{g}_{\text{cat}} \times \text{min}} \right]$$

$$k_2' |_{150^{\circ}\text{C}} = 4.36 \times 10^{-6} \left[\frac{\text{mmol}}{\text{g} \times \text{g}_{\text{cat}} \times \text{min}} \right]$$

$$t_{N|200^{\circ}\text{C}} = 9.76 \text{ [min]}$$

$$k_1' |_{200^{\circ}\text{C}} = 7.04 \times 10^{-5} \left[\frac{\text{mmol}}{\text{g} \times \text{g}_{\text{cat}} \times \text{min}} \right]$$

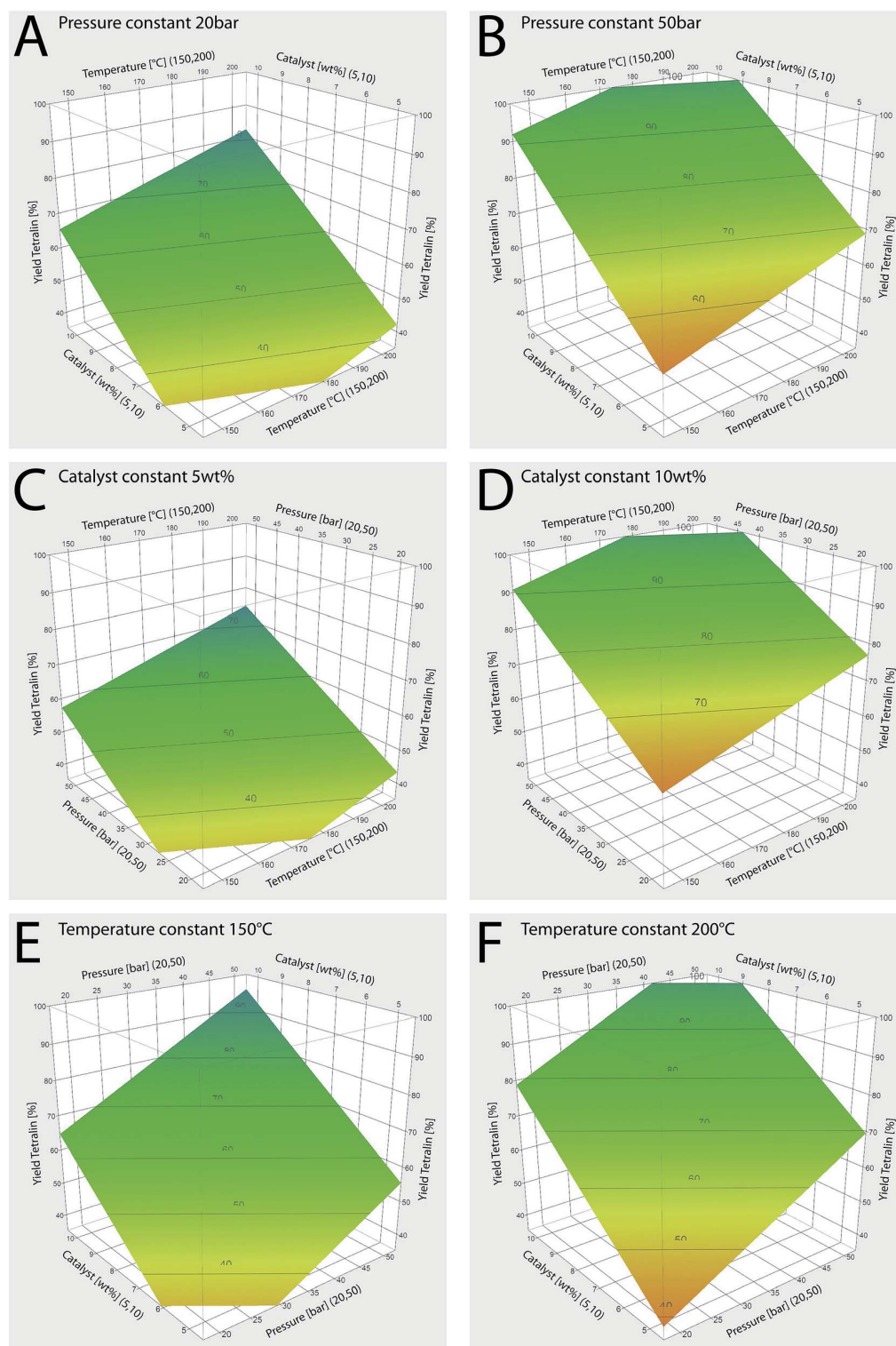


Fig. 4 Prediction variance surface plots.

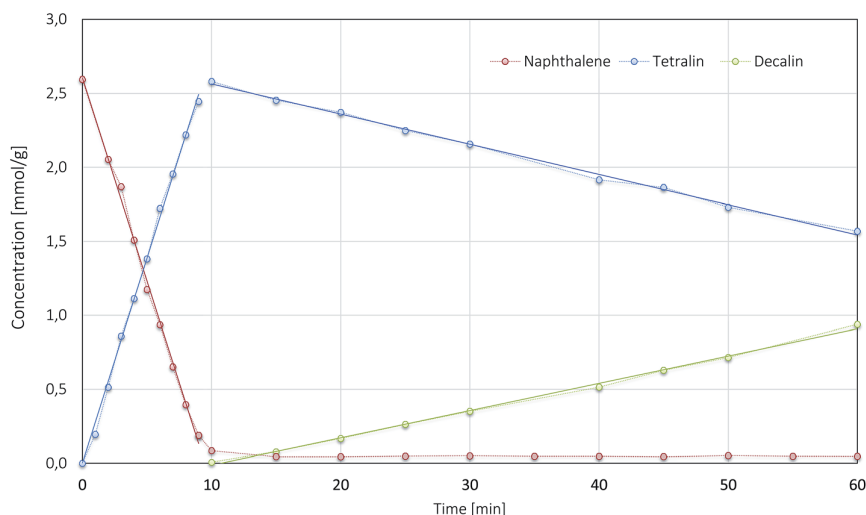


Fig. 5 Kinetics at $T = 150\text{ }^{\circ}\text{C}$, 20 bar, 5% catalyst.

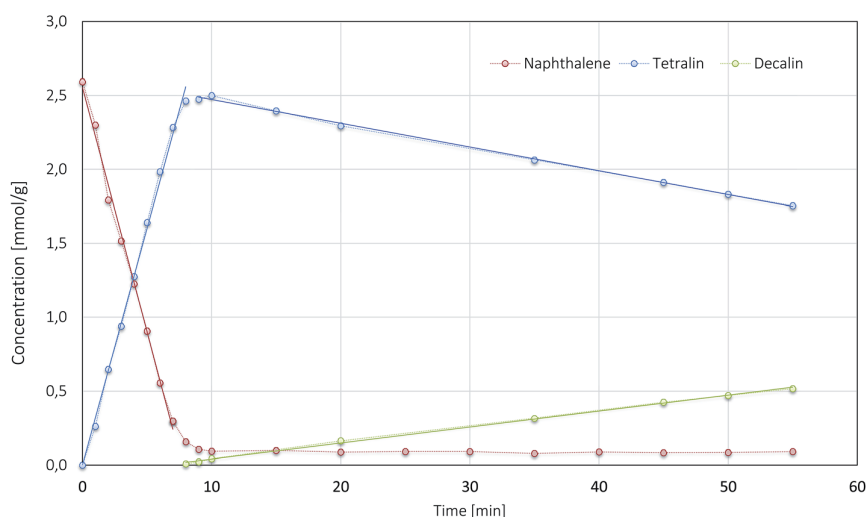


Fig. 6 Kinetic at $T = 200\text{ }^{\circ}\text{C}$, 20 bar, 5% catalyst.

Table 2 Kinetic Equations

| | | | |
|-------------|---|-----------|-----------------------------|
| Naphthalene | $r_N = -k_1$ $c_N = c_{N,0} - k_1 t$ | N-present | $t_N < \frac{c_{N,0}}{k_1}$ |
| Tetralin | $r_T = k_1$ $c_T = k_1 t$ $r_T = -k_2$ $c_T = c_{T(t=t_N)} - k_2(t - t_N)$ $c_T = k_1 t_N - k_2(t - t_N)$ | N-present | $t_N < \frac{c_{N,0}}{k_1}$ |
| | | N-absent | $t_N > \frac{c_{N,0}}{k_1}$ |
| Decalin | $r_D = 0$ $c_D = 0$ $r_D = k_2$ $c_D = k_2(t - t_N)$ | N-present | $t_N < \frac{c_{N,0}}{k_1}$ |
| | | N-absent | $t_N > \frac{c_{N,0}}{k_1}$ |

$$k_2'_{200^{\circ}\text{C}} = 3.93 \times 10^{-6} \left[\frac{\text{mmol}}{\text{g} \times \text{g}_{\text{cat}} \times \text{min}} \right]$$

Analysis of the samples taken during the kinetic experiments at $150\text{ }^{\circ}\text{C}$ and $200\text{ }^{\circ}\text{C}$ and comparison of the results led to a finding concerning the composition of Decalin. It was shown that at $150\text{ }^{\circ}\text{C}$ reaction temperature the ratio of *trans*- to *cis*-Decalin stays constant with reaction time while the ratio at $200\text{ }^{\circ}\text{C}$ reaction temperature rose with time. Fig. 7 shows the ratio of *trans*-Decalin to *cis*-Decalin formed with respect to time. The reason for the increase of the ratio is that at $200\text{ }^{\circ}\text{C}$ the formation of *trans*-Decalin is thermodynamically favored but can be influenced by the used catalyst

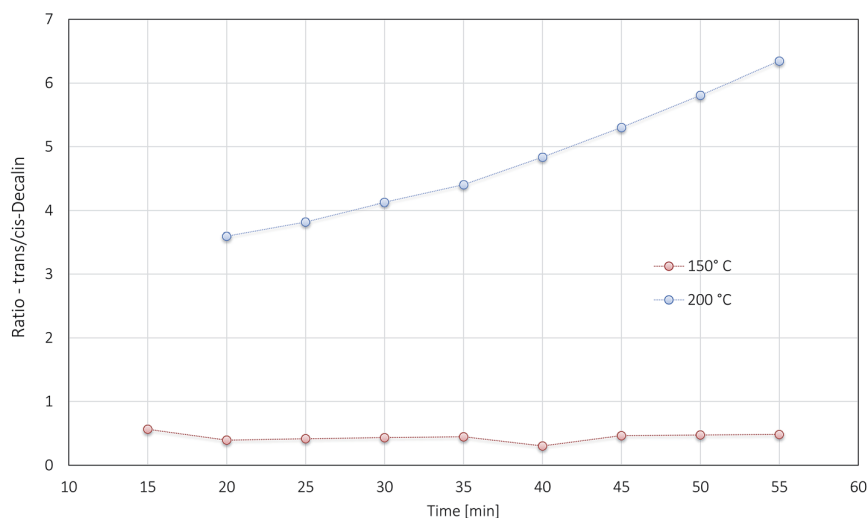


Fig. 7 Ratio of *trans*-Decalin to *cis*-Decalin (20 bar, 5% catalyst).

materials.^{19,20} While isomerization reaction of *cis*-Decalin to *trans*-Decalin were ruled out during reaction by¹⁸ other groups found isomerization from *cis*- to *trans*-Decalin in the magnitude of *trans*-Decalin formation in the reaction stage at 200 °C.²⁰

4. Conclusion

Hydrogenation of Naphthalene was investigated. In the first part of the study several experiments were conducted using design of experiments to investigate the influence of the factors temperature between 150 °C and 200 °C, hydrogen pressure between 20 bar and 50 bar and catalyst load between 5 wt% and 10 wt% on the yield of Tetralin after 5 minutes of reaction. In the second part of the study the kinetics of the reaction of Naphthalene to Tetralin and Decalin were investigated separately for two temperatures, 150 °C and 200 °C. A pressure of 20 bar hydrogen and catalyst load of 5 wt% was chosen for the investigation of the kinetics.

The results of the design of experiments study indicate that:

(1) Influence of the factors is increasing in the order: temperature < pressure < catalyst load.

(2) Highest yield of Tetralin in the design of experiments study was found for 200 °C, 50 bar hydrogen and 10 wt% of catalyst.

The results of the kinetic study indicate that:

(1) The reaction of Naphthalene to Tetralin to Decalin occurs stepwise and not classically consecutive.

(2) All reactions are zero-order reactions.

(3) In the first reaction step selective hydrogenation of Naphthalene to Tetralin occurs with a yield of 96%.

(4) Only after complete consumption of Naphthalene, Tetralin is hydrogenated to form Decalin.

(5) Reaction of Naphthalene to Tetralin is an order of magnitude faster than the reaction of Tetralin to Decalin.

Acknowledgements

This work was funded by the FFG - Austrian Research Promotion Agency, A3Plus task [Nr.: 835804], project bioBOOST.

References

- N. Schwaiger, V. Witek, R. Feiner, H. Pucher, K. Zahel, A. Pieber, P. Pucher, E. Ahn, B. Chernev, H. Schroettner, P. Wilhelm and M. Siebenhofer, Formation of liquid and solid products from liquid phase pyrolysis., *Bioresour. Technol.*, 2012, **124**, 90–94.
- N. Schwaiger, R. Feiner, K. Zahel, A. Pieber, V. Witek, P. Pucher, E. Ahn, P. Wilhelm, B. Chernev, H. Schröttner and M. Siebenhofer, Liquid and Solid Products from Liquid-Phase Pyrolysis of Softwood, *BioEnergy Res.*, 2011, **4**(4), 294–302.
- H. Pucher, N. Schwaiger, R. Feiner, L. Ellmaier, P. Pucher and M. Siebenhofer, Catalytic hydrodeoxygenation of dehydrated liquid phase pyrolysis oil, *Int. J. Energy Res.*, 2014, DOI: 10.1002/er.3205.
- R. Feiner, N. Schwaiger, H. Pucher, L. Ellmaier, P. Pucher and M. Siebenhofer, Liquefaction of pyrolysis derived biochar: a new step towards biofuel from renewable resources, *RSC Adv.*, 2013, **3**, 17898–17903.
- R. Feiner, N. Schwaiger, H. Pucher, L. Ellmaier, A. Reiter, M. Derntl, T. Glatz, P. Pucher and M. Siebenhofer, Kinetics of Biochar Liquefaction, *BioEnergy Res.*, 2014, 1–8.
- R. Feiner, Liquefaction of biogenous feedstocks, PhD Thesis, Graz University of Technology, 2014.
- M. W. Haenel, Catalysis in Direct Coal Liquefaction in *Handbook of Heterogeneous Catalysis*, Wiley-VCH Verlag GmbH, 2008, pp. 3023–3036.
- W. Rittmeister, Naphthalinhydroverbindungen, in *Ullmann's Encyclopedia of Industrial Chemistry*, 3rd edn, 1960, p. 589.

- 9 T. Kaneko, F. Derbyshire, E. Makino, D. Gray, and M. Tamura, Coal Liquefaction, in *Ullmann's Encyclopedia of Industrial Chemistry*, Wiley-VCH Verlag GmbH, 2005, pp. 1–83.
- 10 G. Collin, H. Höke, and H. Greim, Naphthalene and hydronaphthalenes, in *Ullmann's Encyclopedia of Industrial Chemistry*, 2000, pp. 661–670.
- 11 OECD Sids, 1,2,3,4-Tetrahydronaphthalene, 2004.
- 12 T.-C. Huang and B.-C. Kang, The Hydrogenation of Naphthalene with Platinum/Alumina-Aluminum Phosphate Catalysts, *Ind. Eng. Chem. Res.*, 1995, **34**(9), 2955–2963.
- 13 K. C. Pratt and V. Christoverson, Hydrogenation of a model hydrogen-donor system using activated red mud catalyst, *Fuel*, 1982, **61**, 460–462.
- 14 S. Yang and L. M. Stock, *Molecular catalytic hydrogenation of aromatic hydrocarbons and the hydrotreating of coal liquids*, Pittsburgh, PA, USA, 1996.
- 15 P. A. Rautanen, M. S. Lylykangas, J. R. Aittamaa and O. A. I. Krause, Liquid-phase hydrogenation of naphthalene and tetralin on Ni/Al₂O₃: Kinetic modeling, *Ind. Eng. Chem. Res.*, 2002, **41**, 5966–5975.
- 16 A. C. A. Monteiro-Gezork, R. Natividad and J. M. Winterbottom, Hydrogenation of naphthalene on NiMo- Ni- and Ru/Al₂O₃ catalysts: Langmuir–Hinshelwood kinetic modelling, *Catal. Today*, 2008, **130**(2–4), 471–485.
- 17 H. Metzen, B. Schleppehoff, and A. Sinhuber, Patent: Process for the preparation of tetralin by the selective hydrogenation of naphthalene, EP0087597 A1, EP 0087597 A11983, 1983.
- 18 S. Kirumakki, B. Shpeizer, G. Sagar, K. Chary and A. Clearfield, Hydrogenation of Naphthalene over NiO/SiO₂–Al₂O₃ catalysts: Structure–activity correlation, *J. Catal.*, 2006, **242**(2), 319–331.
- 19 C. M. C. Romero, J. W. Thybaut and G. B. Marin, Naphthalene hydrogenation over a NiMo/γ-Al₂O₃ catalyst: experimental study and kinetic modelling, *Catal. Today*, 2008, **130**(1), 231–242.
- 20 A. D. Schmitz, G. Bowers and C. Song, Shape-selective hydrogenation of naphthalene over zeolite-supported Pt and Pd catalysts, *Catal. Today*, 1996, **31**(96), 45–56.

Chapter 12

Hydrocarbon liquid
production via the
bioCRACK process and
catalytic hydroproces-
sing of the product oil



Cite this: *Green Chem.*, 2015, **17**, 2487

Hydrocarbon liquid production *via* the bioCRACK process and catalytic hydroprocessing of the product oil

N. Schwaiger,^{*a,c} D. C. Elliott,^b J. Ritzberger,^c H. Wang,^b P. Pucher^c and M. Siebenhofer^a

Continuous hydroprocessing of liquid phase pyrolysis Bio-oil, provided by BDI-BioEnergy International bioCRACK pilot plant at OMV Refinery in Schwechat/Vienna Austria was investigated. These hydroprocessing tests showed promising results using catalytic hydroprocessing strategies developed for unrefined Bio-oil. A sulfided base metal catalyst (CoMo on Al₂O₃) was evaluated. The bed of catalyst was operated at 400 °C in a continuous-flow reactor at a pressure of 12.1 MPa with flowing hydrogen. The condensed liquid products were analyzed and found that the hydrocarbon liquid was significantly hydro-treated so that nitrogen and sulfur were below the level of detection (<0.05), while the residual oxygen ranged from 0.7 to 1.2%. The density of the products varied from 0.71 g mL⁻¹ up to 0.79 g mL⁻¹ with a correlated change of the hydrogen to carbon atomic ratio from 2.1 down to 1.9. The product quality remained high throughout the extended tests suggesting minimal loss of catalyst activity through the test. These tests provided the data needed to assess the quality of liquid fuel products obtained from the bioCRACK process as well as the activity of the catalyst for comparison with products obtained from hydro-treated fast pyrolysis Bio-oils from fluidized-bed operation.

Received 26th November 2014,
Accepted 12th February 2015

DOI: 10.1039/c4gc02344g

www.rsc.org/greenchem

Introduction

Fast pyrolysis of biomass is a viable technology for the direct production of liquid fuels.¹ Liquid phase pyrolysis of biomass is an alternative technology to fast pyrolysis. Although product classes, such as liquid phase Bio-oil and biochar, are similar, the differences in operation and product composition are significant. Liquid phase pyrolysis is usually powered with a liquid heat carrier.² This heat carrier limits the operation temperature to less than 400 °C according to the boiling point and thermal stability. This temperature limit leads to a higher amount of biochar and less liquid phase Bio-oil production with higher water content and acid number. A major advantage of liquid phase pyrolysis over fast pyrolysis in fluidized bed operation is elevated heat transfer in the liquid heat carrier phase. Also, biochar and inorganics are retained in the liquid heat carrier. Liquid phase Bio-oil is not contaminated with solids. Thus, hot vapor filtration³ for dust removal from the vapor phase is not needed.⁴ However, depending on the heat carrier biomass is partially dissolved in it.

The Bio-oil product from fast pyrolysis and liquid phase pyrolysis, however, is not of sufficient quality for direct use as petroleum refinery feedstock. Catalytic hydroprocessing has been developed to convert the highly oxygenated Bio-oil components into hydrocarbons.⁵ Conventional hydrotreating processes cannot be directly applied for upgrading of fast pyrolysis Bio-oil. Specifically, the necessity of a two-temperature strategy was identified.⁶

The objective of this research project was to develop a catalytic hydrotreating process for the production of crude petroleum refinery feedstock from biomass, specifically from condensate of the bioCRACK process. From bioCRACK pyrolysis two different fractions of condensate, high aqueous Bio-oil and Dehydrated Bio-oil, are collected. These feedstocks need hydroprocessing to produce a refinery compatible hydrocarbon-like feedstock. Previous hydrodeoxygenation studies have been performed in a batch reactor with the bioCRACK Bio-oil and Dehydrated Bio-oil using precious and base metal catalysts at lower temperature. The process resulted in a partially deoxygenated Bio-oil with some improvements in reduced heavy product compared to conventional fast pyrolysis Bio-oil hydroprocessing.⁷

Investigations focused on hydrotreating of condensate from liquid phase pyrolysis of spruce wood pellets. The Bio-oils were produced in a bioCRACK reactor located at the OMV refinery complex in Schwechat, Austria. The Bio-oil products

^aInstitute of Chemical Engineering and Environmental Technology, NAWI Graz, Central Lab Biobased Products, Graz University of Technology, Inffeldgasse 25/C, 8010 Graz, Austria. E-mail: nikolaus.schwaiger@tugraz.at

^bPacific Northwest National Laboratory, PO Box 999, Richland, WA 99352, USA

^cBDI-BioEnergy International AG, Parkring 18, 8074 Grambach/Graz, Austria

were hydrotreated in a bench-scale, continuous-flow, packed-bed catalytic reactor at Pacific Northwest National Laboratory (PNNL).

Experimental

The pyrolysis experiments were performed in the BDI-Bio-Energy International AG bioCRACK pilot plant facility at OMV refinery Vienna/Schwechat. Fig. 1 shows an image of the pilot plant facility. Spruce pellets were the feedstock for liquid phase pyrolysis. VGO (vacuum gas oil) was the liquid heat carrier. The biomass feed rate was between 60–100 kg h⁻¹. The ratio of biomass and VGO varied between 1 : 3 and 1 : 6. Pyrolysis temperature was between 350–400 °C.

The flow sheet of the bioCRACK pilot plant is shown in Fig. 2. Biomass and liquid heat carrier oil are fed simul-



Fig. 1 bioCRACK pilot plant at OMV refinery Vienna/Schwechat.

taneously into the impregnator. From there a biomass heat carrier slurry is transferred into the reactor 1 and 2 where the biomass is immediately heated to 375 °C. The biogenic and the fossil vapors are cooled in the condenser. The settling vessel separates the condensed vapors into an aqueous Bio-oil fraction and the non-polar bioCRACK oil fraction. In the following distillation step high boiling heat carrier residues are separated from the nonpolar bioCRACK oil fraction. After pyrolysis the heat carrier is separated from biochar.

For further lab scale processing the residual heat carrier is separated from biochar by solid liquid extraction. Biochar can then undergo liquefaction.^{8–10}

bioCRACK bio-oil dehydration

Due to the high water content of aqueous Bio-oil, dehydration was tested to raise the energy content and to lower transport volume. Dehydration of flash pyrolysis Bio-oil was already tested,^{11,12} but there is no data available for liquid phase pyrolysis Bio-oil.

Dehydration was performed by short path distillation. The apparatus had a heat exchanger surface of 0.1 m². The heat carrier operating temperature was 130 °C and operating pressure was 130 mbar. It has been reported,¹³ that upgrade of Bio-oil distillate with ethanol may increase economic revenue.

Hydroprocessing

bioCRACK Bio-oil samples of dehydrated Bio-oil and a native Bio-oil were shipped to PNNL. The Bio-oils were hydroprocessed in a mini-hydrotreater (see Fig. 3). The hydrotreater is a single pass, co-current, continuous, down-flow reactor. The system can operate up to 12.4 MPa (1800 psig) with a maximum catalyst temperature of 400 °C. The setup consists of a gas feed and liquid feed system, the reactor and a gas-liquid separation system. The gas feed system consists of a manifold for feeding hydrogen through one mass flow controller and helium through a second mass flow controller. The liquid Bio-oil feedstock is delivered to the pressurized reactor system by two high pressure ISCO syringe pumps. The tubular

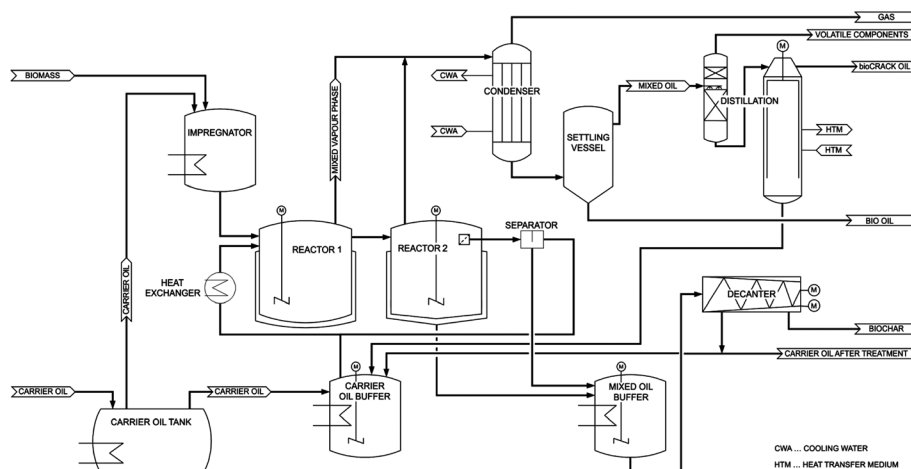


Fig. 2 Process scheme of the bioCRACK pilot plant Vienna/Schwechat.

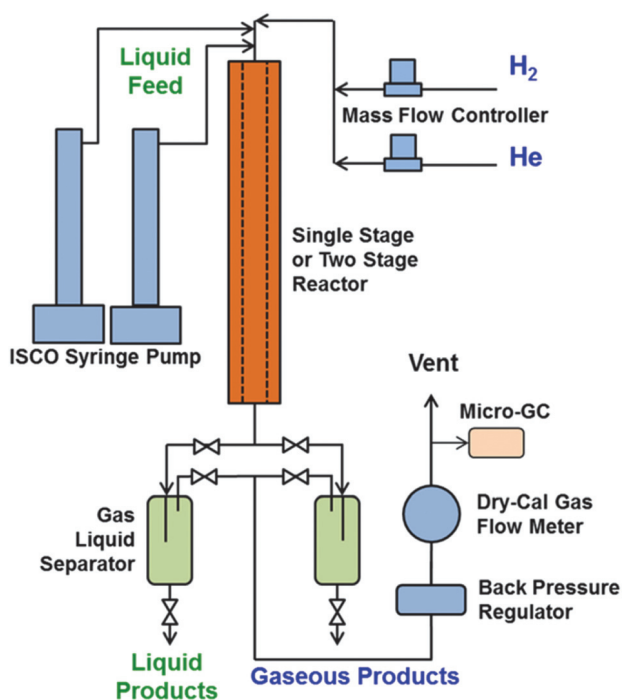


Fig. 3 Schematic of the mini-reactor hydrotreater system.

fixed-bed catalytic hydrotreater is made of 316 stainless steel, 13 mm (1/2") internal diameter by 64 cm long with 40 ml capacity for single stage heater or 24 + 24 ml capacity for two-stage hydrotreating. The reactor is heated by a single heating zone. The liquid feedstock and hydrogen gas entered the top of the catalyst bed and passed downward through the bed in a trickle flow. The temperature of the catalyst bed was monitored by thermocouples in a thermocouple well (5 mm (3/16") tubing). After exiting the catalytic reactor, the liquid products were separated from the gaseous products in one of two pressurized and cooled traps placed in parallel flow downstream of the reactor system. Periodically liquid samples were collected when switching collection vessels and venting/draining the trap. The recovered liquid products were phase-separated, weighed, and sampled for further analysis. The off-gas passed a back-pressure regulator and was then directed through a DryCal gas meter to monitor the gas flowrate. Periodically gas samples were analyzed by an online Inficon Micro-GC 3000 4-Channels micro gas chromatograph with molecular sieve, Plot U, Alumina, and Stabilwax columns. Prior to each hydro-treating test, the micro GC was calibrated using a calibration gas standard.

Campaigns were performed for each feed over the course of a five-day test, and the products and feed were collected to assess performance for each Bio-oil for comparison with the results obtained from processing of fast pyrolysis Bio-oil.

The hydroprocessing tests performed well with CoMo catalyst, sulfided *in situ*. The reactor tube containing the catalyst was heated to 150 °C in H₂ flow, followed by a temperature ramp from 150 °C to 350 °C over 3 h and H₂ flow and sulfiding agent (35% di-tertiarybutyl-disulfide (DTBDS) in decane). Then

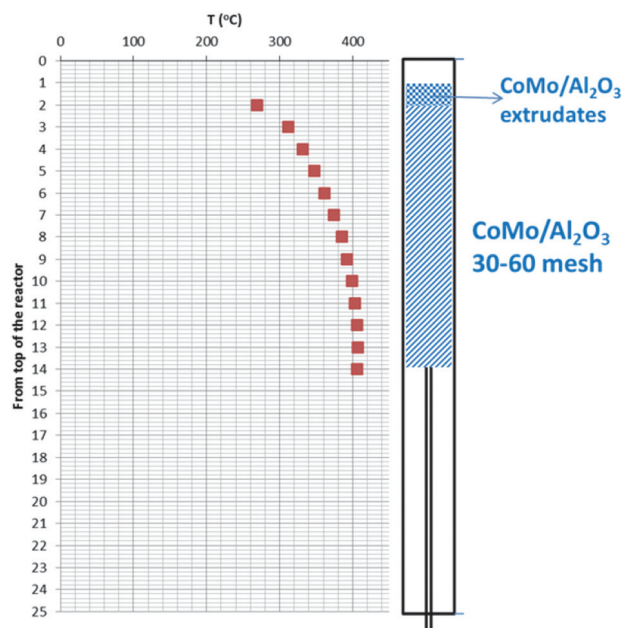


Fig. 4 Schematic of the catalyst bed in the mini-hydrotreater reactor.

temperature was raised to 400 °C and held constant for 5 h with H₂ and sulfiding agent flow.

For the hydroprocessing tests the flow ratio of H₂/liquid was 2508 L H₂ (L Bio-oil)⁻¹. The operating pressure was 12.1 MPa (1750 psi). The Bio-oil feedstock was spiked with DTBDS equaling 150 ppm of sulfur. Fig. 4 shows a schematic of the catalyst bed for the single stage testing mode. The temperatures were monitored at the center line of the catalyst bed by a thermocouple which was adjustable within a full length thermowell. The isothermal part of the catalyst bed is clearly shown and the length of the isothermal part of the catalyst was used to calculate the space velocity.

Analytical methods

The feedstock and Bio-oil products, as produced, were analyzed at BDI-BioEnergy International AG. All liquid and solid products and the feed were characterized by elemental analysis in CHN mode with a Vario macro CHNO-analyzer, from Elementar Analysensysteme. The heat carrier and entrained heat carrier composition and boiling characteristics were determined with a GC-SimDis MXT 2887, 10 m column from Restek and Agilent 7890A GC. Water was measured with GC-TCD. Determination of biomass volatiles was done according to Standard EN 15148. ¹⁴C analytics was done by Beta Analytic Limited. For CO and CO₂ detection an ABB gas analyser with an uras 26 infrared photometer was used and Oxygen was measured with a Magnos 206 detector.

The Bio-oils and hydrotreated products were characterized at PNNL for elemental analysis, including C, H, N, O, & S, Total Acid Number (TAN), water content, metals content, and

by GC-MS. Using a DB-5 column over a temperature program, separation of the Bio-oils was performed and mass spectrometric analysis undertaken with a Mass Selective Detector.

Results

Feedstock

Results from the feedstock analyses are shown in Table 1.

Results of liquid phase pyrolysis according to the bioCRACK process

The yield of the major products (oil, char, and gas) of the bioCRACK process is shown in Fig. 5. The figure shows the mass balance based on ^{14}C analysis of an experiment at 375 °C with a biomass feed of 65 kg h⁻¹. The amount of biomass fed, Bio-oil fractions, and char were determined gravimetrically.

During liquid phase pyrolysis in the bioCRACK process biochar (BCH) and gas/vapor is formed from biomass constituents. Table 2 shows the elemental composition of the product streams. Differently to flash pyrolysis three liquid product streams are formed in the bioCRACK process. The first fraction is a high boiling fraction of decomposed biomass, which is dissolved during liquefaction into the heat carrier. 15 (wt%) of the biogenous carbon feed is solved into this fraction and the concentration of biogenous carbon in this fraction is 2.0 (wt%). The second liquid fraction is the so called bioCRACK oil

Table 1 Composition of feedstock

| | Proximate analysis (wt%) | | | Ultimate analysis (wt%) | | | |
|----------------|--------------------------|--------------|------|-------------------------|------|------|------------|
| | Volatiles | Fixed carbon | Ash | C | H | N | O by diff. |
| Spruce pellets | 84.94 | 14.68 | 0.38 | 50.67 | 6.30 | 0.04 | 42.99 |

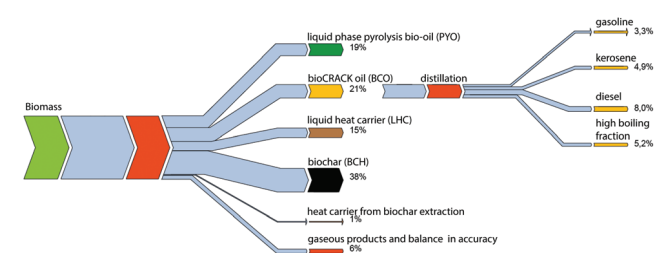


Fig. 5 Biogenous carbon mass balance of liquid phase pyrolysis as performed in the bioCRACK pilot plant at OMV Refinery Vienna.¹⁴

Table 2 Elemental composition of bioCRACK product streams

| Product stream | C (wt%) | H (wt%) | N (wt%) | Residual (wt%) |
|---------------------------|---------|---------|---------|----------------|
| Biochar (BCH) | 80.9% | 5.4% | <1 | 13.5% |
| BioCRACK oil (BCO) | 84.8% | 12.4% | <1 | 2.4% |
| Liquid heat carrier (LHC) | 86.5% | 12.1% | <1 | 0.9% |

Table 3 Major gas components (v/v% of gas)

| Sample | CO (v/v%) | CO ₂ (v/v%) | CO ₂ : CO |
|--------|-----------|------------------------|----------------------|
| | 43.8 | 44.5 | 1.01 |

(BCO). This is a non-polar phase of biomass decomposition products and the degraded heat carrier. During pyrolysis 21% of the biogenous carbon from biomass is directly dissolved into this hydrocarbon fraction and the concentration of biogenous carbon is 6.7 (wt%). The bioCRACK oil can be fractionated into a gasoline, kerosene, diesel and high boiling fraction by distillation or further processed to a Diesel like Fuel by catalytic co-hydrodeoxygenation with Bio-oil.¹⁵

This bioCRACK oil is evaporated together with the Bio-oil fraction, which is the third liquid fraction of the bioCRACK process. The dissolution of biogenous compounds into the heat carrier and the bioCRACK oil phase is the major reason for the low carbon content, the high acid content and the high water- and oxygen content of the polar aqueous bioCRACK Bio-oil.

The major gas components are given in Table 3.

Bio-oil dehydration

During short path distillation Bio-oil was split in two fractions, 74% of condensate and 22% bottom product, latter being used for hydrodeoxygenation. 4% of the feed were lost as light boiling fraction due to low pressure operation at 130 mbar. Table 4 shows the composition of the feed compared to the dehydration products (Bio-oil).

Bio-oil fraction analysis

The results of ultimate, proximate, and water by Karl-Fisher titration analysis are in Table 4. These analyses are of the bioCRACK Bio-oil fractions as recovered from the pilot plant. The organic O contents in the Bio-oils were calculated from the difference in total O (determined by difference) and O in water.

The Bio-oils were analyzed at PNNL. The results are shown in Table 5. The C, H, O composition is calculated from wet oil composition by subtracting the amount of oxygen and hydrogen of the measured moisture content. Detailed trace element analysis of the wet Bio-oils was performed by ICP. The results are shown in Table 6. The Bio-oils are essentially mineral free, but with a significant amount of sulfur. The TAN (total acid number) was also determined by PNNL. Viscosity and density were determined with a Stabinger viscosimeter according to ASTM D7042.

Semi-quantitative analysis of the two bioCRACK feedstocks was performed with gas chromatography-mass spectrometry (GC-MS). With the Agilent peak matching program tentative identifications were applied to the components and their relative quantities were determined based on total ion current. The results are presented in Table 7, showing the relative quantities of the identified components. The two bio-oil fractions show some distinct differences in composition. Overwhelmingly they contain typical fast pyrolysis Bio-oil components, a mixture of guaiacols and light oxygenates. The

Table 4 Bio-oil, ultimate and proximate composition (wet oil basis)

| Sample | C (wt%) | H (wt%) | N (wt%) | O (wt%) | Ash (wt%) | H ₂ O (wt%) | Density (g mL ⁻¹) | pH |
|--------------------|---------|---------|---------|---------|-----------|------------------------|-------------------------------|-----|
| Dehydrated Bio-oil | 50.5 | 7.1 | 0.4 | 41.5 | 0.5 | 9.9 | 1.22 | 2.7 |
| Bio-oil | 23.2 | 9.4 | 0.3 | 67.1 | NA | 56.3 | 1.07 | 2.6 |
| Bio-oil condensate | 14.4 | 9.97 | 0.3 | 75.3 | NA | 68.9 | 1.04 | 3.0 |

Table 5 Analysis of bioCRACK Bio-oils

| Sample name | C (wt% dry) | H (wt% dry) | H/C ratio dry basis | O (wt% dry) | Moisture (wt%) | N (wt% wet) | S (wt% wet) | Density (g mL ⁻¹ @40 °C) | TAN (mg KOH g ⁻¹) | Viscosity (mm ² s ⁻¹ @40 °C) |
|--------------------|-------------|-------------|---------------------|-------------|----------------|-------------|-------------|-------------------------------------|-------------------------------|--|
| Dehydrated Bio-oil | 59.1 | 6.7 | 1.36 | 33.4 | 10.24 | 0.14 | 0.50 | 1.226 | 135 | 105 |
| Bio-oil | 51.1 | 6.2 | 1.45 | 42.6 | 57.43 | <0.05 | 0.03 | 1.097 | 101 | 2.3 |

Table 6 Trace analysis of bioCRACK Bio-oils

| | S (ppm) | Al (ppm) | Si (ppm) | K (ppm) | Fe (ppm) | Ca (ppm) | Mg (ppm) | P (ppm) |
|--------------------|---------|----------|----------|---------|----------|----------|----------|---------|
| Dehydrated bio-oil | 3372 | <15 | <15 | 24 | 39 | 17 | <15 | <15 |
| Bio-oil | 557 | <15 | <15 | <15 | <15 | <15 | <15 | <15 |

Table 7 Components in bioCRACK Bio-oils based on GC-MS analysis

| Component | Dehydrated Bio-oil | | Bio-oil | |
|--|--------------------|-----------------|----------------|----------|
| | Retention time | Quantity | Retention time | Quantity |
| Methyl acetate | 1.756 | 1.3 | 1.737 | 3 |
| Formic acid | | ND ^a | 1.96 | 0.5 |
| Acetic acid | 2.37–2.49 | 6.8 | 2.7 | 25.9 |
| Acetol (hydroxyacetone) | 2.79–3.01 | 3.8 | 2.82 | 21.1 |
| Propionic acid | | ND | 4.20–4.34 | 1.5 |
| 1-Hydroxy-2-butanone | | ND | 5.10–5.16 | 0.3 |
| Butanedial | | ND | 5.74–5.90 | 0.4 |
| Methylene cyclopropane | | ND | 7.92–7.95 | 0.2 |
| Cyclopentenones | | ND | 8.00–8.10 | 0.2 |
| Methyl cyclopentenone | | ND | 10.86–10.90 | 0.4 |
| γ-Butyrolactone | 11.64–11.77 | 0.4 | 11.34–11.44 | 1.3 |
| Methyl furfural | | ND | 12.51 | 0.5 |
| 3-Methyl-2,5-dihydrofuran | | ND | 13.04 | 0.4 |
| Corylone (hydroxymethylcyclopentenone) | 13.79–13.91 | 6.1 | 13.71–14.02 | 7.5 |
| Methyl-2,3-dihydrofuran | 13.92–13.96 | 5 | | ND |
| Trans-cyclopentane-1,2-diol | | ND | 14.05 | 1 |
| Guaiacol | 14.63–14.65 | 1.2 | 14.56 | 2.4 |
| Methyl guaiacol | 16.02–16.08 | 3.8 | 15.99 | 3.8 |
| Catechol | 16.94 | 1.4 | 16.94 | 0.8 |
| Ethyl guaiacol | 17.06 | 3.4 | 17.06 | 2.2 |
| Hydroxy dimethyl cyclopentenone | 17.21 | 0.3 | 17.26 | 1.1 |
| Hydroquinone | 17.76 | 4.1 | 17.81–17.92 | 2.8 |
| Propyl guaiacol | 18.05 | 2.9 | 18.05 | 1.6 |
| Guaiacol formaldehyde (vanillin) | 18.68 | 6.6 | 18.73 | 2.4 |
| Methyl benzaldehyde | 19.03 | 3.6 | | ND |
| Guaiacol ethanone | 19.55 | 4.3 | 19.57 | 1.6 |
| Guaiacol propanone | 19.92 | 8.2 | 19.93 | 3.3 |
| Levoglucosan | 20.15–20.38 | 35.3 | 20.20–20.69 | 13.7 |
| Ethyl homovanillate | 26.54 | 1.4 | 26.58 | 0.3 |

^a ND = not detected.

guaiacol (2-methoxyphenol) compounds have the typical alkyl and carbonyl substituents on the 4 position. There is a significant amount of levoglucosan in both Bio-oil fractions, but significantly lower concentration in the whole Bio-oil. The Bio-oil product has a large number of light oxygenates, which were

not found in the Dehydrated Bio-oil. These compounds, *e.g.* acetic acid and acetol (hydroxyacetone), were separated during distillation. On the other hand the Dehydrated Bio-oil has a larger concentration of all the phenolic compounds, with the exception of guaiacol and methyl guaiacol.

Table 8 Products from hydrotreating bioCRACK Dehydrated Bio-oil (elemental contents are normalized to 100%)

| C content dry basis | H content dry basis | O content dry basis | H/C ratio dry basis | Density, g ml ⁻¹ | Moisture content | Total acid number | Mass balance | Carbon balance |
|---------------------|---------------------|---------------------|---------------------|-----------------------------|------------------|-------------------|--------------|----------------|
| 85.04 | 13.86 | 1.10 | 1.94 | 0.755 | 0.24 | <0.01 | 93.6 | 90.6 |
| 85.55 | 13.24 | 1.21 | 1.84 | 0.784 | 0.26 | <0.01 | 99.2 | 98.5 |
| 85.41 | 13.51 | 1.08 | 1.88 | 0.789 | 0.30 | <0.01 | 92.4 | 88.3 |

Hydroprocessing results

For both of the reported tests the products and data were collected over the entire period with individual products and data sets collected in operating windows from 6 to 12 h long. The hydrogen consumption has been calculated and the yield of gas and oil products determined.

The Dehydrated Bio-oil feedstock was pumped directly into the mini-hydrotreater without pre-processing. The feedstock was assumed to have <0.1% filterable solids content, based on BDI data provided. A fixed bed of pre-sulfided CoMo on alumina catalyst (3.5% CoO and 14% MoO₃) from AlfaAesar (#40435) ground to a 30–60 mesh particle size was used at standard conditions of nominally 400 °C, 12.1 mPa, and a liquid hourly space velocity of 0.2. Three oil samples selected to represent the product over the 54 h test were analyzed as reported in Table 8. Elemental contents are normalized to 100%; S and N were <0.02 and <0.05, respectively.

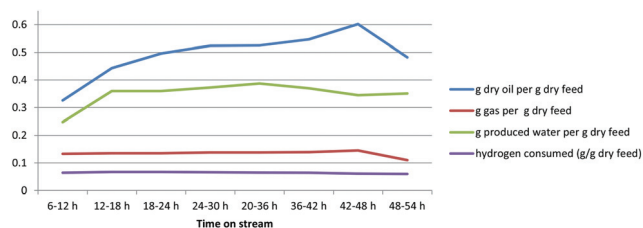
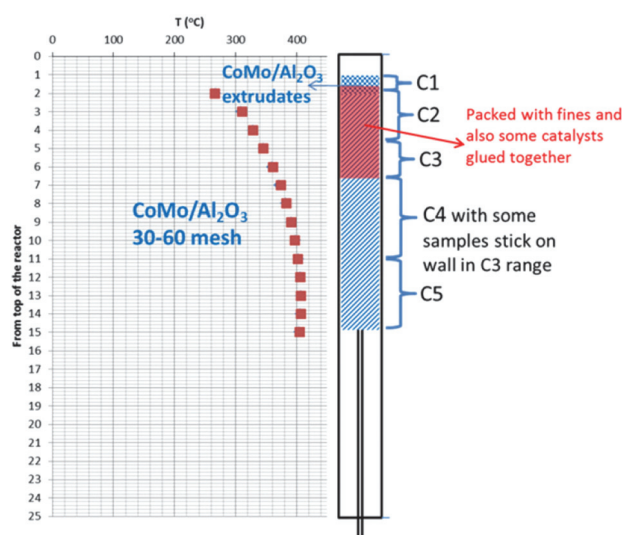
Trace element analysis of the feedstock showed only small amounts of a few expected biomass components, 17 ppm Ca and 24 ppm K with 38 ppm Fe and 3320 ppm S. The iron is likely a corrosion product. The high sulfur level is unexpected. The S number for the feedstock was found by inductively coupled plasma-optical emission spectroscopy (ICP-OES) measurement, but it is similar to that by the thermal method (0.50 wt%). Since a sulfided catalyst was used for the processing there was no conflict. In fact, we added di-tertiarybutyl-disulfide to the feedstock to maintain at least 150 ppm of sulfur.

The operating results as shown in Fig. 6 were fairly consistent throughout the test period. The liquid oil yield from the bioCRACK Dehydrated Bio-oil was 0.5 to 0.6 g g⁻¹, with lower but still significant gas and water production. The hydrogen consumption was a bit higher than typically seen with fast pyrolysis Bio-oil.

Gas products were analyzed through the test using gas chromatography. The gas product was composed of carbon oxides (21–26% CO₂ and 4–5% CO) and alkane hydrocarbon gases (22–25% CH₄, 22–19% C₂, 14–12% C₃, 6–11% C₄, 5% C₅) diluted with the excess hydrogen (93–94 vol% of off gas).

The 316 SS tubular reactor is depicted in Fig. 7 and the area of fouled catalyst after the test is shaded in red.

ICP analysis of the spent catalyst bed showed some evidence of deposits in the bed. As might be expected the feed contaminants, iron, calcium, and potassium, were found at levels higher than in the fresh catalyst with exceptionally high levels at the point in the catalyst bed where the reactants exceeded 300 °C. Zinc and manganese (below detection limit

**Fig. 6** Process results from hydrotreating bioCRACK Dehydrated Bio-oil.**Fig. 7** Schematic of catalytic reactor bed following test.

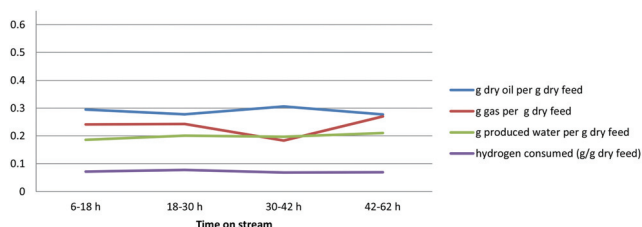
in the feed) also followed this trend, as did chromium and nickel, which are likely reactor wall corrosion products.

A similar test was performed with the bioCRACK Bio-oil product. The Bio-oil feedstock was pumped directly into the mini-hydrotreater without pre-processing. Four oil samples selected to represent the product over the 62 h test were analyzed as reported in Table 9. Elemental contents are normalized to 100%; S and N were <0.05 and <0.05, respectively.

The operating results as shown in Fig. 8 were fairly consistent throughout the four test periods. The liquid oil yield from the bioCRACK Bio-oil was only 0.3 g per g of dry feed with significant gas and water production as well. The yield of dry oil product on a carbon basis is similar to the Dehydrated Bio-oil, at about 50%. The hydrogen consumption was also high at about 7 wt% on a dry feed basis.

Table 9 Products from hydrotreating bioCRACK Bio-oil (elemental contents are normalized to 100%)

| C content dry basis | H content dry basis | O content dry basis | H/C ratio dry basis | Density, g ml ⁻¹ | Moisture content | Total acid number | Mass balance | Carbon balance |
|---------------------|---------------------|---------------------|---------------------|-----------------------------|------------------|-------------------|--------------|----------------|
| 84.30 | 14.96 | 0.74 | 2.11 | 0.712 | 0.36 | <0.01 | 85.6 | 84.9 |
| 83.94 | 15.22 | 0.84 | 2.15 | 0.722 | 0.34 | <0.01 | 85.4 | 81.7 |
| 84.27 | 14.77 | 0.96 | 2.08 | 0.730 | 0.30 | <0.01 | 84.2 | 77.8 |
| 84.41 | 14.91 | 0.68 | 2.10 | 0.726 | 0.44 | <0.01 | 86.5 | 85.2 |

**Fig. 8** Process results from hydrotreating bioCRACK Bio-oil.

Gas products were analyzed through the test using gas chromatography. The gas product was composed of carbon oxides (6–9% CO₂ and 0% CO) and alkane hydrocarbon gases (21–17% CH₄, 30–35% C₂, 25–21% C₃, 18–11% C₄, 0–5% C₅) diluted with the excess hydrogen (95–97 vol% of off gas).

No trace elements were detected in the Bio-oil by ICP (<15 ppm) except sulfur. There were elements found deposited onto the catalyst after the test including Si, Ca, Mg, and Na, which were likely derived from the feedstock. In addition, there were elevated levels of Fe and Cr, which could be attributed to corrosion.

Discussion

The bioCRACK Bio-oil fractions performed well for up to 62 h when using a representative hydrotreating catalyst in a single temperature stage configuration. The light oil phase product was sufficiently hydrotreated so that nitrogen and sulfur were at or below the level of detection, while the residual oxygen content was low, <1%. The density of the products were relatively low compared to literature values for hydrotreated Bio-oil, 0.71 g mL⁻¹ up to 0.79 g mL⁻¹. The lighter products were produced from the Bio-oil fraction which was found to contain lower molecular weight and more saturated components as fed to the hydrotreater. It is no surprise that the product from the higher molecular weight and more aromatic Dehydrated Bio-oil is higher in density. The Dehydrated Bio-oil appears to contain less reactive functional groups, which are less easily deoxygenated as shown by the difference in oxygen analysis, a reduction of 98.1% for the Bio-oil and only 96.6% reduction in the Dehydrated Bio-oil. Since both Bio-oil feedstocks were processed at the same space velocity, the higher oil product yield and lower gas product yield for the dehydrated product is significant. The space velocity of 0.2 used in these tests is also higher than other reports for hydrotreating Bio-oil to similarly high quality hydrocarbon products.

The consistency of the operating results and the products over the time of these experiments suggests little loss of catalyst activity through the test. The apparent drop in oil and gas production in the last data window, when feeding the dehydrated Bio-oil, may be better explained as experimental variability in correction of the higher production in the previous data window. The consistency contrasts with most reports in the literature for hydrotreating Bio-oil.¹⁶ Similar consistency of operation has only been achieved by a pretreatment of low severity hydroprocessing prior to the actual hydrotreating.¹⁷ In addition, a two-temperature stage hydrotreating was used to avoid fouling of the hydrotreating catalyst bed¹⁸ or the use of precious metal catalysts.¹⁹

Conclusions

With this mini-hydrotreater system we can make a preliminary assessment of the hydrotreating results with the bioCRACK feedstocks. We conclude that these feedstocks can be readily hydrotreated based on high yield of deoxygenated liquid hydrocarbon product. The results contrast with those for fast pyrolysis Bio-oil in that the catalyst bed did not foul in these extended runs and this even when using only a single temperature bed with conventional hydrotreating catalyst and without a precious metal catalyst hydroprocessing pretreatment. The tests do not represent optimized conditions, but only a first proof of principle. The oil products have been highly saturated and the hydrogen consumption could probably be reduced by changes in operating parameters such as lower operating pressure and faster throughput to reduce the residence time in the catalyst bed.

Acknowledgements

This research work was supported by BDI-BioEnergy International AG under Work-For-Others contract. The preparation of the publication was performed with support from the U.S. Department of Energy as part of the Bio-oil Stabilization and Commoditization FOA #0686 under Contract No. DE-AC05-76RL01830 at the Pacific Northwest National Laboratory. The authors gratefully acknowledge the support of the Bioenergy Technologies Office and program manager Prasad Gupta. Suh-Jane Lee and Asanga Padmaperuma are acknowledged for their participation in the operations of the minihydrotreater.

Notes and references

- 1 A. V. Bridgwater, *Biomass Bioenergy*, 2012, **38**, 68–94.
- 2 N. Schwaiger, R. Feiner, K. Zahel, A. Pieber, V. Witek, P. Pucher, E. Ahn, P. Wilhelm, B. Chernev, H. Schröttner and M. Siebenhofer, *BioEnergy Res.*, 2011, **4**, 294–302.
- 3 D. Mohan, C. U. Pittman and P. H. Steele, *Energy Fuels*, 2006, **20**, 848–889.
- 4 N. Schwaiger, V. Witek, R. Feiner, H. Pucher, K. Zahel, a. Pieber, P. Pucher, E. Ahn, B. Chernev, H. Schroettner, P. Wilhelm and M. Siebenhofer, *Bioresour. Technol.*, 2012, **124**, 90–94.
- 5 D. C. Elliott, *Energy Fuels*, 2007, **21**, 1792–1815.
- 6 E. Baker and D. Elliott, *US Pat.* 4,795,841, 1989.
- 7 H. Pucher, N. Schwaiger, R. Feiner, P. Pucher, L. Ellmaier and M. Siebenhofer, *Int. J. Energy Res.*, 2014, **38**, 1964–1974.
- 8 R. Feiner, N. Schwaiger and H. Pucher, *RSC Adv.*, 2014, **4**, 34955.
- 9 R. Feiner, N. Schwaiger, H. Pucher, L. Ellmaier, P. Pucher and M. Siebenhofer, *RSC Adv.*, 2013, **43**, 1–6.
- 10 R. Feiner, N. Schwaiger, H. Pucher, L. Ellmaier, A. Reiter, M. Derntl, T. Glatz, P. Pucher and M. Siebenhofer, *Bio-Energy Res.*, 2014, **7**, 1343–1350.
- 11 S. Wang, Y. Gu, Q. Liu, Y. Yao, Z. Guo, Z. Luo and K. Cen, *Fuel Process. Technol.*, 2009, **90**, 738–745.
- 12 Z. Guo, S. Wang, Y. Gu, G. Xu, X. Li and Z. Luo, *Sep. Purif. Technol.*, 2010, **76**, 52–57.
- 13 S. Wang, Q. Cai, X. Wang, L. Zhang, Y. Wang and Z. Luo, *Energy Fuels*, 2014, **28**, 115–122.
- 14 J. Ritzberger, P. Pucher, N. Schwaiger and M. Siebenhofer, *Chem. Eng. Trans.*, 2014, **39**, 1189–1194.
- 15 H. Pucher, N. Schwaiger, R. Feiner, L. Ellmaier, P. Pucher, B. Chernev and M. Siebenhofer, *Green Chem.*, 2015, **17**, 1291–1298.
- 16 E. Furimsky, *Catal. Today*, 2013, **217**, 13–56.
- 17 A. H. Zacher, M. V. Olarte, D. M. Santosa, D. C. Elliott and S. B. Jones, *Green Chem.*, 2014, **16**, 491.
- 18 D. C. Elliott, T. R. Hart, G. G. Neuenschwander, L. J. Rotness, M. V. Olarte, A. H. Zacher and Y. Solantausta, *Energy Fuels*, 2012, **26**, 3891–3896.
- 19 J. Wildschut, F. H. Mahfud, R. H. Venderbosch and H. J. Heeres, *Ind. Eng. Chem. Res.*, 2009, **48**, 10324–10334.

Chapter 13

Biomass Pyrolysis Refinery –
Herstellung von nachhaltigen
Treibstoffen

Biomass Pyrolysis Refinery –
Production of Biofuels from
Lignocellulose

BiomassPyrolysisRefinery – Herstellung von nachhaltigen Treibstoffen

Nikolaus Schwaiger^{1,*}, Roland Feiner¹, Hannes Pucher¹, Lisa Ellmaier², Jürgen Ritzberger², Klara Treusch², Peter Pucher² und Matthäus Siebenhofer¹

DOI: 10.1002/cite.201400099

In der BiomassPyrolysisRefinery wird Lignocellulose in zwei Stufen verflüssigt. In der ersten Stufe wird Lignocellulose durch Flüssigphasenpyrolyse (FPP) in flüssige und feste Zwischenprodukte umgewandelt. Erprobt wird die FPP im Pilotmaßstab in der OMV Raffinerie Schwechat. Dabei entstehen aus der Biomasse Flüssigphasenpyrolyseöl, Pyrolysekohle, Gase und 10–20 % flüssige Pyrolyseprodukte, die direkt in der Raffinerie zu Treibstoffen weiterverwertet werden. In der zweiten Stufe wird Pyrolysekohle in Tetralin als Wasserstoffdonor verflüssigt und das Flüssigphasenpyrolyseöl durch Hydrodeoxygenierung unter Wasserstoffdruck in flüssigen Treibstoff umgewandelt.

Schlagwörter: BiomassPyrolysisRefinery, Flüssigphasenpyrolyse, Hydrodeoxygenierung, Pyrolysekohleverflüssigung

Eingegangen: 08. Juli 2014; *revidiert:* 02. März 2015; *akzeptiert:* 03. März 2015

BiomassPyrolysisRefinery – Production of Biofuels from Lignocellulose

The BiomassPyrolysisRefinery concept consists of two main process steps. In the first step lignocellulosic biomass is converted into pyrolysis oil and pyrolysis char through liquid phase pyrolysis. In the second step these intermediate products are upgraded. Liquid phase pyrolysis oil was upgraded by two-step hydrodeoxygenation. The first step was mild hydrodeoxygenation, the second step was a co-refining with a fossil oil refinery intermediate. Direct liquefaction of pyrolysis char was carried out with the hydrogen donor solvent Tetralin.

Keywords: Biochar liquefaction, BiomassPyrolysisRefinery, Hydrodeoxygenation, Liquid phase pyrolysis

1 Einleitung

Trotz erhöhtem Angebot und fallenden Ölpreisen im Herbst 2014 sind die Folgen des auf CO₂ basierenden Klimawandels weltweit erkennbar [1]. Dabei macht der Transportsektor rund ein Fünftel des Weltenergiebedarfs aus. Die steigende Weltbevölkerung und der damit einhergehende Bedarf an Mobilität führen zwangsläufig zu einer immer größer werdenden Nachfrage an Flüssigtreibstoffen [2]. Da der Hauptteil der Flüssigtreibstoffproduktion auf Erdöl beruht, ist die Entwicklung eines gleichwertigen Biotreibstoffs eine der größten Herausforderungen [3]. Dieser sollte kom-

patibel mit der bestehenden Distributionsinfrastruktur sein und nachhaltig die CO₂-Emissionen senken [4]. Des Weiteren schreibt die Richtlinie 2009/28/EG [5] vor, dass bis zum Jahr 2020 10 % des Endenergieverbrauchs im Verkehrssektor aus erneuerbaren Energien gedeckt werden müssen. Da die Verantwortlichkeit und das Bewusstsein für die Erhaltung der Umwelt sowie die Retardation des Klimawandels durch Treibhausgasemissionen immer mehr in den Vordergrund treten, ist es unabdingbar, fossile Primärenergieträger durch nachhaltige, CO₂-neutrale Biotreibstoffe zu substituieren. Strategien zur Substitution von fossilen Primärenergieträgern sind die Erzeugung von Biokraftstoffen erster- und zweiter Generation; Unter Biokraftstoffen erster Generation versteht man Treibstoffe, die durch Umsetzung von ölhaltigen Feldfrüchten gewonnen werden oder aus glucosehaltigem Getreide fermentiert werden. Die Biokraftstoffe der zweiten Generation zielen hingegen auf eine ganzheitliche Pflanzennutzung ab. Zu den Biokraftstoffen der zweiten Generation gehören unter anderem die indirekte sowie die direkte Verflüssigung von lignocelluloser Biomasse [6].

¹Dr. Nikolaus Schwaiger (nikolaus.schwaiger@tugraz.at), Dr. Roland Feiner, Dr. Hannes Pucher, Prof. Matthäus Siebenhofer, Technische Universität Graz, Central Lab Biobased Products/Institut für Chemische Verfahrenstechnik und Umwelttechnik, Inffelgasse 25C, 8010 Graz, Österreich; ²Lisa Ellmaier, Jürgen Ritzberger, Klara Treusch, Dr. Peter Pucher, BDI-BioEnergy – International AG, Parking 18, 8074 Grambach, Österreich.

in der OMV Raffinerie Wien/Schwechat durchgeführt, die in Abb. 2 gezeigt ist. Die Hydrodeoxygenierung des Flüssigphasenpyrolyseöls und die Verflüssigung des Biochar werden im Labormaßstab in einem 450-mL-Hochdruckautoklaven der Firma Büchi in den Laboratorien des Instituts für Chemische Verfahrenstechnik und Umwelttechnik der TU Graz erforscht.



Abbildung 2. bioCRACK-Pilotanlage der Firma BDI BioEnergy-International AG in der OMV Raffinerie Wien/Schwechat [34].

3.1 Flüssigphasenpyrolyse

Im Unterschied zur Fast- oder Flash-Pyrolyse wird beim BioCrack-Verfahren flüssiges Trägeröl anstatt z. B. Sand als Wärmeträger eingesetzt [19, 20, 25, 26]. Die Biomasse wird in Inertatmosphäre in einem heißen Trägeröl pyrolysiert, wobei die Pyrolysetemperaturen vom Siedepunkt und der Zersetzungstemperatur des Trägermediums abhängen.

Ein Vorteil der Flüssigphasenpyrolyse ist, dass Partikel (Kohle, Asche) im heißen Trägeröl gebunden bleiben. Darüber hinaus ist der Wärmetransport im flüssigen Medium

der Wirbelschicht überlegen. Die Nachteile sind, dass die Partikel nach der Pyrolyse vom Trägeröl getrennt werden müssen und die Pyrolyse aufgrund der Zersetzung und dem Siedeverhalten des Trägeröls temperaturbegrenzt ist. Die Besonderheit der FPP hingegen ist, dass, abhängig vom Trägeröl, ein bedeutender Teil der Biomasse bereits während der Pyrolyse in eine Rohstoff-Fraktion umgesetzt wird.

Abb. 3 zeigt die Bilanz des biogenen Kohlenstoffs bei der Flüssigphasenpyrolyse von Fichtenholzpellets in der bioCRACK-Pilotanlage. Alle Daten wurden basierend auf ¹⁴C-Messungen und der Kohlenstoffbilanz errechnet. Bei diesem Experiment liegt der Bilanzzeitraum bei 38 h. Es wurden 60 kg h⁻¹ Biomasse bei einer Trägeröltemperatur von 375 °C umgesetzt. Als Trägeröl wurde Vakuumgasöl (VGO), ein Intermediat der Erdölraffination, das für die weitere Verwertung zu Diesel teuer in einem Hydrocracker weiterverarbeitet werden muss, eingesetzt. Die elementare Zusammensetzung aller Stoffströme ist in Tab. 1 angegeben.

Die Bilanzdifferenz beschreibt den biogenen Anteil des Pyrolysegases und deckt sich mit den ermittelten Werten der Laborversuche [19]. Während der Flüssigphasenpyrolyse werden 38 % des biogenen Kohlenstoffs zu einem fes-

Tabelle 1. Elementare Zusammensetzung der Produkte und der Edukte der Flüssigphasenpyrolyse von Fichtenholzpellets bei 375 °C in der bioCRACK-Anlage als Durchschnittswert über den Bilanzzeitraum.

| Material | C [%] | H [%] | N [%] | Rest [%] |
|-------------------------------|-------|-------|-------|----------|
| Biomasse (BM) | 49,6 | 6,3 | < 1 | 44,0 |
| Flüssigphasenpyrolyseöl (PYO) | 25,6 | 9,4 | < 1 | 64,6 |
| Biochar (BCH) | 80,9 | 5,4 | < 1 | 13,5 |
| BioCRACK-Öl (BCO) | 84,8 | 12,4 | < 1 | 2,4 |
| Trägeröl (TOL) | 86,5 | 12,1 | < 1 | 0,9 |

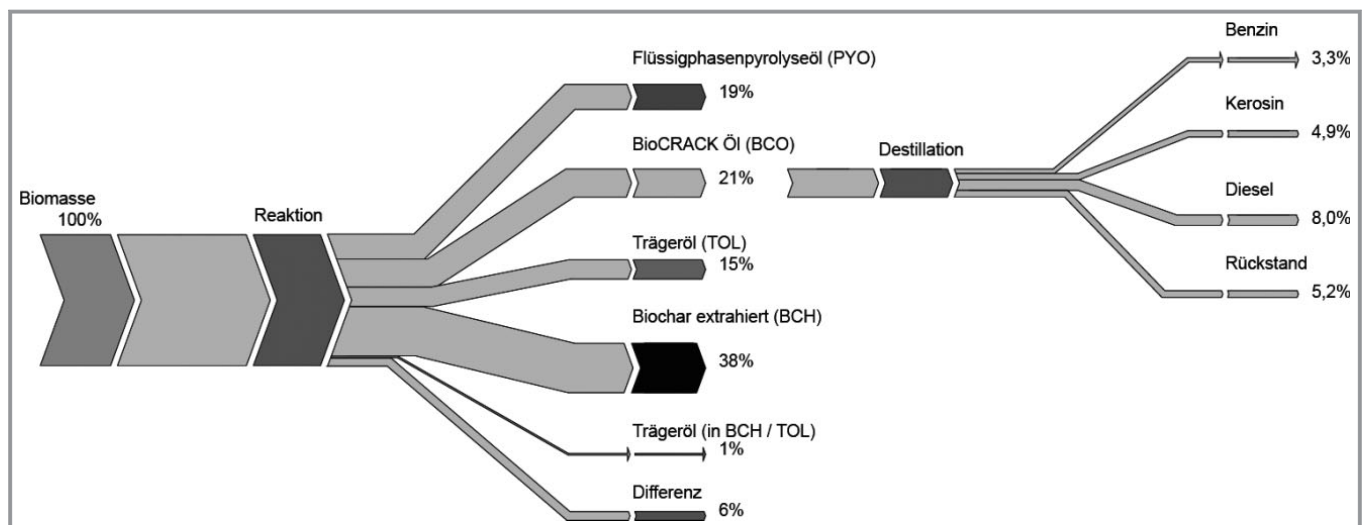


Abbildung 3. Bilanz des biogenen Kohlenstoffs bei der Flüssigphasenpyrolyse [34].

ten Produkt, dem sogenannten Biochar (BCH) umgesetzt. Insgesamt werden 55 % des biogenen Kohlenstoffs verflüssigt. Diese flüssigen Produkte teilen sich in drei Fraktionen auf. Einen Teil bildet das Flüssigphasenpyrolyseöl (PYO). Das sind die sauerstoffreichen wasserlöslichen organischen Verbindungen und das gebildete Reaktionswasser. Die Eigenschaften von PYO werden in Tabs. 2 und 3 gezeigt. Die organischen Komponenten haben eine breite Molekülgrößenverteilung von Methanol bis zu Verbindungen mit einem Molgewicht von mehr als 3000 g mol^{-1} [19]. Ein weiterer Teil der Biomasse wird im Trägeröl (TOL) gelöst. Diese 15 % der Biomasse werden ausschließlich auf Basis der ^{14}C -Analyse und der Kohlenstoffbilanz nachgewiesen. Im Trägeröl wird eine Konzentration von 2 % biogenem Kohlenstoff erreicht. Die dritte flüssige Fraktion, das sogenannte bioCRACK-Öl (BCO) sind die kohlenwasserstofflöslichen Degradationsprodukte der Biomasse, die mit den Degradationsprodukten des Trägeröls aus dem Reaktor ausgetragen werden. Der ^{14}C -Gehalt von BCO und die Zusammensetzung der Komponenten für die spätere Hydrodeoxygenierung werden in Tab. 2 gezeigt.

Tabelle 2. Eigenschaften des eingesetzten Flüssigphasenpyrolyseöls (PYO), BCO und des gebildeten HDO-Treibstoffs.

| | PYO | BCO | HDO-Treibstoff |
|--|------|------|----------------|
| Wassergehalt [%] | 49,6 | 0,1 | 0,2 |
| Heizwert [MJ kg^{-1}] | 9,2 | 40,1 | 41,2 |
| Säurezahl [$\text{mg}_{\text{KOH}} \text{g}^{-1} \text{ Probe}$] | 82,2 | – | – |
| Mittleres Molekulargewicht [g mol^{-1}] | 420 | 370 | 360 |
| Dichte [kg m^{-3}] | 1,09 | 0,88 | 0,87 |
| Viskosität [mPa s] | 3,9 | 8,0 | 4,5 |
| ^{14}C -Gehalt [Gew.-%] | 100 | 9,8 | 28 |

Durch destillative Trennung kann das bioCRACK-Öl (BCO) in Treibstofffraktionen aufgetrennt werden. Die Zuordnung zu diesen drei Treibstoffklassen basiert ausschließlich auf deren Siedebereichen, der Sauerstoffgehalt jeder Fraktion ist für die entsprechende Norm noch zu hoch und die Fraktionen müssen noch hydriert werden.

Die Pyrolysekohle wird nach der Reaktion dekantiert und für die Verflüssigung im Labormaßstab in Hexan vom Trägeröl gereinigt. Die flüssigen Produkte (PYO, BCO) werden über einen Separator getrennt und dann im Labormaßstab hydrodeoxygeniert.

Tabelle 3. Elementare Zusammensetzung des eingesetzten Flüssigphasenpyrolyseöls (PYO), BCO und des gebildeten HDO-Treibstoffs.

| | PYO | BCO | HDO-Treibstoff |
|-------------------|------|------|----------------|
| C-Gehalt [Gew.-%] | 25,6 | 83,6 | 85,5 |
| H-Gehalt [Gew.-%] | 9,2 | 11,8 | 12,1 |
| O-Gehalt [Gew.-%] | 64,9 | 4,2 | 1,9 |
| N-Gehalt [Gew.-%] | >1 | >1 | >1 |

3.2 Verflüssigung von Pyrolysekohle

38 % der Biomasse werden zu Biochar pyrolysiert, dessen Zusammensetzung in Tab. 1 gezeigt wird. Angelehnt an die Verflüssigung von fossiler Kohle [27], wird diese in der Sumpfpphase durchgeführt. Vorversuche zeigten, dass für eine Verflüssigung von Pyrolysekohle ein flüssiges Trägermedium unabdingbar ist. Die Verflüssigung selbst läuft bei 425°C und bis zu 200 bar Wasserstoffdruck ab. Durch heterogene Katalyse in der Flüssigphase ist es kaum möglich reaktiven Wasserstoff an den Ort der Kohle-Depolymerisation bzw. des Bindungsbruchs zu bringen. Ohne Wasserstoffdonor wird hauptsächlich Koks und Teer gebildet. Abb. 4 zeigt den Weg der Kohle-Depolymerisation über den Übergangszustand der Bruchfragmente zur Repolymerisation und der damit einhergehenden Feststoff- und Teerbildung.

Tetralin (1,2,3,4-Tetrahydronaphthalin) hat die Aufgabe, den reaktiven Wasserstoff am Ort der Depolymerisation der Kohlefragmente zum Zeitpunkt des Bindungsbruchs freizugeben. Das soll verhindern, dass es wieder zu einer Repolymerisation und somit zu einer ungewollten Teer- und Koksbildung kommt. Abb. 5 zeigt das Schema der Kohleverflüssigung mit Tetralin. Dabei werden ab 350°C Fragmentradikale gebildet, die dann von Tetralin unter der Bildung von naszierendem Wasserstoff stabilisiert werden. Dabei

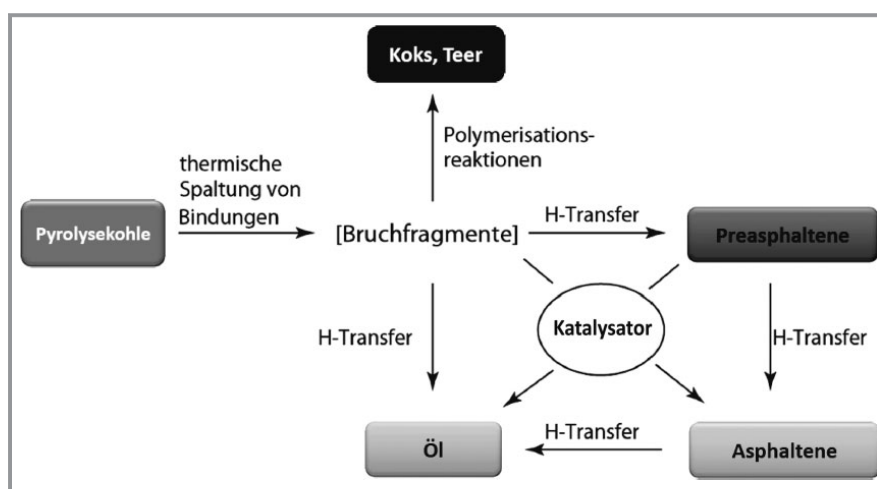


Abbildung 4. Schema der Depolymerisation von Kohle mit und ohne Stabilisierung durch reaktiven Wasserstoff [35].

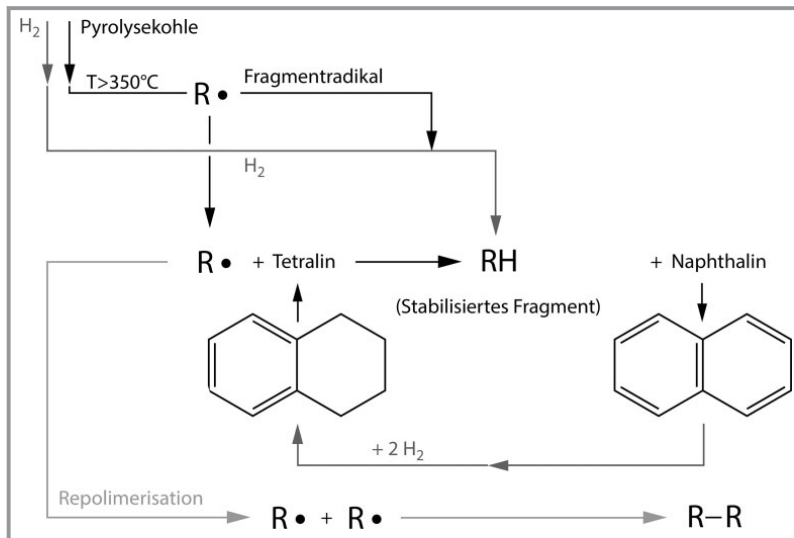


Abbildung 5. Der Shuttle-Effekt des Molekülpaars Tetralin und Naphthalin bei der Verflüssigung von Pyrolysekohle [36].

wird aus Tetralin Naphthalin gebildet und das stabilisierte Fragment geht in Lösung.

Wie in Abb. 4 gezeigt wird, muss aus der Pyrolysekohle nicht direkt öliges Produkt gebildet werden. Es können dabei auch bei Raumtemperatur nicht-kondensierbare Gase, Asphaltene und Präasphaltene entstehen. Aus der Pyrolysekohle gebildetes Öl, Asphaltene und Präasphaltene werden wie folgt definiert: Alle Produkte der Pyrolysekohleverflüssigung, die Hexan löslich sind, werden dem Öl zugeschrieben. Alle Hexan-unlöslichen aber Toluol-löslichen Produkte werden Asphaltene genannt. Alle Toluol-unlöslichen aber in Tetrahydrofuran (THF) löslichen Produkte werden Präasphaltene genannt. Alle weiteren Reaktionsprodukte, die

nicht THF-löslich sind, werden als fester Rückstand bezeichnet.

Die Verflüssigung von Pyrolysekohle in Tetralin kann man in zwei Reaktionsphasen teilen. Einerseits in den Zeitraum bis zum Erreichen der Reaktionstemperatur (die Aufheizphase) und andererseits in die isotherme Phase. Abb. 6 zeigt die Verflüssigung von Pyrolysekohle bei 425 °C und 180 bar Wasserstoffdruck. Man erkennt dabei, dass über 70 % der Kohle nach einer Reaktionszeit von 30 min zu einem Öl abgebaut wurden. Ferner ist ersichtlich, dass zu Beginn mehrheitlich Präasphaltene gebildet werden. Gegen Ende der Reaktionszeit sind die Asphaltene fast gänzlich abgebaut und es entsteht verstärkt Gas.

Abgeleitet von der in Abb. 6 gezeigten Produktverteilung kann unter folgenden Annahmen der Reaktionsverlauf modelliert werden:

- Die Intermediate (Präasphaltene und Asphaltene; PAA) sowie Produkte (Öl und Gas; O+G) werden zusammengefasst.

- Die Kinetik verläuft nach erster Ordnung.
- Die Pyrolysekohle wird in zwei Teile geteilt: die leicht reaktive und die schwer reaktive Pyrolysekohle.
- Das produzierte Wasser wird dem Öl zugerechnet.
- Der Einfluss von Wasserstoffdruck, Korngrößenverteilung, Stofftransport etc. wird vernachlässigt.

Abb. 7 zeigt den Vergleich der Produktbildung mit dem Ergebnis der Modellierung. Es wird deutlich, dass sich die Umsetzung der Kohle sehr gut beschreiben lässt.

Das gebildete Öl ist jedoch nach der Verflüssigung noch kein fertiger Treibstoff. Durch Gelpermeationschromatographie kann gezeigt werden, dass die verflüssigten Produkte eine Molmassenverteilung zwischen 100 und 2000 g mol⁻¹

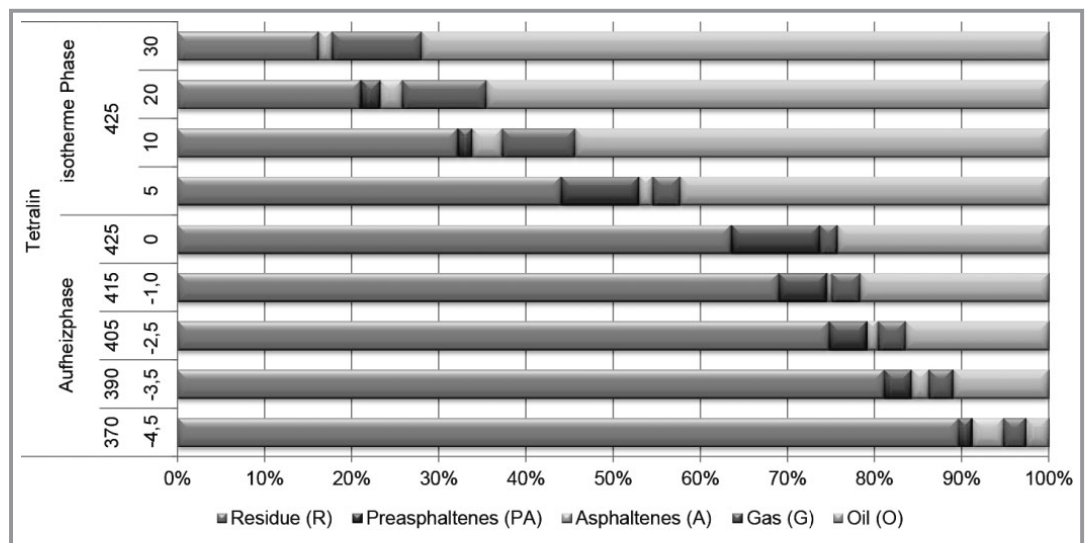


Abbildung 6. Verflüssigung von Pyrolysekohle bei einem Tetralin zu Kohleverhältnis von 3:1 und bei einem Druck von 180 bar [36, 37]. Die Ordinate ist in zwei Einheiten gespalten: einerseits die Reaktionstemperatur [°C] und andererseits die Reaktionszeit [min]; der Zeitpunkt null ist das Erreichen der Reaktionstemperatur.

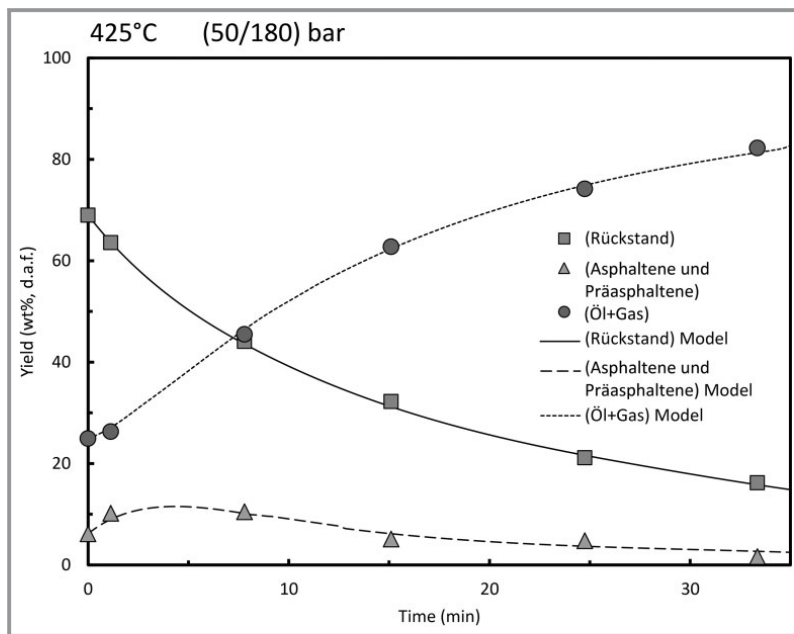


Abbildung 7. Vergleich zwischen Experiment und reaktionstechnischer Modellierung der Verflüssigung von Biochar bei 425 °C und 180 bar Reaktionsdruck bei einem Startdruck von 50 bar Wasserstoff [38].

aufweisen. Dennoch wird die eingesetzte Pyrolysekohle zu über 70 % verflüssigt und der heterogen katalysierten Hydrodeoxygenierung zugänglich gemacht. Darüber hinaus kann das gebildete Naphthalin wieder zu Tetralin rehydriert werden [28].

3.3 Hydrodeoxygenierung von Pyrolyseöl

Wie Abb. 3 zeigt, werden bei einer Pyrolysetemperatur von 375 °C 19 % des biogenen Kohlenstoffs in das wässrige Flüssigphasenpyrolyseöl gelöst. Durch den hohen Wassergehalt und durch den großen Sauerstoffanteil in den Produktmolekülen muss das Pyrolyseöl weiterverarbeitet werden, um einen wirtschaftlichen Mehrwert zu generieren. In Bezug auf Flüssigphasenpyrolyseöl kann man das Pyrolyseöl vor

der Hydrodeoxygenierung entwässern [29] oder direkt mit der gesamten Wasserfracht hydrodeoxygenieren.

Zur Hydrodeoxygenierung eignen sich Edelmetallkatalysatoren, die durch den hohen Preis sehr unattraktiv sind. Als kostengünstige Alternative wurde Raney-Nickel verwendet. Die Hydrodeoxygenierung von Flüssigphasenpyrolyseöl wird in einem zweistufigen Prozess, wie er in Abb. 8 gezeigt wird, durchgeführt [30, 31]. Dabei wird zuerst bei 250 °C mild hydrodeoxygeniert. Bei diesem ersten Schritt werden die organischen Komponenten soweit hydrophobiert, dass es zu einer Phasentrennung kommt [30]. Es entstehen zwei flüssige Phasen, eine organische und eine wässrige Phase. Der Massenanteil der organischen Phase, beträgt nur 22 %, darin finden sich aber 70 % des Energieinhalts (bezogen auf den Heizwert) des eingesetzten Flüssigphasenpyrolyseöls (PYO). Der Kohlenstoffgehalt der wässrigen Phase liegt bei 12,5 %, der Kohlenstoffgehalt der organischen Phase bei 70 %. Der Verlust an organischen Verbindungen in der wässrigen Phase ist gewollt, da es sich bei diesen

größtenteils um kurzkettige sauerstoffreiche Verbindungen (Essigsäure, Hydroxypropanon) handelt, deren Hydrierung nicht sinnvoll ist. In der zweiten Stufe wird das mild hydrodeoxygenierte (stabilisierte) Flüssigphasenpyrolyseöl im Verhältnis 1:2,5 mit dem im bioCRACK-Prozess erzeugten bioCRACK-Öl (BCO) gemeinsam hydriert. Die zwei Komponenten sind vor der Hydrodeoxygenierung nicht mischbar. Die zweite Stufe wird bei 150 bar Wasserstoffdruck und 400 °C betrieben.

Das flüssige Produkt dieser zweiten Stufe zerfällt ebenfalls in eine organische und eine wässrige Phase, wobei bei der zweiten Stufe der Anteil der wässrigen Phase mit 4 % sehr gering ist. Der Massenanteil der organischen Phase beträgt 88 % in denen 96 % der eingesetzten Energie (bezogen auf den Heizwert) vorliegt. Über die zweistufige Hydrodeoxygenierung werden somit 67 % der eingesetzten Energie

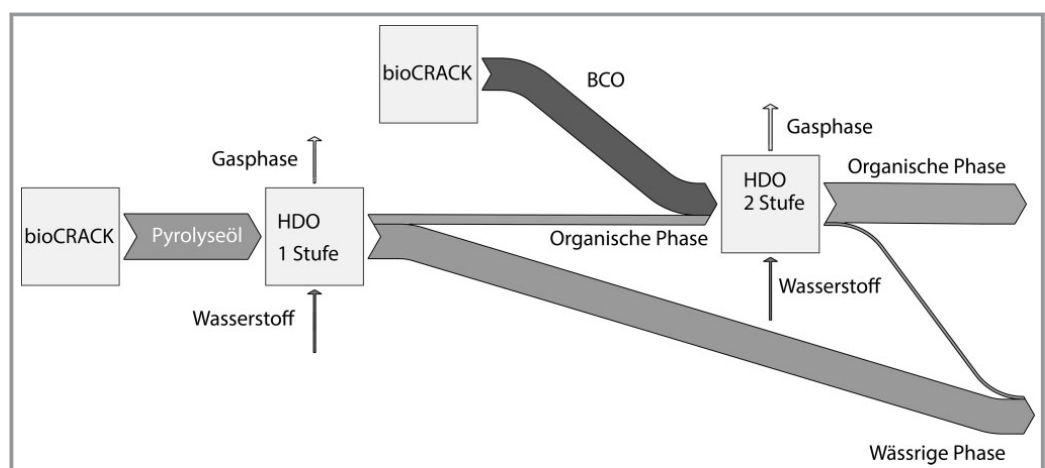


Abbildung 8. Hydrodeoxygenierung von Flüssigphasenpyrolyseöl [30].

(bezogen auf den Heizwert) des eingesetzten Pyrolyseöls in einen Treibstoff mit biogenem Kohlenstoff transferiert. Die Tabs. 2 und 3 zeigen einen HDO-Treibstoff, der den Vorgaben der Diesel-Norm EN-590 schon sehr nahe kommt.

4 Zusammenfassung

Das BiomassPyrolysisRefinery-Konzept zeigt einen neuen Zugang zur Verflüssigung von Biomasse. Als hybrides Verfahren für das Co-Refining von Erdölraffinationsintermediaten und der Pyrolyse kann in drei Abschnitten ein Dieselsatzkraftstoff erzeugt werden. Beim ersten Abschnitt, dem bioCRACK-Prozess, können 21 % des biogenen Kohlenstoffs in BCO gelöst werden. Nach der Destillation sind 16 % des biogenen Kohlenstoffs in Verbrennungsmotoren verwertbar.

Alternativ dazu kann das BCO mit dem Pyrolyseöl gemeinsam verwertet werden. Bei dieser Variante werden 25 % des biogenen Kohlenstoffs in einen dieselähnlichen Treibstoff mit 28 % biogenem Kohlenstoffanteil transferiert. Aus Versuchsergebnissen zur Pyrolyseölverwertung kann abgeleitet werden, dass bei noch nicht optimierter kontinuierlicher Hydrierung [32] insgesamt 18 % der eingesetzten Biomasse verflüssigt werden können.

Welchen Beitrag die Pyrolysekohleverflüssigung zur Biotreibstoff-Herstellung leisten kann, kann noch nicht quantifiziert werden. Die technische Machbarkeit konnte aber bereits bestätigt werden.

Die Autoren möchten der Österreichischen Forschungsförderungsgesellschaft, die dieses Projekt im Rahmen der FFG-Projekte bioBOOST (FFG Nr.: 825564) und bio-CRACK (FFG Nr.: 835804) unterstützt hat, danken.

Literatur

- [1] *Climate Change 2014: Impacts, Adaptation, and Vulnerability. Part A: Global and Sectoral Aspects* (Eds: C. B. Field et al.), Cambridge University Press, Cambridge **2014**.
- [2] M. Balat, *Energy Convers. Manage.* **2011**, *47*, 858. DOI: 10.1016/j.enconman.2010.08.013
- [3] S. Sorrell, J. Speirs, R. Bentley, A. Brandt, R. Miller, *Energy Policy* **2010**, *38*, 5290. DOI: 10.1016/j.enpol.2010.04.046
- [4] *Climate Change 2007: Synthesis Report* (Eds: Core Writing Team, R. K. Pachauri, A. Reisinger), IPCC, Geneva **2007**.
- [5] *Richtlinie 2009/28/EG des Europäischen Parlaments und des Rates*, 23. April **2009**.
- [6] F. Behrendt, Y. Neubauer, *Chem. Eng. Technol.* **2008**, *31*, 667. DOI: 10.1002/ceat.200800077
- [7] R. Rauch, *4. BtL-Kongress*, Berlin, Dezember **2010**.
- [8] H. J. Arpe, *Industrielle Organische Chemie*, Wiley-VCH, Weinheim **2007**.
- [9] D. Leckel, *Energy Fuels* **2009**, *23*, 2342. DOI: 10.1021/ef900064c
- [10] G. A. Olah, *Beyond Oil and Gas: The Methanol Economy*, Wiley-VCH, Weinheim **2009**.
- [11] M. Müller, U. Hübsch, *Dimethyl Ether*, in *Ullmann's Encyclopedia of Industrial Chemistry*, Wiley-VCH, Weinheim **2012**. DOI: 10.1002/14356007.a08_541
- [12] J. Burger, M. Siegert, E. Ströfer, H. Hasse, *Fuel* **2010**, *89*, 3315. DOI: 10.1016/j.fuel.2010.05.014
- [13] F. Fischer, H. Tropsch, *Ber. Dtsch. Chem. Ges.* **1926**, *59*, 830. DOI: 10.1002/cber.19260590442
- [14] R. Plass, *4. BtL-Kongress*, Berlin, Dezember **2010**.
- [15] P. M. Mortensen, J.-D. Grunwaldt, P. A. Jensen, K. G. Knudsen, A. D. Jensen, *Appl. Catal., A* **2011**, *407*, 1–19. DOI: 10.1016/j.apcata.2011.08.046
- [16] A. R. Ardiyanti, A. Gutierrez, M. L. Honkela, A. O. I. Krause, H. J. Heeres, *Appl. Catal., A* **2011**, *407*, 56. DOI: 10.1016/j.apcata.2011.08.024
- [17] F. de Miguel Mercader, M. J. Groeneveld, S. R. A. Kersten, N. W. J. Way, C. J. Schaverien, J. A. Hogendoorn, *Appl. Catal., B* **2010**, *96*, 57. DOI: 10.1016/j.apcatb.2010.01.033
- [18] F. D. M. Mercader, P. Koehorst, *AIChE J.* **2011**, *57*, 3160. DOI: 10.1002/aic.12503
- [19] N. Schwaiger, R. Feiner, K. Zahel, A. Pieber, V. Witek, P. Pucher, E. Ahn, P. Wilhelm, B. Chernev, H. Schröttner, M. Siebenhofer, *BioEnergy Res.* **2011**, *4*, 294. DOI: 10.1007/s12155-011-9132-8
- [20] N. Schwaiger, V. Witek, R. Feiner, H. Pucher, K. Zahel, A. Pieber, P. Pucher, E. Ahn, B. Chernev, H. Schroettner, P. Wilhelm, M. Siebenhofer, *Bioresour. Technol.* **2012**, *124*, 90. DOI: 10.1016/j.biortech.2012.07.115
- [21] M. A. Hubmann, *Master Thesis*, Technische Universität Graz **2010**.
- [22] G. W. Huber, S. Iborra, A. Corma, *Chem. Rev.* **2006**, *106*, 4044. DOI: 10.1021/cr068360d
- [23] A. V. Bridgwater, D. Meier, D. Radlein, *Org. Geochem.* **1999**, *30*, 1479. DOI: 10.1016/S0146-6380(99)00120-5
- [24] D. Meier, O. Faix, *Bioresour. Technol.* **1999**, *68*, 71. DOI: 10.1016/S0960-8524(98)00086-8
- [25] N. Schwaiger, *PhD Thesis*, Technische Universität Graz **2011**.
- [26] T. Willner, in *Biocrudeoil*, Gülzower Fachgespräche, Vol. 28, Fachagentur Nachwachsende Rohstoffe, Gülzow **2008**.
- [27] D. D. Whitehurst, T. O. Mitchell, M. Farcasiu, *Coal liquefaction: The Chemistry and Technology of Thermal Processes*, Academic Press, New York **1980**.
- [28] R. Feiner, N. Schwaiger, H. Pucher, L. Ellmaier, M. Derntl, P. Pucher, M. Siebenhofer, *RSC Adv.* **2014**, *4*, 34955. DOI: 10.1039/C4RA03487B
- [29] H. Pucher, N. Schwaiger, R. Feiner, P. Pucher, L. Ellmaier, M. Siebenhofer, *Int. J. Energy Res.* **2014**, *38*, 1964. DOI: 10.1002/er.3205
- [30] H. Pucher, *PhD Thesis*, Technische Universität Graz **2014**.
- [31] H. Pucher, N. Schwaiger, R. Feiner, L. Ellmaier, P. Pucher, B. Chernev, M. Siebenhofer, *Green Chem.* **2015**, *17*, 1291. DOI: 10.1039/C4GC01741B
- [32] N. Schwaiger, D. C. Elliott, J. Ritzberger, H. Wang, P. Pucher, M. Siebenhofer, *Green Chem.* **2015**, in press. DOI: 10.1039/C4GC02344G
- [33] R. Feiner, *Achema 2012*, Frankfurt, Juni **2012**.
- [34] J. Ritzberger, P. Pucher, N. Schwaiger, M. Siebenhofer, *Chem. Eng. Trans.* **2014**, *39*, 1189–1195. DOI: 10.3303/CET1439199
- [35] M. W. Haedel, in *Handbook of Heterogeneous Catalysis*, Wiley-VCH, Weinheim **2008**.
- [36] R. Feiner, *PhD Thesis*, Technische Universität Graz **2014**.
- [37] R. Feiner, N. Schwaiger, H. Pucher, L. Ellmaier, P. Pucher, M. Siebenhofer, *RSC Adv.* **2013**, *3*, 17898. DOI: 10.1039/c3ra43516d
- [38] R. Feiner, N. Schwaiger, H. Pucher, L. Ellmaier, A. Reiter, M. Derntl, T. Glatz, P. Pucher, M. Siebenhofer, *BioEnergy Res.* **2014**, *7*, 1343. DOI: 10.1007/s12155-014-9469-x

BiomassPyrolysisRefinery – Production of Biofuels from Lignocellulose

Nikolaus Schwaiger^{1,*}, Roland Feiner¹, Hannes Pucher¹, Lisa Ellmaier², Jürgen Ritzberger², Klara Treusch², Peter Pucher² und Matthäus Siebenhofer¹

DOI: 10.1002/cite.201400099

Abstract:

The BiomassPyrolysisRefinery concept consists of two main process steps. In the first step lignocellulosic biomass is converted into pyrolysis oil and pyrolysis char through liquid phase pyrolysis. In the second step these intermediate products are upgraded. Liquid phase pyrolysis oil was upgraded by two-step hydrodeoxygenation. The first step was mild hydrodeoxygenation, the second step was a co-refining with a fossil oil refinery intermediate. Direct liquefaction of pyrolysis char was carried out with the hydrogen donor solvent Tetralin.

Keywords:

Biochar liquefaction, BiomassPyrolysisRefinery, Hydrodeoxygenation, Liquid phase pyrolysis

Received: 8 July 2014; *revised:* 2 March 2015; *accepted:* 3 March 2015

1 Introduction

Although in autumn of 2014 the supply of oil was rising and prices were falling, the effects of CO₂-related climate change were evident worldwide[1]. The transport sector accounts for a fifth of global energy demand. The growing world population necessarily leads to constantly rising demand for mobility and therefore for liquid fuels [2]. Since the majority of liquid fuel production is based on oil, one of the big challenges is to develop an equivalent biofuel [3]. Such a biofuel ought to be compatible with the existing distribution infrastructure and ought to reduce CO₂ emissions sustainably [4]. Also, Directive 2009/28/EC [5] requires that by the year 2020, 10% of the final energy needs of the transport sector must be met by renewable energy. Since the responsibility to preserve the environment and to slow down climate change is becoming increasingly urgent, it is absolutely essential to replace fossil energy sources with sustainable CO₂-neutral biofuels. Two of the possible substitution strategies for fossil energy sources are the production of first and second-generation biofuels. First-generation biofuels are fuels obtained from oil-producing crops or through fermentation of glucose-containing grain. Second-generation biofuels are based on use of total plant biomass. The methods for producing second-generation biofuels include indirect and direct liquefaction of lignocellulosic biomass[6].

¹Dr. Nikolaus Schwaiger (nikolaus.schwaiger@tugraz.at), Dr. Roland Feiner, Dr. Hannes Pucher, Prof. Matthäus Siebenhofer, Technische Universität Graz, Central Lab Biobased Products/Institut für Chemische Verfahrenstechnik und Umwelttechnik, Inffeldgasse 25C, 8010 Graz, Österreich;

²Lisa Ellmaier, Jürgen Ritzberger, Klara Treusch, Dr. Peter Pucher, BDI-BioEnergy–International AG, Parkring 18, 8074 Grambach, Österreich.

The hydrodeoxygenation of the liquid-phase pyrolysis oil and the liquefaction of the biochar are tested at laboratory scale in a Büchi 450-ml high-pressure autoclave in the laboratories of the Institute of Chemical Engineering and Environmental Technology at Graz University of Technology.



Figure2:bioCRACK pilotplant of BDI at OMV refinery Vienna/Schwechat

3.1 Liquid-phase pyrolysis

In contrast to fast or flash pyrolysis, the bioCRACK process uses liquid carrier oil as a heat carrier instead of, for example, sand [19, 20, 25, 26]. The biomass is pyrolysed in a hot carrier oil under an inert atmosphere, at a pyrolysis temperature that depends on the boiling point and the decomposition temperature of the carrier medium. One advantage of the liquid-phase pyrolysis is, that particles (charcoal, ash) remain suspended in the hot carrier oil.

The heat transfer in the liquid medium is also superior to that in the fluidized bed. The disadvantages are, that after the pyrolysis, the particles have to be separated from the carrier oil and that the pyrolysis temperature is limited because of the decomposition and boiling properties of the carrier oil. However, the special characteristic of LPP is that depending on the carrier oil, a large fraction of the biomass is already converted into a rawfuel fraction during the pyrolysis.

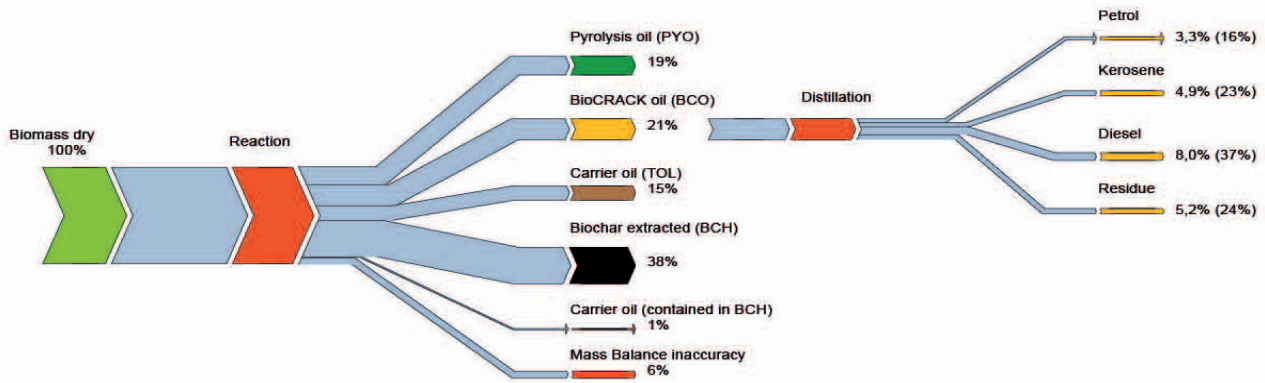


Figure3: Balance of biogenous Carbon during liquid phase pyrolysis [34]

Fig. 3 shows the biogenous carbon balance in the liquid-phase pyrolysis of pine wood pellets in the bioCRACK pilot plant. All the figures shown, were calculated on the basis of ^{14}C measurements and the carbon balance sheet. The balance shown is from the 38-h time point. At a carrier oil temperature of 375°C , biomass was converted at a rate of 60 kg h^{-1} . The carrier oil was vacuum gas oil (VGO), a mineral oil refinery intermediate that can only be converted to diesel by means of a high-cost hydrocracking process. The elemental composition of all the material flows is shown in Table 1.

Table1: Elemental composition of the products and educts of liquid-phase pyrolysis of spruce wood pellets at 375°C in the bioCRACK pilot plant.

| Material | C [%] | H [%] | N [%] | Rest [%] |
|---------------------------------|-------|-------|-------|----------|
| Biomass (BM) | 49.6% | 6.3% | <1 | 44.0% |
| Liquid phasepyrolysis oil (PYO) | 25.6% | 9,4% | <1 | 64.6% |
| Biochar (BCH) | 80.9% | 5.4% | <1 | 13.5% |
| BioCRACKoil (BCO) | 84.8% | 12.4% | <1 | 2.4% |
| Carrieroil (TOL) | 86.5% | 12.1% | <1 | 0.9% |

The balance difference describes the biogenous fraction of the pyrolysis gas and agrees with the measured values from the laboratory experiments [19]. In the course of the liquid-phase pyrolysis, 38% of the biogenic carbon is converted into a solid product, the so-called biochar (BCH). In total, 55% of the biogenic carbon is liquefied. Among the liquid products, three fractions can be identified. One fraction is the liquid-phase pyrolysis oil (PYO). This consists of oxygen-rich, water-soluble organic compounds and the water of reaction. The properties of PYO are shown in Table 2. The organic components have a wide range of sizes, from methanol up to compounds with molecular masses of more than 3000 g mol^{-1} [19]. Another fraction of the biomass dissolves in the carrier oil (TOL). These 15% of the biomass are detected only by means of the ^{14}C analysis and the carbon balance sheet. In the carrier oil, the concentration of biogenous carbon reaches 2%. The third liquid fraction, the so-called bioCRACK-oil (BCO) is made up of the hydrocarbon-soluble degradation products of the biomass that are transported out of the reactor along with the degradation products of the carrier oil. The ^{14}C content of the BCO and the composition of the components for the subsequent hydrodeoxygenation are shown in Table 2.

Table2: Properties of the liquid-phase pyrolysis oil (PYO), BCO and the resultant HDO fuel

| | Liquid phase pyrolysis oil | BCO | HDO Fuel |
|---|-------------------------------|------|----------|
| Water content [%] | 49.6 | 0.1 | 0.2 |
| Lower Calorific value [MJ/kg] | 9.2 | 40.1 | 41.2 |
| Acid number [mg _{KOH} /g _{sample}] | 82.2 | - | - |
| Mean molecular mass [g/mol] | 420 | 370 | 360 |
| Density [kg/m ³] | 1.09 | 0.88 | 0.87 |
| Viscosity [mPa s] | 3.9 | 8.0 | 4.5 |
| ¹⁴ C content [%] | 100 | 9.8 | 28.0 |
| Elemental composition | | | |
| Carboncontent [%] | 25.6 | 83.6 | 85.5 |
| Hydrogencontent [%] | 9.2 | 11.8 | 12.1 |
| Oxygencontent [%] | 64.9 | 4.2 | 1.9 |
| Nitrogencontent [%] | <1 | <1 | <1 |

The bioCRACK oil (BCO) can then be split into fuel fractions by distillation. The classification of these three fuel classes is done solely on the basis of boiling point ranges, but the oxygen content of each fraction is still too high for the corresponding standard, so that the fractions still have to be hydrogenated.

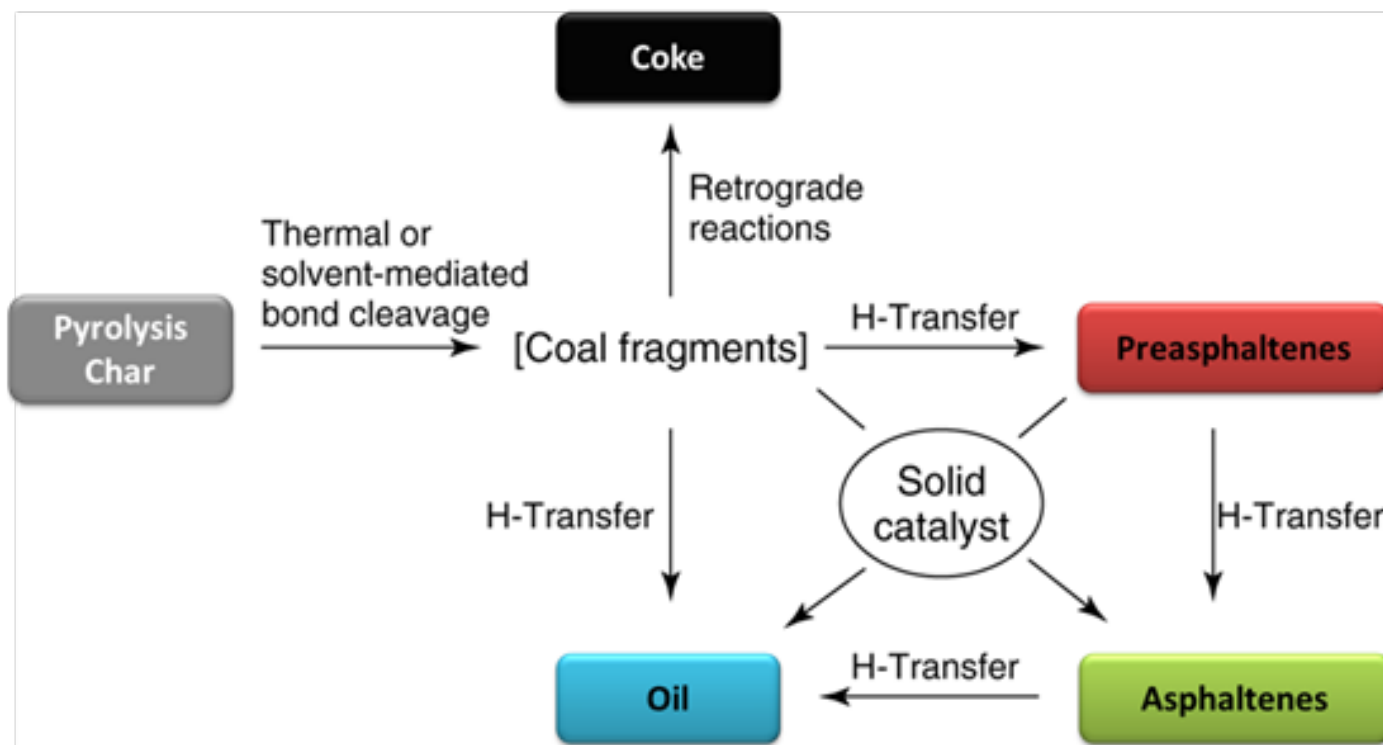


Figure4: Reaction scheme of the depolymerisation of char with and without stabilization by reactive hydrogen [35].

After the reaction, the pyrolysis oil is decanted and separated from the carrier oil by washing in hexane for the

laboratory-scale liquefaction. The liquid products (PYO, BCO) are isolated using a separator and then hydrodeoxygenated at laboratory scale.

3.2 Liquefaction of pyrolysis char

38% of the biomass is pyrolysed to biochar, whose composition is shown in Table 1. In an analogous method to the liquefaction of coal [27], this is done in a sludge. Preliminary experiments showed that for liquefaction of pyrolysis char a liquid carrier medium is needed. The liquefaction takes place at 425°C with a hydrogen pressure of up to 200 bar. With heterogeneous catalysis in the liquid phase it is almost impossible to deliver reactive hydrogen to the sites of coal depolymerization or bond scission. Without a hydrogen donor, mainly coke and tar are formed. Fig. 4 shows the pathway of coal depolymerization via the transition state of cleavage fragments to repolymerization and the resultant formation of solid and tarry products.

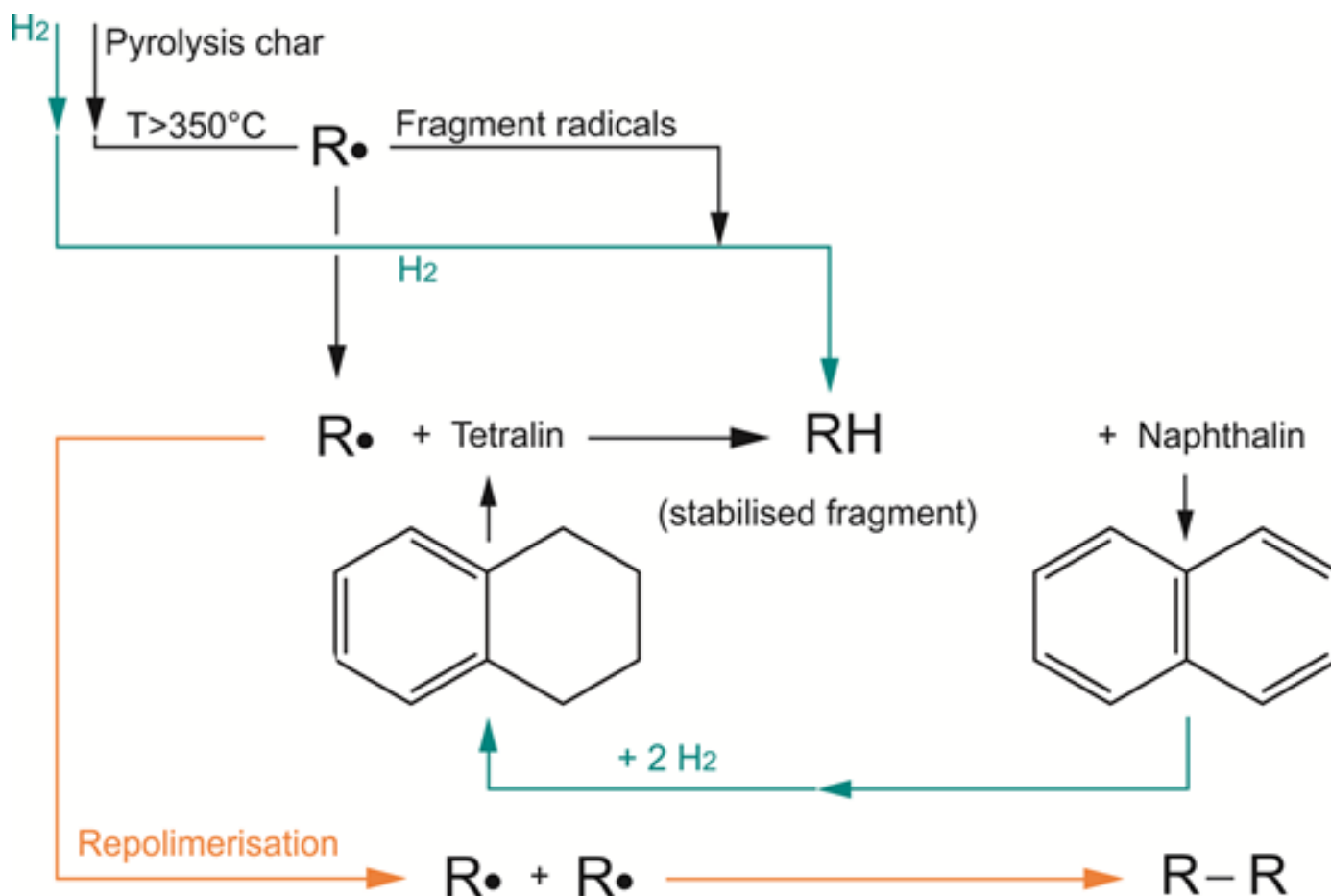


Figure 5: Shuttle mechanism between tetralin and naphthalene in the liquefaction of pyrolysis char [36].

Tetralin (1,2,3,4-tetrahydronaphthalene) is used to release reactive hydrogen at the sites of depolymerization of the cleavage fragments at the moment of bond scission. This is intended to prevent repolymerization and thus the unwanted formation of tar and coke. Fig. 5 shows the reaction scheme of coal liquefaction with tetralin. From 350°C upwards, cleavage-fragment radicals are formed which are then stabilized by tetralin with the formation of nascent hydrogen. This reaction converts tetralin to naphthalene, and the stabilized fragment goes into solution.

As shown in Fig. 4, it is not necessary to form oily products directly from the pyrolysis char. It is also possible, to form at room temperature non-condensable gases, asphaltenes and preasphaltenes. These substances are classified by their solubility as follows: The hexane-soluble products are called oils; those that are hexane-insoluble but toluene-soluble are called asphaltenes; and those that are toluene-insoluble, but tetrahydrofuran (THF)-soluble are called preasphaltenes. All other products that are not soluble in THF are classified as solid residues.

The liquefaction of pyrolysis char in tetralin can be divided into two reaction phases: the warming-up phase

until the reaction temperature is reached and the isothermic phase after it has been reached. Fig. 6 shows the liquefaction of pyrolysis char at 425°C with 180 bar of hydrogen pressure. It can be seen that more than 70% of the char is decomposed into an oil after a reaction time of 30 min. It is also clear that at the beginning of the reaction time, mostly preasphaltenes are formed but towards the end, the preasphaltenes have been almost completely degraded and gas formation increases.

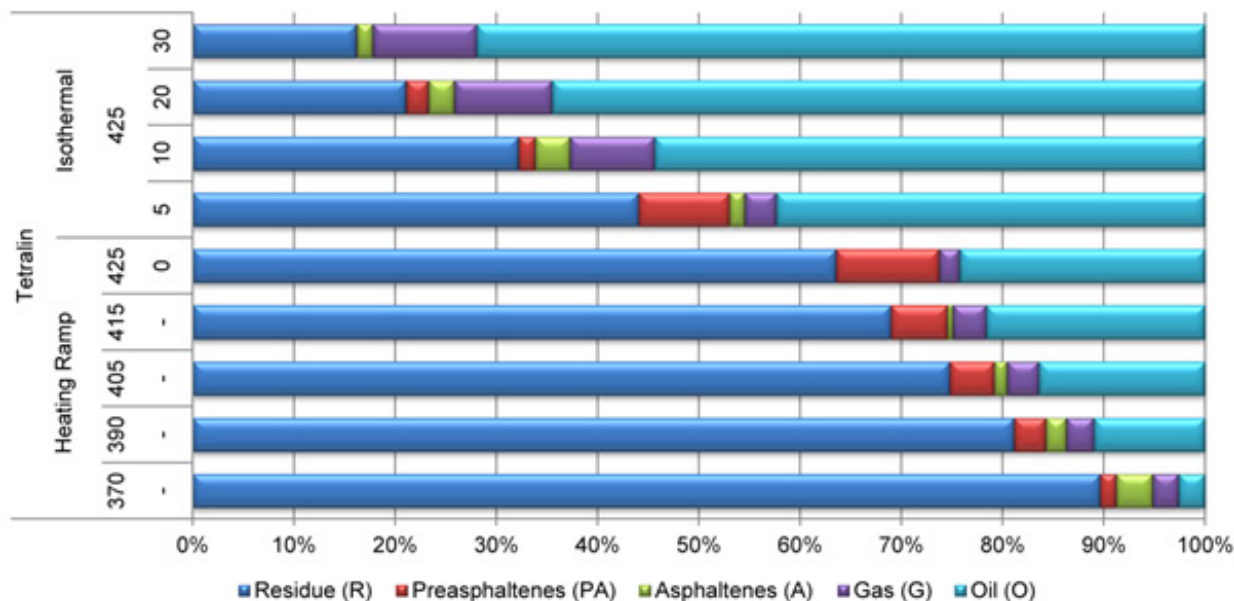


Figure6: Liquefaction of pyrolysis char at a tetralin-to-char ratio of 3:1 and pressure of 180 bar [36, 37]. The Y-axis shows the temperatures in °C reached at different times (relative to the time point t=0 when the reaction temperature is reached).

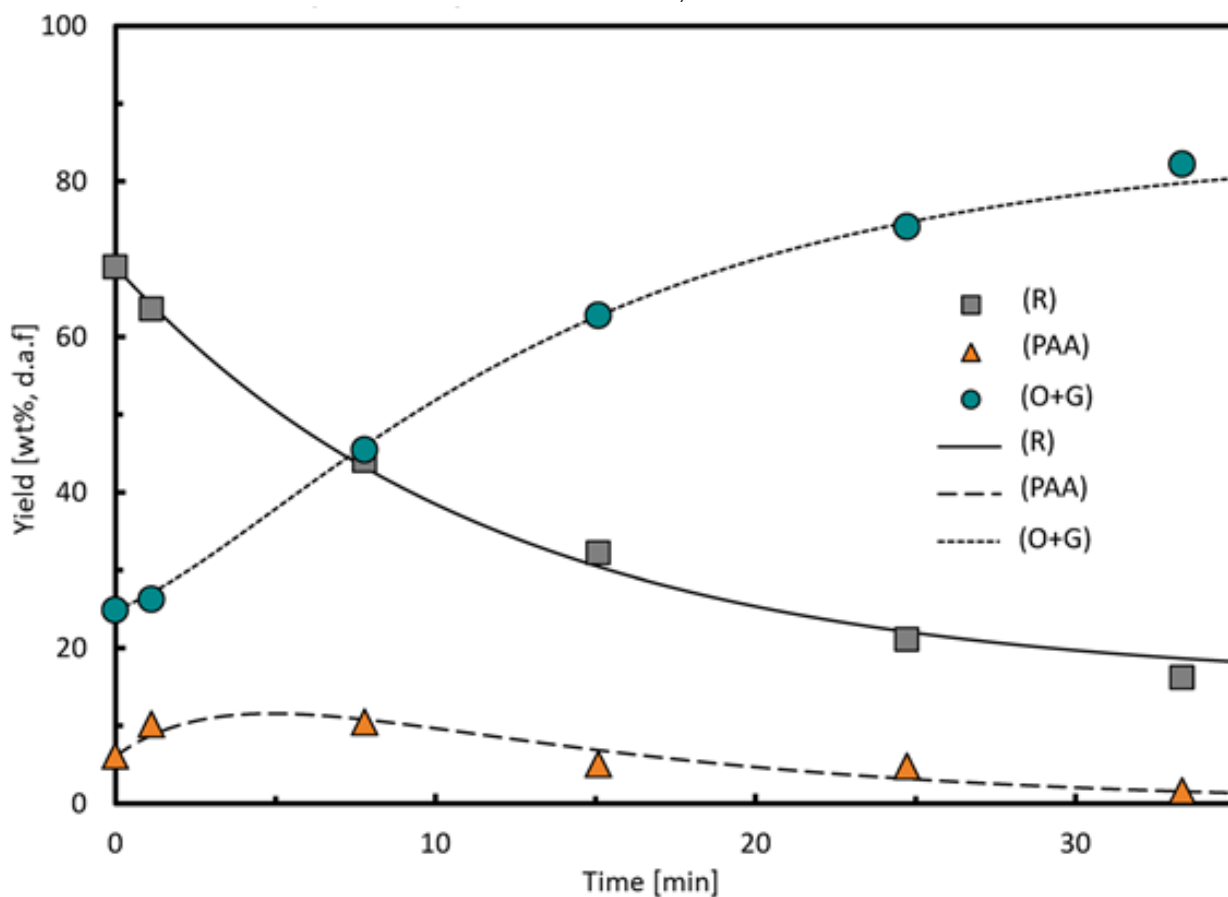


Figure7: Comparison of experimental values and modelling of the liquefaction of pyrolysis char at 425°C and 180 bar reaction pressure, at an initial hydrogen pressure of 50 bar [38].

The progress of the reaction can be modelled based on the relative amounts of the different products shown in Fig. 6 and the following assumptions:

- The intermediates (preasphaltenes and asphaltenes, PAA) and products (oil and gas, O+G) are grouped together.
- The kinetics are first-order.
- The pyrolysis char consists of two subfractions: readily reactive and poorly reactive.
- The water formed is counted as belonging to the oil.
- The effects of hydrogen pressure, particle size distribution, mass transfer, etc. are neglected.

Fig. 7 shows a comparison of the product formation with the results of the modelling. It can be seen that the model describes the conversion of the char very well. However, the oil formed is not yet a usable fuel. Analysis by gel permeation chromatography shows that the liquid products have a range of molecular masses from 100 to 2000 g mol⁻¹.

On the positive side, more than 70% of the pyrolysis char is converted and made accessible to hydrodeoxygenation by heterogeneous catalysis; and additionally, the naphthalene formed is re-hydrogenated back to tetralin [28].

3.3 Hydrodeoxygenation of pyrolysis oil

As shown in Fig. 3, at a pyrolysis temperature of 375°C, 19% of the biogenous carbon dissolves in the wet liquid-phase pyrolysis oil. Because of the high water content and the high oxygen content in the product molecules, the pyrolysis oil has to be further processed in order to generate an economically valuable end product. The oil can be first dehydrated and then hydrodeoxygenated [29] or directly hydrodeoxygenated without prior water separation.

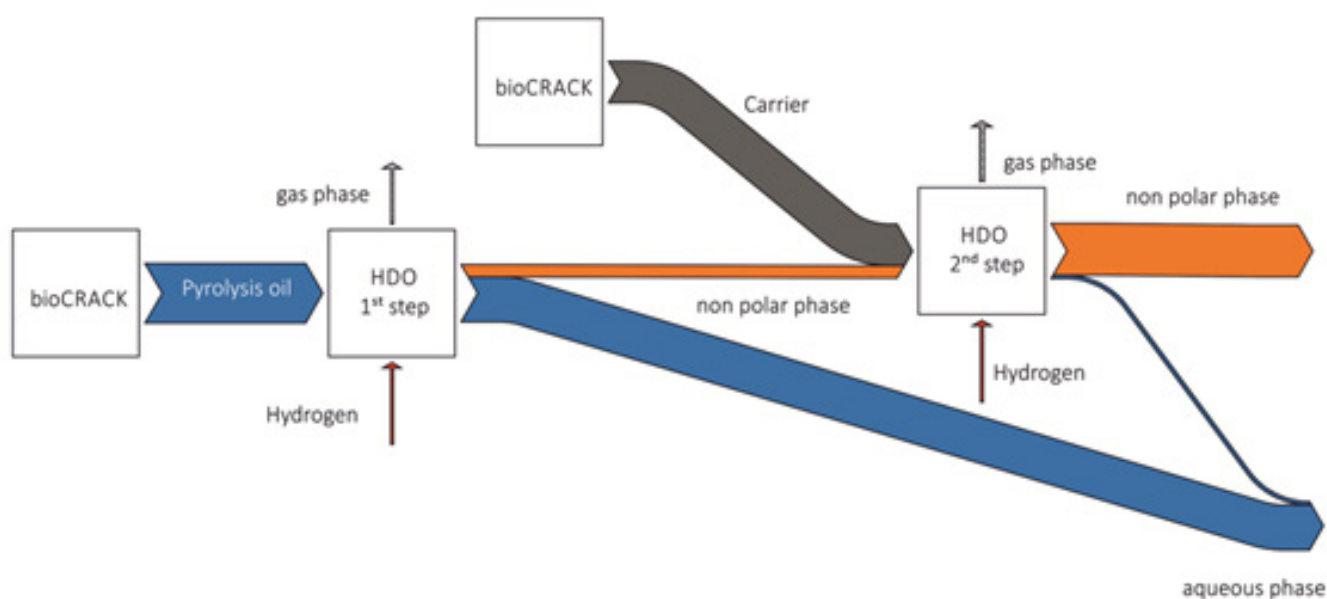


Figure8: Hydrodeoxygenation of liquid-phase pyrolysis oil [30].

In principle, the hydrodeoxygenation can be done with precious-metal catalysts, but in practice these are not an attractive option because of their high price. As a more economical alternative, Raney nickel was used. The hydrodeoxygenation of liquid-phase pyrolysis oil is done in a two-stage process as shown in Fig. 8 [30, 31]. In the first stage, a mild hydrodeoxygenation is done at 250°C. In this first step, the hydrophobicity of the organic components is increased to the point that a phase separation occurs [30], resulting in two liquid phases, one aqueous, one organic. Although the mass fraction of the organic phase is only 22%, it represents 70% of the (calorific) energy content of the liquid-phase pyrolysis oil (PYO). The carbon content of the aqueous phase is 12.5% and that of the organic phase is 70%. The loss of organic compounds in the aqueous phase is desirable, because the compounds involved are mainly short-chain, oxygen-rich compounds (e.g. acetic acid, hydroxypropanone) whose hydrogenation would not be useful. In the second step, the mildly hydrodeoxygenated

(stabilised) liquid-phase pyrolysis oil is hydrogenated in a mixture (at a ratio of 1:2.5) with the bioCRACK oil produced in the bioCRACK process. Before the hydrodeoxygenation, the two components are not miscible. The second stage is performed at 400°C under 150 bar of hydrogen pressure.

The liquid product of this second stage also separates into two phases, although in this case the aqueous phase is a much smaller fraction of the whole, at 4%. The mass fraction of the organic phase is 88%, which contains 96% of the calorific energy of the starting materials. Therefore the two-stage hydrodeoxygenation is able to transfer 67% of the calorific energy of the original pyrolysis oil to a fuel with biogenous carbon. Table 2 shows a HDO fuel that is already very close to the specification of the diesel standard EN-590.

4 Summary

The BiomassPyrolysisRefinery concept demonstrates a new approach to liquefaction of biomass. As a hybrid process for co-refining of intermediates from mineral oil refineries and pyrolysis, it produces a diesel replacement fuel in three steps. In the first stage, the bioCRACK process, 21% of the biogenous carbon is solubilized in BCO. After the distillation, 16% of the biogenous carbon is usable in internal combustion engines.

Alternatively, the BCO can also be worked up together with the pyrolysis oil. In this variant of the process, 25% of the biogenic carbon is transferred to a diesel-like fuel with 28% biogenous carbon. From experimental results on conversion of pyrolysis oil we can conclude that in total 18% of the original biomass can be liquefied by means of an – as yet not optimized – continuous hydrogenation process [32].

It is not yet possible to quantify the contribution that liquefaction of pyrolysis oil can make to the production of biofuels, but the work described here confirms that it is technically feasible.

The authors acknowledge the financial support of the Austrian Research Promotion Agency (FFG) through the FFG projects bioBOOST (FFG Nr.: 825564) and bioCRACK (FFG Nr.: 835804).

5 References

- [1] Climate Change 2014: Impacts, Adaptation, and Vulnerability. Part A: Global and Sectoral Aspects (Eds: C. B. Field et al.), Cambridge University Press, Cambridge 2014.
- [2] M. Balat, *Energy Convers. Manage.* 2011, 47, 858. DOI: 10.1016/j.enconman.2010.08.013
- [3] S. Sorrell, J. Speirs, R. Bentley, A. Brandt, R. Miller, *Energy Policy* 2010, 38, 5290. DOI: 10.1016/j.enpol.2010.04.046
- [4] Climate Change 2007: Synthesis Report (Eds: Core Writing Team, R. K. Pachauri, A. Reisinger), IPCC, Geneva 2007.
- [5] Richtlinie 2009/28/EG des Europäischen Parlaments und des Rates, 23. April 2009.
- [6] F. Behrendt, Y. Neubauer, *Chem. Eng. Technol.* 2008, 31, 667. DOI: 10.1002/ceat.200800077
- [7] R. Rauch, 4. BtL-Kongress, Berlin, Dezember 2010.
- [8] H. J. Arpe, *Industrielle Organische Chemie*, Wiley-VCH, Weinheim 2007.
- [9] D. Leckel, *Energy Fuels* 2009, 23, 2342. DOI: 10.1021/ef900064c
- [10] G. A. Olah, *Beyond Oil and Gas: The Methanol Economy*, Wiley-VCH, Weinheim 2009.
- [11] M. Müller, U. Hübsch, Dimethyl Ether, in *Ullmann's Encyclopedia of Industrial Chemistry*, Wiley-VC, Weinheim 2012. DOI: 10.1002/14356007.a08_541

- [12] J. Burger, M. Siegert, E. Ströfer, H. Hasse, *Fuel* 2010, 89, 3315. DOI: 10.1016/j.fuel.2010.05.014
- [13] F. Fischer, H. Tropsch, *Ber. Dtsch. Chem. Ges.* 1926, 59, 830. DOI: 10.1002/cber.19260590442
- [14] R. Plass, 4. BtL-Kongress, Berlin, Dezember 2010.
- [15] P. M. Mortensen, J.-D. Grunwaldt, P. A. Jensen, K. G. Knudsen, A. D. Jensen, *Appl. Catal., A* 2011, 407, 1 – 19. DOI: 10.1016/j.apcata.2011.08.046
- [16] A. R. Ardiyanti, A. Gutierrez, M. L. Honkela, A. O. I. Krause, H. J. Heeres, *Appl. Catal., A* 2011, 407, 56. DOI: 10.1016/j.apcata.2011.08.024
- [17] F. de Miguel Mercader, M. J. Groeneveld, S. R. A. Kersten, N. W. J. Way, C. J. Schaverien, J. A. Hogendoorn, *Appl. Catal., B* 2010, 96, 57. DOI: 10.1016/j.apcatb.2010.01.033
- [18] F. D. M. Mercader, P. Koehorst, *AIChE J.* 2011, 57, 3160. DOI: 10.1002/aic.12503
- [19] N. Schwaiger, R. Feiner, K. Zahel, A. Pieber, V. Witek, P. Pucher, E. Ahn, P. Wilhelm, B. Chernev, H. Schröttner, M. Siebenhofer, *BioEnergy Res.* 2011, 4, 294. DOI: 10.1007/s12155-011-9132-8
- [20] N. Schwaiger, V. Witek, R. Feiner, H. Pucher, K. Zahel, A. Pieber, P. Pucher, E. Ahn, B. Chernev, H. Schroettner, P. Wilhelm, M. Siebenhofer, *Bioresour. Technol.* 2012, 124, 90. DOI: 10.1016/j.biortech.2012.07.115
- [21] M.A.Hubmann, Master Thesis, Technische Universität Graz 2010. [22] G. W. Huber, S. Iborra, A. Corma, *Chem. Rev.* 2006, 106, 4044. DOI: 10.1021/cr068360d
- [23] A. V. Bridgwater, D. Meier, D. Radlein, *Org. Geochem.* 1999, 30, 1479. DOI: 10.1016/S0146-6380(99)00120-5
- [24] D. Meier, O. Faix, *Bioresour. Technol.* 1999, 68, 71. DOI: 10.1016/S0960-8524(98)00086-8
- [25] N. Schwaiger, PhD Thesis, Technische Universität Graz 2011. [26] T. Willner, in *Biocrudeoil*, Gülzower Fachgespräche, Vol. 28, Fachagentur Nachwachsende Rohstoffe, Gülzow 2008.
- [27] D. D. Whitehurst, T. O. Mitchell, M. Farcasiu, *Coal liquefaction: The Chemistry and Technology of Thermal Processes*, Academic Press, New York 1980.
- [28] R. Feiner, N. Schwaiger, H. Pucher, L. Ellmaier, M. Derntl, P. Pucher, M. Siebenhofer, *RSC Adv.* 2014, 4, 34955. DOI: 10.1039/C4RA03487B
- [29] H. Pucher, N. Schwaiger, R. Feiner, P. Pucher, L. Ellmaier, M. Siebenhofer, *Int. J. Energy Res.* 2014, 38, 1964. DOI: 10.1002/er.3205
- [30] H. Pucher, PhD Thesis, Technische Universität Graz 2014. [31] H. Pucher, N. Schwaiger, R. Feiner, L. Ellmaier, P. Pucher, B. Chernev, M. Siebenhofer, *Green Chem.* 2015, 17, 1291. DOI:10.1039/C4GC01741B
- [32] N. Schwaiger, D. C. Elliott, J. Ritzberger, H. Wang, P. Pucher, M. Siebenhofer, *Green Chem.* 2015, in press. DOI: 10.1039/C4GC02344G
- [33] R. Feiner, *Achema* 2012, Frankfurt, Juni 2012.
- [34] J. Ritzberger, P. Pucher, N. Schwaiger, M. Siebenhofer, *Chem. Eng. Trans.* 2014, 39, 1189 – 1195. DOI: 10.3303/CET1439199 [35] M. W. Haenel, in *Handbook of Heterogeneous Catalysis*, Wiley-VCH, Weinheim 2008.
- [36] R. Feiner, PhD Thesis, Technische Universität Graz 2014. [37] R. Feiner, N. Schwaiger, H. Pucher, L. Ellmaier, P. Pucher, M. Siebenhofer, *RSC Adv.* 2013, 3, 17898. DOI: 10.1039/c3ra43516d
- [38] R. Feiner, N. Schwaiger, H. Pucher, L. Ellmaier, A. Reiter, M. Derntl, T. Glatz, P. Pucher, M. Siebenhofer, *BioEnergy Res.* 2014, 7, 1343. DOI: 10.1007/s12155-014-9469-x

Chapter 14

Conclusion

14 Conclusion

The last chapter of this thesis is a short summary of the presented biomass liquefaction project based on liquid phase pyrolysis. Figure 1 shows a schematic of the lab scale batch reactor, which provided the data of the basic biomass liquefaction mechanisms of liquid phase pyrolysis.

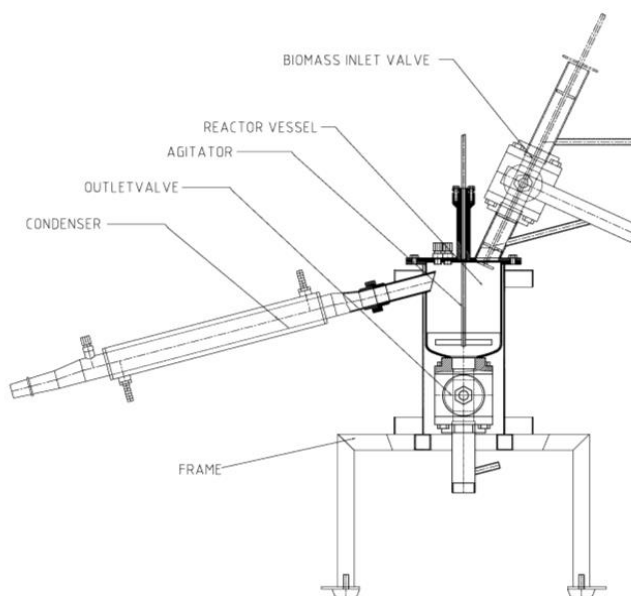


Figure 1: Schematic of the Liquid phase pyrolysis lab scale batch reactor [1]

Main outcome of these experiment series was the relationship of liquid product formation and biomass carburation at $T=350^{\circ}\text{C}$. This context is shown in in Figure 2.

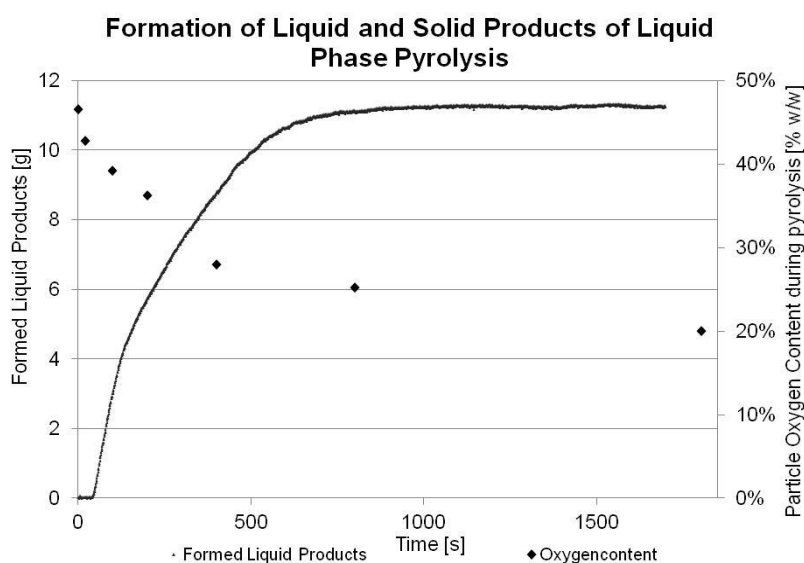


Figure 2: Kinetics of biomass liquefaction and biomass carburation during liquid phase pyrolysis at $T=350^{\circ}\text{C}$ [2]

The liquefaction process is finished after 800 s. The first 100 s are dedicated to biomass dewatering and afterwards formation of liquid CHO-products is predominant. Contrarily to

liquid product formation carburation is finished after 1800 s. These findings classified liquid phase pyrolysis to a special type of intermediate pyrolysis [2].

Consequently on its way to a new biomass conversion technology, BDI Bioenergy International AG built a pilot plant based on these outcomes and the balances of Mertlitz [3] and Pucher. This conversion technology is partially based on liquid phase pyrolysis. The intension of the BDI Bioenergy International AG process is to liquefy biomass **and** degrade the liquid heat carrier to produce a renewable fuel. The registered trade name of this liquefaction method is the bioCRACK process.

Juni 2015
87. Jahrgang
CITAH 87 (6)
665-864 (2015)
ISSN 0009-286 X

www.CIT-journal.com

Chemie Ingenieur Technik

Verfahrenstechnik · Technische Chemie · Apparatewesen · Biotechnologie

6 | 2015

Themenheft:
Reaktionstechnik

Gastherausgeber:
Elias Klemm
Jörg Sauer

Herausgeber:
DECHEMA
GDCh
VDI-GVC

WILEY-VCH



Figure 3: The bioCRACK pilot plant at OMV refinery Vienna/Schwechat [4]

The bioCRACK pilot plant is shown in Figure 3. It was in operation from June 2012 until December 2014. Various biomass feeds were tested; examples are soft wood, hard wood,

miscanthus and wheat straw. The different types of biomass did not affect the biomass to fuel conversion rate heavily [5].

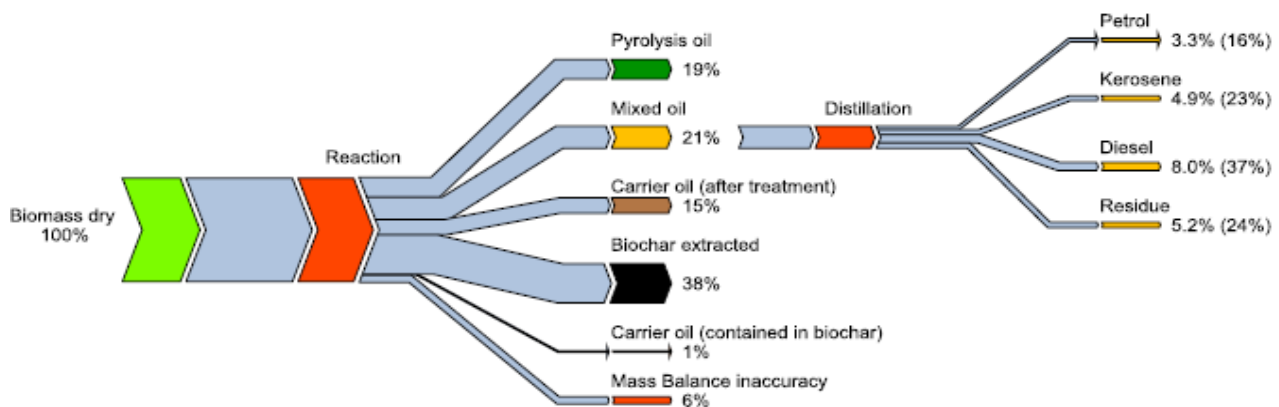


Figure 4: Biogenous carbon balance at T=375 °C [6]

Figure 4 shows the balance of biogenous carbon during the bioCRACK Process. It is shown that in a first step 21% of the carbon can be transferred directly into fuel fractions. Moreover 15% are transferred into a heavy fuel fraction, which can be further processed by fluid catalytic cracking [7]. Anyway Figure 4 shows that a further processing of the side streams biochar and pyrolysis oil is needed. This was performed in the FFG project (Austrian research promotion agency; Österreichische Forschungsförderungsgesellschaft) bioBOOST.

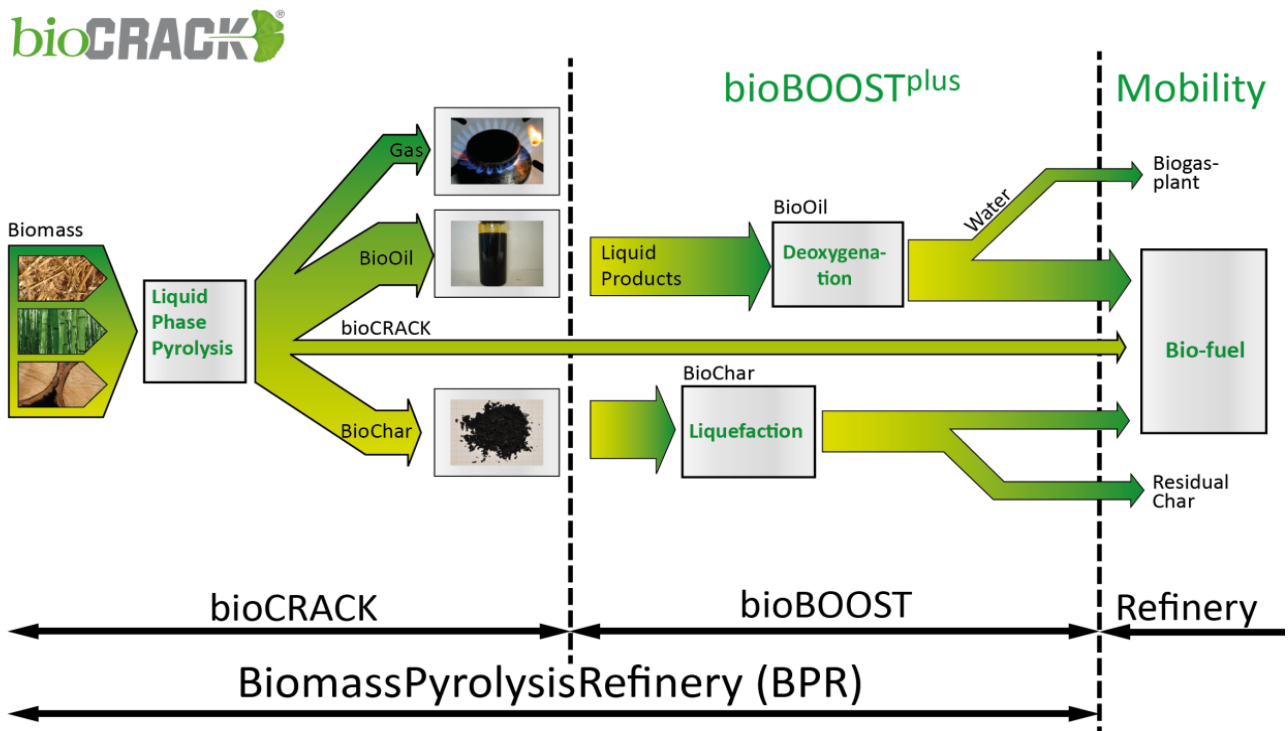


Figure 5: Product streams in the BiomassPyrolysisRefinery [8]

The first intention was to hydrodeoxygenate the liquid phase pyrolysis oil. Hydrodeoxygenation was performed in a two-step process in a 450 ml high pressure batch reactor. The first step was a low temperature hydroxygenation at 250°C with Raney-Nickel under hydrogen atmosphere (HDO1). The second step was a co-hydrodeoxygenation in a ratio

Conclusion

of 1:2.5 with the mixed oil from the bioCRACK process (HDO2). This was done under severe conditions at 400°C and 250 bar hydrogen pressure. Product and feed composition and properties are shown in Table 1. It was possible to produce a Diesel with 28% biogenous carbon content.

Table 1: Results of the two-step hydrodeoxygenation of liquid phase pyrolysis oil [9]

| | Pyrolysis oil | HDO1 | HDO2 | Diesel |
|---------------------------------|---------------|------|------|--------|
| Water Content [wt.%] | 50 | 11 | 0.2 | 0.02 |
| LHV [MJ/kg] | 8.7 | 26.4 | 41.2 | 42.5 |
| Density [kg/m ³] | 1070 | 1100 | 870 | 835 |
| Viscosity [mPa s] | 4 | 163 | 4.5 | 4 |
| Biogenous carbon [wt.%] | 100 | 100 | 28 | <7 |
| Elemental analysis on wet basis | | | | |
| Carbon Content [wt.%] | 25.6 | 62.5 | 85.5 | 85.9 |
| Hydrogen Content [wt.%] | 9.2 | 8.3 | 12.1 | 13.3 |
| Oxygen Content [wt.%] | 64.9 | 28.7 | 1.9 | <1 |
| Nitrogen Content [wt.%] | <1 | <1 | <1 | <1 |

The second part of the bioBOOST project was to liquefy the biochar, produced during the bioCRACK process. Biochar is the non-liquefied residur of the biomass, which is shown in Figure 6. It is easily remarkable that biochar, produced by the bioCRACK process, is the residual decomposition product of the lignin enriched structures in the wood cells. In detail it is the remaining middle lamella and primary wall.

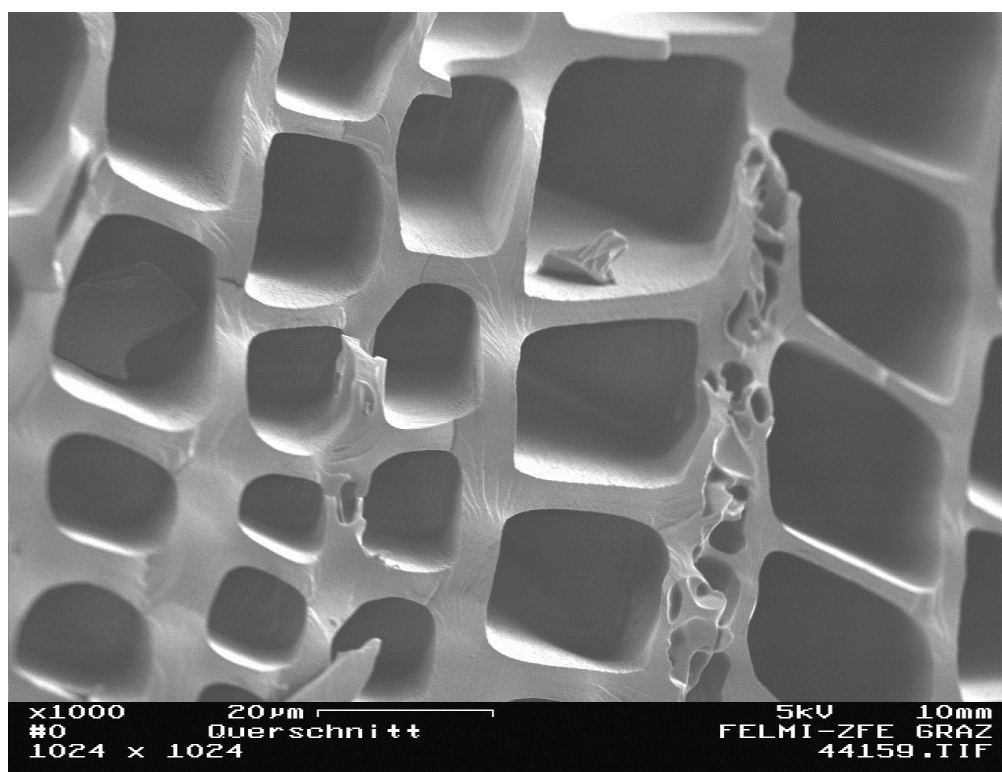


Figure 6: Biochar from liquid phase pyrolysis [10]

To liquefy biochar highly reactive hydrogen is a necessity. Heterogeneous catalysis is not able to provide this reactive hydrogen quantity at reaction conditions of 425°C and 180 bar. It is absolutely essential to provide this reactive hydrogen at the site of carbon-carbon bond rupture. A possibility to solve this problem is to supply reactive hydrogen with the tetralin-naphthalin hydrogen donor system.

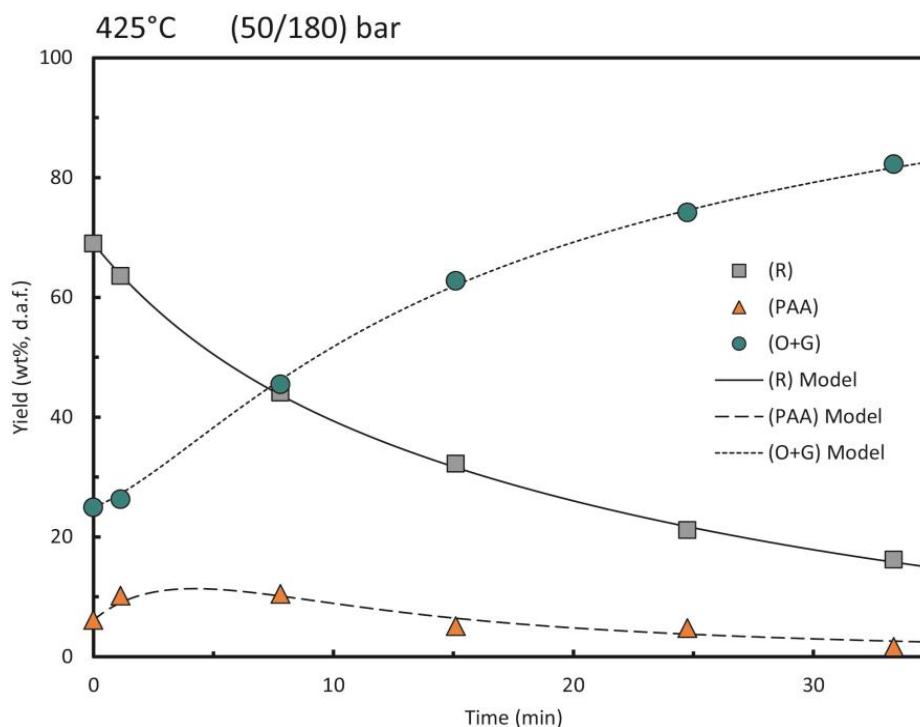


Figure 7: Biochar liquefaction and modelling in tetralin as hydrogen donor at 425°C and 180 bar hydrogen pressure (R; Residue, PAA; Preasphaltenes and Asphaltenes, O+G; Oil and gaseous products) [11]

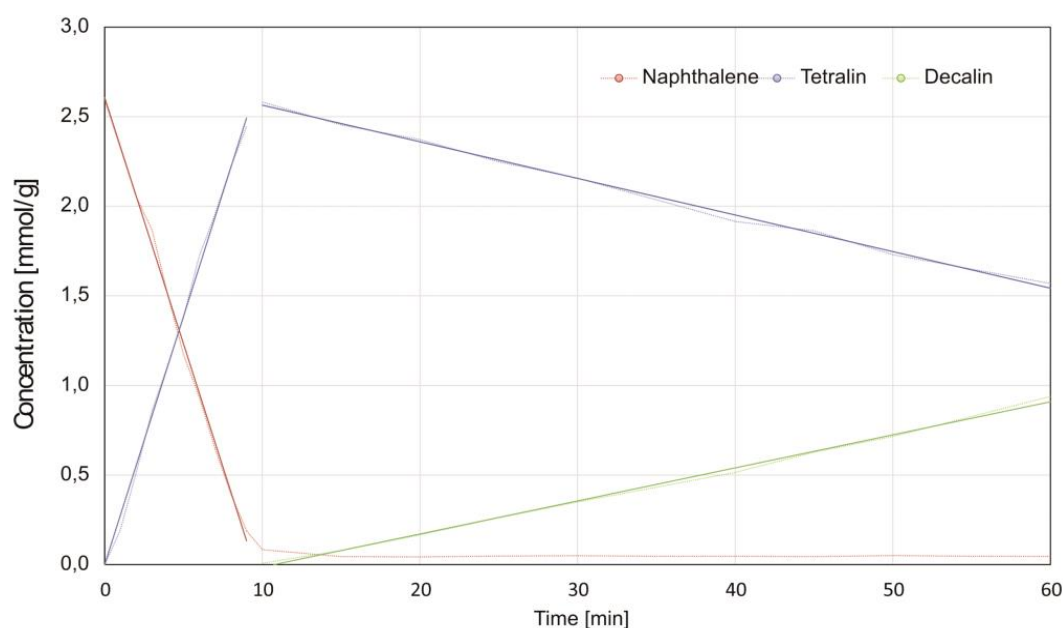


Figure 8: Naphthalene hydrogenation with Raney Nickel at 150°C [12]

Under these process parameters it is possible to convert more than 80% of the solid biochar into liquids and to model the degradation process as Figure 7 shows. Products of this liquefaction step are short chain alkanes and asphaltenes and preasphaltenes and gaseous products. To form a whole cycle with a hydrogen donor, rehydration is obvious. Naphthalene rehydrogenation is shown in Figure 8. Naphthalene is first hydrogenated to tetralin in a first order reaction. After full consumption of naphthalene, tetralin is further hydrogenated to both cis- and trans-decalin isomers, which are presented as decalin in Figure 8.

To sum up: This habilitation thesis presents an alternative biomass liquefaction route. In pilot scale 15% of biomass is directly convertible into liquid fuels, with the hydrodeoxygenation of the liquid phase pyrolysis oil additional 5% of the biomass can be transferred into liquid fuels. The impact of biochar liquefaction for liquid fuel production cannot be evaluated yet.

14.1 List of Figures

| | |
|---|---|
| FIGURE 1: LIQUID PHASE PYROLYSIS LAB SCALE BATCH REACTOR [1]..... | 1 |
| FIGURE 2: KINETICS OF BIOMASS LIQUEFACTION AND BIOMASS CARBURATION DURING LIQUID PHASE PYROLYSIS AT T=350°C [2] | 1 |
| FIGURE 3: THE BIOCRAK PILOT PLANT AT OMV REFINERY VIENNA/SCHWECHAT [4] | 2 |
| FIGURE 4: BIOGENOUS CARBON BALANCE AT T = 375 °C [6] | 3 |
| FIGURE 5: PRODUCT STREAMS IN THE BIOMASSPYROLYSISREFINERY [8] | 3 |
| FIGURE 6: BIOCHAR FROM LIQUID PHASE PYROLYSIS [9] | 4 |
| FIGURE 7: BIOCHAR LIQUEFACTION AND MODELLING IN TETRALIN AS HYDROGEN DONOR AT 425°C AND 180BAR HYDROGEN PRESSURE (R; RESIDUE, PAA; PREASPHALTENES AND ASPHALTENES, O+G; OIL AND GASEOUS PRODUCTS) [10] | 5 |
| FIGURE 8: NAPHTHALENE HYDROGENATION WITH RANEY NICKEL AT 150°C..... | 5 |

14.2 List of Tables

| | |
|--|---|
| TABLE 1: RESULTS OF THE TWO-STEP HYDRODEOXYGENATION OF LIQUID PHASE PYROLYSIS OIL..... | 4 |
|--|---|

1. Schwaiger N, Feiner R, Zahel K, et al. (2011) Liquid and Solid Products from Liquid-Phase Pyrolysis of Softwood. *BioEnergy Res* 4:294–302. doi: 10.1007/s12155-011-9132-8
2. Schwaiger N, Witek V, Feiner R, et al. (2012) Formation of liquid and solid products from liquid phase pyrolysis. *Bioresour Technol* 124:90–4. doi: 10.1016/j.biortech.2012.07.115
3. Mertlitz V (2010) Flüssigphasen-Pyrolyse biogener Edukte (Grundlagen) . Graz : s.n., 2010. Technische Universität Graz
4. Schwaiger N, Feiner R, Pucher H, et al. (2015) Chemie Ingenieur Technik - Titelbild. 87:665–864.
5. Ritzberger J (2016) Flüssigphasenpyrolyse - Prozessmodellierung und Scale-Up. Technische Universität Graz
6. Ritzberger J, Pucher P, Schwaiger N, Siebenhofer M (2014) The BioCRACK Process-A Refinery Integrated Biomass-to-Liquid Concept to Produce Diesel from Biogenic Feedstock. *Chem Eng Trans* 39:1189–1194.
7. Berchtold M, Fimberger J, Reichhold A, Pucher P (2016) Upgrading of heat carrier oil derived from liquid-phase pyrolysis via fluid catalytic cracking. *Fuel Process Technol* 142:92–99. doi: 10.1016/j.fuproc.2015.09.028
8. Feiner R (2014) Hydrierende Verflüssigung biogener Einsatzstoffe. Technische Universität Graz
9. Pucher H, Schwaiger N, Feiner R, et al. (2015) Biofuel production from liquid phase pyrolysis oil: A two-step HDO process. *Green Chem* 17:1291–1298. doi: 10.1039/C4GC01741B
10. Schwaiger N (2011) REAKTIONSTECHNISCHE ANALYSE FÜR DIE OPTIMIERUNG DER FLÜSSIGPHASENPYROLYSE; REAKTIONSMECHANISMEN DER FLÜSSIGPHASENPYROLYSE VON LIGNOCELLULOSE. Graz University of Technology
11. Feiner R, Schwaiger N, Pucher H, et al. (2014) Kinetics of Biochar Liquefaction. *BioEnergy Res* 7:1343–1350. doi: 10.1007/s12155-014-9469-x
12. Feiner R, Schwaiger N, Pucher H, et al. (2014) Chemical loop systems for biochar liquefaction: hydrogenation of Naphthalene. *RSC Adv* 4:34955. doi: 10.1039/C4RA03487B

